Waveguiding in electrooptic langmuir-blodgett films

Cresswell, J.P.

WAVEGUIDING IN ELECTROOPTIC LANGMUIR-BLODGETT FILMS

by

J.P. Cresswell BSc. MSc.
St. John's College

A Thesis submitted in partial fulfilment
of the requirements for the degree of PhD.

School of Engineering and Computer Science
University of Durham
February 1992

DECLARATION

I hereby declare that the work carried out in this thesis has not been previously submitted for any degree and is not currently being submitted in candidature for any other degree.

Signed.....

Candidate

The work in this thesis was carried out by the candidate.

Signed.....

Director of Studies

Signed.....

Candidate

DEDICATION

This thesis is dedicated to my parents

Acknowledgements

There are a great many people without whom this thesis would have turned out differently or not at all. First of all I would like to thank my supervisor Dr. Mike Petty for his enthusiasm, advice and tolerance over the past three years. Also the other members of the Molecular Electronics for providing a good working environment and excellent coffee room conversation. I must mention especially Mr. Chris Pearson for teaching me how to dip. Special thanks also to the chemists in the group, Dr. John Tsibouklis for the supply of materials and Dr. Yiping Song for FTIR work.

Outside the group, I am very grateful to Dr. Graham Cross for sharing his knowledge of polymer waveguide fabrication and electrooptic measurements. Mr. Brian Blackburn and his colleagues in the mechanical workshop are thanked for construction and maintenance of the troughs and surface plasmon resonance equipment and thanks go too to the electronics workshop and Mr. Peter Friend for the electronic parts of these devices. Mr. Norman Thompson and Mr. Chris Pearson (again) kept the evaporators, water system and (sometimes) the spectrophotometer in working order. Mr. Frank Spence ran an efficient ordering system and is now in well-earned retirement. Finally thanks to Ms. Julie Morgan and Mrs. Kay Seaton for photography and drawing for the papers and this thesis.

In the big world outside Durham I would like to thank Dr. Simon Allen of ICI for the oligomers and Dr. Norman Ratcliffe of British Aerospace (now of Bristol Polytechnic) for the aminonitrostilbenes. Furthest away of all, many thanks to Dr. Yuri Lvov of the Institute of Crystallography, Moscow for the X-ray measurements and for his hospitality when I visited him. The financial support of SERC and ICI is gratefully acknowledged.

Ultimately however, the contents of this thesis are nobody's fault but mine.

Abstract

This thesis describes work on the waveguiding and second-order nonlinear optics of Langmuir-Blodgett (LB) films. A number of new monomeric materials are assessed for their LB deposition and their second-order nonlinear properties. Both the Pockels effect and second harmonic generation are studied. One new chromophore, diphenyl butadiyne is shown to possess exceptional nonlinear effects in monolayer form with $\chi^{(2)}(-\omega;\omega,0) = 2.7 \times 10^{-10}$ mV^{-1}. A novel aminonitrostilbene carboxylic acid with $\chi^{(2)}(-\omega;\omega,0) = 1.43 \times 10^{-10}$ m V^{-1} is also described.

Polymeric LB materials have been found to possess greater stability than monomers but the deposition properties are often poor. Two oligomers are investigated, these both form high-quality LB layers and one gave $\chi^{(2)}(-\omega;\omega,0) = (3.4+1.0j)\times 10^{-11}$ m V^{-1}.

Two alternate-layer systems are considered. The first, of an amidonitrostilbene and a novel functionalised diarylalkyne deposits to 150 bilayers, but the nonlinear coefficients are shown to diminish after fewer than ten layers. X-ray diffraction, waveguiding and Fourier transform infra-red measurements are also performed. The second system alternates the two oligomers; only films of fewer than seven layer are studied due to the low value of Pockels effect and second-harmonic generation detected.

A novel method of waveguide fabrication combining solution dipped polymer layers with LB films is introduced. This technique allows the rapid fabrication of waveguides with nonlinear properties. Monomode waveguides are produced and their electrooptic properties measured. These are the first such measurements on an LB film waveguide. It is shown theoretically that such waveguides could be used to produce modulators of similar figures of merit to those made from poled-polymers but that an order of magnitude improvement in $\chi^{(2)}(-\omega;\omega,0)$ is needed to match lithium niobate systems.

CONTENTS

Chapter 1
Introduction

As perceived limits in electronic devices have been approached there has been an immense increase in interest in optical methods of signal transmission and processing. The major advantages of optics are seen to be its greater available bandwidth and the parallelism which may be achieved by using a broad wavefront. The first of these advantages has already been used to great effect in fibre optic communications where a much larger number of channels can be compressed into a single fibre as compared to traditional wires. However none of the signal processing is carried out optically, for example routing is achieved after converting the signals back to the electronic domain.

Nonlinear optical devices have many potential applications in the processing of optical signals and a number of modulators, wavelength filters and switching systems have been demonstrated. Many of these make use of inorganic materials (eg. gallium arsenide, lithium niobate) but there has also been a great deal of work done on organics in the hope of finding materials with larger nonlinearities.

Among the organic structures investigated have been Langmuir-Blodgett (LB) films. These films are attractive for nonlinear optics because they offer the possibility of engineering films with highly aligned molecules, controlled symmetry and hence large nonlinear coefficients. However, the materials used are often of poor thermal stability and the problem of producing the nonlinear waveguide structures needed for practical devices has yet to be addressed.

The work in this thesis investigates a number of new Langmuir-Blodgett materials designed for second-order nonlinear optics. The fabrication and assessment of nonlinear waveguides is also described. Chapter 2 introduces the general theory of linear and nonlinear optics for any type of material. Chapter 3 then explains the advantages of confined light structures for studying and using nonlinear effects and describes the theory of two such structures: the Kretchmann surface plasmon resonance system, and optical waveguides. Chapter 4 looks at the fabrication of

Langmuir-Blodgett films, applies the general optical theory of Chapter 2 to this particular case and provides an overview of past work on the nonlinear optics of LB films. The experimental methods used are given in Chapter 5. Chapter 6 is the first results chapter, it lists the materials studied and describes their Langmuir-Blodgett deposition properties. Chapter 7 gives the results from characterisation of the monolayers. The production of practical nonlinear devices will require films of much greater thickness than a single monolayer, one technique for achieving this is to produce structure formed of alternate-layers of a pair of LB materials. Chapter 8 is concerned with the characterisation of two alternate-layer systems, one of which is studied by optical waveguiding. However, a number of drawbacks were identified in the conventional method of producing LB film waveguides and Chapter 9 introduces a new technique. These novel waveguides are investigated for their propagation and electrooptic properties. Finally, Chapter 10 draws together conclusions from the whole thesis and makes suggestions for further work.

Chapter 2
Linear and Nonlinear Optics Theory

Optics theory may be broadly divided into two areas; those of linear and nonlinear optics. This division is defined by the form of the mathematical relationship between optical electric field and the induced polarisation. This chapter introduces, in general terms, the concepts required for the study of the optical properties of Langmuir-Blodgett films.

2.1 Linear Optics

As light is an electromagnetic wave its propagation properties are determined by the medium's response to electric and magnetic fields. In particular the response depends on permitivitty and permeability. For most materials the relative permeability is equal to unity so their effect on electromagnetic waves is due solely to their dielectric properties. A full description of linear optics will be found in any optics textbook, eg. reference 1.

The polarisation state of light is defined as the direction of its electric field vector (**E**). This vector always lies at right angles to the direction of propagation. This electric field induces an electronic displacement (**D**) in a medium such that:

$$\mathbf{D} = \epsilon_0 \hat{\epsilon}_r \mathbf{E} \tag{2.1}$$

where $\hat{\epsilon}_r$ is a second rank tensor known as the relative permittivity (the contribution to displacement of dc polarisation has been omitted).

A second definition of **D** is:

$$\mathbf{D} = \epsilon_0 \mathbf{E} + \mathbf{P} \tag{2.2}$$

where **P** is the polarisation induced in the material. This leads to a further relationship:

$$\mathbf{P} = \epsilon_0 \hat{\chi} \mathbf{E} \tag{2.3}$$

where $\hat{\chi}$ $(= \hat{\epsilon}_r - 1)$ is the susceptibility tensor (also of second rank).

It is the linearity of this electric field-polarisation relationship which defines linear optics.

2.1.1 Anisotropy in Linear Optics

In linear optics all the media properties are described by the relative permittivity tensor, this may be converted to a refractive index tensor by taking the square root of each element. The real part of refractive index controls effects such as reflection (by Fresnel formulae), refraction (by Snell's Law) and the velocity of propagation. The imaginary part represents loss.

For any non-optically active dielectric it is possible to diagonalise the permittivity tensor by suitable choice of principal axes. Equation 2.1 can then be rewritten as:

$$\begin{pmatrix} D_x \\ D_y \\ D_z \end{pmatrix} = \begin{pmatrix} \epsilon_{11} & 0 & 0 \\ 0 & \epsilon_{22} & 0 \\ 0 & 0 & \epsilon_{33} \end{pmatrix} \begin{pmatrix} E_x \\ E_y \\ E_z \end{pmatrix} \tag{2.4}$$

Light is only able to propagate as a single mode (ie. its electric and magnetic fields changing only as regards phase) if the dielectric displacement and electric field, perpendicular to the wavevector, are colinear (this is a consequence of the derivation of the wave equation for em waves in a dielectric from Maxwell's equations). However, in the general anistropic case it is readily shown that any polarisation of incident light may be resolved into two orthogonal polarisations propagating with different velocities in the medium. These two resolved polarisations define the ordinary and extraordinary rays which possess distinct refractive indices and therefore different angles of refraction at an interface. A medium with two refractive indices is said to be birefringent.

Three distinct levels of anisotropy can be identified:

i) Isotropic Medium : $\epsilon_{11} = \epsilon_{22} = \epsilon_{33}$

Here there is no anisotropy and all polarisations and propagation directions experience the same refractive index. The distinction between ordinary and extraordinary rays does not apply.

ii) Uniaxial Medium : $\epsilon_{11} = \epsilon_{22} \neq \epsilon_{33}$

For most ray directions and polarisations both ordinary (refractive index $= \sqrt{\epsilon_{11}} = \sqrt{\epsilon_{22}}$) and extraordinary (refractive index $= \sqrt{\epsilon_{33}}$) rays are generated. The exception is for light travelling in the z direction (the 'optic axis') where all polarisations are governed by the ordinary refractive index.

iii) Biaxial Medium : $\epsilon_{11} \neq \epsilon_{22} \neq \epsilon_{33}$

In this case there are two optic axes of transmission where the light may be resolved into orthogonal polarisations of equal velocity. Otherwise ordinary and extraordinary rays are produced.

An elegant graphical construction called the index ellipsoid[2] allows the refractive index experienced by any wave in any type of medium to be visualised. Generally the equation of the ellipsoid surface is determined by a set of six B parameters:

$$B_1 x^2 + B_2 y^2 + B_3 z^2 + B_4 yz + B_5 xz + B_6 xy = 1 \qquad (2.5)$$

where:

$$B_1 = \frac{1}{\epsilon_{11}} \qquad B_2 = \frac{1}{\epsilon_{22}}$$

$$B_3 = \frac{1}{\epsilon_{33}} \qquad B_4 = \frac{1}{\epsilon_{23}}$$

$$B_5 = \frac{1}{\epsilon_{13}} \qquad B_6 = \frac{1}{\epsilon_{12}}$$

(note that from the symmetry rules for second-rank tensors $\epsilon_{23} = \epsilon_{32}$ etc. and if the system is diagonalised B_4, B_5 and B_6 are set to zero)

The distance between the origin and the ellipsoid surface in the direction of the electric field vector is equal to the square of the refractive index. The cross section of the ellipsoid for the uniaxial crystal lithium niobate viewed along the y-axis is shown in figure 2.1. Light polarised in the x-direction experiences the ordinary index n_o, whilst light polarised in the z-direction is governed by the extraordinary index n_e. For a biaxial medium the existence of two optic axes is easily visualised as being equivalent to stating the any general ellipsoid possesses two directions defining circular cross-sections.

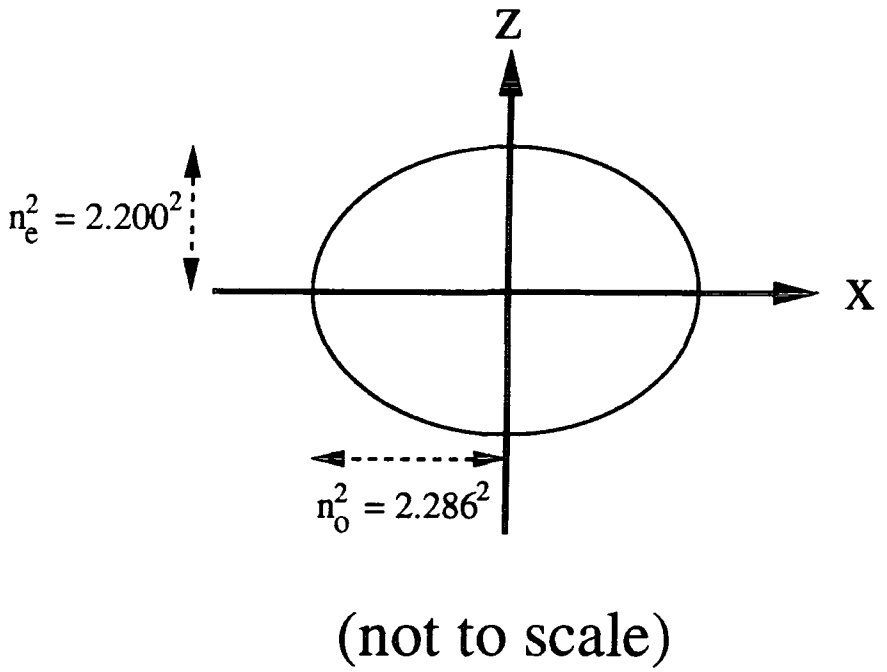

Figure 2.1 - Cross-section of the index ellipsoid of lithium niobate

2.2 Nonlinear Optics

As explained in the previous section, linear optics is defined by the linearity of the electric field polarisation relationship. In nonlinear optics this is replaced by a series expansion[3]:

$$\frac{\mathbf{P}}{\epsilon_0} = \chi^{(1)}\mathbf{E} + \chi^{(2)}\mathbf{EE} + \chi^{(3)}\mathbf{EEE}. \ldots . \tag{2.6}$$

$\chi^{(2)}$ is called second-order susceptibility and $\chi^{(3)}$ third order susceptibility etc. In practice these quantities are tensors, starting with a third rank tensor for second-order susceptibility and increasing in rank as the series progresses.

Nonlinear optics may be subdivided according to the significance of the higher order susceptibilities. For the materials in this thesis $\chi^{(2)}$ is most important, this situation is described as second-order nonlinear optics.

2.3 Second-Order Nonlinear Optics

Neglecting the linear contribution to polarisation, we may write:

$$\frac{P_k}{\epsilon_0} = \chi^{(2)}_{klm} E_l E_m \tag{2.7}$$

where $klm = 1, 2, 3$ and summation over repeated subscripts is assumed. Note that the electric field relationship is no longer simply a square law as the interaction may involve two separate field components. When one or more of these components is at an optical frequency second-order nonlinear effects start to manifest themselves.

2.3.1 The Pockels Effect

One situation giving rise to nonlinear effects is a combination of one optical field with one of lower frequency. A simple example is when the x-direction field is optical (written as $E_1(\omega)$) and a dc field is applied in the y-direction ($E_2(0)$). Ignoring any dc polarisations but including both first and second-order terms gives:

$$\frac{P_k}{\epsilon_0} = \chi^{(1)}_{k1} E_1(\omega) + \chi^{(2)}_{k12} E_1(\omega) E_2(0) + \chi^{(2)}_{k21} E_2(0) E_1(\omega) \tag{2.8}$$

Applying a basic symmetry relationship[4] for third rank tensors that $\chi^{(2)}_{k12} = \chi^{(2)}_{k21}$ leads to:

$$\frac{P_k}{\epsilon_0} = \{\chi^{(1)}_{k1} + 2\chi^{(2)}_{k12} E_2(0)\} E_1(\omega) \tag{2.9}$$

By analogy with the linear situation it is clear that the linear susceptibility has been modified by an additional dc field dependent term. This is equivalent to a relative permittivity change:

$$\Delta\epsilon_{k1} = 2\chi^{(2)}_{k12} E_2(0) \tag{2.10}$$

This electrically controlled change to permittivity is called the Pockels effect. The general expression for any orientation of field and medium is:

$$\Delta\epsilon_{kl} = 2\chi^{(2)}_{klm} E_m \tag{2.11}$$

The dc-field may be replaced by a higher frequency field (eg up to microwave).

Another method commonly used to quantify the change in refractive index from the Pockels effect is based on the index ellipsoid and the so called electrooptic (or r) coefficients[5]. It is useful to briefly consider this technique to allow comparision between r coefficients for a material and its $\chi^{(2)}_{klm}$

The r coefficients determine the change in the B coefficients of the index ellipsoid when a field is applied:

$$\Delta B_i = r_{ij} E_j \tag{2.12}$$

(note that the r coefficients form a 6x3 matrix are are therefore do not constitute a tensor)

Temporarily discarding the subscripts, $B = \frac{1}{\epsilon}$, therefore $\Delta B = \frac{1}{\epsilon^2}\Delta\epsilon$. Hence, comparing equations 2.11 and 2.12 and using the definitions of B_i given after equation 2.5 it can be shown that:

$$\chi^{(2)}_{kkm} = \frac{1}{2}\epsilon^2_{kk} r_{km} \tag{2.13a}$$

$$\chi^{(2)}_{23m} = \frac{1}{2}\epsilon^2_{23} r_{4m} \tag{2.13b}$$

$$\chi^{(2)}_{13m} = \frac{1}{2}\epsilon^2_{13} r_{5m} \tag{2.13c}$$

$$\chi^{(2)}_{12m} = \frac{1}{2}\epsilon^2_{12} r_{6m} \tag{2.13d}$$

2.3.2 Second Harmonic Generation

A second case involving the production of nonlinear effects is when both the interacting fields are at optical frequencies. The simplest example of this is the interaction with itself of one optical field along one of the principal axes, eg $E_1(\omega)$:

$$\frac{P_k}{\epsilon_0} = \chi^{(1)}_{k1} E_1(\omega) + \chi^{(2)}_{k11} E_1(\omega) E_1(\omega) \tag{2.14}$$

Explicitly introducing the time dependence as $E_1(\omega) = E^0_1 \cos\omega t$ and rewriting the cosine squared term as a second harmonic cosine produces:

$$\frac{P_k}{\epsilon_0} = \chi^{(1)}_{k1} E^0_1 \cos\omega t + \frac{1}{2}\chi^{(2)}_{k11}\{1 + E^0_1 E^0_1 \cos 2\omega\} t \tag{2.15}$$

The second harmonic polarisation term gives rise to the emission of light at this frequency. This process is called second harmonic generation (SHG).

In calculating the magnitude of second harmonic produced it is essential to consider the effect of the phase of the fundamental and harmonic beams. Although the

fundamental will produce SHG at every point along its path through the medium the phase may lead, in some cases, to destructive interference. The situation is similar to coupling between modes in an optical directional coupler; maximum transfer only occurs if both modes travel at the same velocity. Generally the second harmonic field magnitude after propagating through a sample of length l is given by[5]:

$$|E_{2\omega}|^2 = \frac{\omega^2 d^2}{n_{2\omega}^2 c^2}|E_\omega|^4 l^2 \mathrm{sinc}^2(\Delta k l/2) \tag{2.16}$$

where n_ω is the refractive index at the fundamental, and $\Delta k = 2k_\omega - k_{2\omega}$ (this is a measure of the velocity difference between the two frequencies). d is equal to half the relevant tensor element of $\chi^{(2)}$, this type of notation is often used by experimentalists.

This equation may be converted into terms of intensity (I) by use of the relationship:

$$I = \frac{1}{2} cn\epsilon_0 |E|^2 \tag{2.17}$$

which gives:

$$I_{2\omega} = \frac{8\pi^2 d^2 l^2 I_\omega^2}{\lambda_\omega^2 n_\omega^2 n_{2\omega} c\epsilon_0} I_\omega^2 \mathrm{sinc}^2(\Delta k l/2) \tag{2.18}$$

The production of practical devices for efficient generation of second-harmonic at low input powers requires that the sinc term be made equal or close to unity. This means that Δk must be zeroed by ensuring that both the fundamental and second-harmonic wave travel at the same velocity. In general this cannot be achieved due to dispersion but a number of special techniques can overcome this limitation. For example, in a birefringent crystal it can be arranged (for a suitable incident angle) that the fundamental has an ordinary index equal to the extraordinary index at the second harmonic (or vice versa). Phase matching may also be achieved in waveguides (see chapter 3).

It should be emphasised that $\chi^{(2)}$ $(= 2d)$ as measured by SHG will be different to that from the Pockels effect, this is due to the difference in input and output frequency. In cases where it is necessary to distinguish between the two values the following notation is used; $\chi^{(2)}(-\omega;\omega,0)$ for the Pockels effect; $\chi^{(2)}(-2\omega;\omega,\omega)$ for SHG. The frequency before the semicolon refers to the output and is shown as negative, the two input frequencies are given after the semicolon, separated by a comma.

2.3.3 Other Second-Order Nonlinear Effects

In equation 2.15 there is a dc term related through $\chi^{(2)}$ to the square of the input field. This process is known as optical rectification and is simply an intensity dependent dc polarisation.

If, instead of interacting a single input beam with itself to give SHG, two inputs of differing optical frequency are used sum and difference frequencies will be produced.

2.4 Materials for Second-Order Nonlinear Optics

The polarisation-field equation for a second-order nonlinear material is given by (with tensor nature omitted):

$$\frac{P(E)}{\epsilon_0} = \chi^{(1)}E + \chi^{(2)}EE \tag{2.19}$$

If the direction of the electric field is reversed this would give an equal and opposite polarisation in a centrosymmetric material. Therefore:

$$\frac{P(-E)}{\epsilon_0} = \frac{-P(E)}{\epsilon_0} = -\chi^{(1)}E + \chi^{(2)}EE = -\chi^{(1)} - \chi^{(2)}EE \tag{2.20}$$

Clearly the only solution to this is $\chi^{(2)} = 0$, which leads to the first requirement for second-order nonlinear materials; they must be non-centrosymmetric.

A second requirement is apparent from the need for the material to work at op-

tical frequencies, namely that its hyperpolarisability must be based on electronic processes.

A number of inorganic materials display significant second-order properties, notably lithium niobate and potassium dihydrogen phosphate (KDP). However, considerable effort has been put into the design of organic materials in the hope of realising larger values of $\chi^{(2)}$. A number of design criteria have been established to point the synthetic chemist in the correct direction.

2.4.1 Organic Materials

The polarisation of a molecule may be expressed as a Taylor series expansion of similar form as that for a macroscopic material[5]:

$$p = p_0 + \alpha E + \beta EE + \gamma EEE. \ . \ . \tag{2.21}$$

where p_0 is the ground state polarisation, α the polarisability and β the second-order hyperpolarisability etc (the tensor nature of the polarisabilities has been neglected). For an organic medium to exhibit large second-order nonlinear properties its molecules must have a large β.

To give large values of hyperpolarisability at optical frequencies it is clear that the electrons of the organic molecule must be relatively free to move. Intuitively this implies that such a molecule would also possess a high linear polarisability. Electron mobility in organics is achieved by conjugated π bond systems.

In the vast majority of cases, the overall properties of an organic material are determined solely by those of the individual molecules, that is to say that intermolecular processes are of little importance. This means that the individual molecules must satisfy the requirement of asymmetry. As the optical properties are determined by the π electrons the implication is that their distribution must be asymmetric, this is achieved by the use of donor and acceptor groups. In addition to the need for asymmetric molecules it is, of course, also essential that the overall structure be

non-centrosymmetric in terms of molecular alignment.

A number of equations have been derived to estimate the magnitude of β from other properties of the molecule. The system of π electrons between acceptor and donor groups can be regarded as an example of intramolecular charge transfer. By considering the perturbation produced during second harmonic generation (from a source of energy $\hbar\omega$) an equation for β in such systems has been obtained[5]:

$$\beta = \frac{3e^2\hbar^2 W f \Delta\mu}{2m[W^2 - (2\hbar\omega)^2][W^2 - (\hbar\omega)^2]} \tag{2.22}$$

where W is the energy gap, $\Delta\mu$ the difference between excited and ground state dipole moments, e and m the electron charge and mass respectively, and f the oscillator strength of the charge transfer.

From the denominator it is seen that the presence of a transition at either the fundamental or double frequency will maximise β. However this will also lead to strong absorption at one of these wavelengths, depleting either the input or output wave. In practice a trade-off clearly exists with the best solution being a transition slightly shifted from one of the wavelengths. If the molecule is to be used in the visible region the need for such a transition indicates that it will be coloured. It is worth noting that a transition at the second harmonic will not enhance $\chi^{(2)}$ for the Pockels effect.

For a large β it is also necessary to maximise $\Delta\mu$, unfortunately the practical and theoretical study of excited dipole moments is extremely difficult due to their short lifetimes. In practice it is often found that a large ground state dipole moment leads to good second-order properties.

The dipole moment of a molecule depends on the product of the charge separated and the length of separation. Hence it is obviously an advantage to have a long conjugated π electron system to maximise the dipole moments. This relationship has been quantified[6]:

$$\beta \propto L_\pi^3 \tag{2.23}$$

where L_π is the length of the conjugated system.

A similar equation exists for polarisability:

$$\alpha \propto L_\pi^3 \tag{2.24}$$

so there is a correlation between having a high linear polarisability and good non-linear properties.

To summarise, the molecule should have a long conjugated π electron system, donor and acceptor groups to give intramolecular charge transfer and a transition close to either the fundamental or second harmonic frequency. These properties will often be found in highly coloured and highly polarisable molecules.

2.5 Summary

Most optical materials show a linear relationship between the electric field of the light and induced polarisation, and can be described by a single tensor of relative permittivity. However some media exhibit nonlinearity in this relationship, this leads to a number of useful effects, for example second harmonic generation and the Pockels effect. Design rules exist to allow chemists to design organic molecules for nonlinear optics.

References

1. G.R. Fowles *Introduction to Modern Optics* (Holt, Rinehart and Winston 1975).
2. T.S. Narasimhamurty, *Photoelastic and Electro-optic Properties of Crystals* (Plenum 1981) p48.
3. R.G. Byer in *Nonlinear Optics* ed P.G. Harper, B.S. Wherrett (Academic press 1977) p51.

4. J. Zyss, D.S. Chemla in *Nonlinear Optical Properties of Organic Molecules and Crystals* ed D.S. Chemla, J. Zyss (Academic Press 1987) pp 23-191.

5. A. Yariv, *Quantum Electronics* (Wiley 1989) pp298-310.

6. J.F. Nicoud, R.J. Twieg, in *Nonlinear Optical Properties of Organic Molecules and Crystals* ed D.S. Chemla, J. Zyss (Academic Press 1987) pp 233.

Chapter 3

Theory of Electromagnetic Surface Modes and Guided Wave Optics

3.1 The Importance of Confinement in Nonlinear Optics

For convenient study and practical application of nonlinear optical effects it is advantageous to confine the light intensity within small dimensions (typically of the order of microns) instead of allowing it to propagate freely within the bulk of a material (bulk optics).

This confinement may be achieved by guiding the light in a thin layer (as a guided mode) or binding it at an interface (as an electromagnetic surface mode). There are several advantages compared to bulk optics, the most important of these will now be listed:

(i) Enhancement of the scale of the nonlinear effect

For most of the nonlinear processes described in Chapter 2 the detected output depends upon the input intensity raised to a power greater than unity. It is therefore clear that for a given optical input power a greater effect will be observed if this power is confined to a small area. For example in a second harmonic generation experiment reducing the area by a factor of two will double the fundamental intensity, which will quadruple the second harmonic intensity. After allowing for the reduction in area it is obvious that the output power has been doubled. The length of interaction between the light and the nonlinear medium is also important, the low loss associated with optical waveguiding allows devices to be several centimetres long.

(ii) Reduction in the amount of nonlinear material required

This is particularly important for materials which are only available in film form eg. Langmuir-Blodgett films. Clearly for any high cost material it will be an advantage to reduce the amount required.

(iii) Reduction in size and weight of devices

The use of unconfined light implies a need for lenses, mirrors and other bulk optical components. In a world accustomed to microelectronic scale devices the guided wave optical equivalents are likely to prove more commercially acceptable. In addition, confined light devices are relatively cheap to make using techniques adapted from integrated circuit production[1].

(iv) Ease of integration with fibre optics

Optical fibres work by a system of waveguiding, the light is guided in a small core (typically 4 to 100 microns) surrounded by a flexible cladding. As nonlinear waveguides could easily be made to similar dimensions to the core, the passage of light between the two may be simply achieved. The joining process could be as straight forward as gluing the fibre to the end of the waveguide[2].

(v) Convenience of application of electric fields

Some nonlinear optical processes require the application of an electric field which then alters the properties of the nonlinear medium. The most widely used example is the Pockels effect, which is employed in phase and intensity modulators and other integrated optical devices. To provide a large field for small applied voltage the electrode gap must be small. This *may* be achieved in bulk optics by using transparent electrodes perpendicular to the direction of light propagation[3] but a waveguide approach offers greater interaction lengths (in bulk optics the length is limited to the electrode gap).

(vi) Suitability for phase matching

As explained in chapter 2, for efficient second harmonic generation it is essential that both the fundamental and harmonic waves propagate at the same velocity. In the case of a waveguide this may be achieved by ensuring that the effective index of a mode at the fundamental wavelength is equal to that for another mode at the harmonic (see section 3.6 for an explanation of waveguide modes).

3.2 Electromagnetic Surface Modes - Confinement at an interface

An electromagnetic surface mode is a bound state existing at the interface between two media. For nonlinear optics it is those modes excitable by light which are of interest: these have been enumerated in different ways by Burstein[4] and Welford[5]. To understand the properties of these modes it is instructive to consider the behaviour of light at the boundary of two semi-infinite media, this is referred to as the single interface situation.

3.2.1 The Single Interface System

The axes are as defined in figure 3.1, the two media are separated by the $z = 0$ plane and the wavevectors $\mathbf{k}_i$ of the incident, transmitted and reflected light lie in the xz plane. For a bound field at the interface it is essential to have a surface charge, from classical electromagnetic theory it is clear that an electric field perpendicular to the interface is needed. This cannot be provided by s-polarised light, so only p-polarisation will be considered. Hence the electric field vectors lie in the xz plane. Medium 1 is taken as having a permittivity ϵ_1 and medium 2, ϵ_2. The first physical constraint on the problem is Snell's law, writing this in permittivity form we have:

$$\sqrt{\epsilon_1}\sin\theta_1 = \sqrt{\epsilon_2}\sin\theta_2 \tag{3.1}$$

Multiplying by the wavevector in free space k_o and recalling that $k_i = k_o\epsilon_i$, Snell's law can be viewed as conservation of the wavevector x-component $k_{1,x} = k_{2,x} = k_x$ between the two layers.

The electric ($\mathbf{E}$) and magnetic ($\mathbf{H}$) fields of the light are described by Maxwell's equations:

$$\nabla \times \mathbf{H} = \epsilon_o\epsilon_i\frac{\partial \mathbf{E}}{\partial t} \tag{3.2a}$$

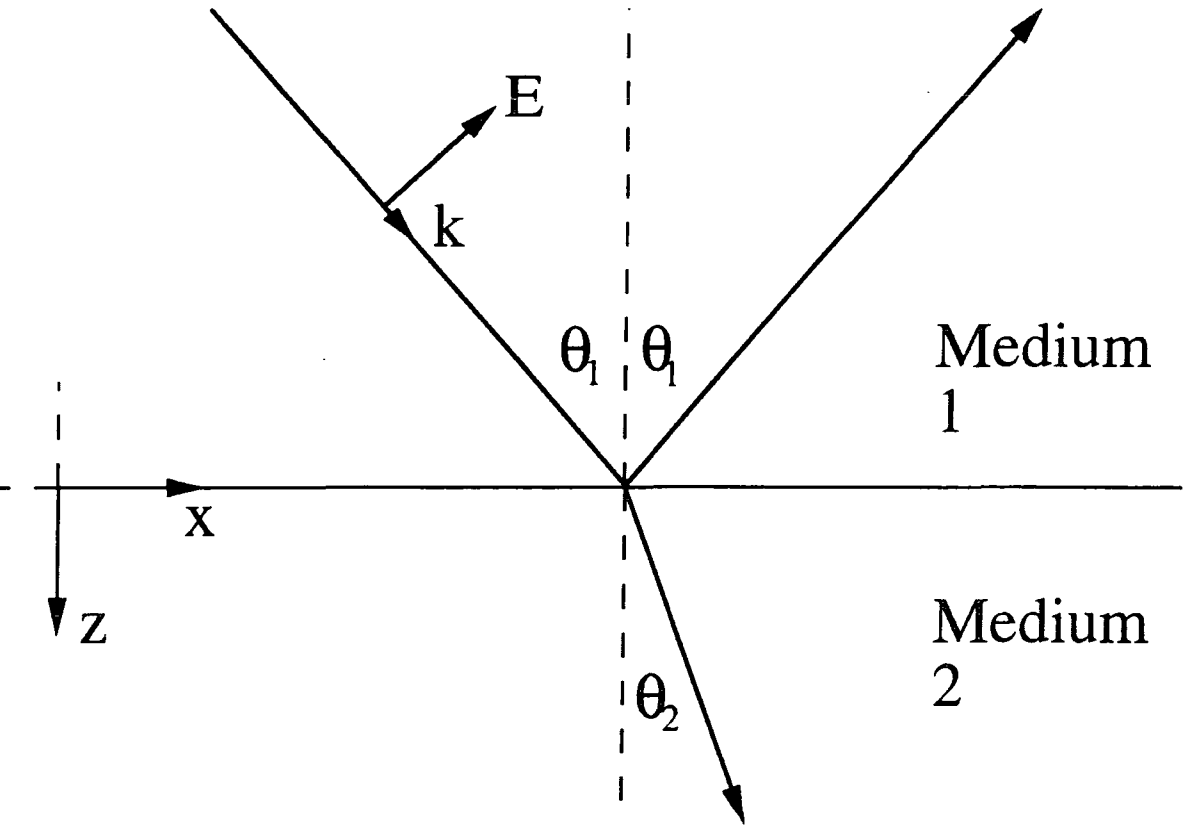

Figure 3.1 - Definition of axes

$$\nabla \times \mathbf{E} = -\mu_o \frac{\partial \mathbf{H}}{\partial t} \tag{3.2b}$$

(non magnetic media and absence of free charge have been assumed)

For the chosen geometry

$$\frac{\partial \mathbf{E}}{\partial \mathbf{y}} = 0 \quad , \quad \frac{\partial \mathbf{H}}{\partial \mathbf{y}} = 0 \quad , \quad E_y = 0 \qquad \text{and} \qquad H_x = H_z = 0$$

and for propagating waves in the x-direction solutions must be of the form $e^{j(k_x x - \omega t)}$. This allows simplification to

$$k_x H_y = \omega \epsilon_o \epsilon_i E_z \tag{3.3a}$$

$$\frac{\partial H_y}{\partial z} = j\omega \epsilon_o \epsilon_i E_x \tag{3.3b}$$

$$jk_z E_z + \frac{\partial E_x}{\partial z} = j\omega\mu_o H_y \tag{3.3c}$$

and elimination of H_y, E_z gives a single wave equation in E_x.

$$\frac{\partial^2 E_x}{\partial x^2} + (\omega\epsilon_o\epsilon_i\mu_o - k_x^2)E_x = 0 \tag{3.4}$$

Hence the wavevector z-component is given by

$$k_{i,z} = \sqrt{k_o^2\epsilon_i - k_x^2} \tag{3.5}$$

The fields in the two media may then be generally represented by:

Medium 1 :

$$E_x = A_1 e^{jk_{1,z}z} + B_1 e^{-jk_{1,z}z} \tag{3.6a}$$

Medium 2 :

$$E_x = A_2 e^{jk_{2,z}z} + B_2 e^{-jk_{2,z}z} \tag{3.6b}$$

(A_i and B_i are arbitrary coefficients and the x and time dependence have been omitted)

The final pair of conditions on the problem are those connected with field continuity at the interface. Both E_x and H_y must be continuous, for convenience the H_y condition may be rewritten as continuity of $\epsilon_i \int E_x dz \quad (= \frac{\epsilon_i}{k_{i,z}}(A_i e^{jk_{i,z}z} - B_i e^{-jk_{i,z}z}))$.

Welford[5] defines surface mode solutions as those cases when only one electromagnetic wave exists in each medium. For practical confinement these surface modes must be bound at the interface, mathematically this requires the wave solution to decay exponentially away from the boundary in both media. However such a strict mathematical requirement can only occur for lossless media as no means of

exciting the mode is provided. Therefore the definition of a bound surface mode can be broadened to include all those where the wave solutions contain a measure of exponential decay character.

Following Welford[5] in setting one of the waves in each medium to zero let $A_1 = B_2 = 0$ (the choice of these two coefficients to zero is arbitrary but, as no decision has been made on the sign of $k_{i,z}$, there is no loss of generality).

Applying the two boundary conditions gives:

$$B_1 = A_2 \tag{3.7a}$$

$$\frac{\epsilon_1}{k_{1,z}} = \frac{\epsilon_2}{k_{2,z}} \tag{3.7b}$$

When substituted into equation (3.5) this gives the following:

$$k_x^2 = k_o^2 \sqrt{\frac{\epsilon_1 \epsilon_2}{\epsilon_1 + \epsilon_2}} \tag{3.8a}$$

$$k_{1,z}^2 = k_x^2 \frac{\epsilon_1}{\epsilon_2} \tag{3.8b}$$

$$k_{2,z}^2 = k_x^2 \frac{\epsilon_2}{\epsilon_1} \tag{3.8c}$$

As the wave is propagating in the x-direction k_x is real and it follows that if both media have positive real permittivities the z-components of the wavevectors are real. Hence no bound surface wave is excited.

If one or more of the media are lossy but both have positive real parts of permittivity then values of $k_{i,z}$ may be found corresponding to bound modes. These modes are referred to as Zenneck modes[6].

The case of two lossless media with permittivity real parts of opposite signs gives entirely imaginary $k_{i,z}$. The bound modes of this ideal system are called Fano modes[7].

The combination of a lossless medium with a positive permittivity (ϵ_1) with another of negative real part and positive imaginary part ($\epsilon_2 = -|\epsilon_2^{'}| + \epsilon_2^{''}$) also gives rise to bound surface modes, these are known as lossy Fano modes (note that $|\epsilon_2^{'}| > 2\epsilon_1$ to achieve the required wavevectors). Although this is again an ideal situation (as all materials exhibit loss) it is close to the practical system of dielectric and metal. These modes are also termed *surface plasmon polaritons* (SPP's); *plasmon* because the optical properties of the metal are consistent with its electrons behaving as a free electron plasma; *polariton* to indicate the coupling of photons with polar excitations in the metal.

3.2.2 Optical Excitation of Surface Plasmon Polaritons

Optical excitation of SPP's requires matching of both energy (ie. optical frequency or wavelength) and momentum (wavevector). The x-component of the SPP wavevector at a given wavelength (ie free space wavevector k_o) is:

$$k_x^2 = k_o^2 \sqrt{\frac{\epsilon_1 \epsilon_2}{\epsilon_1 + \epsilon_2}} \tag{3.9}$$

whilst light in medium i can provide x-components between zero and $k_o \epsilon_i$ depending on angle of propagation.

For a metallic medium 2 it is easily proved that $k_x^2 > k_o^2 \epsilon_1$ so the momentum is too great for excitation from medium 1. It is also immediately clear that excitation from medium 2 cannot even provide the correct sign of k_x^2.

The conclusion is that the modes of the single interface system cannot be directly excited optically, this is unsuprising as our criterion for a bound surface mode was its lack of optical radiation or excitation. There is an obvious analogy with optical waveguides where the light is confined in a film or channel to prevent radiation loss.

The method of excitation for SPP's is analogous to the prism coupling technique for optical waveguides and is termed the *attenuated total reflection* or ATR method.

The requirement for a x-component of wavevector in medium 1 greater than that available from propagating waves dictates that evanescence in the z-direction is needed. Such waves are found within a few wavelengths of a boundary exhibiting total internal reflection. If a metal-dielectric interface is brought close to this surface SPP's will be excited. This is known as the Otto arrangement[8] if the dielectric is nearer the total internally reflecting boundary (figure 3.2); if the situation is reversed it is named after Kretschmann[9] (figure 3.3). In each case the total internal reflection is attenuated at the SPP matching condition, this is referred to as *surface plasmon resonance* or SPR. The use of prisms is solely to allow the reflectivity of the system to be monitored, if they were replaced by glass slides the SPP would still be excited but the reflected wave would be trapped within the slide by total internal reflection.

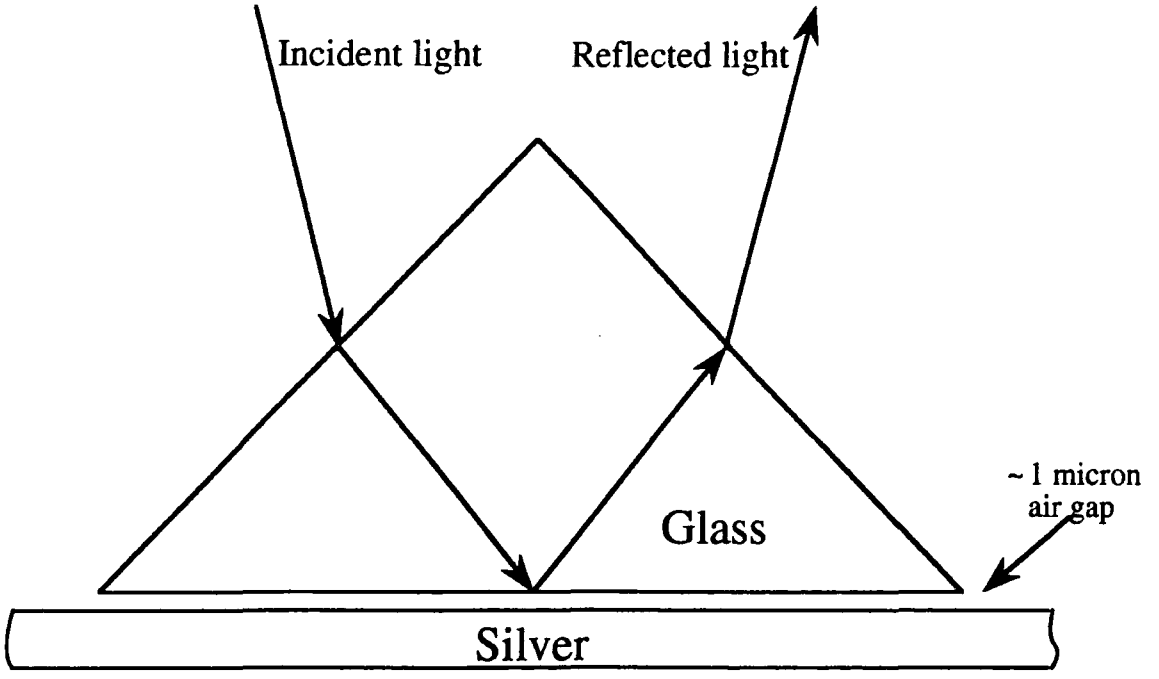

Figure 3.2 - Otto SPR arrangement

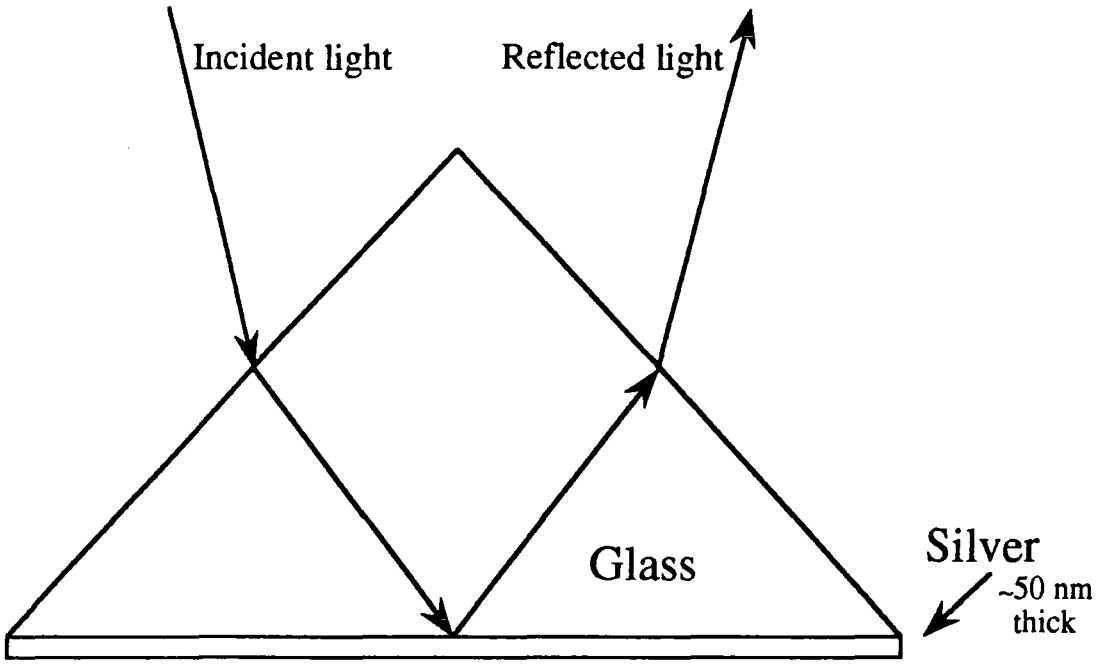

Figure 3.3 - Kretschmann SPR arrangement

Practically, the Kretschmann system is superior as it may be readily constructed by vacuum evaporation of a metal onto glass. Whilst it is possible to produce analytic expressions describing the fields and reflectivity of the arrangement it is more useful to use numerical methods on a computer. This allows easy extension of the model to more complex structures. The model written for this thesis is described in section 3.4. However optical waveguides will be discussed first as they may be described by similar techniques.

3.3 Optical Waveguides

A second method of light confinement is to use an optical waveguide here the light is bound (guided) within a thin film or channel of material[10]. As in the case of waves bound at an interface the requirements for guiding may be described in terms of the wavevector components within a number of media.

The simplest example is that of a slab waveguide in which a 2- dimensional guiding medium is bounded by two semi-infinite media on either side (figure 3.4). The

solutions to Maxwell's equations are again of the form given in equation (3.6) and the condition for guiding is that the solutions in the semi-infinite media are both exponentially decaying. The requirements of Snell's law and the boundary conditions must, of course, again be satisfied.

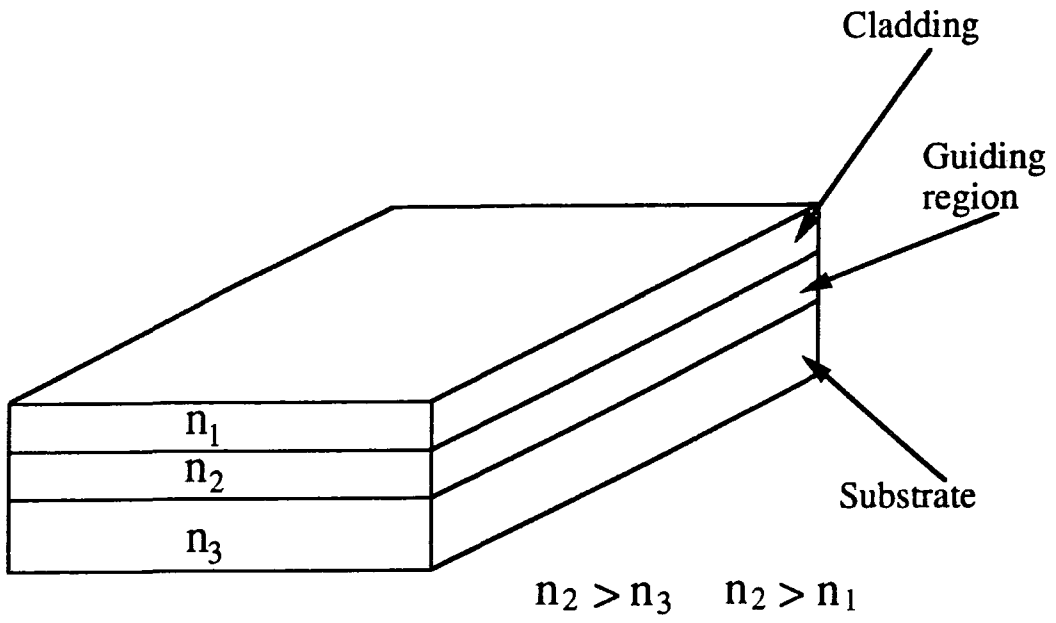

Figure 3.4 - Slab waveguide

The media parameters for guiding are found to be that the guiding medium must have the greatest refractive index and that its thickness must be greater than a certain minimum value. The reason for these requirements become clear if the structure is considered using a ray model rather than a Maxwell equation electromagnetic field model. To fully confine a ray within a medium it must be unable to escape at any interface ie. it must be totally reflected. The conditions for total internal reflection are that the confining (incident) medium must be of the greater refractive index and that the angle of incidence angle (θ) must satisfy

$$\theta > \sin^{-1}(n_1/n_2)$$

where n_1 is the refractive index of the incident medium and n_2 the index of the second medium.

However, the total internal reflection condition does not fully specify the requirements for waveguiding. It is also essential the ray should undergo a $2m\pi$ (m=integer) phase change in its two reflections and associated transits across the guiding medium. This is to maintain coherence of the wavefront. As the reflections introduce a phase change the guiding region must be sufficiently thick to build this up to 2π; this is the reason for the minimum thickness. The phase condition also dictates that only certain angles of ray can lead to waveguiding. These angles define the modes, a Maxwell's equation technique for finding them is given in section 3.6. For a more detailed explanation of waveguide theory see Marcuse[10]

The simple slab waveguide may be developed into a multiple slab guide, in which propagating wave solutions exist in all layers except the outside, or the graded index waveguide (which has a constantly varying refractive index). Channel guides which confine the light in two dimensions are also possible. For a discussion of these waveguides the reader is again referred to Marcuse[10].

Numerical methods of modelling single and multiple slab waveguides are discussed in the next sections.

3.4 Theory of waves in plane parallel structures

The configurations used for excitation of surface plasmon polaritons and the guiding of light in slab waveguides are both examples of a series of plane parallel media. Although (in the simplest case) each of these problems consists of only three layers of optical material the experimental work of this thesis requires the ability to model structures of greater complexity. Therefore a number of programs were developed with the power to consider any number of plane parallel layers.

The theory used develops naturally from that described for two media in section 3.2. The main points will be briefly restated before extension to more layers. The symbols and axis definitions are identical to section 3.2

(i) Snell's Law

This basic relation describing refraction is found to be equivalent to conservation of z-component of wavevector.

$$k_x = k_{1,x} = k_{2,x} = k_{3,x} \quad \ldots\ldots \tag{3.10}$$

(ii) Solutions to Maxwell's Equations

Medium i :

$$E_x = A_i e^{jk_{i,z}z} + B_i e^{-jk_{i,z}z} \tag{3.11}$$

where $k_{i,z} = \sqrt{k_o^2 \epsilon_i - k_x^2}$.

The A_i and B_i are arbitrary constants to be found using boundary conditions.

(iii) Boundary Conditions

E_x and $\epsilon_i \int E_x dz$ must be continuous at all boundaries.

This is a full description of the problem for any number of layers, all that is required is to manipulate the equations into a form suitable for computer numerical techniques.

3.4.1 Reduction of problem to simultaneous equation form

Figure 3.5 shows the definitions of layer thicknesses for the structure. The boundary of media 1 and 2 occurs at $z = z_1(= 0)$, media 2 and 3 at $z = z_2$ and media i and $i + 1$ at $z = z_i$.

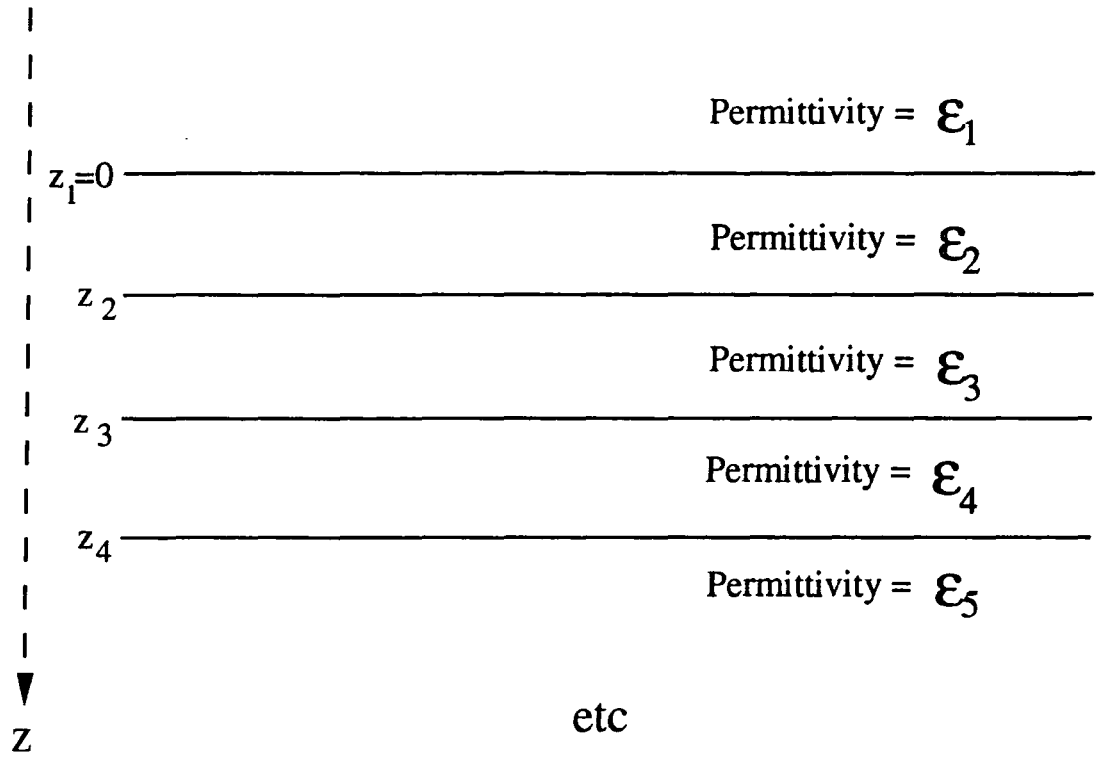

Figure 3.5 - Definitions of symbols in multilayer stack

Applying the boundary conditions gives a pair of equations for each interface.

At $z = z_1 = 0$:

$$A_1 + B_1 - A_2 - B_2 = 0 \tag{3.12a}$$

$$\frac{\epsilon_1}{k_{1,z}}(A_1 - B_1) - \frac{\epsilon_2}{k_{2,z}}(A_2 - B_2) = 0 \tag{3.12b}$$

At $z = z_2$:

$$A_2 e^{jk_{2,z}z_2} + B_2 e^{-jk_{2,z}z_2} - A_3 e^{jk_{3,z}z_2} - B_3 e^{-jk_{3,z}z_2} = 0 \tag{3.12c}$$

$$\frac{\epsilon_2}{k_{2,z}}(A_2 e^{jk_{2,z}z_2} - B_2 e^{-jk_{2,z}z_2}) - \frac{\epsilon_3}{k_{3,z}}(A_3 e^{jk_{3,z}z_2} - B_3 e^{-jk_{3,z}z_2}) = 0 \tag{3.12d}$$

At $z = z_i$:

$$A_i e^{jk_{i,z}z_i} + B_i e^{-jk_{i,z}z_i} - A_{i+1} e^{jk_{i+1,z}z_i} - B_{i+1} e^{-jk_{i+1,z}z_i} = 0 \tag{3.12e}$$

$$\frac{\epsilon_i}{k_{i,z}}(A_i e^{jk_{i,z}z_i} - B_i e^{-jk_{i,z}z_i}) - \frac{\epsilon_{i+1}}{k_{i+1,z}}(A_{i+1} e^{jk_{i+1,z}z_i} - B_{i+1} e^{-jk_{i+1,z}z_i}) = 0 \tag{3.12f}$$

For a problem of n-layers this gives $2 \times (n-1)$ equations. However there are $2n$ unknowns (the A_i and B_i for each layer) - clearly two further equations are needed. At this point the methods used for surface plasmon polaritons and slab waveguides diverge.

3.5 Application of the theory to the Kretschmann SPR arrangement

In the Kretschmann arrangment the problem is one of multilayer reflection: the light is incident from medium 1 and we wish to know the reflectivity of the whole system, as this is a monitor of surface plasmon polariton excitation. If we choose $k_{1,z}$ to be positive it is clear that the term $A_1 e^{jk_{1,z}z}$ represents a wave travelling in the positive z direction (the incident wave) and $B_1 e^{-jk_{1,z}z}$ is the reflected wave. As reflectivity is defined as the intensity ratio of the forward and reverse waves $(=|\frac{B_1^2}{A_1^2}|)$ it is possible to normalise by A_1. This reduces by one the number of unknowns.

In the last (semi-infinite) layer the $B_i e^{-jk_{i,z}z}$ term represents either an incident wave from $x = \infty$ (for real positive $k_{i,z}$) or, if the solution is evanescent, it is an exponentially growing term. The former case is inconsistent with the Kretschmann configuration whilst the latter is non-physical. Hence $B_i = 0$.

There are now $2(n-1)$ each of equations and unknowns so the problem may be arranged as a set of simultaneous equations and solved by Gaussian elimination[11]. Fortran 77 and GHOST 80 graphics routines were used to write software capable of generating and solving this set of equations (all programs are given in Appendix 3).

Figure 3.6 shows reflectivity against angle for a Kretschmann structure of glass, silver (500 Å) and air. The angle (θ) represents the x-component of the incident light wavevector as $k_x = k_o\sqrt{\epsilon_1}\sin\theta$. Only B_1 need be calculated to produce this graph but the other coefficients allow the field and Poynting vector profiles of the whole system to be plotted. For example, figure 3.7 illustrates the maximum in E present at the interface supporting the surface plasmon polariton.

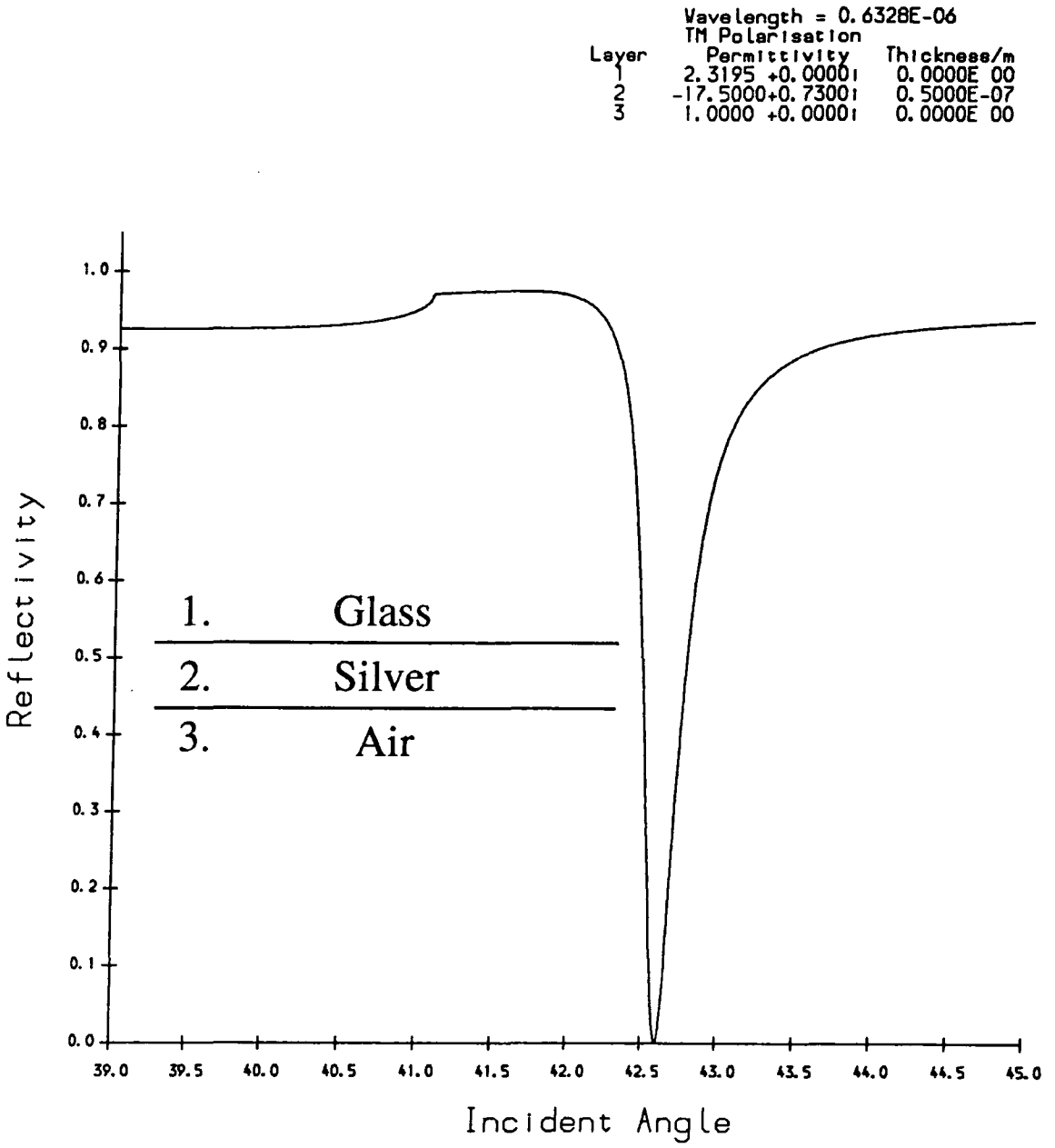

Figure 3.6 - Reflectivity vs angle graph for Kretschmann SPR

The software written is also capable of considering more complex structures; for example, the addition of a further layer on the air side of the silver (figure 3.8) . The presence of a large electric field at this interface means that the reflectivity properties are changed significantly even by a thin layer. The change in ϵ in the vicinity of the SPP causes a large change in its wavevector. In this case the addition

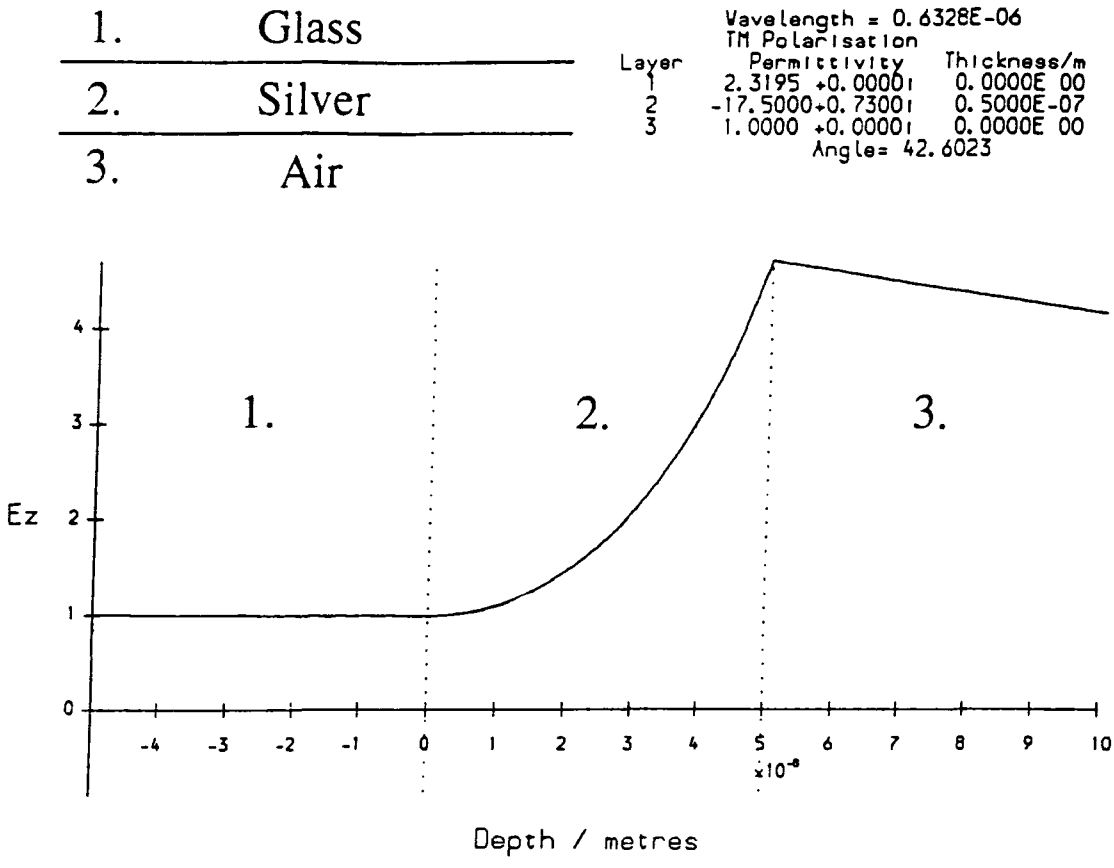

Figure 3.7 - Field maximum in Kretschmann SPR

of a 3 nm layer has shifted the resonant angle by approximately 0.25 degrees.

3.6 Application of the theory to Optical Waveguides

For an n-layer waveguiding structure there are again $2n$ coefficients describing the field and $2(n-1)$ boundary conditions. The condition for waveguiding is that the solutions in the two outside layers must be exponentially decaying. For positive imaginary $k_{i,z}$ in these layers this may be stated mathematically as:

$$B_1 = A_n = 0$$

because these terms would indicate exponentially growing solutions.

Therefore the problem is reduced to $2(n-1)$ equations and $2(n-1)$ unknowns, a solvable set of simultaneous equations. This set of equations has no constant

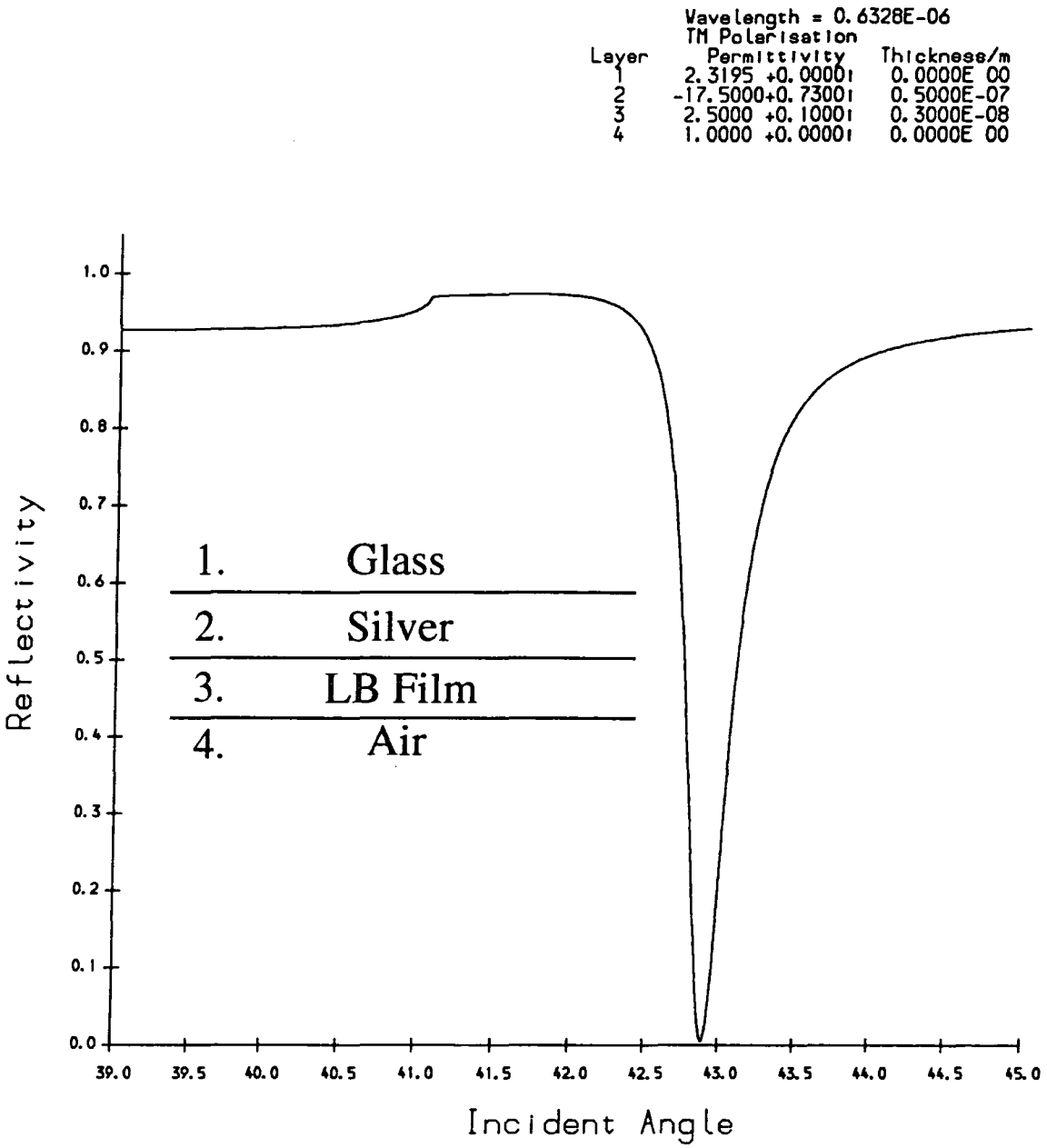

Figure 3.8 - Reflectivity vs angle for Kretschmann SPR with LB film

terms (ie. no terms other than those involving the unknowns), and the situation is known as *homogeneous*[12]. The equations may be repesented in matrix form as:

$$\mathbf{A}.\mathbf{X} = \mathbf{0}$$

where **A** is a boundary condition matrix and **X** is a column vector of A_i and B_i

coefficients. Solutions only exist for this equation when the determinant of matrix A is zero. This occurs for a finite number of values of k_x, ie. this an eigenvalue problem and the valid wavevector components define the only possible eigenmodes of the system.

A program was written to identify the modes of a waveguide system, again Fortran 77 and GHOST 80 graphics were used. An iterative method was used to locate the determinant zeros. Figure 3.9 shows the TE modes of a substrate-film-air waveguide, the wavevectors have been converted to effective index (n_{eff}), defined as $\frac{k_x}{k_o}$.

If any of the layers are lossy there are no determinant zeros. This is because the assumption of exponentially decaying solutions in the outside layers is invalid, if loss is present an input wave is needed to maintain the field profile. Strictly speaking it is incorrect to refer to modes in a lossy system as waves are unable to propagate in an unchanging manner in the x-direction. However there are still only a finite number of valid wavevectors and these may be found by finding *minima* of the determinant.

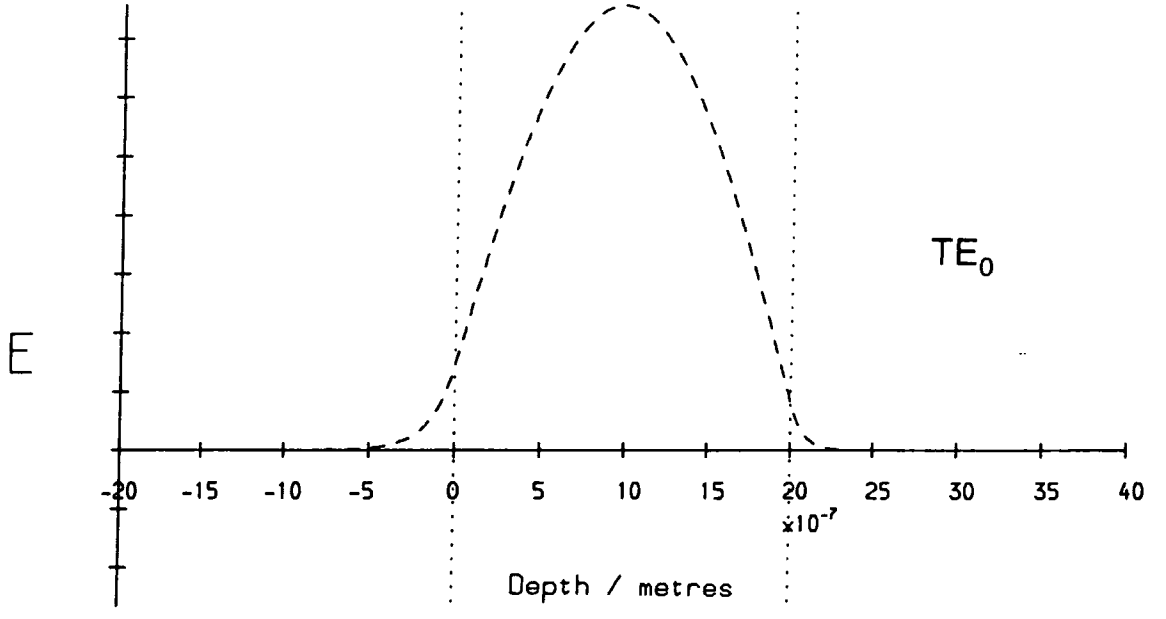

Figure 3.9 - Modes in a substrate-film-air slab waveguide

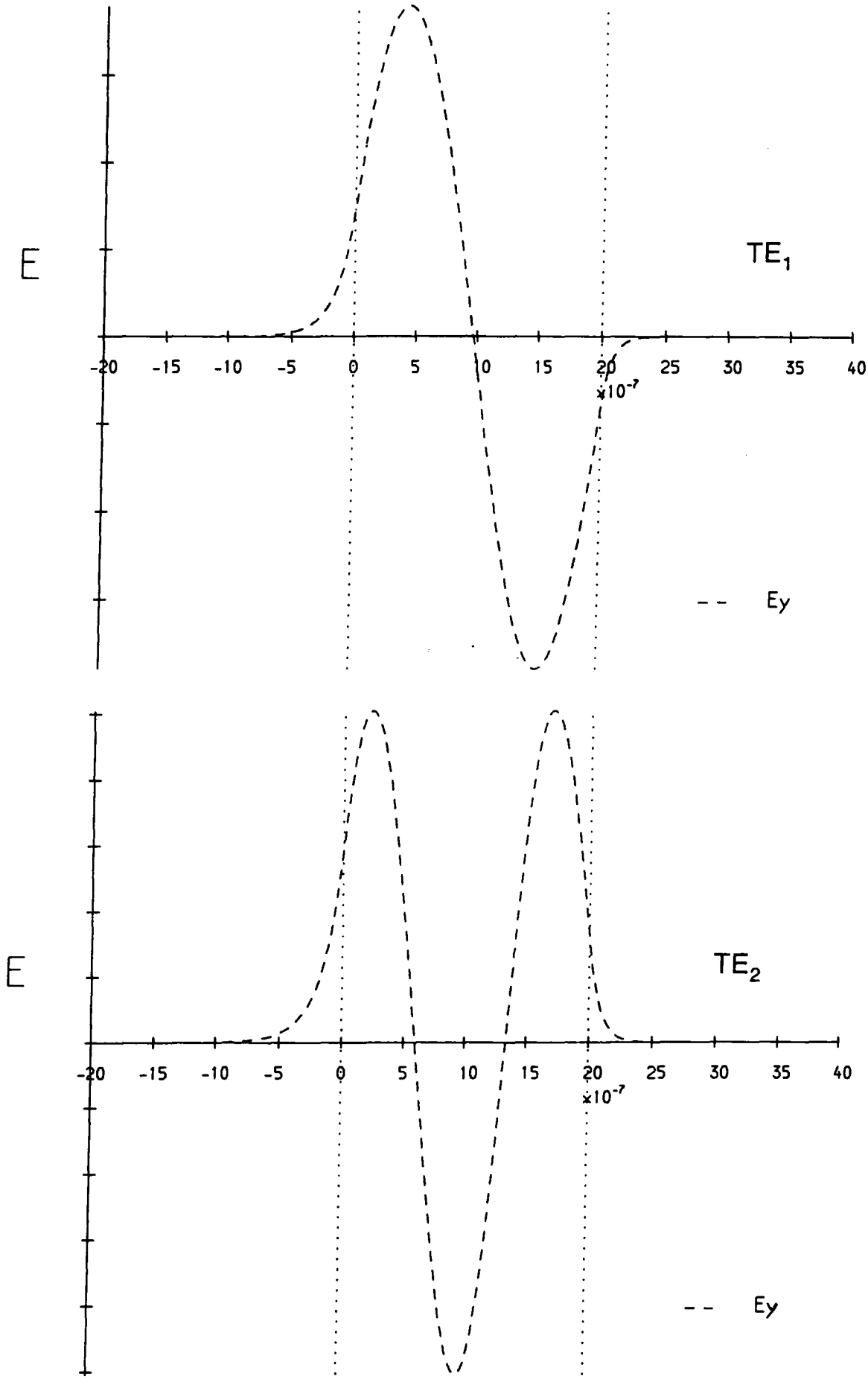

Figure 3.9 - Modes in a substrate-film-air slab waveguide

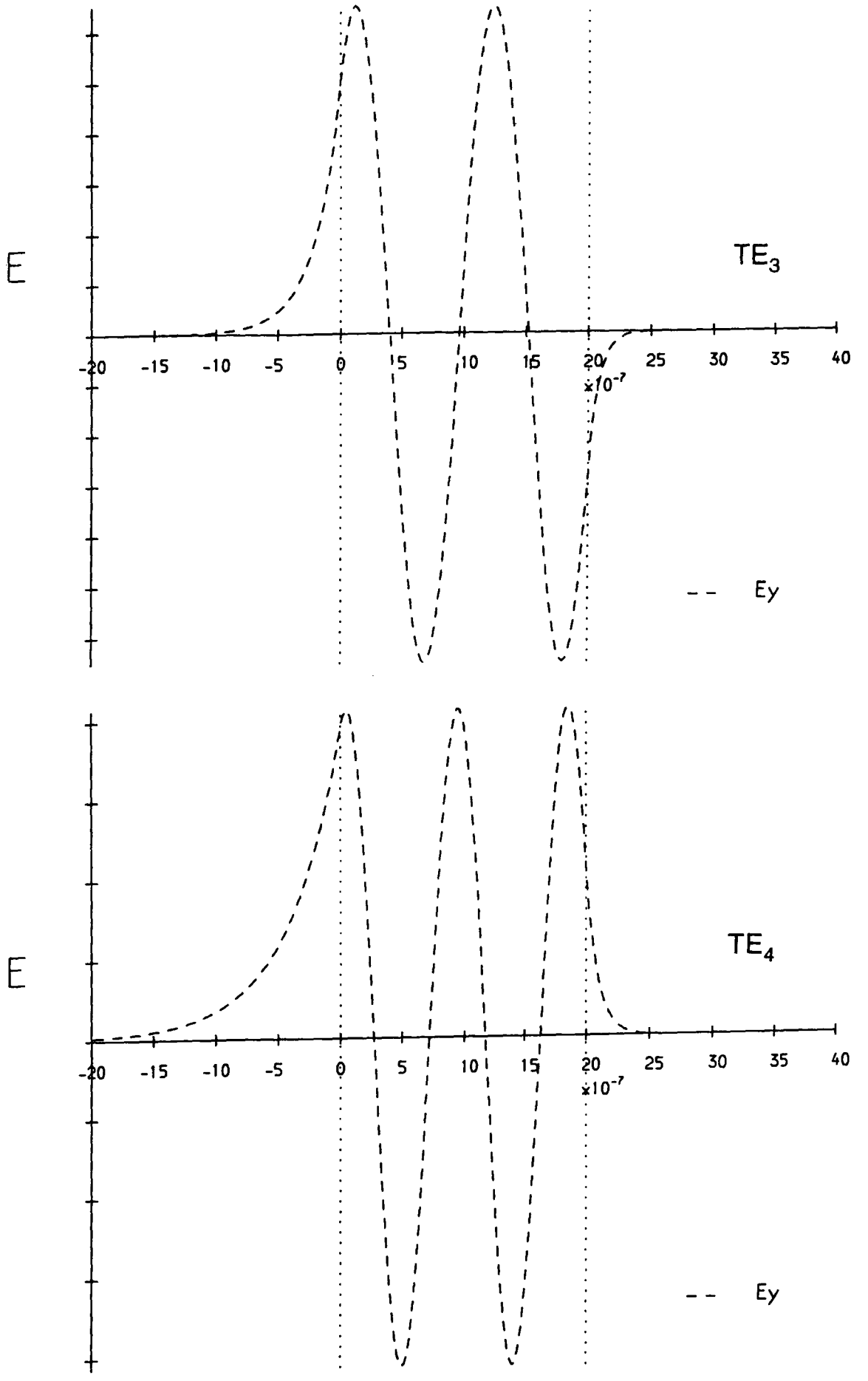

Figure 3.9 - Modes in a substrate-film-air slab waveguide

3.7 Summary

The effect of nonlinear susceptibility on the propagation of light is increased if this light is confined in a small region. This may be achieved by exciting an electromagnetic surface mode (eg. a surface plasmon polariton) or a waveguide mode. Practically the simplest examples of this are the Kretschmann SPR arrangement and slab waveguides. These structures may both be modelled by solving Maxwell's equations for a multilayer dielectric structure.

References

1. *J. Lightwave Tech.* **6 (6)** issue 6 (1988).
2. P.S. Chung, *J. Lightwave Tech.* **5 (12)** pp1721-6 (1987).
3. J.P. Huignard, *J. Optics* **18 (4)** pp181-6 (1987).
4. E. Burstein in *Polaritons*, Ed. E. Burstein and F de Martini, (Pergamon 1974) p1-3.
5. K.R. Welford in *Surface Plasmon Polaritons*, (Institute of Physics 1988) p25-78.
6. J. Zenneck, *Ann. Physik* **23** p846 (1907).
7. U. Fano, *J. Opt Soc. Am.* **31** p213 (1941).
8. A. Otto, *Phys. Stat. Solidi.* **26** p99 (1970).
9. E. Kretschmann, *Z. Physik* **241** pp313-24 (1971).
10. D. Marcuse, *Introduction to Optical Waveguides* (Academic Press 1974)
11. F. Scheid, *Numerical Analysis* 1st ed. (Mc-Graw Hill 1968).
12. D.M. Young, R.T. Gregory, *A survey of numerical analysis* vol 1 (Addison Wesley 1972).

Chapter 4
Langmuir-Blodgett Films

This chapter introduces Langmuir-Blodgett (LB) films and describes their process of fabrication. The general theory of linear and second-order nonlinear optics from chapter 2 is then applied to the particular case of these films. Finally the previous work on waveguiding and second-order nonlinear optics in LB films is reviewed.

4.1 Langmuir-Blodgett Deposition

Langmuir-Blodgett (LB) deposition is the process of transferring monomolecular solid layers, floating on a liquid subphase, to a solid substrate. It takes its name from the two original co-workers in the field, Irving Langmuir[1], who was the first to transfer such a layer to a substrate, and Katherine Blodgett[2,3], who subsequently refined the technique.

The LB process is described in a number of reviews and books, notably those by Gaines[4] and Roberts[5], these both contain much historical background and provide a broad view of the field. This section concentrates on describing the technique as actually applied to producing the films characterised for this thesis.

4.1.1 The Langmuir Troughs

All the troughs used were of the constant perimeter type[6] and manufactured in the department's own workshop. All used PTFE tape barriers controlled for deposition by feedback electronics and a Wilhelmy plate pressure sensor. The simplest trough consisted of a single barrier system providing one area for a film. The dipping head was operated by a dc motor driving a micrometer.

As will be explained in section 4.1.3, LB films of a single material are generally centrosymmetric. To produce films without a centre of symmetry (eg. for nonlinear optics) two materials are used, deposited with the layers alternating. Two distinct types of alternate-layer troughs were used to produce these multilayer structures.

The first of these[7] utilised a rotating roller as a substrate mount, separating two independent subphase areas controlled by a single PTFE constant perimeter barrier (figure 4.1). The roller was driven by a dc motor through a reduction gearbox and was able to lower the substrate through one subphase region and raise it through the other (figure 4.2). By spreading different monolayers on each side, alternate-layer structures could be produced.

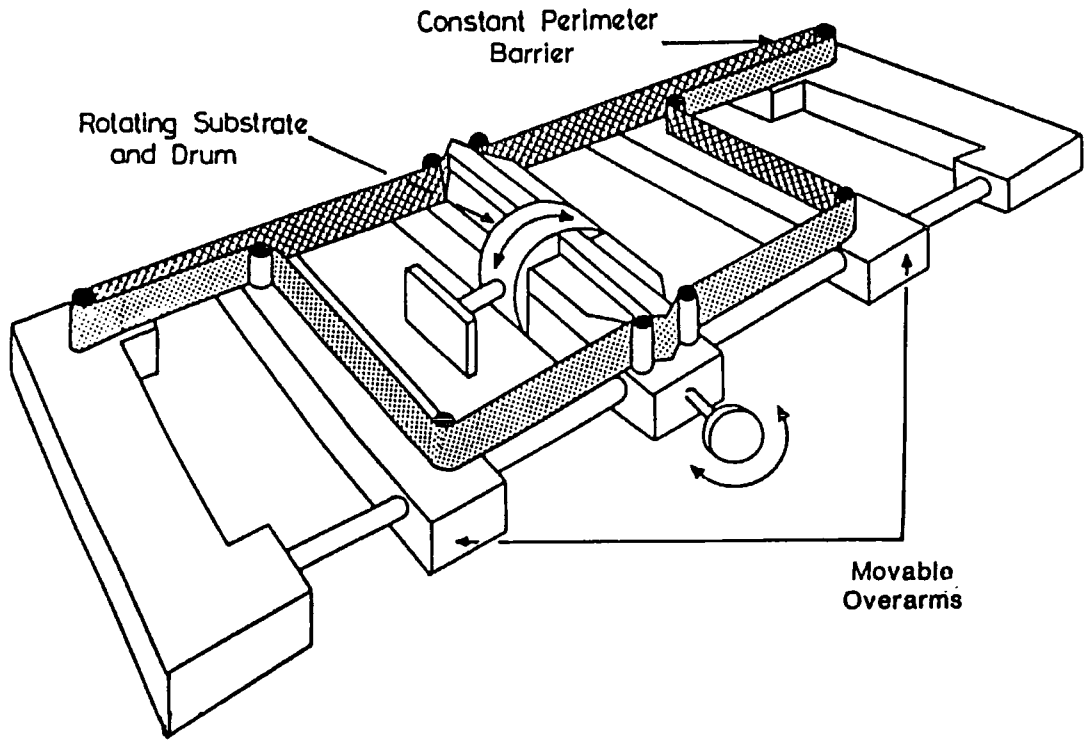

Figure 4.1 - Rotary type alternate-layer Langmuir trough

The second alternate-layer trough was based on a system described by Daniel *et al* [8]. It consisted of a fixed barrier with a 'canal' through it, again this separates

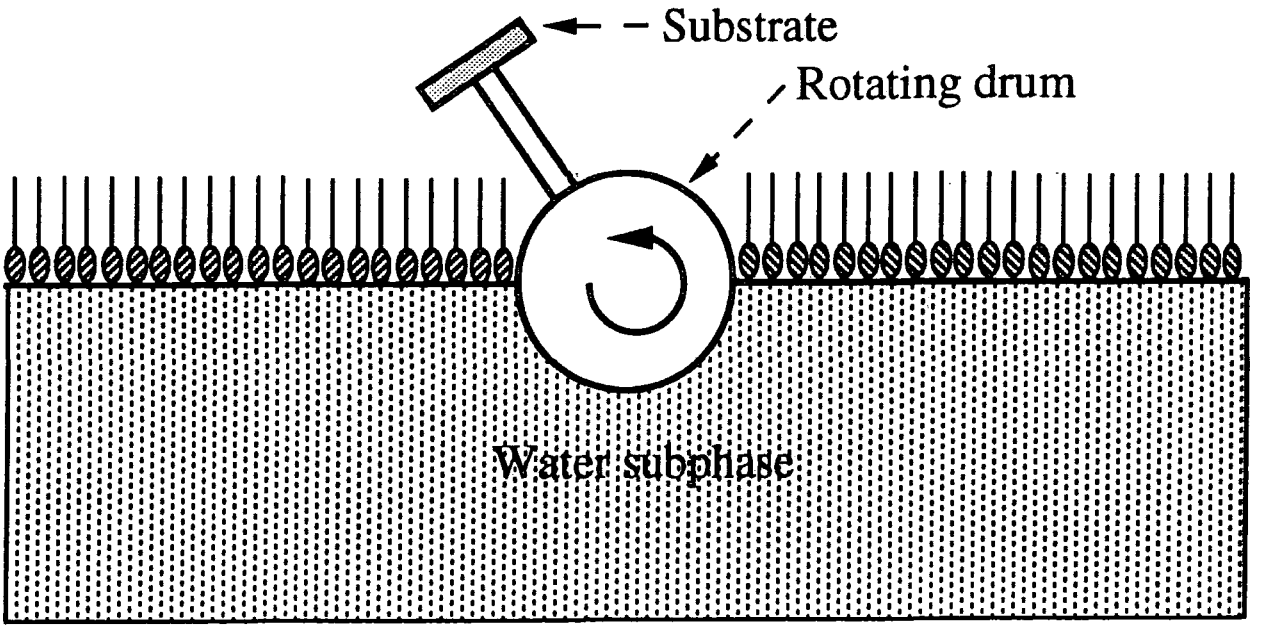

Figure 4.2 - Side view of rotary trough

two isolated controllable areas (figure 4.3). The purpose of the canal was to allow a substrate holder to pass between the two areas whilst holding the substrate in the subphase, permitting the production of alternate-layers.

Environmental conditions can have a significant effect on the quality of the films produced, for example dust in the air or subphase could be deposited in the layer and bacterial contamination has also been observed. In order to reduce the risk of film pollution all of the deposition was carried out in a clean room (nominally class 10000). The subphase was of pure water, this was treated by reverse osmosis to remove organic materials, deionised, exposed to ultra-violet light to kill bacteria and filtered to 0.2 microns. Monitoring of conductivity and total organic content was routinely performed.

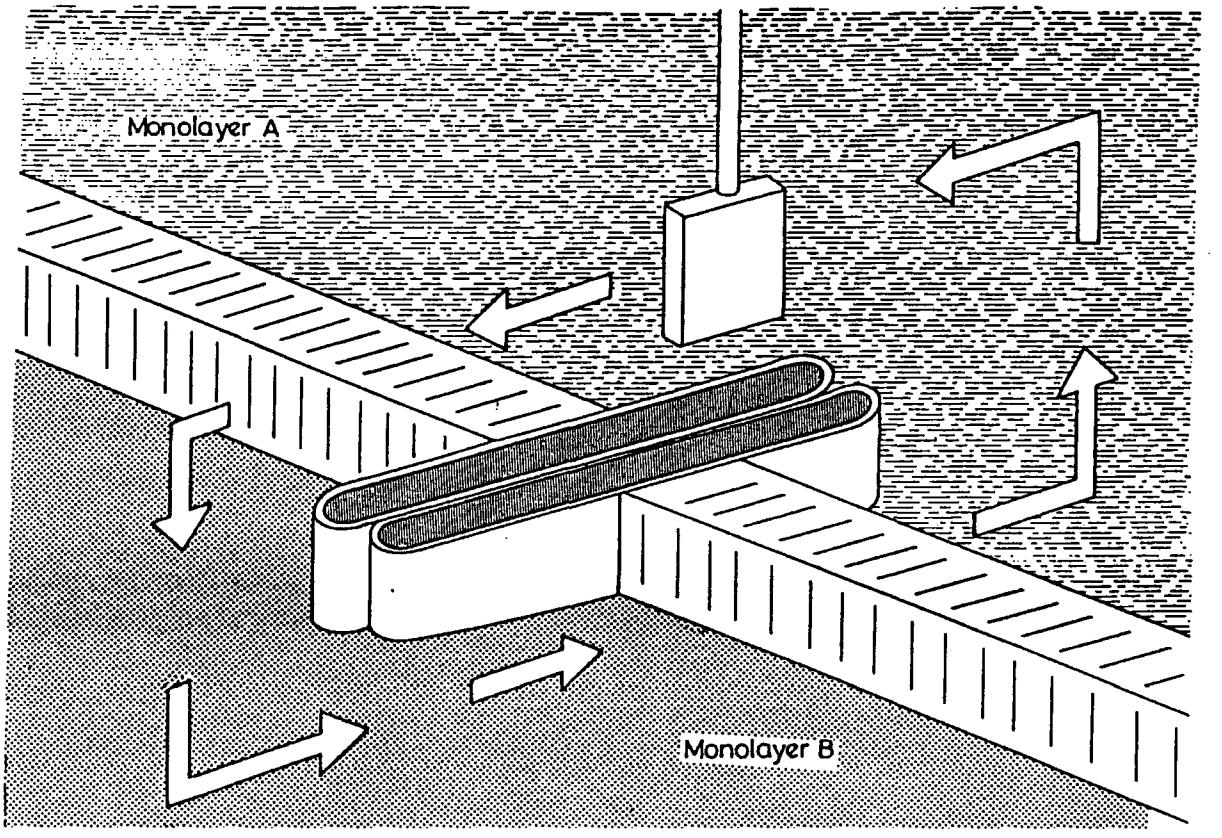

Figure 4.3 Canal type alternate-layer Langmuir trough

4.1.2 Preparation and Characterisation of Floating Monolayers

Where possible materials for study were dissolved in chloroform at concentrations of approximately 1 g l^{-1}. The solution ($\sim 100\mu l$) was then spread dropwise onto the subphase from a microsyringe. After allowing the chloroform to evaporate, the layer was compressed by slowly reducing the barrier area. If the material was being studied for the first time, or if new subphase conditions were being investigated, a plot of surface pressure against area was produced. This is called an isotherm (by analogy with pressure-area plots for bulk materials) and, in principle, allows predictions to be made as to the suitability of the material for LB work and of the best deposition conditions[9].

An extreme case of an isotherm of a material unsuited to LB deposition is when no pressure rise is seen on compression, this may be explained by dissolution into the

subphase. The more general shape of an isotherm is shown in figure 4.4. As the material is compressed an increase in pressure is observed until the film collapses (ie. ceases to be a monolayer) at point C. Before this occurs sudden changes in gradient may be seen (point T_1) or perhaps a 'plateau' region (T_2). These may be tentatively associated with phase transitions. An in-depth study has been undertaken into the phases of docosanoic acid by measuring the X-ray diffraction pattern for different sections of the isotherm[10]. The results showed that a large number of different types of molecular packing were present ie. with rectangular or hexagonal symmetry and several molecular tilt angles. This is analogous to the large numbers of mesophases present in liquid crystals. By taking the approximately linear section for each 'phase' and extrapolating back to zero pressure (points P_1 and P_2) it is possible to estimate the area occupied by a single molecule in the unstressed phase. This, however, is a rather arbitrary process and areas per molecule are sometimes quoted at a given surface pressure. Films are usually deposited at a region with large gradient (to give good pressure control for small change in area) and away from a phase transition (to produce single phase films).

A further test as to the probability of successful LB film formation is the suction test[11]. Here a tube connected to a suction pump is used to remove a portion of a controlled film in a region away from the pressure sensor. If the barriers fail to respond it is clear that the pressure at the sensor is unchanged and the suction tube has simply formed a hole in the film. This indicates that the film is rigid enough to withstand holes in its structure instead of reducing its area to maintain the surface pressure. An attempt to form LB films with such a material is likely to fail as the region under the dipping head will not be replenished as film transfer occurs. If however the suction test leads to an immediate reduction in barrier area, LB film deposition is a possibility, although this in no way guarantees that the layer will transfer to the substrate.

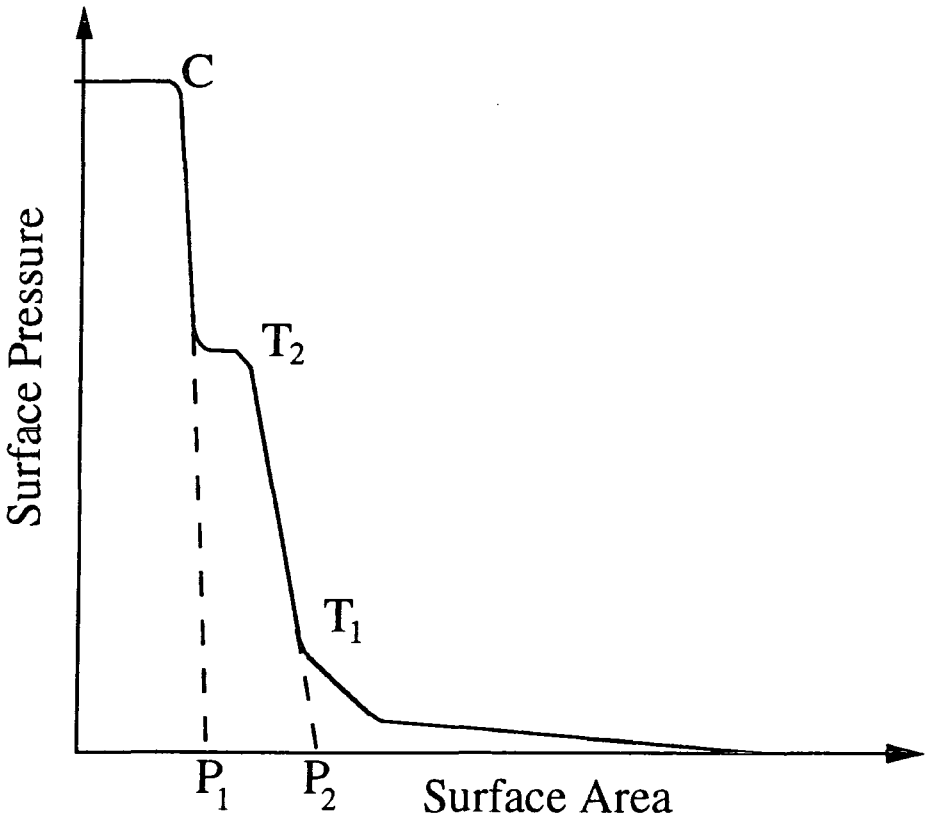

Figure 4.4 - LB film isotherm

4.1.3 Transfer of Monolayers to a Substrate

After compression and control at constant surface pressure, the floating monolayer may be transferred to a substrate. The substrate materials used were glass, silver-coated glass, quartz, silicon and silicon dioxide-coated silicon. In all cases the substrates were cleaned by scrubbing in a solution of teepol and then rinsing thoroughly (for silver-coated glass this cleaning was carried out before vacuum coating). Substrates were either left in a their natural hydrophilic state or treated with dimethyl-dichlorosilane solution to give a hydrophobic surface (the silver-coated glass was always left untreated).

Figure 4.5 represents a floating monolayer of 'classical' LB molecules, ie. they consist of a hydrophilic head group linked to a hydrophobic alkyl chain. When a substrate passes down into the subphase it picks up a layer with the hydrophobic end closest to the substrate. For this reason hydrophobic substrates were always dipped downstroke first. However, the molecular orientation is reversed on the upstroke and the hydrophilic end is closest to the substrate. Hydrophilic substrates

were lowered into the subphase before monolayer compression to allow the first transfer to be on an upstroke.

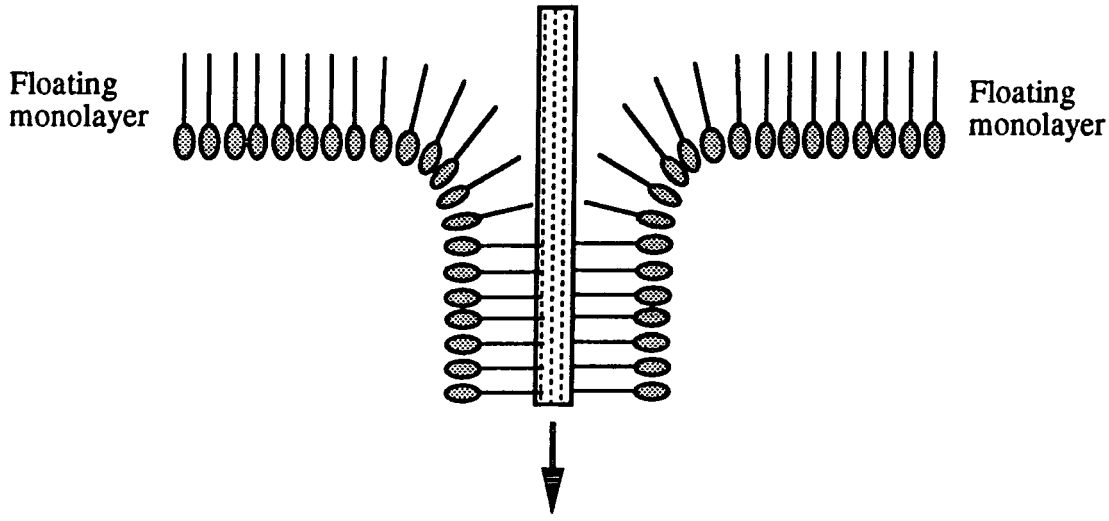

Downstroke dipping. Molecules transfer hydrophobic end first. Substrate should be hydrophobic to assist transfer by depressing meniscus.

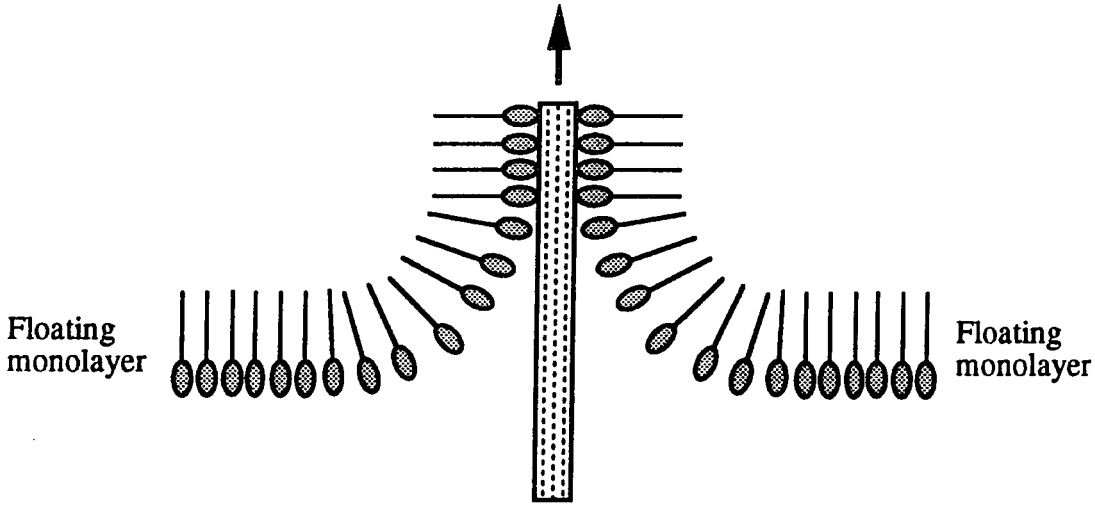

Upstroke dipping. Molecules transfer hydrophilic end first. Substrate should be hydrophilic to assist transfer by raising meniscus.

Figure 4.5 - Hydrophilic and hydrophobic LB film transfer

Subsequent layers may be transfered on repeated strokes, the layers stacking head to head and tail to tail. In some cases transfer may only take place on the down-stroke (X-type) or the upstroke (Z-type). Transfer on both strokes is called Y-type (figure 4.6).

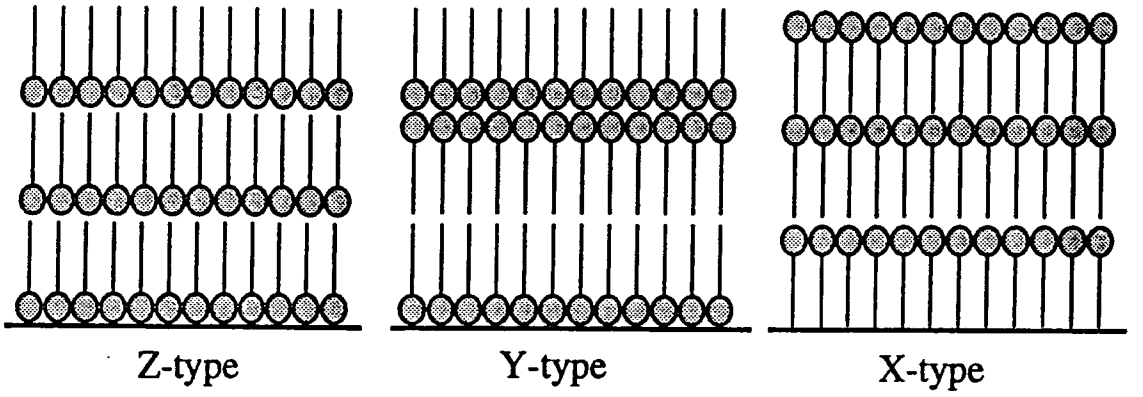

Figure 4.6 - X, Y and Z-type LB films

During monolayer transfer both the surface pressure and area were monitored to give a 'dipping record' (figure 4.7). The pressure should remain constant due to the feedback system; the area reduces as layers are transferred to the substrate. Study of the area plot will reveal which strokes produce transfer and this allows the deposition type to be identified. The transfer ratio may also be measured; this is defined as the ratio of substrate area coated to the reduction in area of the floating monolayer.

It is obvious that Y-type films with an even number of layers are centrosymmetric due to the reversed orientation of the upstroke film relative to the downstroke (films with an odd number of layers will possess a solitary unpaired layer). However, X

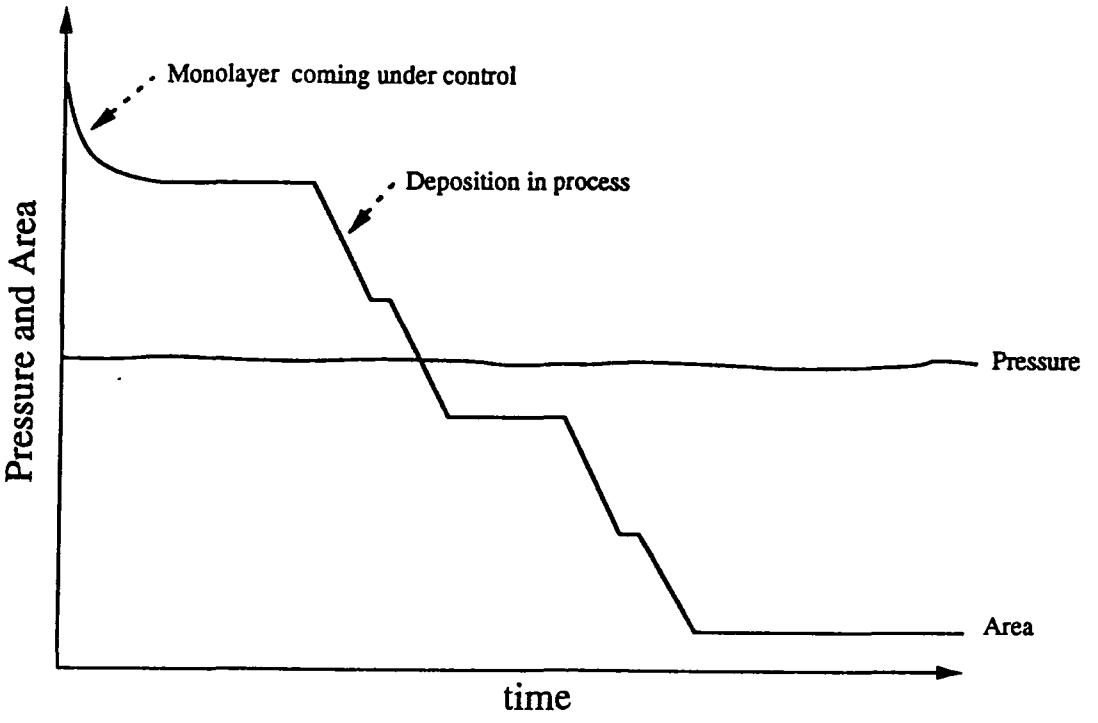

Figure 4.7 - LB film dipping record

and Z-type films (in principle) lack a centre of symmetry as the molecules are arranged head to tail. This means that they may be suited to nonlinear optics.

The alternate-layer technique is a another method of producing asymmetric structures. Here the films are Y-type but the material transferring on the upstroke is different to that on the downstroke. It is evident from figure 4.8 that such films are non-centrosymmetric.

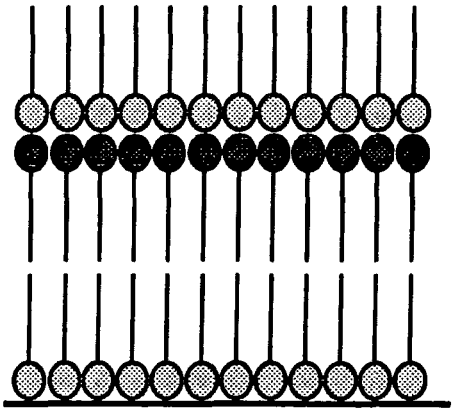

Figure 4.8 - Alternate-layer LB film

4.2 Linear Optics of Langmuir-Blodgett Films

Classical LB film materials consist of rod-shaped molecules that are amphiphilic. An example (Stearic Acid) is shown in figure 4.9, a hydrophilic carboxylic acid head group is linked to a hydrophobic alkyl chain.

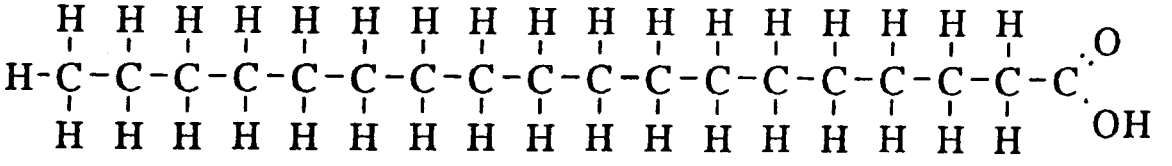

Figure 4.9 - Stearic acid molecule

It is clear that the molecules approximate to a system with axial symmetry. If the z-direction is chosen to lie along the molecular axis the microscopic polarisability tensor ($\widehat{\alpha}$) is diagonal with $\alpha_{11} = \alpha_{22} \neq \alpha_{33}$. The overall properties of the film will depend on the distribution of molecular alignments. Experimental evidence

supports a number of possiblities depending on film quality (quality here means the extent to which molecules align colinearly).

A high quality LB film may be considered as an arrangement of molecules all aligned in the same direction (figure 4.10) with a preferred tilt at an angle ϕ to the substrate normal. All the molecular axes lie in a plane containing the direction of dipping and the substrate normal. The macroscopic consequence of the molecular symmetry is that the film is uniaxially anisotropic with the principal axes along and orthogonal to the molecular axis (figure 4.10). (Reference 12 demonstrates that such films are, in fact, slightly biaxial but two of the indices are very close together and the film is therefore approximately uniaxial).

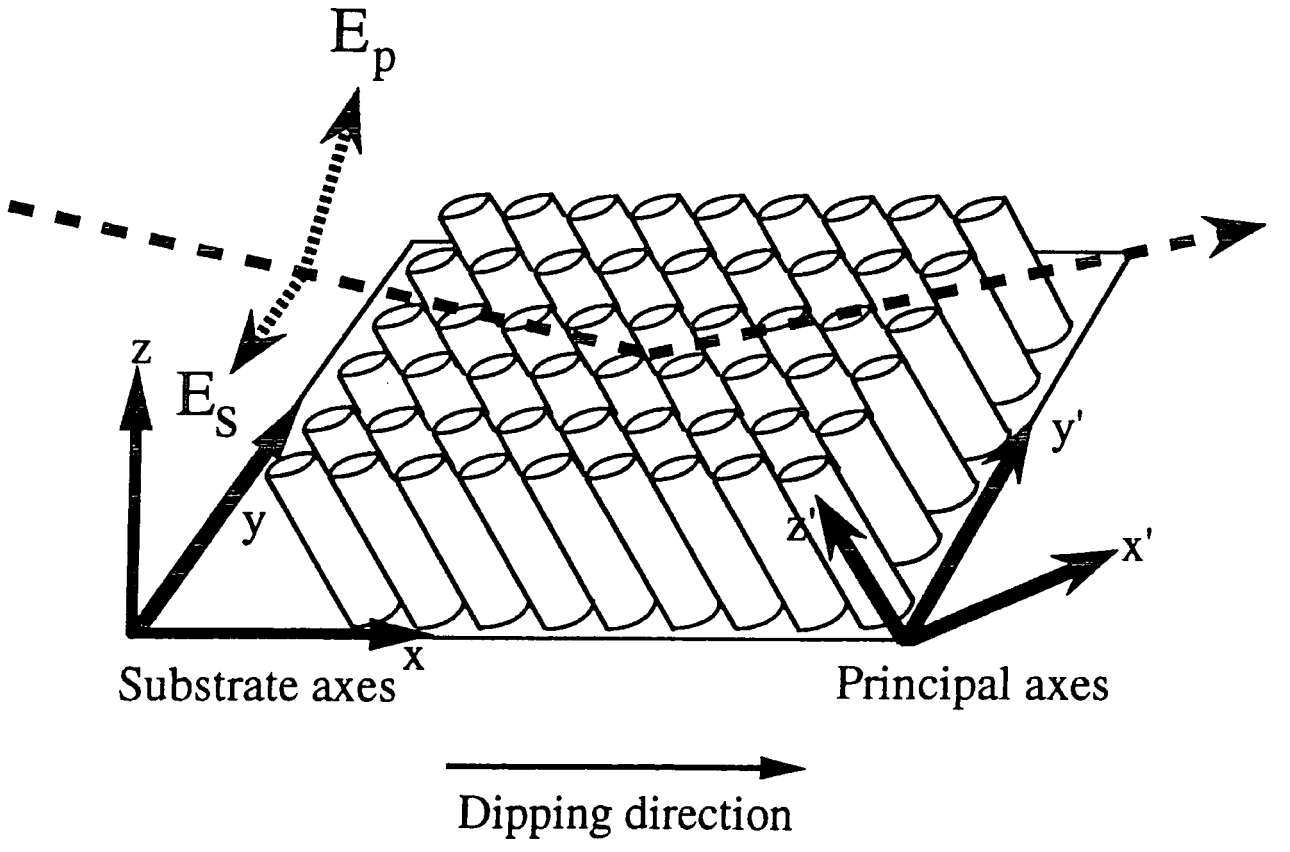

Figure 4.10 - Uniaxial LB film showing molecular alignment, principal axes and p and s-polarisation

It is important to consider the implications for p and s-polarised light incident on uniaxial film. Light of s-polarisation has its electric field vector laying within the plane of the substrate whereas p-polarisation has the electric field coming out of the plane (figure 4.10). Neither of these polarisations are eigenmodes unless the light propagates along the dipping direction. Except for this special case polarisation mixing will occur between the input and output.

A second possible case is that the film consists of regions with two distinct orientations, both at an angle ϕ to the normal and within the same plane, but one leaning along the dipping direction and the other away from it. This scheme is supported by the evidence of reference 13. This type of film will again only have p and s-polarisation eigenmodes for light along the dipping direction. A variation on this system has been observed where the tilt directions take up two orthogonal orientations each at 45 degrees to the dipping direction[14].

It is also likely that for some films the crystal domains will be at other orientations to the dipping direction eg. 60 and 120 degrees. Here the condition for p and s-eigenmodes is again propagation along the direction of molecular tilt.

All of these models can only be approximations to the true situation, in particular the tilt angle will only be an expectation value with a distribution around this. The comments about eigenmodes only apply if a single crystal domain is being probed, for domains smaller than the beam size polarisation mixing is almost certain to occur. In the limiting case of small domains and a large spread of tilt angles the film will approximate to amorphous.

In the case of alternate-layer LB films, the overall structure may be viewed as a single layer rather than modelling it as a repeating grating-like structure. This is because the scale of the layer alternation is much less than the wavelength of light; effectively the optical properties of the overall system represent an averaging of those for the two layer types. All of the models described above also apply to alternate-layer films.

4.3 Langmuir-Blodgett films for Second-Order Nonlinear Optics

Similar rules for molecular design apply to LB nonlinear materials as to other organics. The additional requirement is that the molecule should be amphiphilic to improve its deposition properties. This is generally achieved by attaching a hydrophobic alkyl chain to a polar headgroup which possesses a large β.

The need for a non-centrosymmetric structure dictates the modes of dipping which may be used, ie. X-type, Z-type or alternate-layer. A single monolayer is, of course, also a non-centrosymmetric system and is ideally suited for initial investigation of a new material.

In studies of second-harmonic generation it is expected that a square law relationship between the number of layers and the second harmonic intensity be observed. This is a consequence of equation 2.18, which is reproduced below:

$$I_{2\omega} = \frac{8\pi^2 d^2 l^2 I_\omega^2}{\lambda_\omega^2 n_\omega^2 n_{2\omega} c\epsilon_0} I_\omega^2 \mathrm{sinc}^2(\Delta k l/2) \tag{2.18}$$

For small values of film thickness, (l) it follows that $\mathrm{sinc}(\Delta k l/2) \rightarrow 1$. Hence:

$$I_{2\omega} \propto l^2 \tag{4.1}$$

This condition is often regarded as a quality test of nonlinear LB films. If the measured relationship is sub-quadratic the value of $\chi^{(2)}$ is reducing as more layers are deposited. This is likely to be due to worsening alignment of the active headgroup.

The earliest report of second-order properties in LB films was that of Aktsipetrov et al[15] in which SHG from a monolayer of an azo dye, 4-nitro-4'-octadecy-azobenzene (NAB) is described. The same group later studied Z-type multilayers of the same material and observed a square law relationship up to 6 layers[13].

The first report of nonlinear alternate-layer structures was by Girling *et al* [16]. Clearly for such structures a pair of materials is required, this may consist of one active and one passive ('spacer') material[17] or a pair of active ones[18]. In the

latter case the molecules must be complementary, ie the positions of the donor and acceptor groups should be reversed relative to the alkyl tail. This is shown schematically in figure 4.11. An unusual method of producing non-centrosymmetric films is given in reference 29. Here Y-type films of a single material are used but the alignments of the chromophores gives in-plane asymmetry.

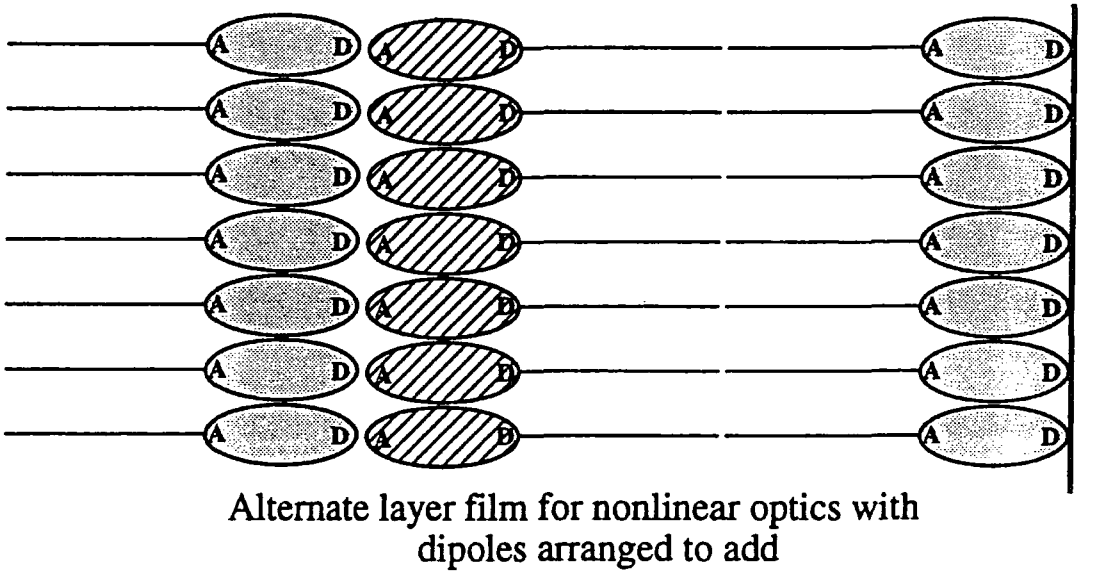

Figure 4.11 - Alternate-layer LB film for nonlinear optics

A number of other materials have been investigated, both in monolayer and multilayer form. Numerical results are summarised in table 4.1, with a number of the best organic and inorganic materials included for comparision. The values are either quoted in or may be derived from the cited references; a table of SI to esu conversions is given in Appendix 1. It should be noted that all of the papers concerned with the Pockels effect in LB films perpetuate a mathematical error in reference 22, namely that $\chi^{(2)}(-\omega;\omega,0) = \Delta\epsilon/E$. There should, of course, also be a factor of 2 in the denominator; the figures in table 4.1 take this into account.

Material	r $/10^{-12}$ m V^{-1}	$\chi^{(2)}(-\omega;\omega,0)$ $/10^{-12}$ m V^{-1}	$\chi^{(2)}(-2\omega;\omega,\omega)$ $/10^{-22}$C V^{-2}	$\beta(-2\omega;\omega,\omega)$ $/10^{-50}$ C m^3 V^{-2}	Reference
Inorganics					
$LiNbO_3$	30.8	361	7.08		19
$Sr_{0.75}Ba_{0.25}Nb_2O_6$	1340	17500			
KDP	9.7	22.6	0.11		19
DKDP	26.4	66.8			
Organic Crystals					
MNA		343	44.3	16.7	20,21
Langmuir-Blodgett Films					
Hemicyanine		61.1	10.8	115	22,23
NAB			1.6		13
Ru-CTP				40 - 60	24
DPNA		19.4	59	115	25,26
Phenylhydrazone			66.7	148	27
Stilbazium			231	741	27
Merocyanine			270	1500	28
DCANP			0.69		29
Azo dyes			3.6 - 8.4	30 - 70	30
Polysiloxane				35	31
Ru-bipyridene				25.9	32

Table 4.1 - Nonlinear Coefficients for LB Materials compared to standard organics and inorganics

For the Pockels effect strontium barium niobate has clearly the largest coefficients but it is only available in ceramic form. This makes it poorly suited to waveguide fabrication. Lithium niobate is the most widely used material; waveguides may be easily made and the value of $\chi^{(2)}$ is large. LB films of hemicyanine are however of

comparable activity. Very few LB films have been assessed for their Pockels effect so it is possible that better materials than hemicyanine may have already been synthesised.

For second-harmonic generation, organic materials have much higher coefficients that inorganics, in many cases this is due to matching an absorption in the material to the required second harmonic. The largest molecular hyperpolarisabilities are seen in merocyanine Langmuir-Blodgett films, these however lose their effects when protonated and must be used in an alkaline atmosphere. However the stable stilbazium salt is of similar activity.

4.3.1 Second Harmonic Generation from Langmuir-Blodgett Films

A number of mathematical analyses have been produced to model the generation of second harmonic light from LB films[15,28,33]. All start from a classic paper by Bloembergen and Pershan dealing with SHG from thin uniaxial films[34]. This theory is developed by reference 15 to include the effects of reflection of the fundamental at the film surfaces. The resultant equations are subsequently simplified in reference 33. Using angles and media subscripts as shown in figure 4.13 the field amplitude relationships for each input and output polarisations are (for SI units):

$$\frac{E_p^{2\omega}}{(E_p^{\omega})^2} = \frac{\omega \cos\varphi_2 \chi_{pp}}{2c(\sqrt{\epsilon_2^{2\omega}}\cos\varphi_0 + \sqrt{\epsilon_0^{2\omega}}\cos\phi_2} \times \left(\frac{2\sqrt{\epsilon_0^{\omega}}\cos\theta_2\cos\theta_0}{\sqrt{\epsilon_0^{\omega}}\cos\theta_2 + \sqrt{\epsilon_2^{\omega}}\cos\theta_0}\right)^2 \qquad (4.2a)$$

$$\frac{E_s^{2\omega}}{(E_p^{\omega})^2} = \frac{\omega \chi_{ps}}{2c(\sqrt{\epsilon_2^{2\omega}}\cos\varphi_0 + \sqrt{\epsilon_0^{2\omega}}\cos\varphi_2} \times \left(\frac{2\sqrt{\epsilon_0^{\omega}}\cos\theta_2\cos\theta_0}{\sqrt{\epsilon_0^{\omega}}\cos\theta_2 + \sqrt{\epsilon_2^{\omega}}\cos\theta_0}\right)^2 \qquad (4.2b)$$

$$\frac{E_p^{2\omega}}{(E_s^{\omega})^2} = \frac{\omega \cos\varphi_2 \chi_{sp}}{2c(\sqrt{\epsilon_2^{2\omega}}\cos\varphi_0 + \sqrt{\epsilon_0^{2\omega}}\cos\phi_2} \times \left(\frac{2\sqrt{\epsilon_0^{\omega}}\cos\theta_0}{\sqrt{\epsilon_2^{\omega}}\cos\theta_2 + \sqrt{\epsilon_0^{\omega}}\cos\theta_0}\right)^2 \qquad (4.2c)$$

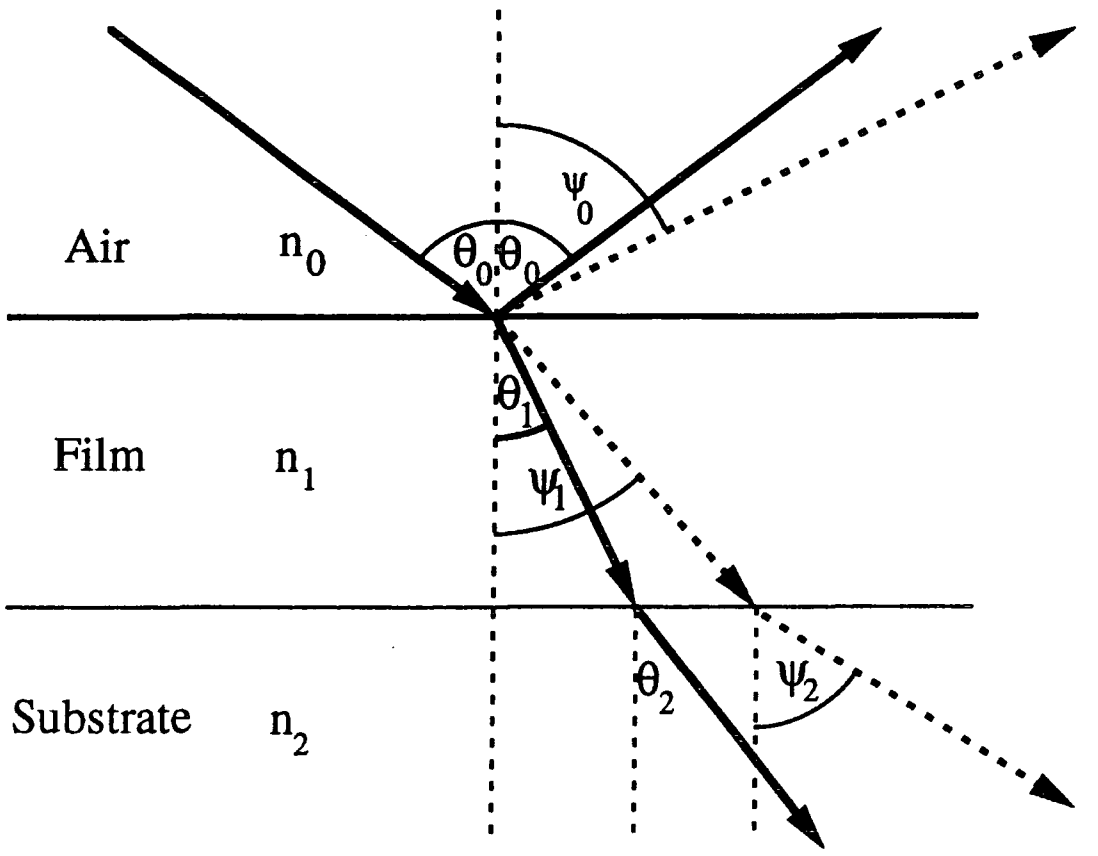

Figure 4.12 - Angles for fundamental (solid) and harmonic (dashed) waves

$$\frac{E_s^{2\omega}}{(E_s^{\omega})^2} = \frac{\omega \chi_{ss}}{2c(\sqrt{\epsilon_2^{2\omega}}\cos\varphi_0 + \sqrt{\epsilon_0^{2\omega}}\cos\varphi_2} \times \left(\frac{2\sqrt{\epsilon_0^{\omega}}\cos\theta_0}{\sqrt{\epsilon_2^{\omega}}\cos\theta_2 + \sqrt{\epsilon_0^{\omega}}\cos\theta_0}\right)^2 \qquad (4.2d)$$

These apply for both reflected and transmitted waves. In each case the second-order susceptibilities are effective values rather than an individual tensor component. In order to derive these coefficients in tensor terms it is necessary to consider which components are driven by a particular input polarisation and which contribute to the relevant output polarisation. Mathematically this can be stated in terms of the unit input and output field vectors, $e_{2\omega}$ and e_{ω} respectively

$$\chi^{(2)}_{eff} = \sum \mathbf{e}_{2\omega} . \hat{\chi}^{(2)} . \mathbf{e}_{\omega} . \mathbf{e}_{\omega} \tag{4.3}$$

For example, in the case of s-polarised input to s-polarised output both the fields are in the y direction and only one component, $\chi^{(2)}_{222}$ contributes. For the other situations more than one field component is involved and there are angle factors to consider. Assuming that the second harmonic propagates at the same angle as the fundamental within the film the full expressions are:

$$\chi^{(2)}_{pp} = \chi^{(2)}_{333} \sin^3\theta_1 + 2\chi^{(2)}_{331} \sin^2\theta_1 \cos\theta_1 + \chi^{(2)}_{311} \sin\theta_1 \cos^2\theta_1 +$$

$$\chi^{(2)}_{133} \sin^2\theta_1 \cos\theta_1 + 2\chi^{(2)}_{131} \sin\theta_1 \cos^2\theta_1 + \chi^{(2)}_{111} \cos^2\theta_1 \tag{4.4a}$$

$$\chi^{(2)}_{ps} = \chi^{(2)}_{233} \sin^2\theta_1 + 2\chi^{(2)}_{231} \sin\theta_1 \cos\theta_1 + \chi^{(2)}_{211} \cos^2\theta_1 \tag{4.4b}$$

$$\chi^{(2)}_{sp} = \chi^{(2)}_{322} \sin\theta_1 + \chi^{(2)}_{122} \cos\theta_1 \tag{4.4c}$$

$$\chi^{(2)}_{ss} = \chi^{(2)}_{222} \tag{4.4d}$$

Fortunately the situation is, in many cases, simpler for an LB film than for a general uniaxial plate. Depending on the molecular orientation, crystal domain size and beam size extra symmetries may exist. For example, reference 33 quotes equations for a film rotationally invariant about the substrate normal, this occurs if the domains have random orientation with respect to the dipping direction and are much smaller than the beam diameter. In practice it may be possible to derive structural information from the dependence of the second harmonic intensity on the fundamental's polarisation and angle[13].

4.3.2 The Pockels Effect in Langmuir-Blodgett films

Most Pockels effect measurements on LB films have been carried out using a modified Kretschmann surface plasmon resonance arrangement with the film deposited onto the silver layer[22]. The full experimental arrangement and theory is given in section 5.2. Figure 4.13 shows the field directions involved. The low-frequency field is along the film normal and that of the light in a direction related by refraction to the resonant angle (θ_r). The angle may be found from Snell's law.

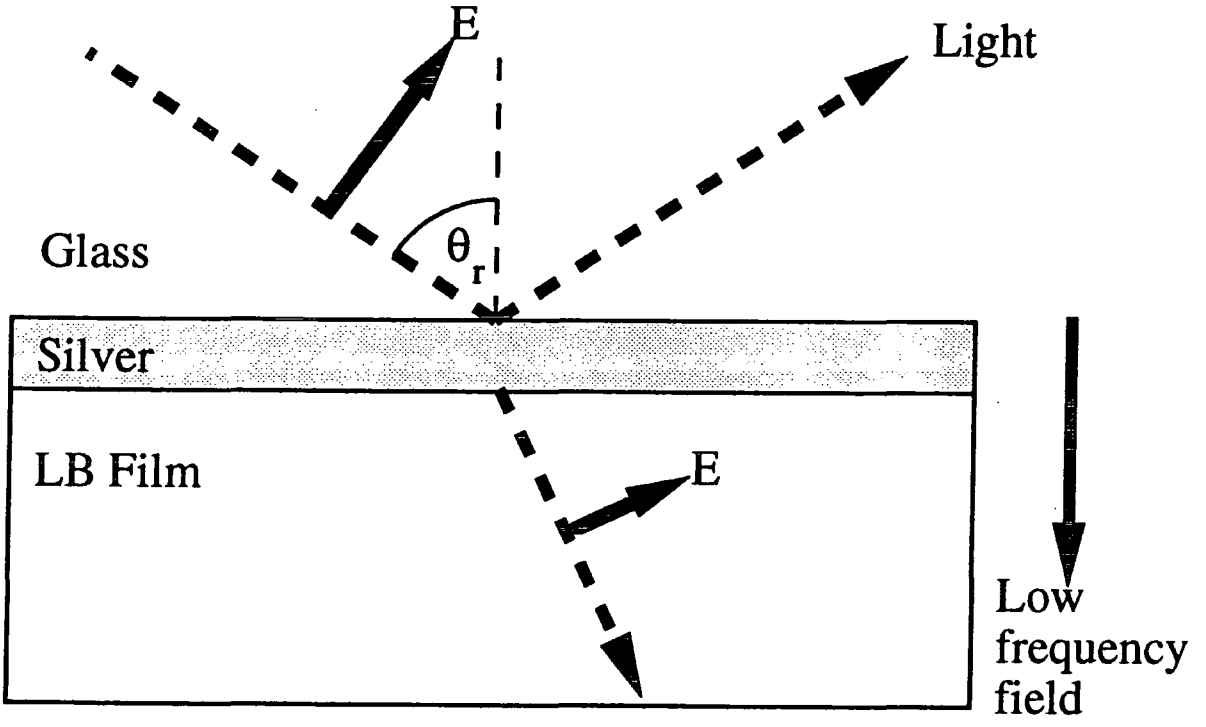

Figure 4.13 - Electric field directions for Pockels effect measurements

As the technique can only use p-polarised inputs and outputs only a single second-order coefficient is obtained and it is not possible to separate the effects of different tensor elements. The overall effect is due to a mixture of all elements involving x and z field components.

However, as it is possible to distinguish an increase in refractive index from a decrease, measurement of the Pockels effect determines the sign of $\chi^{(2)}(-\omega;\omega,0)$ for the material. Second harmonic experiments give no sign information as the intensity depends on the square of $\chi^{(2)}(-2\omega;\omega,\omega)$. A full discussion of the experimental techniques of Pockels effect measurement in LB films is given in sections 5.2 and 5.3.

4.4 Waveguiding in Langmuir-Blodgett Films

As explained in chapter 3, any application of nonlinear optical materials is likely to involve some form of optical confinement, eg a waveguide. A number of workers have studied waveguides of LB films, initially using fatty acids but more recently involving materials with second-order nonlinear properties.

Pitt and Walpita[35] carried out extensive studies on cadmium stearate waveguides formed by the deposition of arachidic acid layers from a subphase containing cadmium ions. These guides were characterised by prism coupling which allows the measurement of the mode effective indices. From these results the layer index, anisotropy and thickness were obtained. Structures of up to 281 layers are described, these exhibited two guided modes for each polarisation.

Waveguiding has also been observed in LB films of preformed polymers [36]. These guides were found to have an attenuation of 10 dB cm^{-1} at 633 nm and could be modified to include active nonlinear groups in the polymer.

Bosshard *et al* [37] produced waveguides of the nonlinear LB film material 2-docosylamino-5-nitropyridene; the attenuation was similar to that for the preformed polymer guides. This material is of the 'herring-bone' type and and was studied as non-centrosymmetric Y-type films. Although second-harmonic generation was obtained, the experiment was performed through-plane rather than using guided light.

The major technical drawbacks of LB film waveguides are their high attenuation and slow speed of fabrication. Also, nothing is known about the electrooptic

properties of the films for guided light. Methods of overcoming these problems are discussed in chapter 9.

4.5 Summary

The Langmuir-Blodgett method allows the production of molecular monolayers and multilayers. The films will, in general, possess a degree of molecular alignment giving rise to uniaxial linear optical properties. Non-centrosymmetric structures may be fabricated, with suitable materials gives rise to second-order nonlinear effects. These effects may be studied by second harmonic generation and by measurement of the Pockels effect.

References

1. I. Langmuir, *Trans. Faraday Soc.* **15** pp62-74 (1920).
2. K.B. Blodgett, *J. Am. Chem. Soc.* **56** p495 (1934).
3. K.B. Blodgett, *J. Am. Chem. Soc.* **57** pp1007-22 (1935).
4. G.L. Gaines, *Insoluble Monolayers at Liquid-Gas Interfaces* (Wiley-Interscience 1966).
5. G.G. Roberts in *Langmuir-Blodgett Films* ed. G.G. Roberts (Plenum 1990).
6. M.C. Petty in *Langmuir-Blodgett Films* ed. G.G. Roberts (Plenum 1990) pp102-5.
7. B. Holcroft, M.C. Petty, G.G. Roberts, G.J. Russell, *Thin Solid Films* **134** pp83-8 (1985).
8. M.F. Daniel, J.C. Dolphin, A.J. Grant, K.E.N. Kerr, G.W. Smitch, *Thin Solid Films* **133** pp235-42 (1985).
9. R.A. Hann in *Langmuir-Blodgett Films* ed. G.G. Roberts (Plenum 1990) pp19-23.
10. R.M. Kenn, C. Bohm, A.M. Bibo, I.R. Peterson, H. Mohwald, J. Als-Nielsen,

K. Kjaer, *J. Phys. Chem.* **95** pp2092-7 (1991).

11. S. Baker, *PhD. thesis*, University of Durham p92 (1985).

12. W.L Barnes, J.R. Sambles, *Surface Science* **177** pp399-416 (1986).

13. O.A. Aktsipetrov, N.N. Akhmediev, I.M. Baranova, E.D. Mishina, V.R. Novak, *Soviet Physics JETP* **62** (3) pp524-30 (1985).

14. A. Bonnerot, P.A. Chollet, H. Frisby, M. Hoclet, *Chemical Physics* **97** pp365-77 (1985).

15. O.A. Aktsipetrov, N.N. Akhmediev, E.D. Mishina, V.R. Novak, *JETP Letters* **37** pp207-9 (1983).

16. I.R. Girling, P.V. Kolinsky, N.A. Cade, J.D. Earls, I.I. Peterson, *Optics Communications* **55** (4) pp289-92 (1985).

17. P. Stroeve, D.D. Saperstein, J.F. Rabolt, *J. Chem. Phys* **92** (11) pp6958-67 (1990).

18. D.B. Neal, M.C. Petty, G.G. Roberts, M.M. Ahmad, W.J. Feast, I.R. Girling, N.A. Cade, P.V. Kolinsky, I.R. Peterson, *Electronic Letters* **22** (9) pp460-2 (1986).

19. T. Kondo, N. Ogasawara, S. Umegaki, R. Ito, *Springer Proc. in Physics vol 36* (Springer-Verlag 1989) pp218-21.

20. T. Yoshimura, Y. Kubota, *Springer Proc. in Physics vol 36* (Springer-Verlag 1989) pp222-26.

21. R. Morita, T. Kondo, N. Ogasawara, S. Umegaki, R. Ito, *Springer Proc. in Physics vol 36* (Springer-Verlag 1989) pp202-5.

22. G.H. Cross, I.R. Girling, I.R. Peterson, N.A. Cade, *Electronics Letters* **22** pp1111-3 (1986).

23. I.R. Girling, N.A. Cade, P.V. Kolinsky, R.J. Jones, I.R. Peterson, M.M. Ahmad, D.B. Neal, M.C. Petty, G.G. Roberts, W.J. Feast, *J. Opt. Soc. Am. B* **4** pp950-5 (1987).

24. T. Richardson, G.G. Roberts, M.E.C. Polywka, S.G. Davies, *Thin Solid Films* **160** pp231-9 (1988).

25. J.C. Loulergue, M. Dumont, Y. Levy, P. Robin, J.P. Pocholle, M. Papuchon, *Thin Solid Films* **160** pp399-405 (1988).

26. I. Ledoux, D. Josse, P.V. Vidakovic, J. Zyss, R.A. Hann, P.F. Gordon, B.D. Bothwell, S.K. Gupta, S. Allen, P.Robin, E. Chastaing, J.C. Dubois, *Europhysics Letters* **3** pp803-9 (1987).

27. D. Lupo, W. Prass, U. Scheunemann, A. Laschewsky, H. Ringsdorf, I. Ledoux, *J. Opt. Soc. Am. B* **5** pp300-8 (1988).

28. I.R. Girling, N.A. Cade, P.V. Kolinsky, C.M. Montgomery, *Electronics Letters* **21** pp169-70 (1985).

29. C. Bosshard, M.Kupfer, P.Gunter, C. Pasquier, S. Zahir, M. Seifert, *Applied Physics Letters* **65** pp1204-6 (1990).

30. L.S. Miller, P.J. Jones, R.S. Sethi, M.J. Goodwin, R. Marsden, G.W. Gray, R.M. Scrawston, *Organic Materials for Nonlinear Optics 89* pp361-6 (Royal Society of Chemistry, London 1989).

31. N. Carr, M.J. Goodwin, A.M. McRoberts, G.W. Gray, R. Marsden, R.M. Scrawston, *Makromol. Chem. Rapid Commun.* **8** pp487-93 (1987).

32. H. Sakaguchi, H. Nakamura, T. Nagamura, T. Ogawa, T. Matsuo, *Chem. Lett.* pp1715-8 (1989).

33. A. Scheelen, P. Winant, A. Persoons in *Organic Molecules for Nonlinear Optics and Photonics* ed. J. Messier, F. Kazjar, P. Prasad (Kluwer Academic 1991).

34. N. Bloembergen, P.S. Pershan, *Phys. Rev.* **128** p606 (1962).

35. C.W. Pitt, L.M. Walpita, *Thin Solid Films* **68** pp101-27 (1980).

36. R.H. Tredgold, M.C.J. Young, P. Hodge, E. Khoshdel, *Thin Solid Films* **151** pp441-9 (1987).

37. Ch. Bosshard, M. Kupfler, P. Gunter, C. Pasquier, S. Zahir, M. Seifert, *Appl. Phys. Lett.* **56**(13) pp1204-6 (1990).

Chapter 5
Experimental Techniques

The Langmuir-Blodgett films were characterised for their structural and optical properties using a number of techniques. Refractive index and layer thickness were obtained from ellipsometry and surface plasmon resonance results. The second-order nonlinear properties were studied by measuring the Pockels effect in a surface plasmon resonance system and by second harmonic generation. Optical waveguides were investigated by prism and end-fire coupling. X-ray diffraction and Fourier transform infra-red measurements were used to assess the degree of order in the films.

5.1 Ellipsometry

Ellipsometry[1] is the measurement of the elliptical polarisation state of light, generally after reflection from one or more parallel interfaces. The measured polarisation may then be used to calculate the refractive indices of the materials separated by the interfaces or, in the case of multiple layers, the thickness of the material.

The general situation for a multilayer structure is shown in figure 5.1. The overall effect of the multilayer stack could be calculated by a similar technique to section 4.4 but for ellipsometry it is usual to express the reflection in terms of the Fresnel coefficients[2] for the individual interfaces. For each interface there are a number of reflection coefficients, one for each possible combination of incident and reflected polarisation. There is also an equivalent set of transmission coefficients.

These coefficients can then by combined to give the overall reflection for the stack by allowing for the phase changes across each layer. If there is no mixing between polarisations this reflection behaviour can be fully described by two coefficients, the amplitude reflectance of p-polarised input to p-polarised output (R_{pp}) and the equivalent for s-polarisation (R_{ss}).

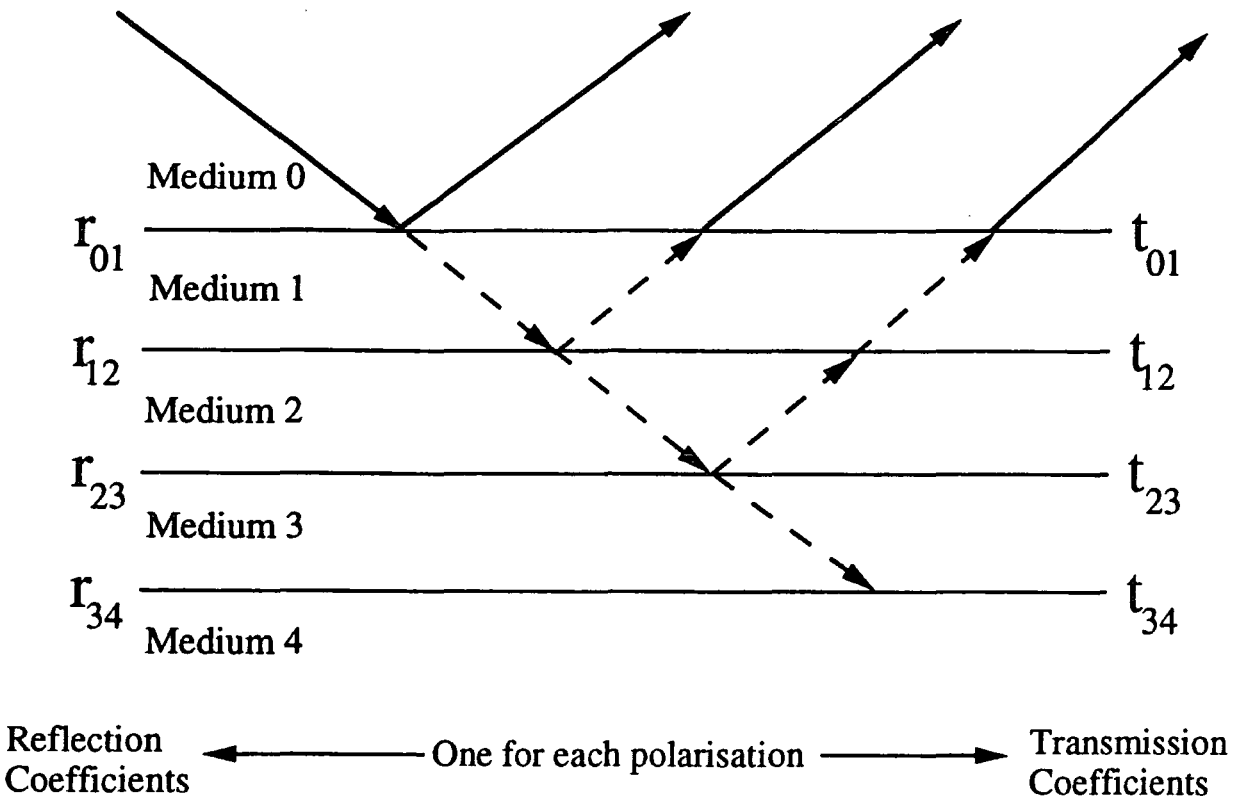

Figure 5.1 - Multilayer stack for ellipsometry

In ellipsometry it is usual to measure indirectly the ratio of these quantities:

$$\frac{R_{pp}}{R_{ss}} = \tan\psi e^{j\Delta} \tag{5.1}$$

by finding ψ and Δ the so called ellipsometric angles[3]

By far the most common method of measuring the ellipsometric angles is by use of a null-ellipsometer[4] and this is the type of machine used at Durham University in the study of LB films.

5.1.1 Practical details of the Rudolph nulling ellipsometer

The ellipsometer used in the Molecular Electronics Group at Durham University is a Rudolph Research AutoEl-IV, this is an automated ellipsometer in which all measurements and calculations are carried out by built-in computer programs. The

operator only has to ensure correct sample alignment and that the program chosen is appropriate to the sample under study.

Figure 5.2 shows the optical arrangement of the AutoEl-IV, the salient features are as follows: a white light source is filtered and collimated to to give monochromatic unpolarised light, this is then passed through a rotatable prism polariser (P); the resulting linearly polarised light is then incident on a quarter-wave plate, referred to as a compensator (C); the compensator output will, in general, be elliptically polarised; the light is then reflected from the sample (S) to be studied and passes through the analyser (A) which is a second prism polariser; the final intensity of the light is monitored by a photomultiplying tube (PMT) . This system is called a PCSA ellipsometer[5] because of the order of its optical elements.

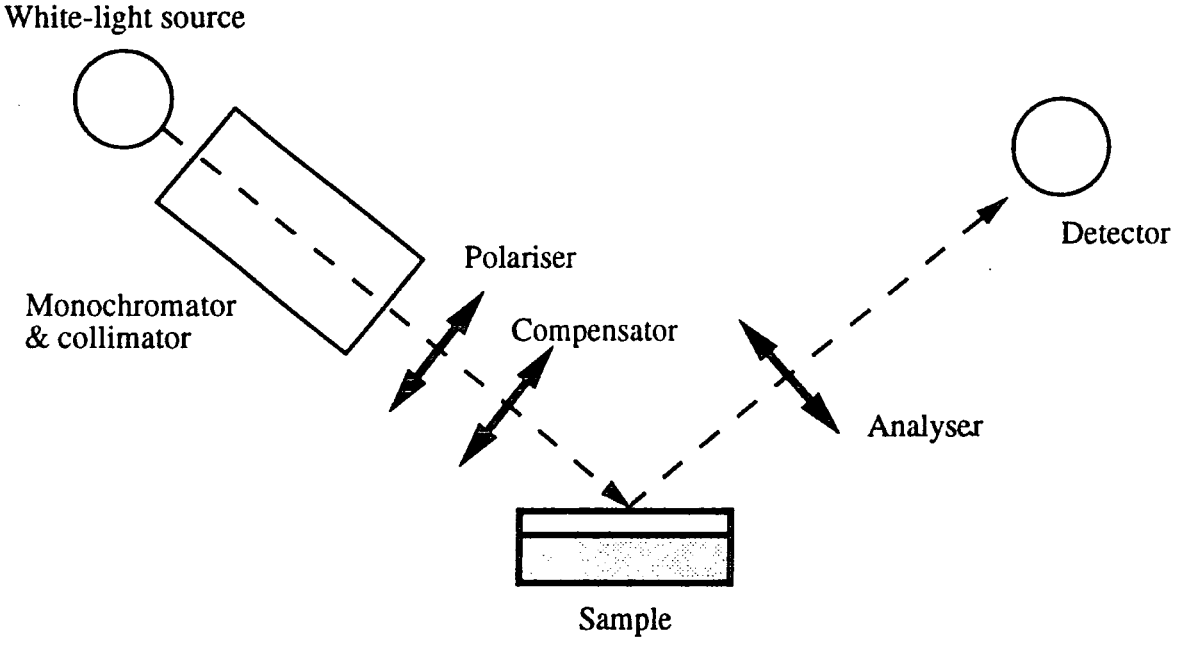

Figure 5.2 - Optical system of Rudolph AutoEl-IV ellipsometer

The reflection of elliptically polarised light from the sample gives, in general, elliptical output. The intensity transmitted through the whole system may be minimised by aligning A to lie across the smaller axis of the ellipse (see figure 5.3). There is,

however, a special case for certain angle of P in which the light reflected from S will be linearly polarised. In this case adjustment of A leads to zero (null) transmitted intensity. This special case is found by alternate adjustment of P and A until no further reduction in PMT ouput is seen, this process is known as nulling. In the AutoEl-IV nulling is carried out automatically by rotating P and A using stepper motors. Hence, this is an auto-nulling PCSA ellipsometer.

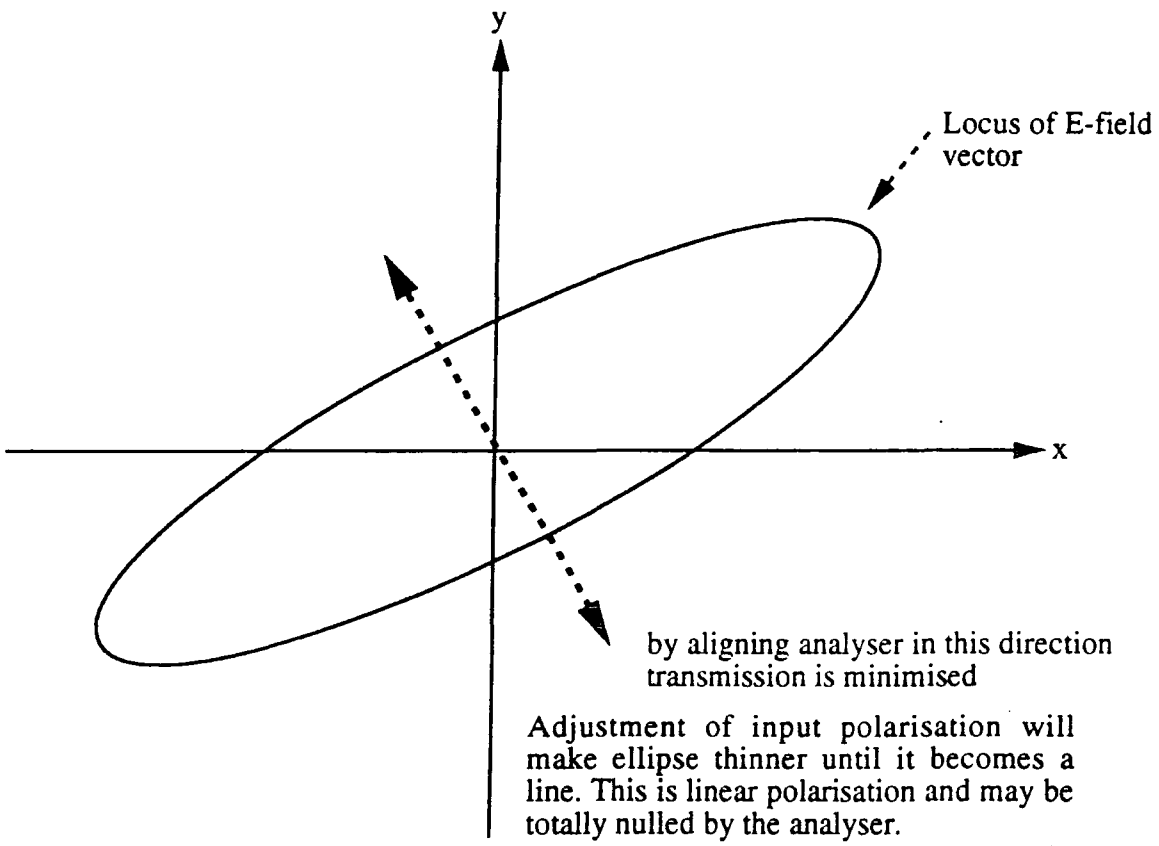

Figure 5.3 - Elliptically polarised light

In practice symmetry considerations show that more than one pair of P and A exist, related by simple formulae[4]. By finding more than one of these pairs of results the overall error may be reduced; this is known as working in more than one zone.

The values of P and A may be used to calculate the ellipsometric angles ψ and Δ which are then fed into the appropriate program to find some of the sample parameters. A total of two parameters may be calculated for a single set of ellipsometric angles although more information can be found by varying the angle of incidence or measuring a number of samples of different thicknesses.

5.1.2 Ellipsometry of LB films - The Isotropic Model[6]

The AutoEl-IV contains a number of built in programs for the study of samples: one of these is for an isotropic, lossless film on an isotropic substrate. Although this does not accurately represent the situation for LB films, it is the nearest approximation amongst the provided software.

The first step is to find the refractive index of the substrate, as this has not been assumed lossless it is a complex quantity. The Fresnel amplitude reflection coefficients for angle of incidence ϕ_0 (the zero indicates its measurement in the incident medium - see figure 5.4 for the definition of symbols) are:

$$R_{pp} = \frac{N_2^2 \cos\phi_0 - N_0(N_2^2 - N_0^2 \sin^2\phi_0)^{\frac{1}{2}}}{N_2^2 \cos\phi_0 + N_0(N_2^2 - N_0^2 \sin^2\phi_0)^{\frac{1}{2}}} \qquad (5.2a)$$

$$R_{ss} = \frac{N_0 \cos\phi_0 - (N_2^2 - N_0^2 \sin^2\phi_0)^{\frac{1}{2}}}{N_0 \cos\phi_0 + (N_2^2 - N_0^2 \sin^2\phi_0)^{\frac{1}{2}}} \qquad (5.2b)$$

$$R_{ps} = R_{sp} = 0 \text{ because s and p are eigenpolarisations.} \qquad (5.2c)$$

As $N_0 = 1$ and ϕ_0 is known the only two parameters to be found are the real and imaginary parts of N_2. Measurement of ψ and Δ for the system provide enough information to calculate these without ambiguity. The calculation must be carried out numerically as it is not possible to produce an analytical expression for the substrate index in terms of the ellipsometric angles.

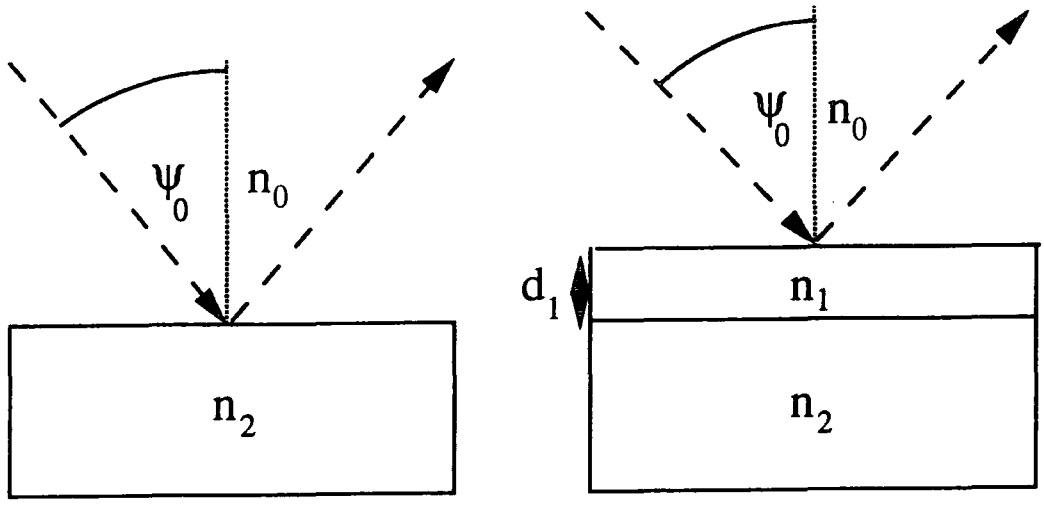

Figure 5.4 - Definition of symbols for ellipsometry

For the ambient-film-substrate system the overall amplitude reflection coefficient is given by combining the coefficients for the two layers after allowing for the phase change β across the film (thickness d_1). These expressions are of the form:

$$r = \frac{r_{01} + r_{12}e^{-j2\beta}}{1 + r_{01}r_{12}e^{-j2\beta}} \tag{5.3}$$

where $\beta = 2\pi(\frac{d_1}{\lambda})(N_1^2 - N_0^2 \sin^2 \phi_0)^{\frac{1}{2}}$.

The r_{01} and r_{12} must be for the correct polarisation.

As the film has been chosen to be lossless there are only two unknowns, the real part of N_1, and d_1. These may again be calculated from ψ and Δ with the only ambiguity being a repetition of results after a half wavelength cycle of d_1. This represents no problem if the approximate layer thickness is known, in the case of LB films the correct results will almost invariably be those for the first cycle (ie the thinnest).

If the layer thickness is known it is possible to measure the loss in the LB layer, this could also be achieved by measuring a series of samples of different thicknesses. Unfortunately the AutoEl-IV only allows calculations to be carried out on results

from a single sample. To include loss or anisotropy in the model it is neccessary to measure ψ and Δ on the AutoEl-IV and feed these into a separate computer for calculations.

5.1.3 Ellipsometry of LB films - The Uniaxial Model

The molecules used to form LB films are typically rod-like, they will therefore exhibit two refractive indices - along the rod and perpendicular to it. When these molecules are deposited it is clear that the film will not satisfy our isotropic model unless the molecules are totally disordered. As explained in section 4.2 a more accurate model of the system is to consider the film as uniaxial with the molecular axes tilted away from the substrate perpendicular (see figure 5.5).

Generally for a uniaxial layer, the two eigenpolarisations are along the optical axis and perpendicular to it. In the case of tilted molecules these will not normally be the s and p polarisations. However, if the molecular axes lie in the plane of incidence, s and p *are* eigenpolarisations so there is no reflection between the two states ($r_{sp} = r_{ps} = 0$). For this case the mathematics can be simplified by resolving the refractive indices into an in-plane (ordinary) component N_{1o} and a perpendicular (extraordinary) component N_{1e}. It is now possible to write down expressions for the amplitude reflection of the two polarisations[7].

$$R_{pp} = \frac{r_{01pp} + r_{12pp}e^{-j2\beta_p}}{1 + r_{01pp}r_{12pp}e^{-j2\beta_p}} \tag{5.4a}$$

$$R_{ss} = \frac{r_{01ss} + r_{12ss}e^{-j2\beta_s}}{1 + r_{01ss}r_{12ss}e^{-j2\beta_s}} \tag{5.4b}$$

where

$$r_{01pp} = \frac{N_{1o}N_{1e}\cos\phi_0 - N_0(N_{1e}^2 - N_0^2\sin^2\phi_0)^{\frac{1}{2}}}{N_{1o}N_{1e}\cos\phi_0 + N_0(N_{1e}^2 - N_0^2\sin^2\phi_0)^{\frac{1}{2}}} \tag{5.5a}$$

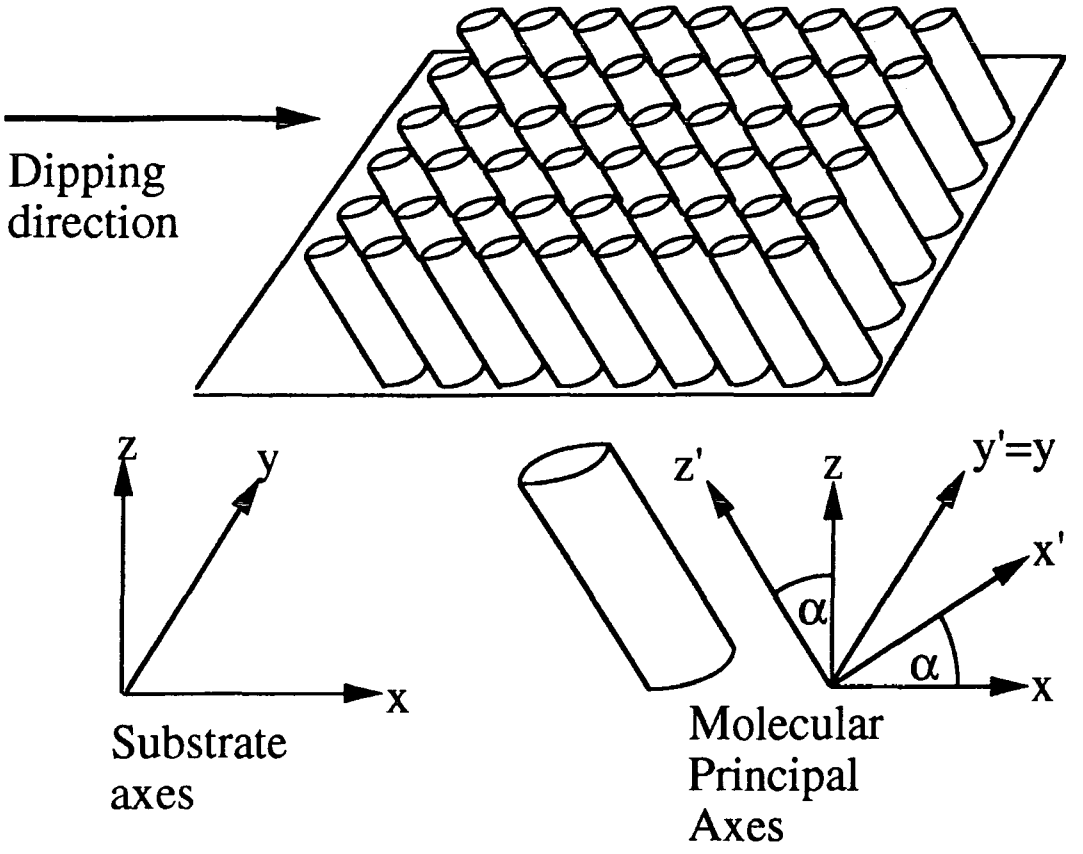

The molecules are tilted with respect to the substrate normal by an angle α but the molecular axis remains in the xz plane. Therefore light incident in this plane has p and s polarisations as eigenmodes.

Figure 5.5 - Uniaxial LB film

$$r_{12pp} = \frac{-N_{1o}N_{1e}\cos\phi_2 - N_2(N_{1e}^2 - N_2^2\sin^2\phi_2)^{\frac{1}{2}}}{N_{1o}N_{1e}\cos\phi_2 + N_2(N_{1e}^2 - N_0^2\sin^2\phi_2)^{\frac{1}{2}}} \qquad (5.5b)$$

$$r_{01ss} = \frac{N_0\cos\phi_0 - (N_{1o}^2 - N_0^2\sin^2\phi_0)^{\frac{1}{2}}}{N_0\cos\phi_0 + (N_{1o}^2 - N_0^2\sin^2\phi_0)^{\frac{1}{2}}} \qquad (5.5c)$$

$$r_{12ss} = \frac{-N_2 \cos\phi_2 - (N_{1o}^2 - N_2^2 \sin^2\phi_2)^{\frac{1}{2}}}{N_2 \cos\phi_2 + (N_{1o}^2 - N_2^2 \sin^2\phi_2)^{\frac{1}{2}}} \tag{5.5d}$$

$$\beta_p = 2\pi(\frac{d_1}{\lambda})(\frac{N_{1o}}{N_{1e}})(N_{1e}^2 - N_0^2 \sin^2\phi_0)^{\frac{1}{2}} \tag{5.6a}$$

$$\beta_s = 2\pi(\frac{d_1}{\lambda})(N_{1o}^2 - N_0^2 \sin^2\phi_o)^{\frac{1}{2}} \tag{5.6b}$$

and from Snell's law

$$N_0 \sin\phi_0 = N_2 \sin\phi_2 \tag{5.7}$$

Each of the refractive indices is a complex quantity, therefore there are potentially a large number of unknowns. If a lossless film is assumed and the refractive indices of substrate and ambient are known, the unknowns are reduced to the real parts of N_{1o} and N_{1e}, and the film thickness d_1.

The problem is still under-specified for solution by ellipsometry of a single sample but the use of multiple samples can provide results. Den Engelsen[7] describes a technique using up to twenty samples of different numbers of layers and by fitting theoretical ellipsometric results to experimental data he is able to determine both the uniaxial refractive indices and the film thickness for each sample. The only assumption he makes is that all layers have the same refractive indices. A possible variation on his technique would be to apply a further constraint: that the film thickness is proportional to the number of layers deposited. This does not reduce the validity of the model in any way as a variation in the thickness of individual LB layers would also lead to a refractive index change.

A computer program was written to analyse ellipsometric results by this method (see Appendix 3 for Fortran 77 source code). The number of layers, Δ and ψ were input for each sample and results found for single layer thickness, N_{1o} and N_{1e}.

Fitting was carried out by a method of swiftest descent[8]. The results may easily be transformed to the molecular axes if the tilt angle of the molecules is known.

As an extra assumption has been made, less values are being fitted for (previously the thickness of each sample was treated as an unknown). This should reduce the number of samples required for satisfactory results. A comparision between results from the isotropic model, Den Engelsen's uniaxial model and this new method is given in section 7.1.

5.2 Surface Plasmon Resonance

The wavevector of a Surface Plasmon Polariton is highly dependent on the optical properties of the materials close to the interface along which it propogates. This sensitivity is a product of the high electric field strength at this boundary (see figure 3.7), typically more than ten times that of the incident light. This field induces polarisation in the adjacent layers, hence the wavevector is dependent on their permittivity. Also, if the layer thickness is such that the SPP's perpendicular decay length is split between more than one layer, the wavevector will vary with layer thickness. This high degree of sensitivity makes surface plasmon resonance a valuable technique for measuring the properties of LB layers deposited close to a boundary supporting an SPP.

5.2.1 Experimental Arrangement for Surface Plasmon Resonance

Surface Plasmon Resonance was detected using a Kretschmann configuration[9] (figure 5.6). Here a thin silver film is used, deposited onto a dielectric (ie. glass in this case). The p-polarised light is incident from the dielectric and the SPP is produced on the opposite side of the silver. The reflected intensity as a function of angle is monitored.

The practical arrangement is shown in figure 5.7. HeNe laser light (632.8 nm) is used, the laser is plane polarised and is adjusted to give p-polarisation by rotation

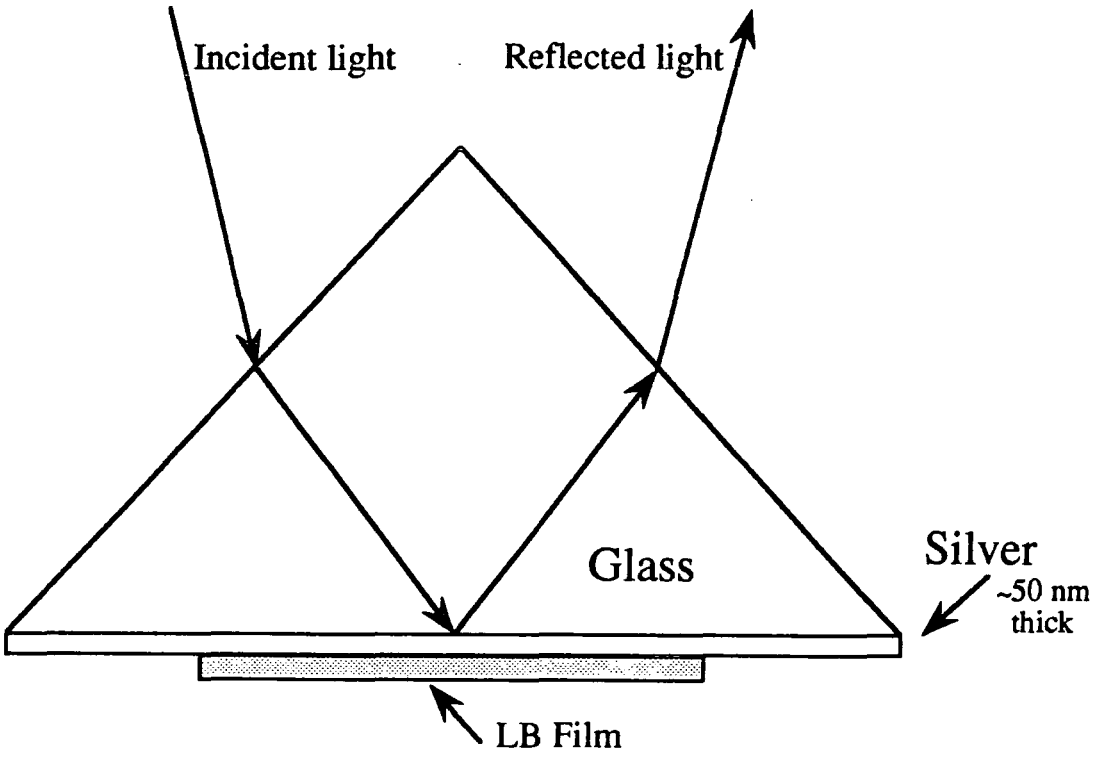

Figure 5.6 - Kretschmann SPR arrangment

within its mount. The glass (n=1.52) prism is mounted on a motorised rotation stage (minimum step size 0.004 degrees) allowing the angle of incidence to be varied. The reflected light is detected by a photodiode also mounted on a rotation stage. The two stages are linked by a gear system so that a θ movement of the prism table gives a 2θ turn of the photodiode; this ensures that the reflected beam always strikes the diode. Instead of depositing the silver film directly onto the prism a silvered slide is used, index matched to the prism by microscope immersion fluid. This is purely for experimental convenience, it is easier to mount microscope slides on a Langmuir trough and the need to have one prism per sample is removed.

The whole system is under computer control (BBC Master Series). The diode voltage is detected at a digital multimeter (which the computer reads via an IEEE interface) as the rotation stages are moved by a stepper motor. This builds up a set of data points giving reflected intensity against number of steps. To convert the number of steps into an angle of incidence it is necessary to calibrate the stage

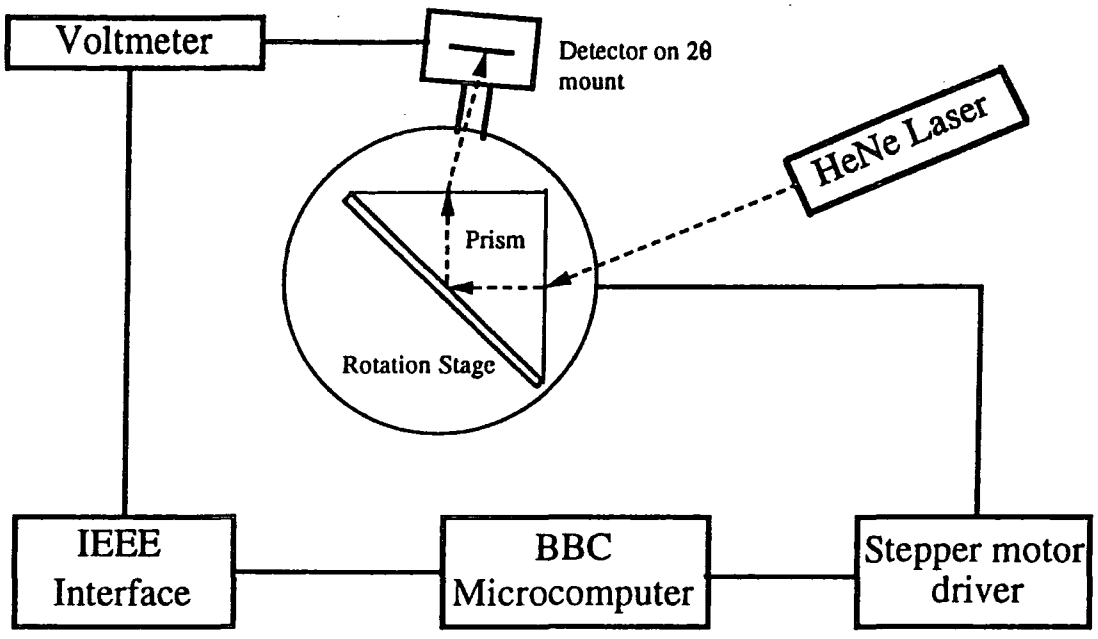

Figure 5.7 - Practical setup for observing Kretschmann SPR

at a datum point. This is achieved by using a plain glass prism with no silvered slide and searching for the critical angle. Knowledge of the prism refractive index allows calibration via the usual Snell's law formula.

The diode voltage was theoretically corrected for reflection loss at the two prism faces to give a set of reflected intensities for the Kretschmann arrangement only. The method of normalising these intensities to give reflectivity is described in the next section.

5.2.2 Fitting of experimental SPR data

The permittivities and thicknesses of the layers in an SPR system may be calculated using the theory described in section 3.5. As the equations cannot be analytically inverted to give layer properties in terms of reflectivities it is neces-

sary to use numerical analysis to find the required values. The technique used is one on minimising the difference between the experimental reflectivity - angle curve and its theoretical counterpart.

The simplest system for Kretschmann SPR consists of a thin silver film separating two dielectric media, in this case glass and air. The two dielectrics may be considered as semi-infinite as their boundaries are too remote from the silver-dielectric interfaces to influence the SPR. Given the permittivities of the glass and air it is obvious that the system is described by just three unknowns, the real and imaginary parts of the silver permittivity and its thickness. By varying these three parameters it should be possible to arrive at a theoretical curve which matches the experimental one. In practice the parameters are iterated to minimise the mean square error $\overline{\sigma^2}$ where

$$\overline{\sigma^2} = \sum (R_i^t - R_i^e)^2 \tag{5.8}$$

where R_i^t is the theoretical reflectivity at the ith angle of measurement and R_i^e is the experimental reflectivity at the same angle[8]. The iterative steps were chosen by a method of swiftest descent. The partial derivatives of $\overline{\sigma^2}$ were calculated with respect to each of the three parameters and the next search point is in a direction opposite to the vector of the three derivatives, ie

$$\begin{pmatrix} \epsilon' \\ \epsilon'' \\ t_l \end{pmatrix}_{i+1} = \begin{pmatrix} \epsilon' \\ \epsilon'' \\ t_l \end{pmatrix}_{i} - s \begin{pmatrix} \frac{\partial \overline{\sigma^2}}{\partial \epsilon'} \\ \frac{\partial \overline{\sigma^2}}{\partial \epsilon''} \\ \frac{\partial \overline{\sigma^2}}{\partial t_l} \end{pmatrix} \tag{5.9}$$

where the i subscript indicates the ith estimate of the parameters and s is the step length to the next estimate (the vector of partial derivatives is normalised to unit length). The step length used is that which gives the smallest mean square error at the next point. The iterative process may be terminated in three ways, by exceeding the maximum number of iterations; by reducing the error to a preset threshold; or when no further improvement in fit occurs. For the best possible

results the latter method should be used.

The method of normalisation used is to equalise the maximum reflectivity of the experimental curve with the reflectivity of the theoretical curve at the same angle (for the current parameter estimates). As the fitting progresses the curve is re-normalised for every iteration. The validity of this approach was confirmed by fitting to a de-normalised set of theoretically generated data. The parameters obtained were close to those originally used to produce the curve; the residual errors are due to the curve only being sampled at a finite number of points (figure 5.8).

For the simple glass-silver-air system it was discovered that the three parameters could be uniquely identified from the SPR curve, provided that an angular range covering both the critical and resonanant angles was used. This is in agreement with reference 10. Typically the average reflectivity difference between theory and experiment was less than 0.5% (figure 5.9).

To fit the properties of Langmuir-Blodgett films on silver it was found to be essential to already know the silver parameters. This was achieved in a number of ways

i) measuring the SPR of a silvered slide before depositing the LB layers,

ii) measuring the SPR of a slide from the same evaporator run as the slide with LB layers

iii) leaving part of the slide uncoated by an LB film.

The best results were obtained from method i), as this allowed the same part of the same slide to be used both before and after LB deposition. Inhomogeneity of the silver films reduced the effectiveness of methods ii) and iii).

After establishing the silver parameters, fitting for the LB layers was attempted.

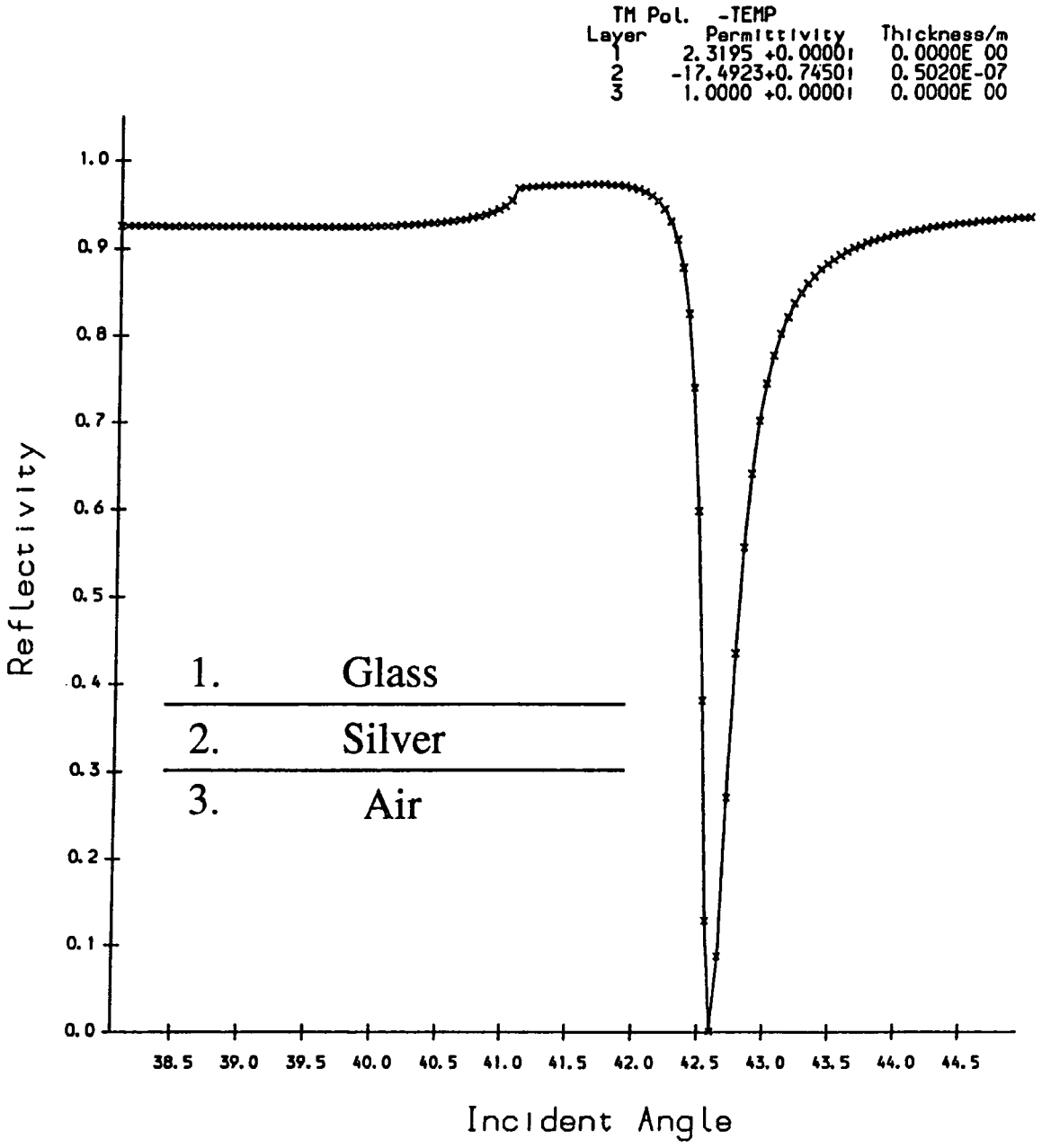

Figure 5.8 - Silver SPR curve fitted to theoretically generated data

It immediately became clear that no unique solution could be found but rather a range of possiblities exist. This is illustrated by figure 5.10 which shows a fit to a theoretically generated curve ($\epsilon_r = 2.5 + 0.05j, t_l = 300\mathring{A}$). Although the fit is mathematically correct it is seen that the layer parameters are not correct.

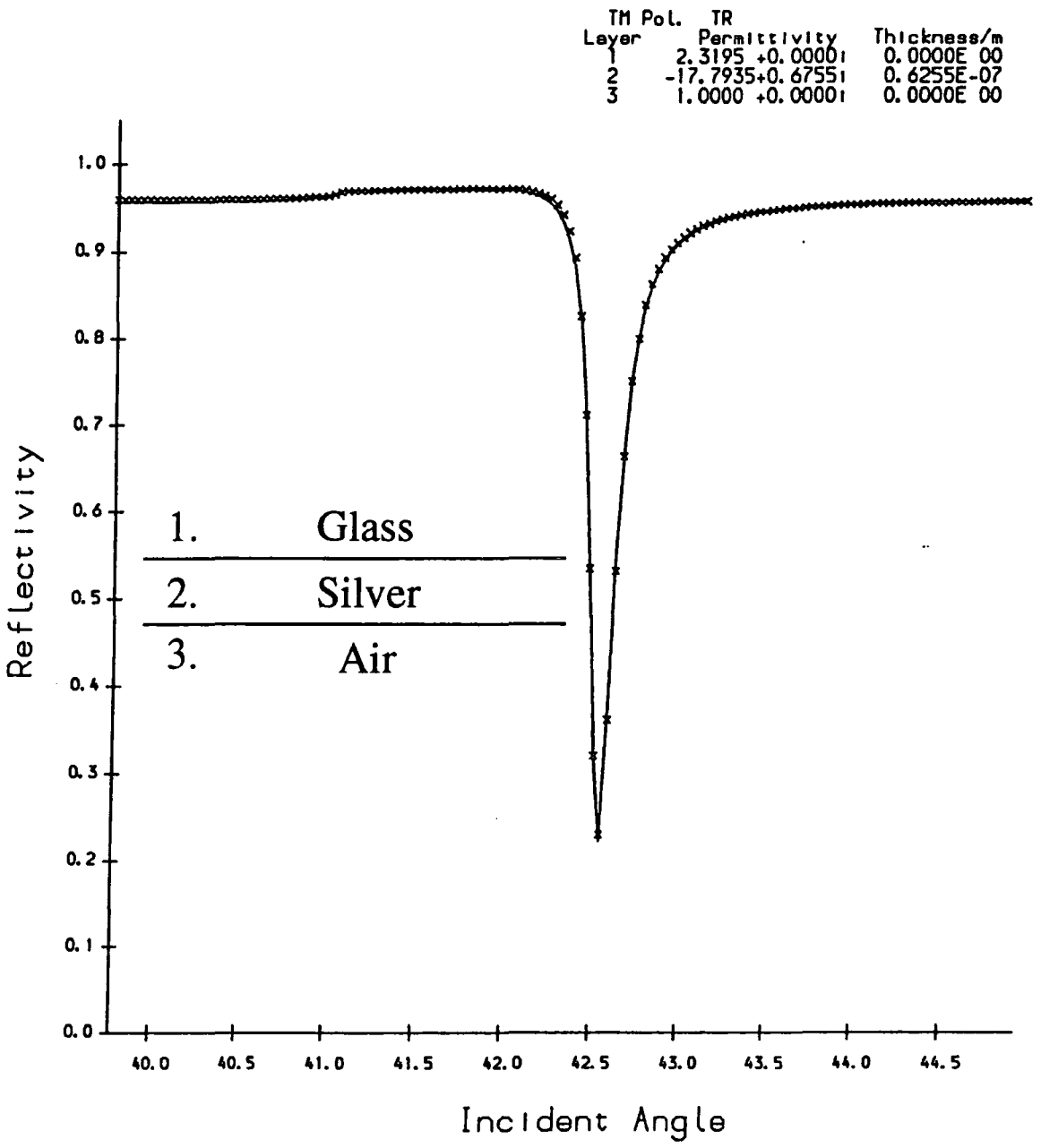

Figure 5.9 - Fitted experimental SPR curve

For LB films (or any other dielectric layer) at least one of the parameters must be known before fitting commences; the other parameter(s) may then be found. The usual method used for the work in this thesis was to find the layer thickness from ellipsometry and then use this result to obtain the permittivity from SPR. This is more satisfactory than using the permittivity given by ellipsometry as this

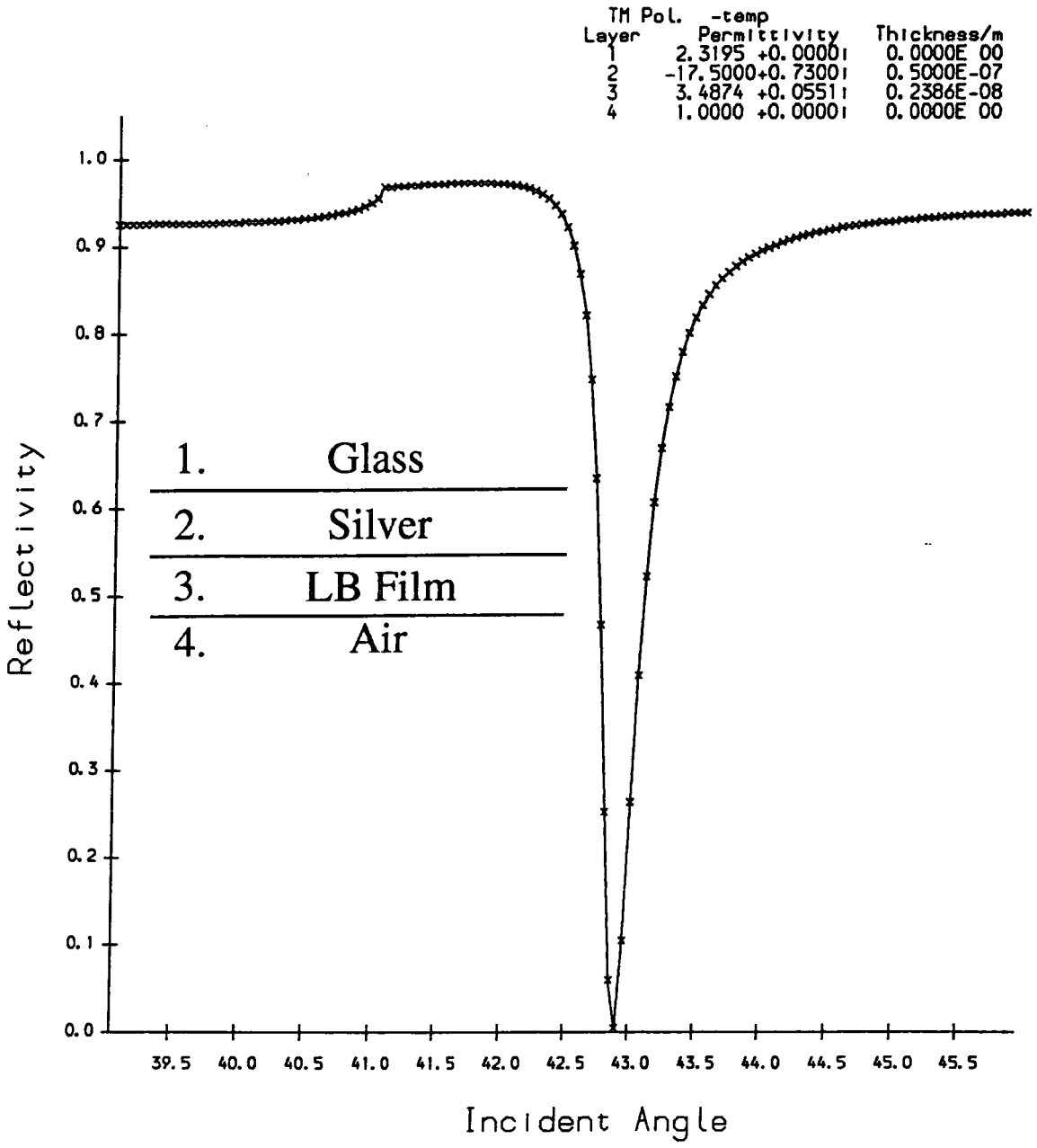

Figure 5.10 - Experimental SPR curve fitted to incorrect parameters

will vary with angle of incidence for uniaxial films. Figure 5.11 shows a fitted SPR curve for a glass-silver-film-air arrangement, the LB film is a monolayer of the dye JT11 (the minima below the critical angle are due to interference with light reflected from the back electrode of the Pockels effect measurement rig - see next section).

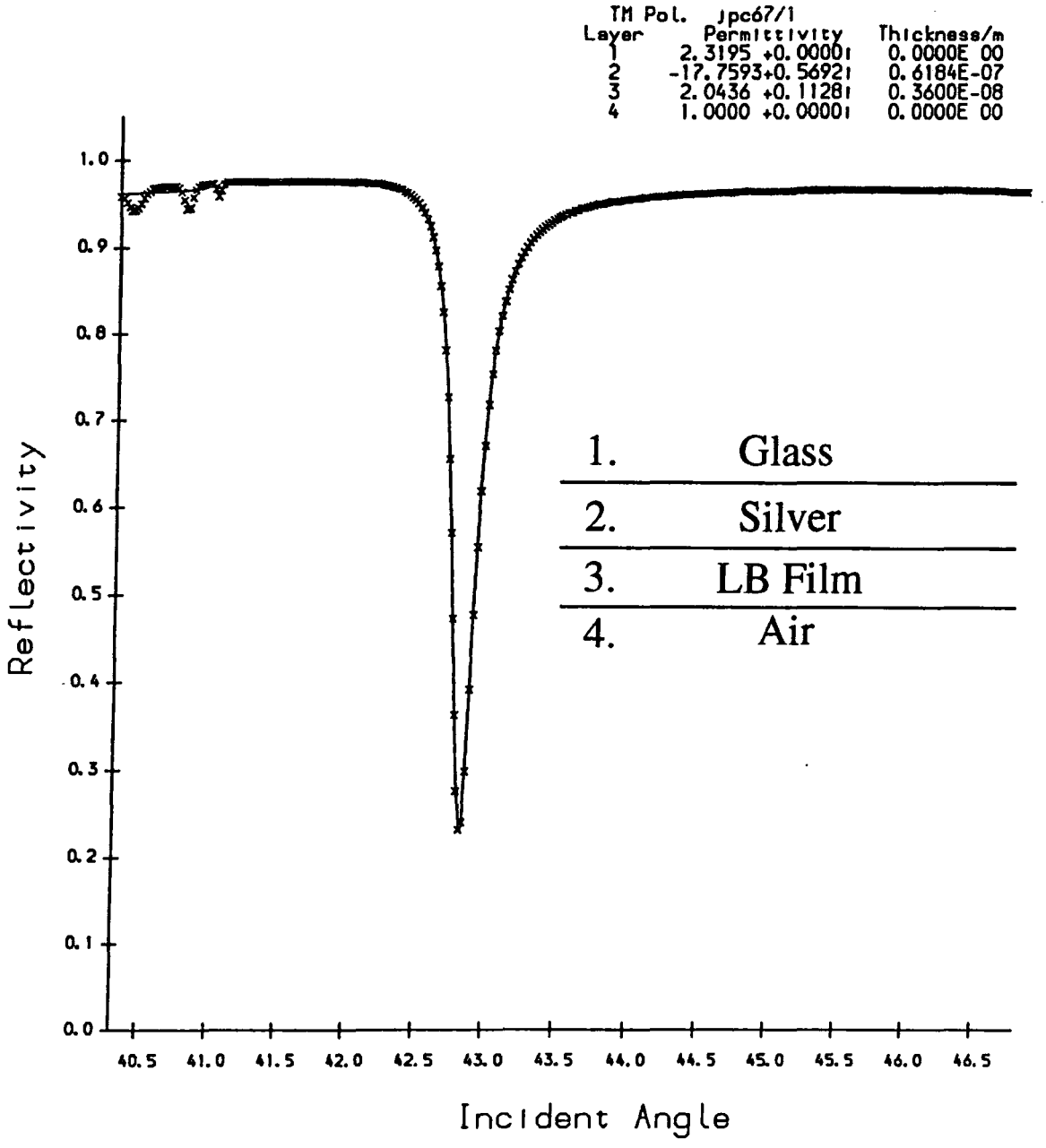

Figure 5.11 Experimentally fitted silver-LB film SPR curve

5.3 Pockels Effect Measurement

The large dependence of SPP wavevector on the optical properties of adjacent layers makes SPR a sensitive tool for detecting small variations in these properties. For example, it may be used to sense changes due to gas absorption[11], condensation of new layers[12] or changes due to intensity dependent refractive index[13].

The Pockels effect is a process by which the refractive index (or permittivity) of a medium changes on application of an electric field. If an experimental arrangment is produced to apply this electric field whilst exciting an SPP it is clear that the small permittivity changes will lead to a change in SPP's wavevector. These changes in wavevector will then lead to reflectivity changes close to the angle of SPR.

If it is assumed that the reflectivity change is due to the permittivity variation of one of the layers near to the SPP interface this can be expressed as:

$$\Delta R = \frac{\partial R}{\partial \epsilon'}\Delta\epsilon' + \frac{\partial R}{\partial \epsilon''}\Delta\epsilon'' \tag{5.10}$$

where the relative permittivity of the layer is $\epsilon_r = \epsilon' + i\epsilon''$.

This is the situation for an electrooptic LB film deposited on an (assumed non-electrooptic) silver layer. Any change in layer thickness (due to electrostriction or piezoelectricity) would also cause a reflectivity change, but these effects are very small and may be neglected (see appendix 2 for a proof of this).

5.3.1 Experimental Arrangement for Pockels effect measurement

The Pockels effect was studied using a modified Kretschmann SPR arrangment[14] (figure 5.12). An indium tin oxide (ITO) transparent electrode has been added, spaced away from the silver and LB film by a photoresist insulator. The resist has been etched away in the region of laser incidence so that the LB film is bounded by air and the surface plasmon resonance angle is therefore unchanged. An ac. electric field is applied between the ITO and the silver layer (ground) which causes variation in the permittivity of the film, and this in turn leads to a reflectivity change close to the resonant angle. The system uses a lock-in amplifier to measure this change; a reflectivity change down to 2×10^{-7} can be detected in this manner. Figure 5.13 shows an SPR curve together with the change in reflectivity due to an applied field.

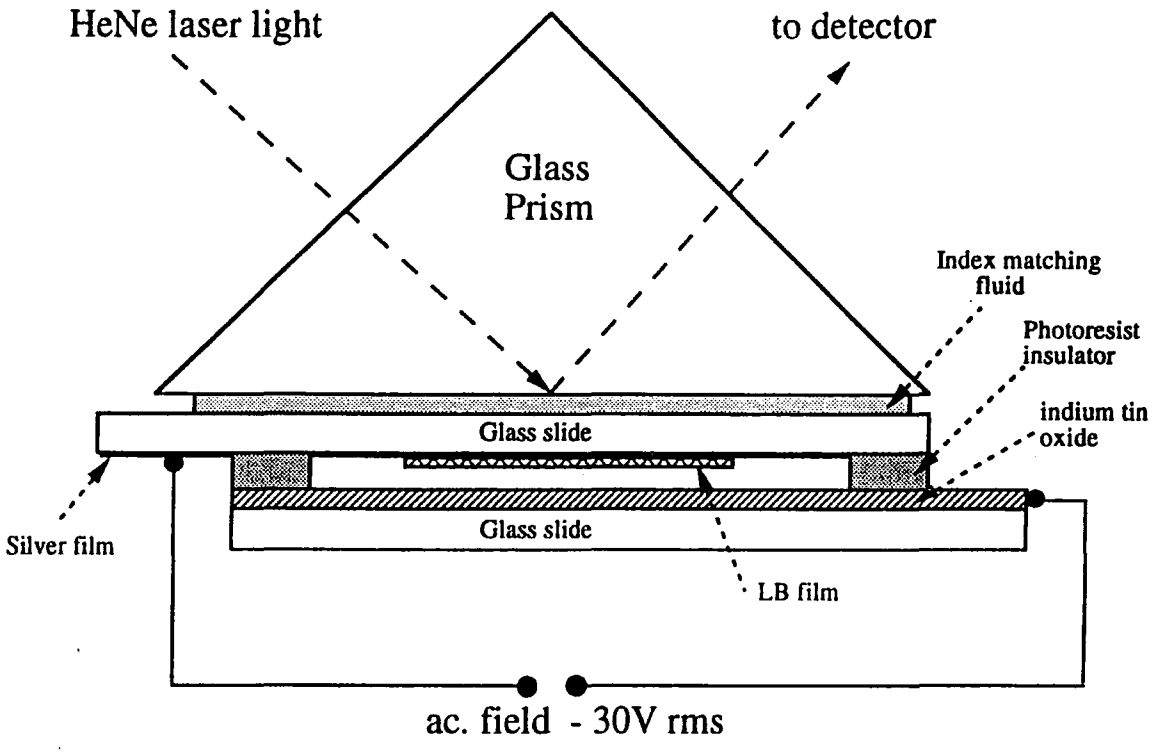

Figure 5.12 - Pockels effect measurement rig

The fitting procedure is extremely strightforward. Equation 5.10 shows that the change in reflectivity is the scaled sum of changes in the real and imaginary parts of permittivity. The scale factors are simply the derivatives of reflectivity with respect to the two parts of permittivity. These derivatives may be calculated numerically at any angle from the permittivities and layer thicknesses obtained from SPR fitting and ellipsometry. It is then a simple matter to find $\Delta\epsilon'$ and $\Delta\epsilon''$ by an iterative process. A computer program was written in Fortrtan 77 to perform this task (see Appendix 3) A typical fit between theory and experiment is show in figure 5.14.

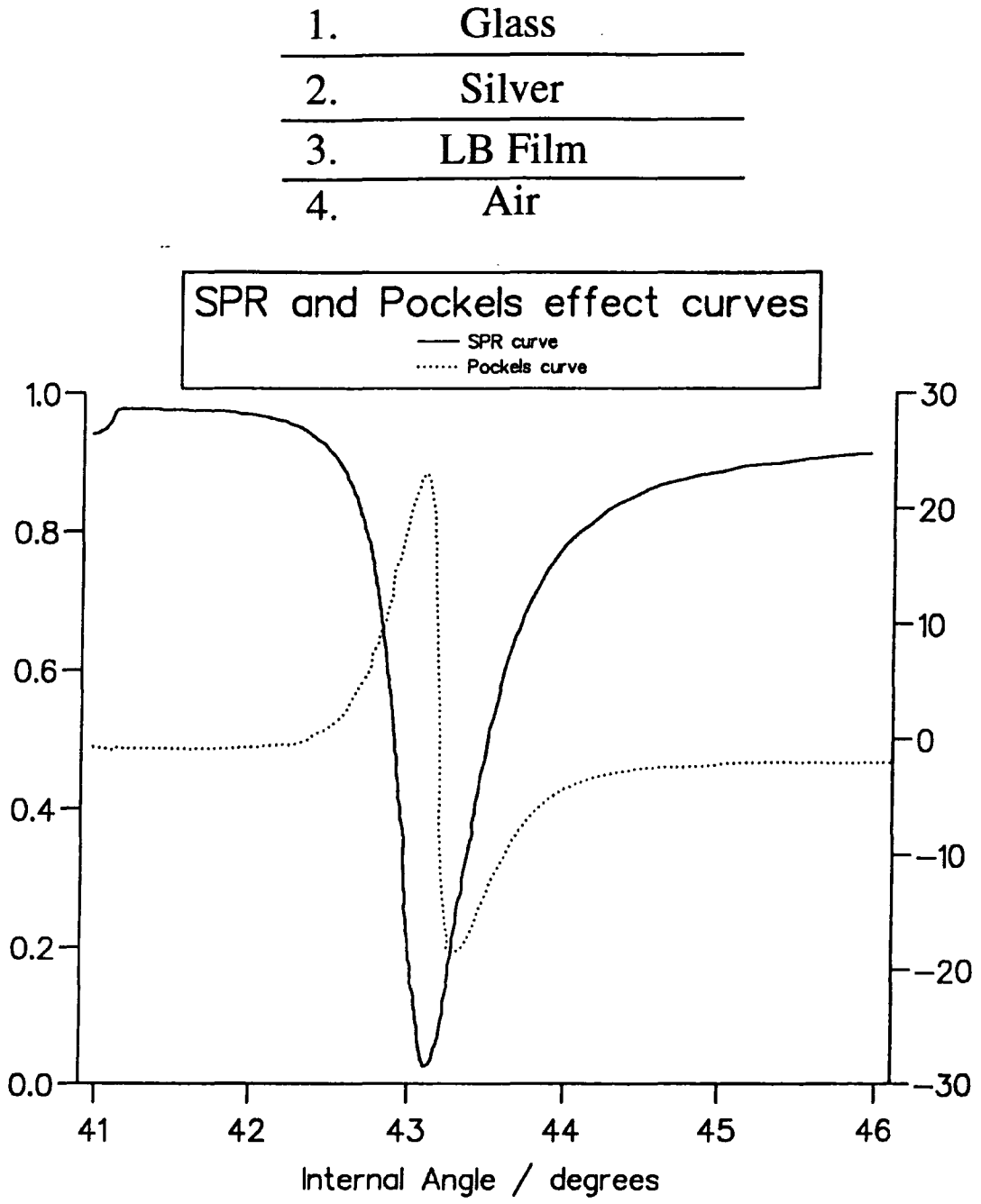

Figure 5.13 - SPR and Pockels effect curves

The second-order nonlinear polarisability is then given by:

$$\chi^{(2)}(-\omega;\omega,0) = \frac{\Delta\epsilon' + j\Delta\epsilon''}{E} \tag{5.11}$$

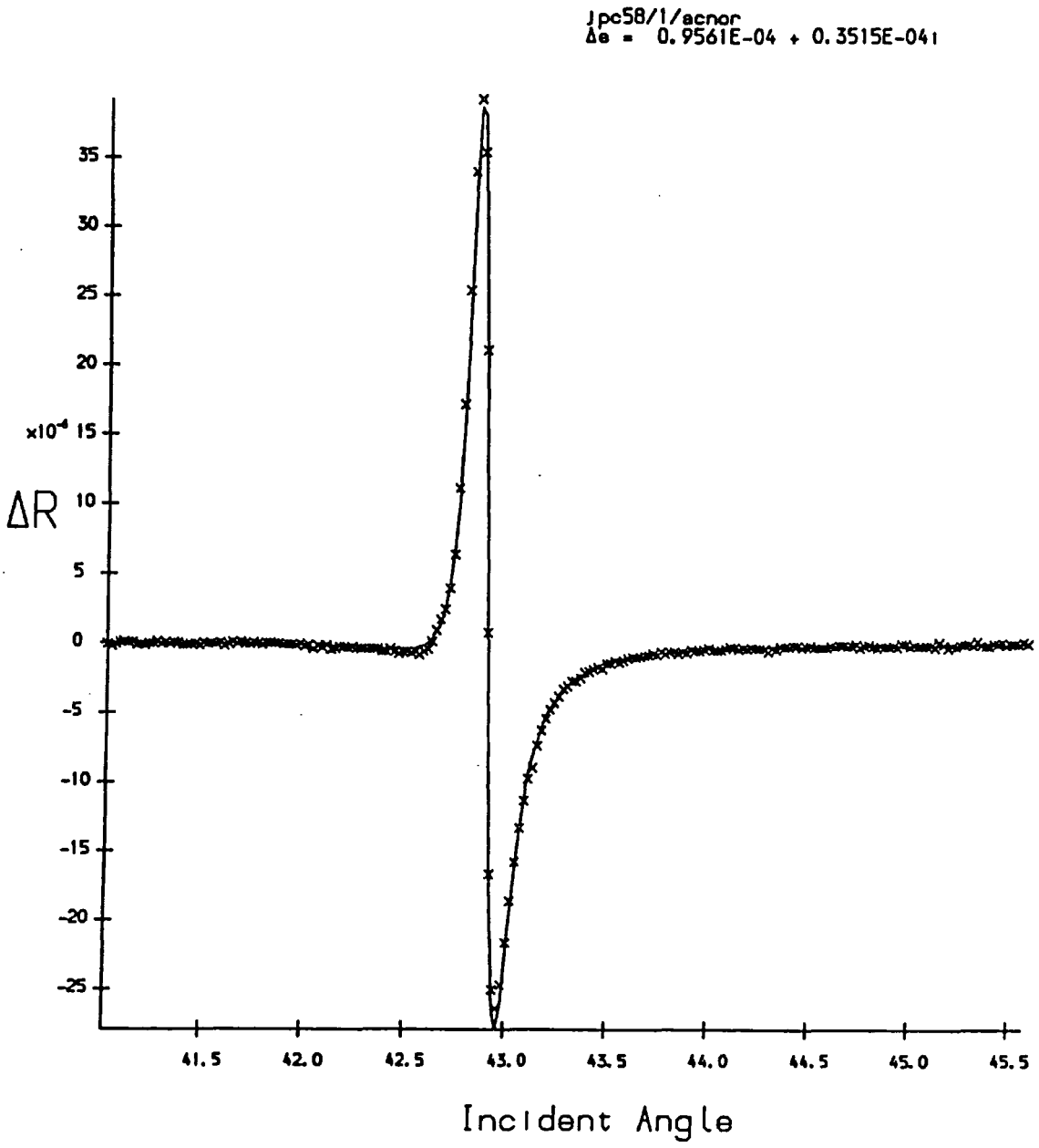

Figure 5.14 - Fitted Pockels effect curve for hemicyanine monolayer

where E is the electric field.

The electric field is the applied rms voltage divided by the electrode gap (6.8 microns from capacitance measurements) and divided by the dc. permittivity of the LB film. This permittivity will typically be greater than or equal to the optical permittivity (as measured by SPR), except when a strong absorption resonantly

enhances the optical value. For the purposes of field calculation the optical value was used unless a low frequency value was also available.

It is clear from equation 5.11 that the sign of $\chi^{(2)}$ may be measured by the Pockels effect. This is in contrast to second harmonic generation where its square is found and sign information is lost. Measurement of the sign of $\chi^{(2)}$ identifies the orientation of the nonlinear chromophores within the film. For the purposes of obtaining the sign of $\chi^{(2)}$ it is important to ensure that the reflectivity change is detected in-phase with the applied field rather than antiphase. This is accomplished by setting the lock-in amplifier phase to 180 degrees to cancel out the inverting effect of the photodiode driver circuit. If the silver film is defined as the ground electrode, a material with positive $\chi^{(2)}$ will shift the resonance to a larger angle. This gives rise to a positive reflectivity change at angles below resonance and a negative change above resonance. Hence it is clear from reference 14 that a hemicyanine monolayer transferred on the upstroke is an example of a material with positive $\chi^{(2)}$.

5.4 Second Harmonic Generation

Second harmonic generation measurements were performed using a Nd- YAG laser at 1.065 μm. Q-switched pulses of 7 ns duration and upto 100 mJ energy were incident on the LB film samples mounted at 45^o to the beam. The fundamental was then removed by 0.532 μm bandpass and infra-red blocking filters allowing the second harmonic to be detected using a photomultiplier. Measurements were made both in reflection and transmission (see figure 5.15)

The magnitude of the input fundamental pulses was measured using a photodiode and then integrating across the pulse length with a boxcar. The input energy was controlled by crossed polarisers and neutral density filters. The second harmonic signal from the photomultiplier was also integrated using the boxcar.

The square law relationship between input intensity (I_ω) and output intensity ($I_{2\omega}$) was confirmed by taking measurements at several input energies. Therefore

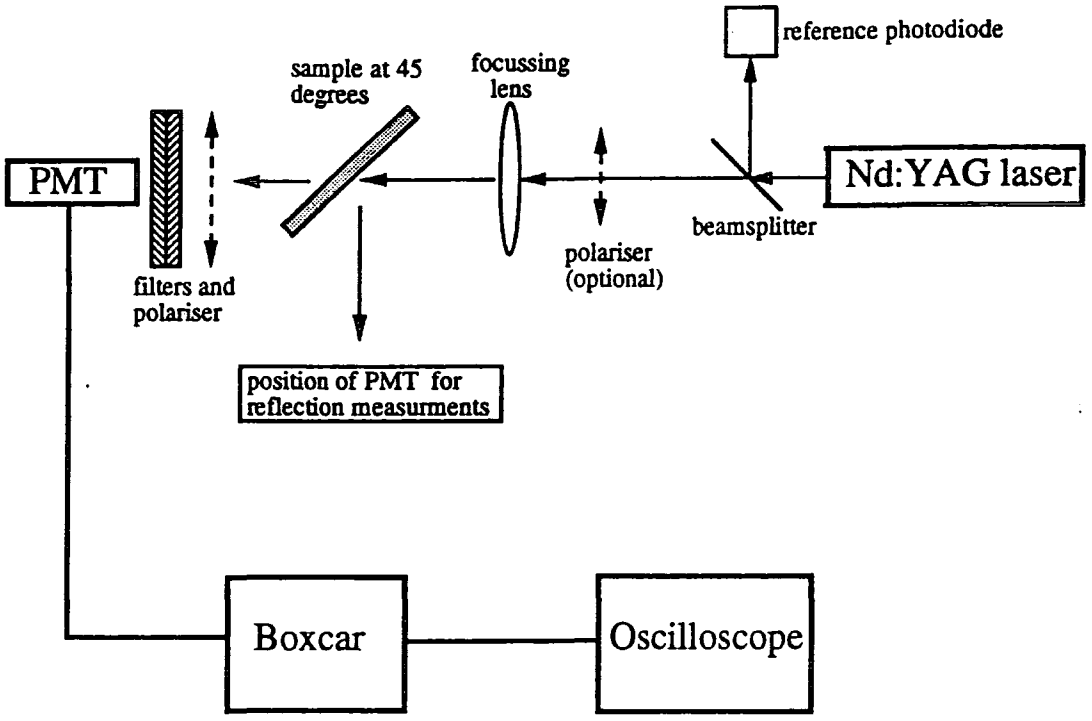

Figure 5.15 - Arrangement for observing SHG

a figure of merit (F) for a sample may be defined as:

$$F = \frac{I_{2\omega}}{I_{\omega}^2}$$

Intensity values (in arbitrary units) may be calculated from the photodiode (E_{PD}) and photomultiplier (E_{PMT}) integrated outputs after making suitable allowance for the presence of neutral density filters (ND_i for input fundamental path, ND_o before the photomultiplier).

The figure of merit is then given by:

$$F = \frac{E_{PD}.10^{ND_i}}{E^2_{PMT}.10^{ND_o}}$$

To provide quantitative results it is necessary to compare with the second harmonic output of a known reference. A monolayer of hemicyanine dye was chosen for this and all results quoted such that its figure of merit is unity.

5.5 Optical Waveguiding

As described in section 3.3 waveguiding provides a convenient method of confining light within a thin layer for the study of nonlinear optical effects. Special techniques are needed to couple light into and out of the waveguide. This may be achieved either by end-fire coupling or prism coupling.

5.5.1 End-fire Coupling into Optical Waveguides

The principle of end-fire coupling is extremely simple. Laser light is focused to a small spot on the end of the waveguide using a microscope objective lens, this light then couples into the waveguide and a magnified image of the output light observed using a second lens at the far end of the guide (see figure 5.16).

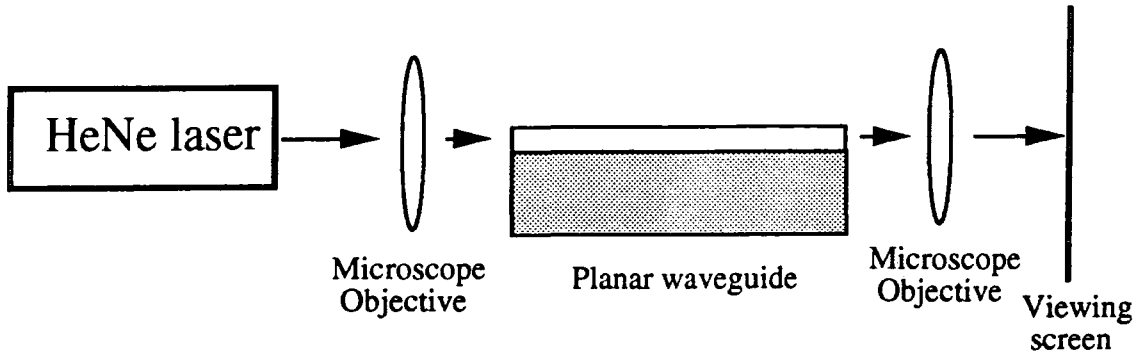

Figure 5.16 - End-fire coupling

In practice their are a number of requirements for successful coupling. Smoothly cleaved or polished end-faces are needed on the guide to prevent scattering of the input and output light. Also the small size of both the light spot and waveguiding layer means that alignment is critical. The objective lenses and waveguide need to be mounted on micron resolution positioners, the arrangement used at Durham is shown in figure 5.17.

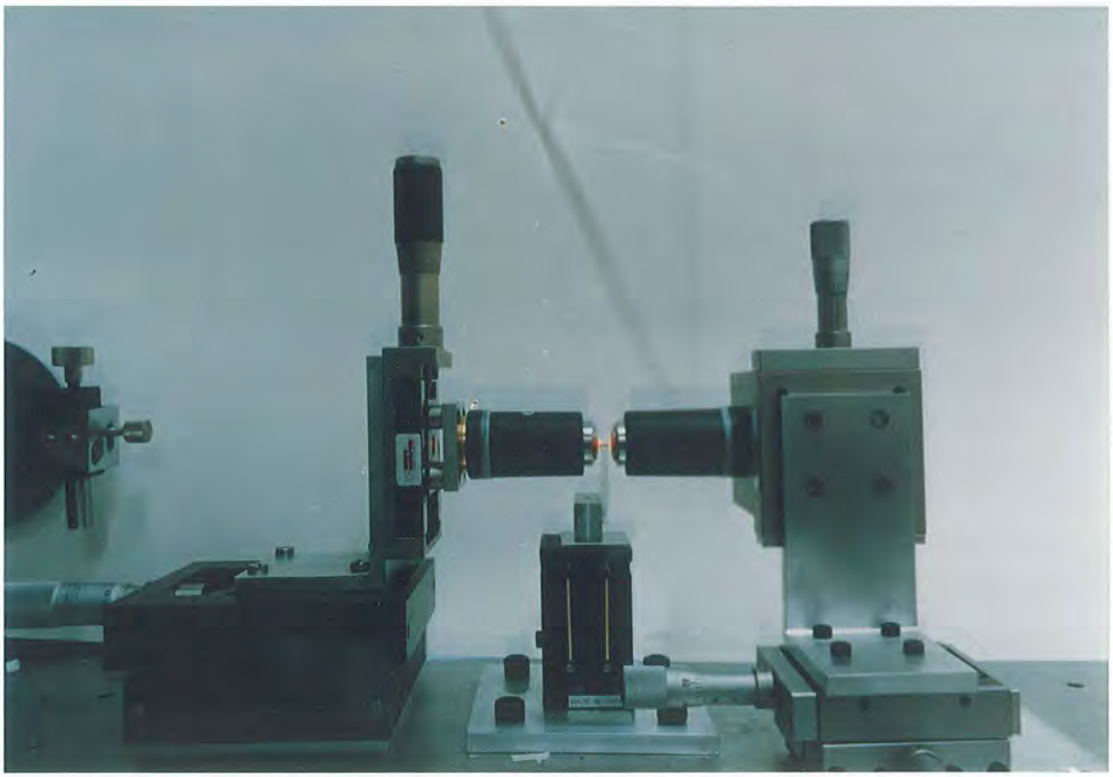

Figure 5.17 - Photograph of the Durham end-fire rig

The first step of the coupling process is to focus the input lens onto the end face of the substrate. If the height of the waveguide is adjusted so the the light is just above the plane of the guide interference fringes will be observed at the output. As the guide is slowly raised the repeat distance of these fringes increases until, at

the point of disappearing, the light is incident on the actual waveguiding region. Final adjustment of the xy position of the two lenses and their focus should now give a magnified output image of the light profile within the guide.

In addition to providing confirmation of waveguiding and information about the intensity profile this technique may be used to study phase modulation by the Pockels effect. If electrodes are deposited on the waveguide and a field applied a refractive index change will occur. For a suitable arrangement of field direction and electrooptic tensor of the guide this will only affect one light polarisation, therefore the other polarisation may be used as a reference. The phase modulation can then be detected by a change in the polarisation properties of the output.

The most important parameter of any waveguide modulator is V_π, the voltage required to give a π radian phase change. Thus in general the phase change (Γ_m) due to a modulating voltage V_m is given by $\Gamma_m = \pi(V_m/V_\pi)$. Yariv[15] describes a technique for measuring the electrooptic properties of a crystal, this can be readily adapted for end-fire studies on a waveguide. The arrangement of figure 5.18 is used. Light is launched with the polarisation at 45 degrees in order to excite equally the TM and TE modes and their relative phase is adjusted by a Soleil-Babinet compensator to give circularly polarised output from the waveguide. Application of a modulating field alters the relative phase of the modes, this may be detected through a second polariser as an intensity modulation I_m. The size of the modulation is given by:

$$\frac{I_m}{I_i} = \frac{\pi V_m}{2V_\pi}$$

where I_i is the input intensity to the waveguide.

Hence V_π for the waveguide may be calculated.

5.5.2 Prism Coupling into Optical Waveguides

Prism coupling[16] provides a method of directly measuring the effective index of

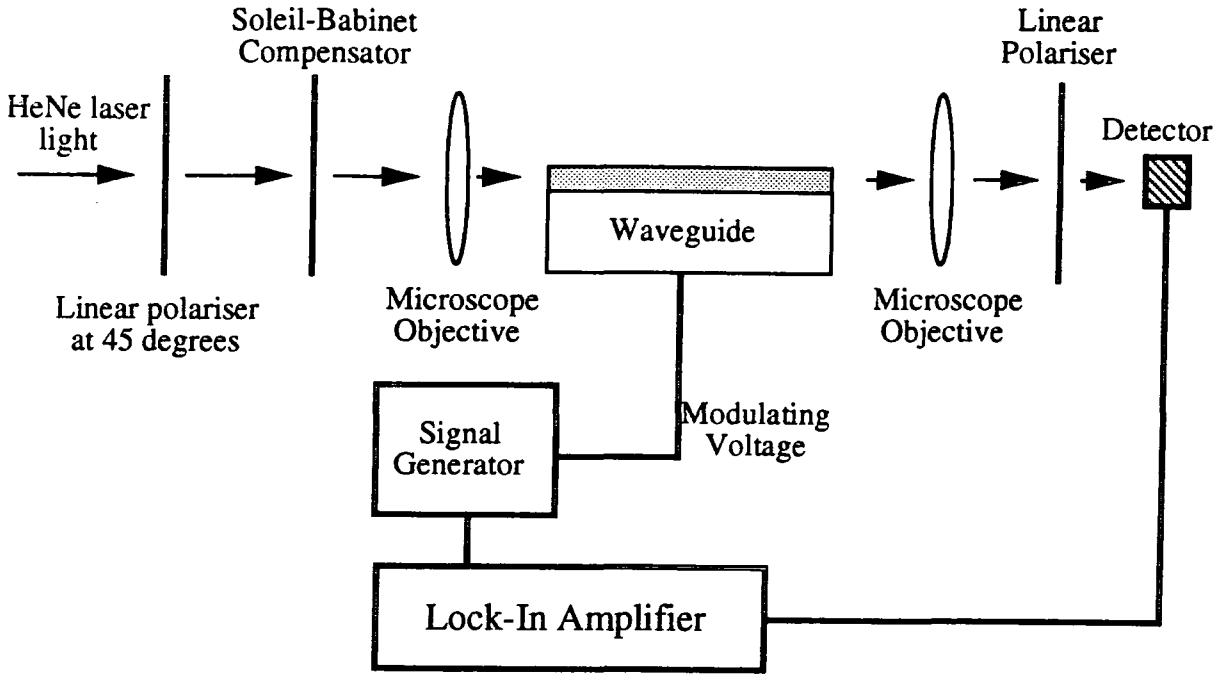

Figure 5.18 - System for measuring the waveguide electrooptic properties

the modes in a waveguide (see section 4.6). As shown in figure 5.19 the input light is incident on a prism the base of which is brought close to the waveguide. Coupling takes place in the region of total internal reflection for the prism so only evanescent waves are present in the region beyond the base. Hence the air gap must be of the order of the decay length of these waves (typically $\sim \lambda$).

For coupling to occur the wavevector z-component of the light in the waveguide must match that of one of the guided modes, ie:

$$k_o n_p \cos\theta = k_o n_{eff}$$

Therefore coupling occurs only for a finite number of discrete angles, one for each guided mode.

A second prism may be added to the arrangment to couple light out of the waveg-

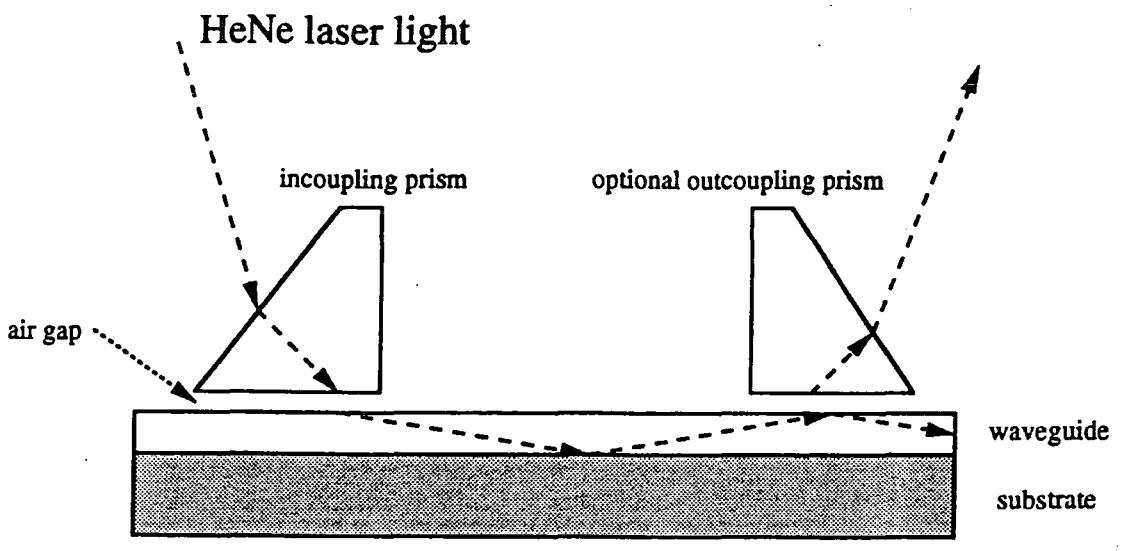

Figure 5.19 - Prism coupling

uide; by varying the distance between the prisms the waveguide propagation loss may be measured.

5.6 X-ray Diffraction

Langmuir-Blodgett multilayers may be studied using X-ray diffraction; typically of the order of 50 layers are required. The X-ray measurements for this thesis were carried out by Dr. Yuri Lvov at the Institute of Crystallography, Moscow. A purpose built position- sensitive small-angle X-ray diffractometer was used[17]. The Cu Kα radiation (λ=0.154 nm) was nickel filtered and collimated by a three-slit collimator. The paths of incident and scattered beams were under vacuum. The detector sensitivity was 0.1 mm (equivalent to an angular resolution of approximately 0.01^o); the diameter of the X-ray beam was assumed to be 0.04^o.

Two quantities could be derived from the X-ray diffraction results, the repeat distance for the structure and the radius of correlation. The repeat distance d_r is found from the usual Bragg formula:

$$2d_r \sin\theta = n\lambda$$

The radius of correlation is a measure of the interlayer order in the material and may be found from the width of the diffraction peaks. It is defined as the distance over which a mismatch equal to half the layer spacing builds-up in the structure.

5.7 Fourier Transform Infra-Red Spectroscopy

A number of films were studied for their infra-red absorption properties using a Fourier transform method. This work was carried out by Dr. Y. Song of the Department of Chemistry, Durham University.

Two distinct experimental configurations were used, Reflection Absorption Infra-Red Spectroscopy (RAIRS) and Attenuated Total Reflection (ATR). For the RAIRS technique films were deposited onto silver coated slides, the measurement was then performed at a glancing incidence (85 degrees). This method is only sensitive to film properties normal to the substrate. For the ATR measurements the films were coated onto a zinc selenide crystal and the results obtained are an average of all directions in the film. For both techniques the spectra produced consist of a series of absorption bands. Comparision of band position with published data allows the assignment of the absorption with an individual bond type within the molecule.

By comparing the results from RAIRS and ATR the presence of orientation dependent absorption can be detected, this property is known as linear dichroism. If no such orientation dependence is present the two spectra will differ only in amplitude, ie. all absorption bands will be in the same ratio. If however the material is dichroic each individual band will occur in the two spectra in a proportion related to the orientation of its assigned bond. Calculation then allows each bond angle to be found and the overall molecular alignment to be established.

5.8 Summary

Langmuir-Blodgett films may be readily studied for their linear optical, nonlinear

optical and structural properties by a number of methods. These include ellipsometry, surface plasmon resonance, second harmonic generation, X-ray diffraction and Fourier transform infra-red spectroscopy. Waveguiding systems may be investigated by prism and end-fire coupling.

References

1. R.M.A. Azzam *Surface Science* **56** pp6-18 (1976).
2. E. Hecht *Optics* (Addison Wesley 1987) pp94-104.
3. R.M.A. Azzam, N.M. Bashara, *Ellipsometry and Polarised Light* (North Holland 1977) pp173-4.
4. R.M.A. Azzam, N.M. Bashara, *Ellipsometry and Polarised Light* (North Holland 1977) pp166-9.
5. R.M.A. Azzam, N.M. Bashara, *Ellipsometry and Polarised Light* (North Holland 1977) pp175-180.
6. R.M.A. Azzam, N.M. Bashara, *Ellipsometry and Polarised Light* (North Holland 1977) pp283-8.
7. D. Den Engelsen, *J. Opt. Soc. Am.* **61** pp1460-6.
8. W.H. Press, B.P. Flannery, S.A. Teukolsky, W.T. Vetterling, *Numerical Recipes* (Cambridge University Press 1986) p302.
9. E. Kretschmann, *Z. Physik* **241** p313.
10. S. Cowen, J.R. Sambles *private communication.*
11. J.P Lloyd, C. Pearson, M.C. Petty, *Thin Solid Films* **160** p431.
12. J.R. Sambles, J.D. Polland. G.W. Bradbury, *Opt. Commun.* **63** (5) pp298-300.
13. Y.J. Chen, G.M. Carter, *Appl. Phys. Lett.* **41** (4) pp307-9.
14. G.H. Cross, I.R. Girling, I.R. Peterson, N.A. Cade, *Elec. Lett.* **22** pp1111-3

(1986).

15. A. Yariv, *Optical Electronics* pp292-3 Holt, Rinehart and Winston (1985).

16. R. Ulrich, R. Torge, *Applied Optics* **12** (12) (1973).

17. L. A.Feigin, Y.M. Lvov, V.I. Troitsky *Soviet Scientific Reviews Physics Reviews* **11** (4) pp285-376 (1989).

Chapter 6
Langmuir-Blodgett Deposition Results

This chapter catalogues the materials investigated and describes their Langmuir-Blodgett deposition properties.

6.1 Materials from the literature

A number of compounds previously used for Langmuir-Blodgett deposition were selected from the literature for further study. These were chosen to serve four purposes:

i) for producing mixed monolayers to enhance the film forming properties of the novel compounds;

ii) to form alternate-layer systems with novel molecules;

iii) to carry out Pockels effect measurements on materials previously assessed by second harmonic generation; and

iv) to establish the correct operation of new equipment and mathematical methods by comparing results with those of other workers.

Fatty acids are by far the most widely studied LB materials, having been investigated by the earliest workers in the field[1,2]. They are also among the most readily deposited molecules and are often mixed with less amenable substances to improve their properties. The fatty acids used were 22-tricosenoic acid[3] (22-TA), and stearic acid[4] (see figure 6.1). The latter is frequently deposited with divalent ions in the subphase (eg. cadmium), this leads to the deposition of salt or mixed salt/acid films.

An amphiphilic diacetylene was also used to form mixed monolayers. Not only does this form high quality LB films but also these films are polymerisable for greater stability. Diacetylenes are categorised by the position of the triple bonds;

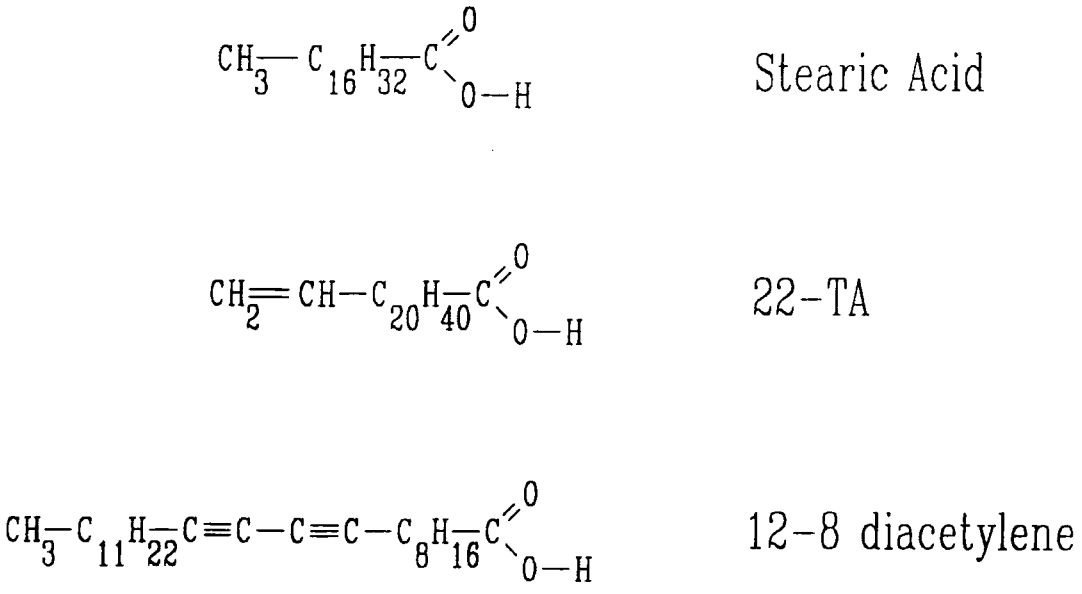

Figure 6.1 - Fatty acid molecules

the example used here is known as 12-8 diacetylene[5], from the numbers of carbon atoms on each side of the diacetylene group (figure 6.1).

Two nonlinear dyes were chosen from the literature for further investigation, these are shown in figure 6.2. Hemicyanine has been previously studied for its second harmonic generation[6] and Pockels effect response[7], both as a pure film and as a mixture with 22-TA[8]. 4-HANS[9] (4-*n*-Heptadecylamido-4′-nitrostilbene) has also been well studied for second harmonic generation (alone and alternated with hemicyanine) but not for its Pockels effect. The two dyes are complementary in terms of donor-acceptor orientation, the relevant groups are clearly marked in figure 6.2. Therefore, one or the other should be suitable for alternation with any novel material.

6.2 Novel Compounds

A number of novel materials were obtained from a variety of sources for investigation of their LB deposition and nonlinear optical properties. All of these were

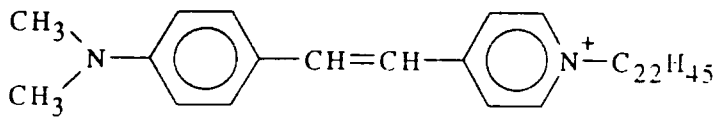

Hemicyanine

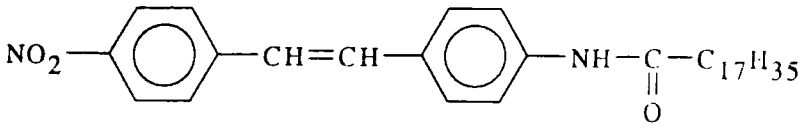

4-HANS

Figure 6.2 - Hemicyanine and 4-HANS

designed following the rules outlined in section 2.4.1, that is they contain donor and acceptor groups separated by a π electron system. This is expected to give rise to significant second-order nonlinear properties. The molecules were also, on the whole, designed to be amphiphilic which should lead to successful LB deposition.

6.2.1 Functionalised diarylalkynes

This group of compounds was synthesised by Dr. John Tsibouklis of the Chemistry Department, University of Durham[10]. A benzene ring and a pyridinium group are linked by an alkyne bridge to from an extended π electron system. The pyridinium moiety acts as the acceptor group, a number of different donor groups were then attached to the benzene ring in the para position to provide a series of compounds. The two examples studied for this thesis used a bromine and methoxy donor respectively, the results of other materials in the series have been reported previously[11]. The hydrophobic alkyl chains were attached to the pyridinium donor, this means that the sign of $\chi^{(2)}$ will be the same as for hemicyanine (ie. positive for a monolayer transferred on the upstroke).

The two molecules, JT3 and JT11 are shown in figure 6.3. In the solid state both were very dark blue-black powders.

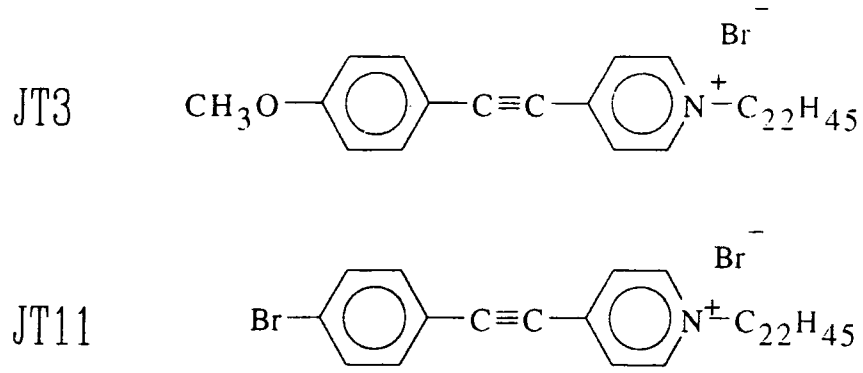

Figure 6.3 - Functionalised diarylalkynes

6.2.2 Diphenyl butadiynes

These contain two benzene rings joined by a diacetylene group and were synthesised by Dr. John Tsibouklis[12]. In each case an acceptor group was formed by attaching a nitro moiety in the para position of one of the rings. A variety of groups were joined to the other benzene ring to act as donors (see figure 6.4). The design of these molecules was also intended to give the possibility of polymerisation at the diacetylene groups by exposure to ultra-violet light. This would leave the conjugated system intact so should not reduce the nonlinear effects. All these materials were coloured pale yellow.

6.2.3 pNA and mNA derivatives

A number of nitroanilines have been studied for their nonlinear optical properties, these include para-nitroaniline (pNA), meta-nitroaniline (mNA) and 2-methyl-4-nitroaniline (MNA) (figure 6.5). Derivatives of pNA and mNA derivatives were prepared with the amine group replaced by an amide and a hydrophobic alkyl chain attached to make them suitable for Langmuir-Blodgett deposition. These materials were synthesised by Dr. John Tsibouklis to study their pyroelectric properties; the opportunity was also taken to investigate their nonlinear optical effects. The

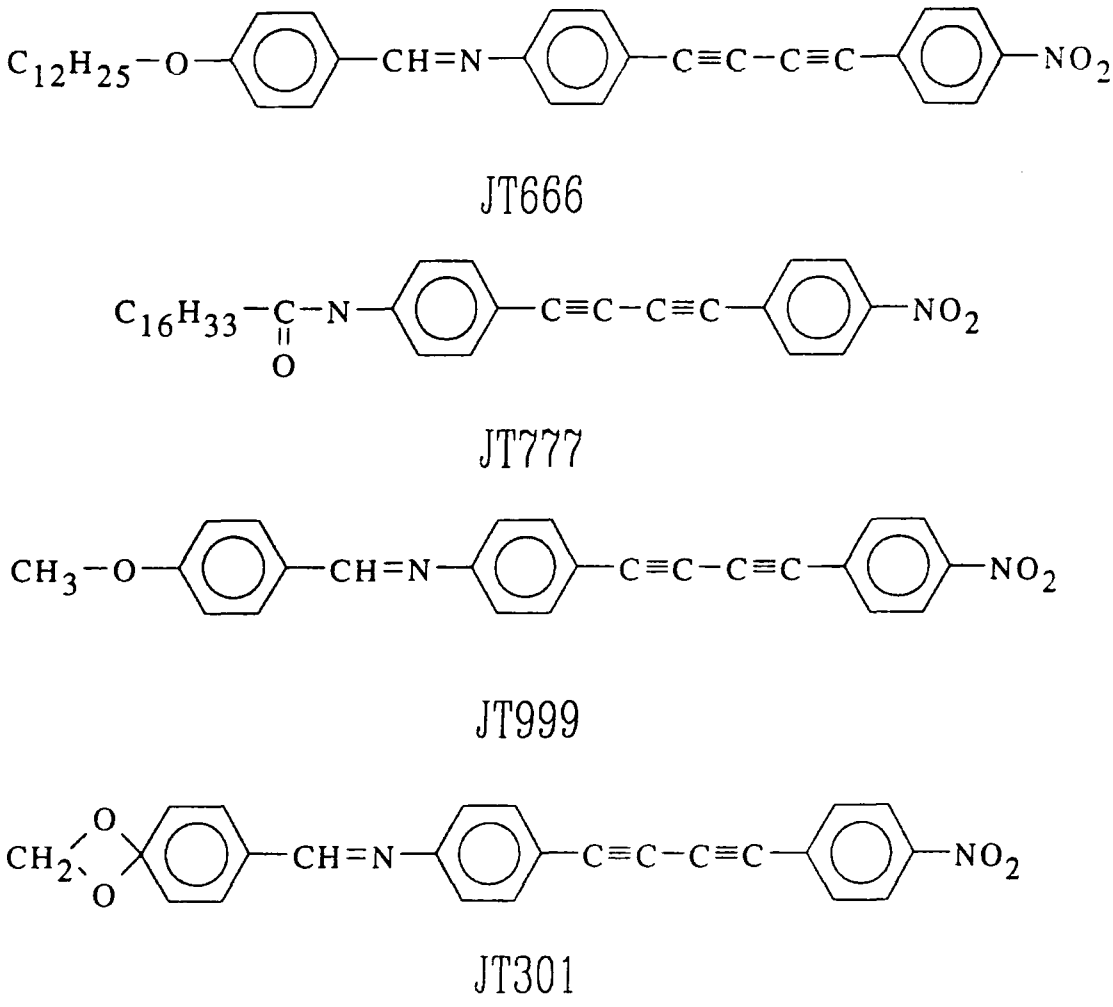

Figure 6.4 - Diphenyl butadiynes

molecules are shown in figure 6.5, JYT19 and JYT21 are the derivatives of pNA and mNA respectively. Both were white powders.

It is interesting to note that although pNA has a larger β than mNA[13], it shows no second-order effects as a crystal due its centrosymmetric structure.

6.2.4 Aminonitrostilbene carboxylic acids and methyl esters

Several stilbene based dyes have already been studied for their nonlinear properties. These include a stilbazium salt [14], an amidonitrostilbene[9] (4-HANS) and an

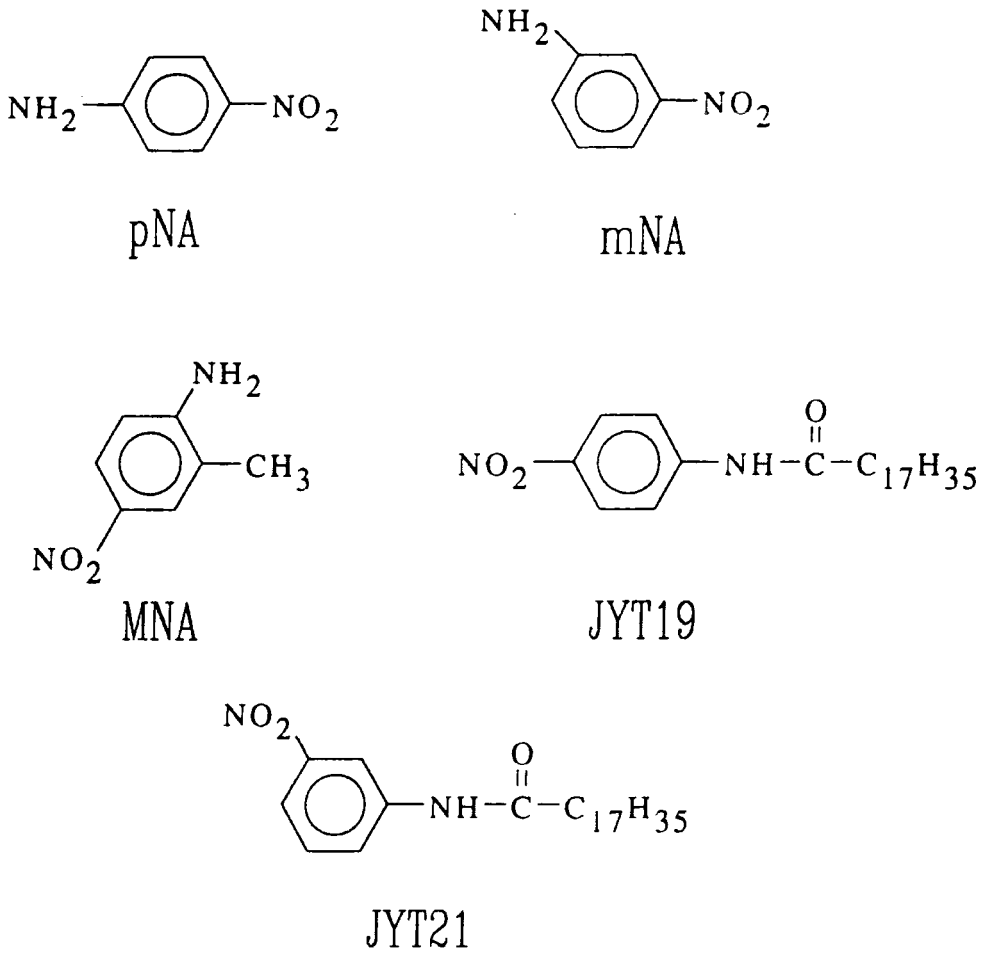

Figure 6.5 - Nitroaniline derivatives

aminonitrostilbene[8]. The stilbazium material exhibits one the largest second-order susceptibilities for a Langmuir-Blodgett film at $\chi^{(2)}(-2\omega;\omega,\omega) = 231 \times 10^{-22}$C V^{-2}, whilst the value for 4-HANS is more modest (2×10^{-22}C V^{-2}).

A group of aminonitrostilbene carboxylic acids was provided by Dr. N. Ratcliffe of British Aerospace, along with one aminonitrostilbene methyl ester (see figure 6.6). Similar substances have already been demonstrated to show second harmonic generation[15]. As the materials differ only the lengths of chains attached they are expected to possess roughly similar values of $\chi^{(2)}$; however their Langmuir-Blodgett properties may differ. The carboxylic acid and ester groups are expected to be hydrophilic and the alkyl chain to be hydrophobic but it is unclear how the chromophores will align. For example, the chromophore in 4-HANS is terminated

by a nitro group which sits in the subphase, if these compounds behave similarily then a negative value of $\chi^{(2)}$ will result. However the acid and ester groups may prove to be more strongly hydrophilic, in which case the nitro group may be forced to point away from the subphase. The direction of the Pockels effect signal will therefore help to determine the true orientation.

All the above compounds were red in solid form.

MA

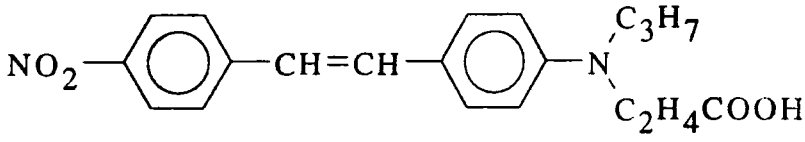

1-19A

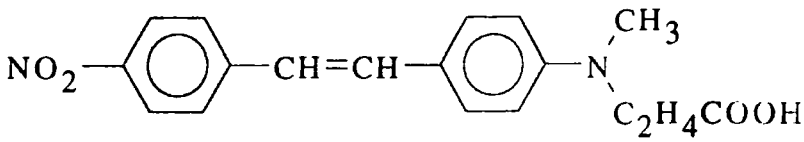

GSC

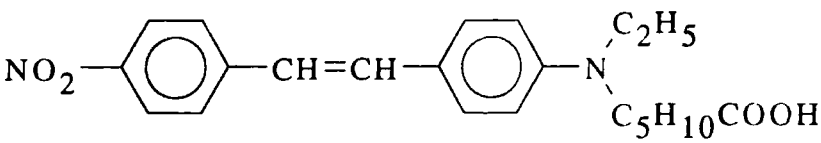

1-40A

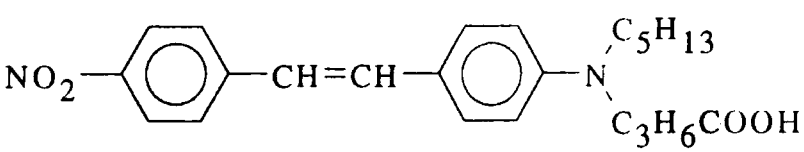

1-40II

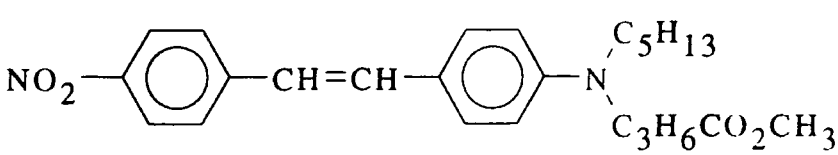

Figure 6.6 - Aminonitrostilbenes

6.2.5 Oligomeric Materials

Although substantial nonlinear effects have been obtained in LB films, their thermal and mechanical properties are usually poor. In an effort to solve these problems polymers have been tried[16,17]. However it is often found that their film forming properties are inferior to those of monomeric LB materials. A possible compromise is to utilise oligomers which are expected to show greater stability than monomers whilst retaining their excellent deposition properties.

A pair of oligomers was provided for study by Dr S. Allen of ICI Wilton Materials Research Centre. The molecular structures are given in figure 6.7. The red material S119191 derives its nonlinearity from the long conjugated azobenzene systems (three per molecule). These are polarised by the nitro acceptor and amide donor groups. The hydrophobic chains are joined to the acceptor side, this is expected to give rise to positive $\chi^{(2)}$ for an upstroke transferred monolayer. Second harmonic generation results for monolayers and layers alternated with a fatty acid have already been reported by ICI[18]. The second oligomer (S122699) is white and contains only a short conjugated system (a single benzene ring) and no acceptor group. This molecule is designed as a passive spacer for alternation with the active material.

6.2.6 Miscellaneous Compounds

A pair of functionalised 4-pyrrolidino-pyridenes (JT9 and JT15), differing only in alkyl chain length, was synthesised by Dr. John Tsibouklis (figure 6.8). Both were white in colour.

Similarily, two functionalised 4-N-dimethylaminopyridenes were obtained from the same source. These have a short conjugated system of a single pyridinium group with an amine donor attached (JT10 and JT12). JT10 was coloured pale orange/pink but JT12 was white.

For all these four materials the hydrophobic chain is joined to the pyridinium

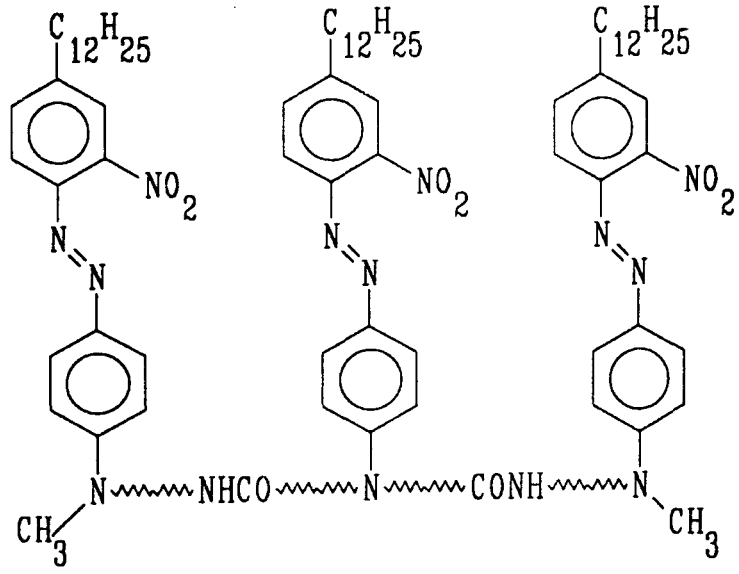

S119191

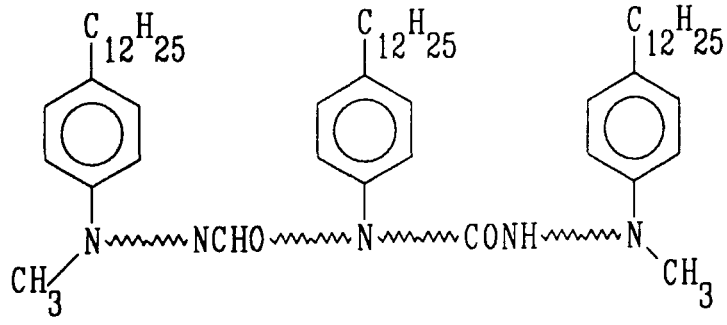

S122699

Figure 6.7 - Oligomeric NLO materials

donor. This arrangement is the same as for hemicyanine thus a similar sign of $\chi^{(2)}$ was anticipated.

An asymmetrically disubstituted stilbene was also provided by Dr. John Tsibouklis (JT201). This was white in solid form.

JT9

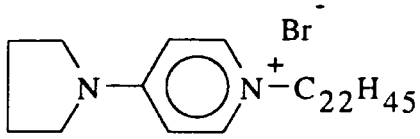

JT15

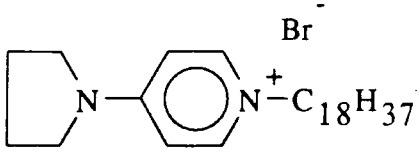

JT10

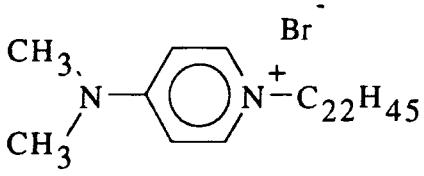

JT12

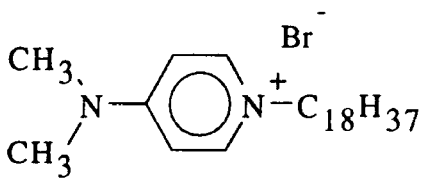

JT201

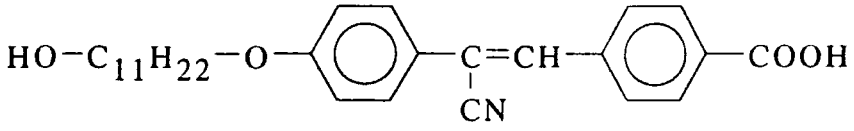

Figure 6.8 - Miscellaneous materials

6.3 Langmuir-Blodgett Deposition

All the materials were dissolved in chloroform at concentrations of approximately 1 g l^{-1}, with the exception of JT201 which was insoluble in this solvent. JT201 was also insoluble in benzene, dichloromethane and acetonitrile; however tetrahydrofuran was subsequently identified as a suitable solvent.

The solutions were then spread dropwise onto the subphase surface of the trough in quantities of 50, 100 or 200 μl and slowly ($\sim 10^{-3}$ nm^2 molecule^{-1} s^{-1}) compressed to produce isotherms. A suitable pressure having been chosen by reference to the isotherm, the materials were controlled and their area change with time noted. If a stable area was obtained an attempt to transfer films to substrates was then made. In cases where no transfer occurred the rigidity of the film was examined by the suction test.

6.3.1 Materials from the literature

The Langmuir-Blodgett properties of fatty acids have been extensively studied previously and suitable film transfer conditions established. For this reason, no further studies were carried out. Films transferred readily to hydrophobic, hydrophilic and silvered glass at a surface pressure of 30 mN m^{-1}

The hemicyanine dye has been studied for its LB film deposition, second harmonic generation and Pockels effect. The alteration to its properties by forming mixed monolayers with 22-TA have also been looked at[8]. As with all monomeric LB materials, its thermal and mechanical properties are poor. In an effort to improve these it was decided to form mixed monolayers of hemicyanine with a diacetylene monomer and then polymerise the latter by exposure to ultra-violet light. This should give a film containing hemicyanine molecules within a polydiacetylene matrix.

As a first step towards working on mixed layers, films of pure diacetylene were prepared using the conditions described in Reference 9 (pH 6.1, 15 mN m^{-1} surface pressure). As expected, Y-type deposition was observed. Solutions of hemicyanine and diacetylene were then mixed at several ratios (molar percentage of hemicyanine 5.9 mol%, 12.4 mol%, 19.5 mol% 27.4 mol%). Isotherms were produced for each mixture and the changing shapes are shown in figure 6.9. In each case the forms are simple and show no signs of phase transitions, except for 27.4 mol% hemicyanine where a small point of inflection is noted at just above 35 mN m^{-1}. The molecular area scale of the isotherms is the average area for the two types of molecules.

For all molar proportions the monolayer could be controlled at 35 mN m^{-1} and the area stabilised after 60 minutes. The mixture with 27.4 mol% hemicyanine was also controlled at 25 mN m^{-1} in order to prepare films away from the inflection point of the isotherm.

Film transfer was accomplished onto hydrophobic glass slides at all molar ratios.

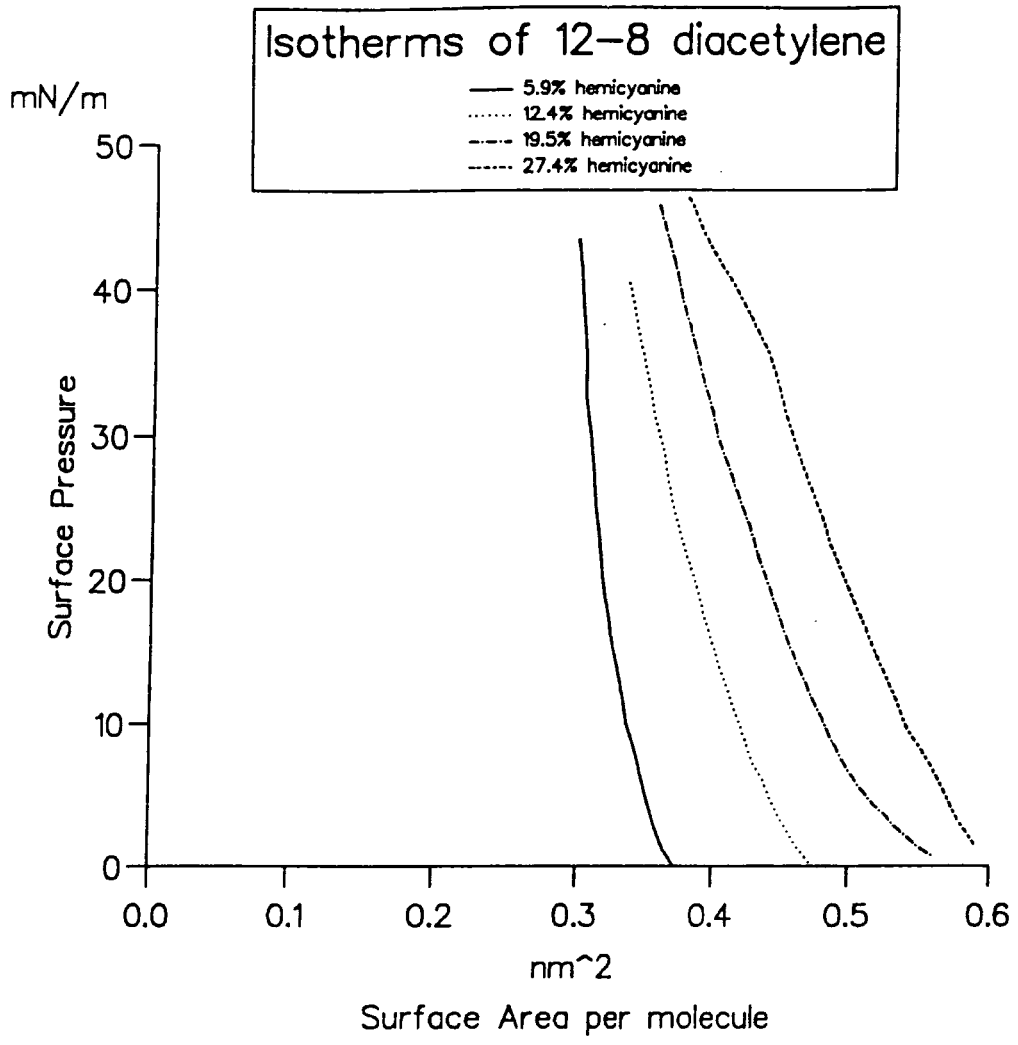

Figure 6.9 - Isotherms of diacetylene and hemicyanine mixtures

For the two smallest hemicyanine concentrations Y-type deposition was observed for up to 20 layers (pH 6.2, 35 mN m^{-1}). At 19.5 mol% of hemicyanine the transfer had become Z-type (pH 6.2, 35 mN m^{-1}) and 10 layers were readily deposited. For the largest hemicyanine concentration deposition varied between Y-type and Z-type. At 35 mN m^{-1} three times as much material was transferred on the upstroke as compared to the downstroke. On changing the surface pressure to 25 mN m^{-1} Y-type deposition was noted for three cycles then a gradual change to Z-type occurred.

To understand the LB behaviour of these mixtures it is important to realise that

pure diacetylene transfers Y-type while hemicyanine is regarded as a Z-type material. For the mixtures with smaller molar proportions of hemicyanine, it is clear that the diacetylene is dominating the properties. As the amount of hemicyanine increases the transfer tends towards Z-type. At 27.4 mol% the transfer properties varied with time which may indicate that the molecular ratio of the floating monolayer is also changing. This would be due to different transfer rates for the two materials.

Monolayer and multilayer (10 to 20 layers) samples were produced at all four ratios for study of their polymerisation and nonlinear optical properties.

The dye 4-HANS has been studied in depth in the literature for its LB film and nonlinear optical properties. However, it has since been found that the original synthesis method for this material in fact led to an equimolar mixture of 4-HANS and stearic acid[19]. Therefore deposition studies were carried out on the newly available pure material.

The isotherm for pure 4-HANS is shown in figure 6.10. Extrapolation of the straight line region to zero pressure gives a molecular area of 0.21 nm^2. The monolayer was controlled at 30 mN m^{-1} but transfer to hydrophobic and hydophilic substrates was impossible. A suction test was performed on the layer, it was found to be extremely rigid and large amounts of material could be removed without affecting the surface pressure at the sensor.

In order to reduce the rigidity of the layer, mixtures were produced with stearic acid and 22-TA. The effect on the isotherm of different molecular proportions of 22-TA is illustrated in figure 6.11, similar results were obtained for mixtures with stearic acid. The molecular area occupied by the fatty acid has been assumed to be the same as for a pure material. Therefore the area axis shows the area remaining per molecule of 4-HANS. In all cases it was possible to control the monolayer at 30 mN m^{-1}.

The deposition properties are summarised in table 6.1. As the amount of fatty acid was increased the transfer properties improved and the rigidity became less.

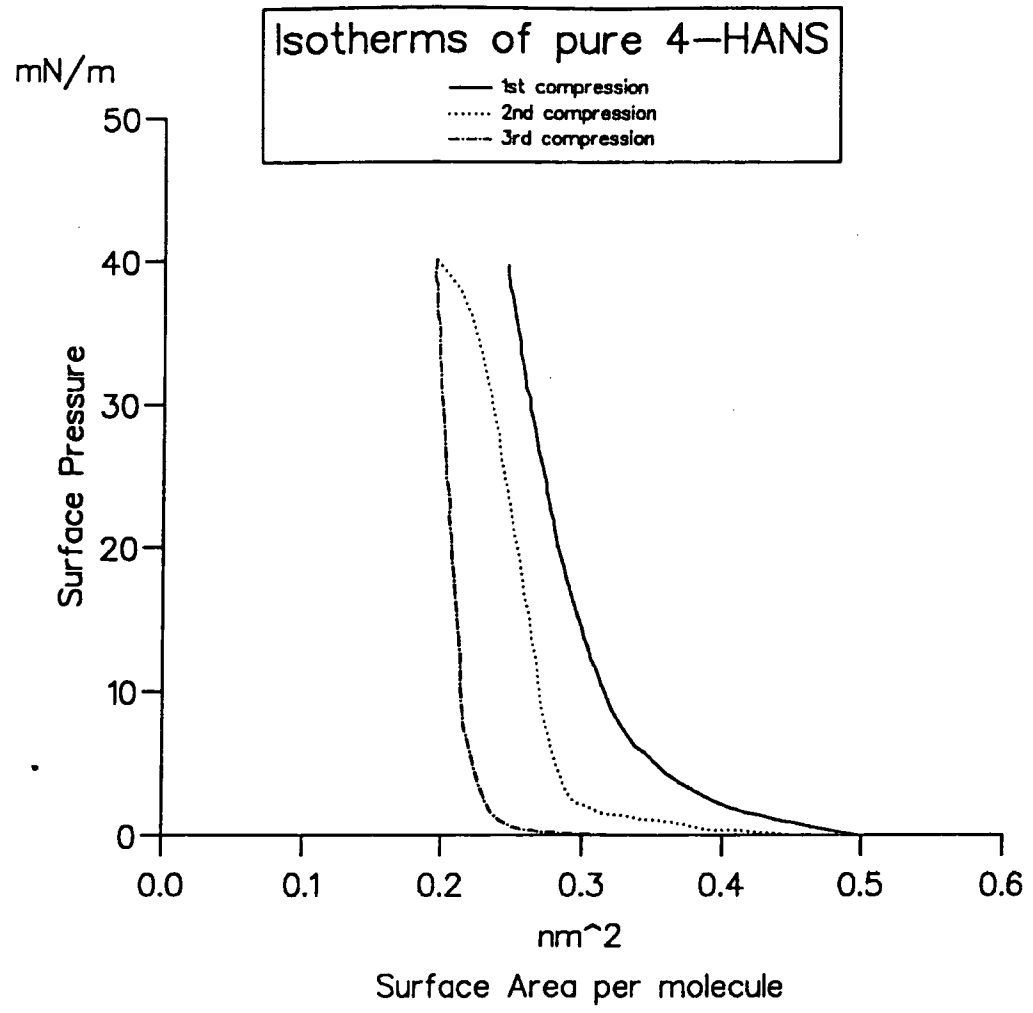

Figure 6.10 - Isotherms of pure 4-HANS

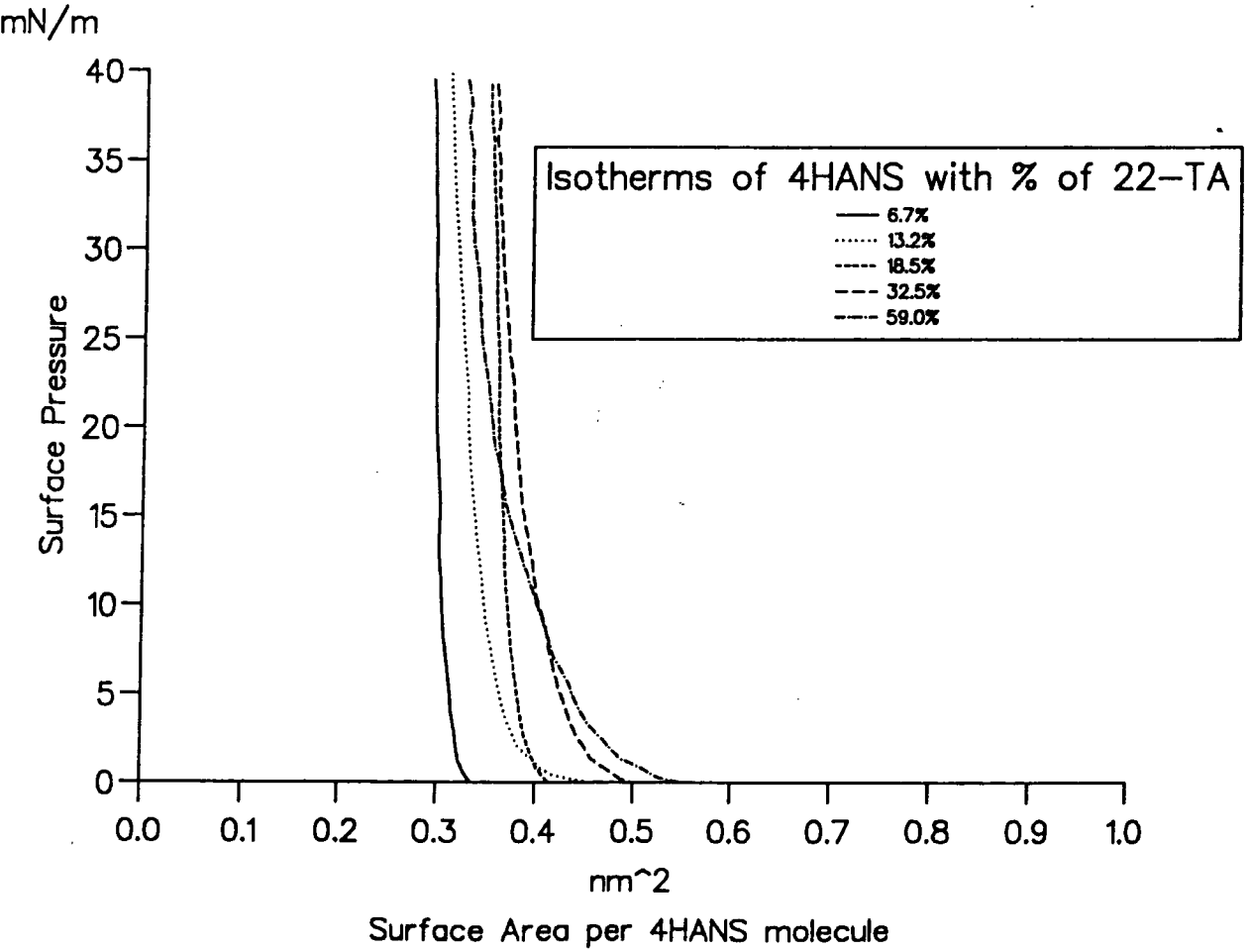

Figure 6.11 - Isotherms of 4-HANS mixed with 22-TA

Clearly, for Y-type deposition, an approximately 50/50 mixture with a fatty acid is required. This is in agreement with the observation that the previous impure material was an equimolar mixture with stearic acid.

4-HANS molar %	stearic acid molar %	Monolayer Deposition	Multilayer Deposition
82.0	18.0	Yes	No[a]
75.0	25.0	Yes	No[a]
47.0	53.0	Yes	Y-type
4-HANS molar %	22-TA molar %	Monolayer Deposition	Multilayer Deposition
93.3	6.7	No	No
87.1	12.9	Yes	No
81.5	18.5	Yes	Poor
76.3	23.7	Yes	Z-type
67.5	32.5	Yes	Z-type
41.0	59.0	Yes	Y-type

[a] Picks up on upstroke, falls off on down stroke

Table 6.1 - Transfer of mixed 4-HANS:stearic acid films

6.3.2 Functionalised diarylalkynes

The Langmuir-Blodgett deposition properties of the first of these materials, JT3, have already been reported[11]. It forms Z-type layers at a surface pressure of 30 mN m^{-1}. Monolayers were prepared on hydrophilic glass and silver coated glass.

The isotherm of the other material, JT11, is shown in figure 6.12a. It consists of three distinct straight line regions, the last of these extrapolates to zero pressure

to give a surface area per molecule of 0.48 nm^2. The form of the isotherm is qualitatively similar to those of fatty acids. The floating monolayer was stable over a period of 15 minutes at a surface pressure of 30 mN m^{-1}. Reliable Y-type deposition was possible onto hydrophobic and hydrophilic substrates with a transfer ratio of 0.96 $\pm$ 0.05 in each case.

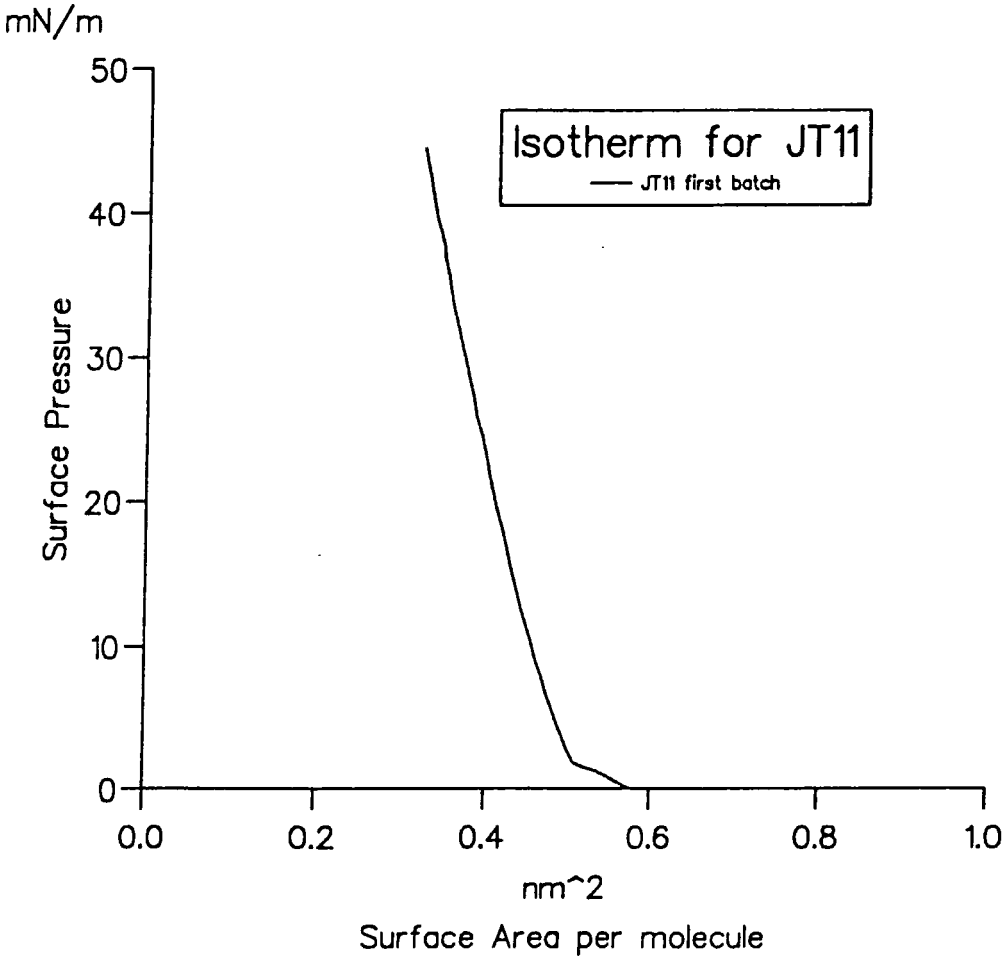

Figure 6.12a - Isotherm of JT11 (first batch)

A second batch of JT11 exhibited somewhat different properties. The isotherm immediately after spreading is shown in figure 6.12b; a plateau feature is clearly visible. The time taken for area stability at 30 mN m^{-1} was increased to about

60 minutes. If the material was left to control at this pressure for 1 hour before taking an isotherm the shape returned to that for the first batch. This behaviour suggests the presence of an impurity which slowly dissolves into the subphase over a period of 1 hour. Despite this no such impurity could be found by high pressure liquid chromatography.

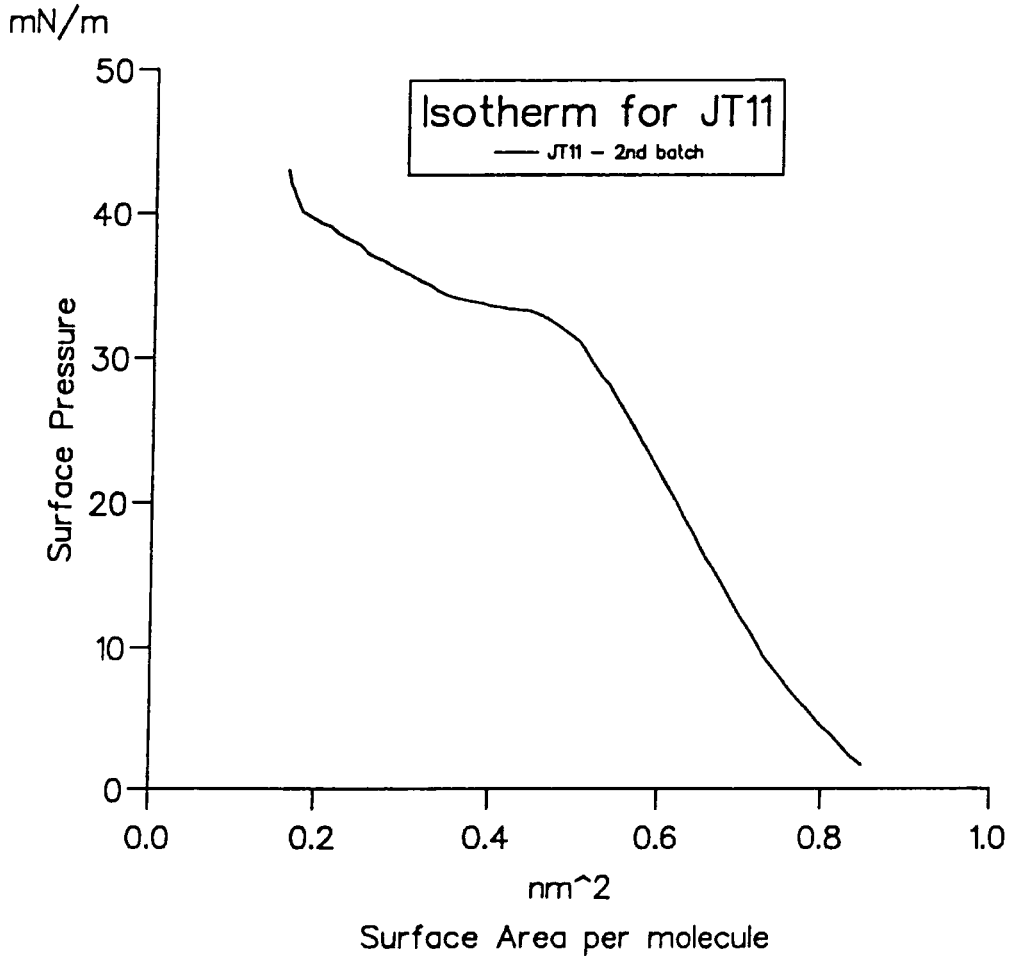

Figure 6.12b -Isotherm of JT11 (second batch)

6.3.3 Diphenyl butadiynes

The first member of this series, JT301, was only available in very small quantities;

thus a solution of just 0.16 g/l was made up (in chloroform). The isotherm is shown in figure 6.13; extrapolation to zero pressure gave a surface area of 0.22 nm^2 per molecule. Control was possible at 25, 35 and 45 mN m^{-1} but deposition onto hydrophobic glass was impossible at any of these surface pressures. Transfer onto hydrophilic glass (3 Y-type layers) and silver coated glass (monolayer) was performed at 25 mN m^{-1}.

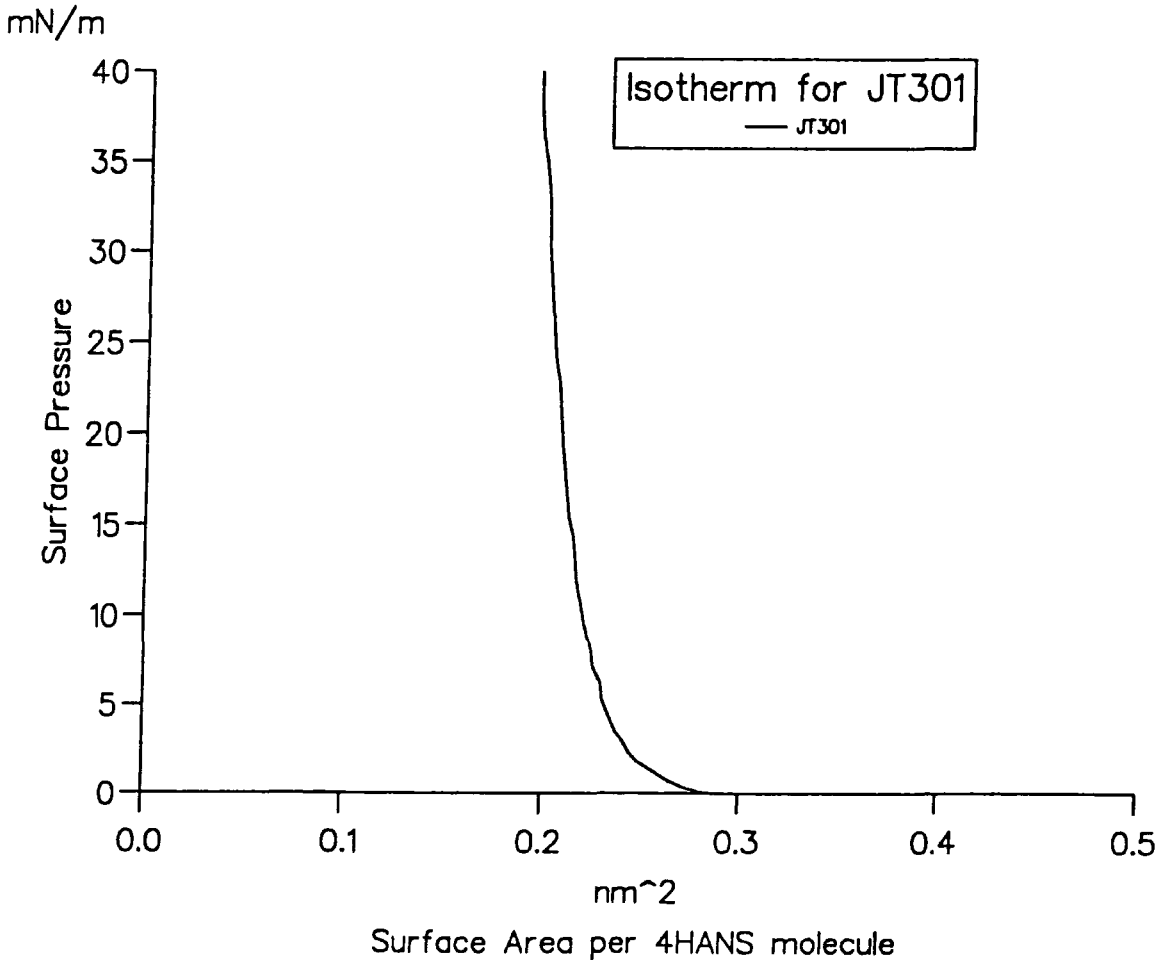

Figure 6.13 - Isotherm of JT301

A series of JT666 isotherms was produced by successive recompressions of one layer (figure 6.14). On the initial compression only a small 'plateau' feature was

noted. The area per molecule for the final isotherm is 0.20 nm^2. The monolayer controlled at 20 mN m^{-1} but no deposition occurred. Reduction of the surface pressure to 15 mN m^{-1} allowed Z-type transfer onto hydrophilic glass (4 layers) and silver coated glass. However, the reproduceability of the transfer was poor and on some occasions no deposition was noted. The transfer ratio was calculated to be 0.15 and the films were observed to be patchy.

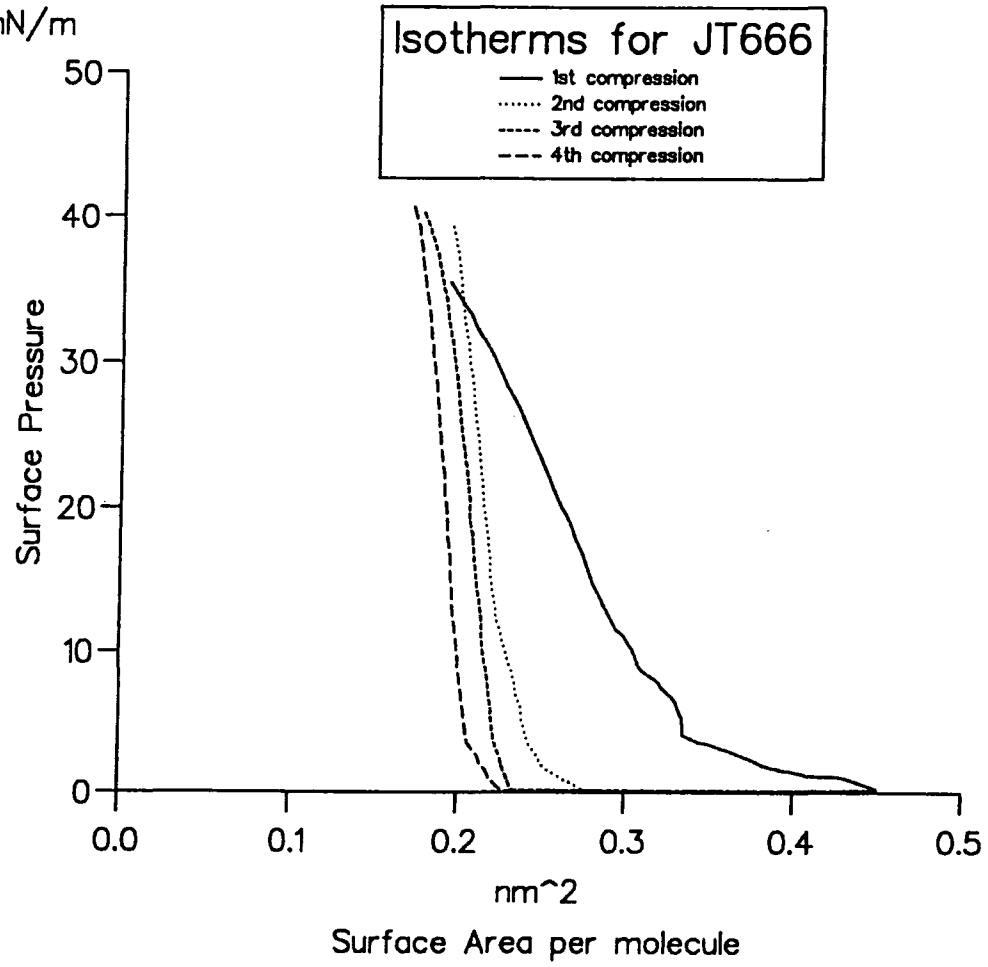

Figure 6.14 - Isotherm of JT666

In an effort to improve the properties of JT666, mixtures with 22-TA were used. For 10 vol % of 22-TA, no improvement in transfer was noted, the films remained

patchy and the deposition mode Z-type. With 50 molar% of 22-TA, the transfer ratio was 0.5 for the downstroke and 1.0 for the upstroke, the latter figure suggests that non-patchy monolayers could be produced. A monolayer was deposited onto silver coated glass for the Pockels effect to be measured.

Isotherms were also prepared for JT777 and JT999; these are shown in figure 6.15. Monolayers of JT777 were deposited onto glass and silver coated glass using mixtures with 10 vol % 22-TA but multilayer transfer was not possible.

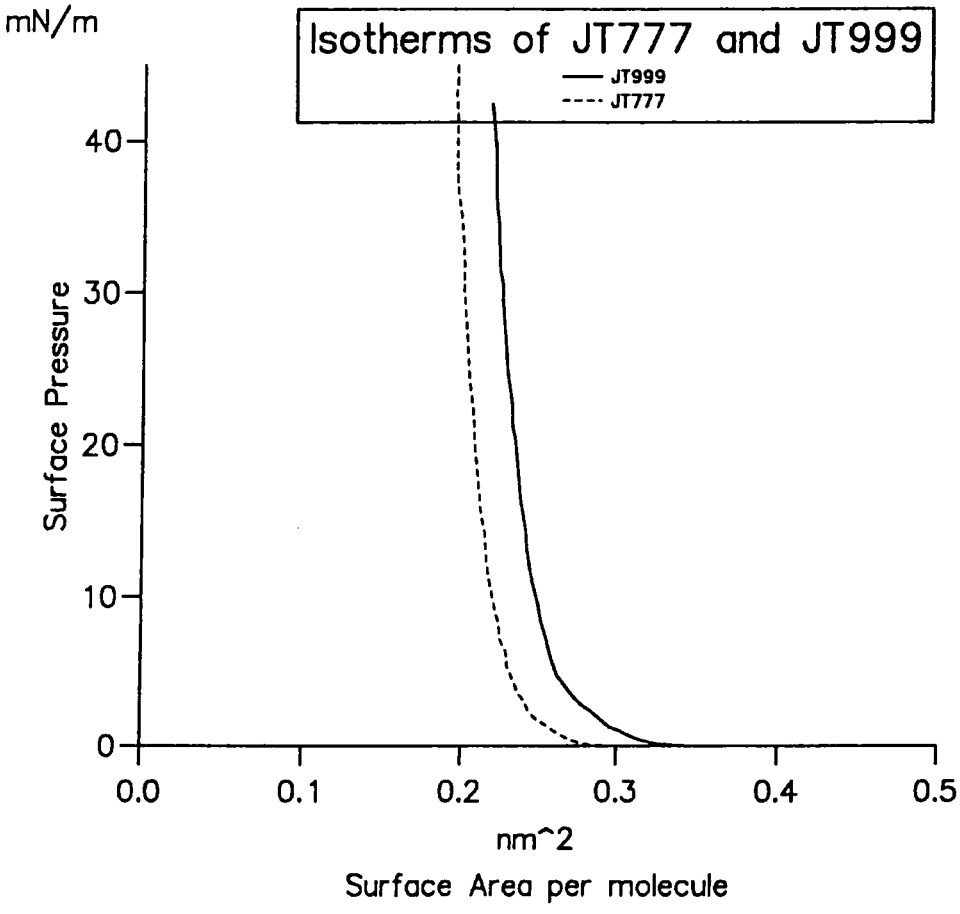

Figure 6.15 - Isotherms of JT777 and JT999

6.3.4 pNA and mNA derivatives

The isotherms of JYT19 and JYT21 are very similar in form and are shown on the same axes in figure 6.16. In both cases a pressure maximum is apparent at an area per molecule of 0.35-0.40 nm^2. It is likely that some rearrangement of the floating molecules then takes place. On further reduction of the area the pressure falls before a second rise is observed. The deposition properties were identical. Using a surface pressure of 30 mN m^{-1} and hydrophilic glass, transfer occurred on the up-stroke but the layer fell off on the down stroke. On hydrophobic glass, Y-type deposition was obtained.

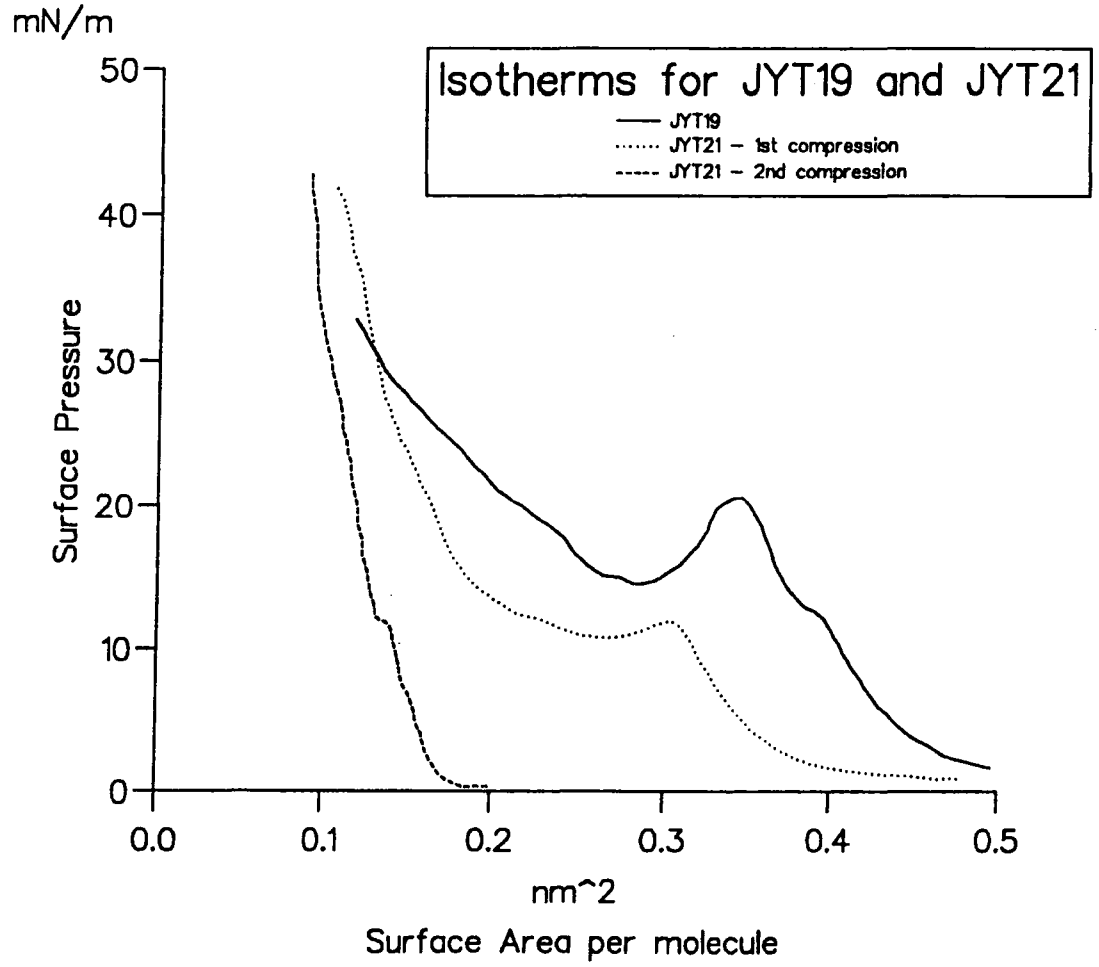

Figure 6.16 - Isotherms of JYT19 and JYT21

Mixtures of the two materials with 22-TA were also made, the isotherms are shown in figure 6.17. The area occupied by the 22-TA molecules was assumed to be equal to that occupied by the same molecules in a pure film,. therefore the surface area axis is marked in surface area per JYT19/21 molecules.

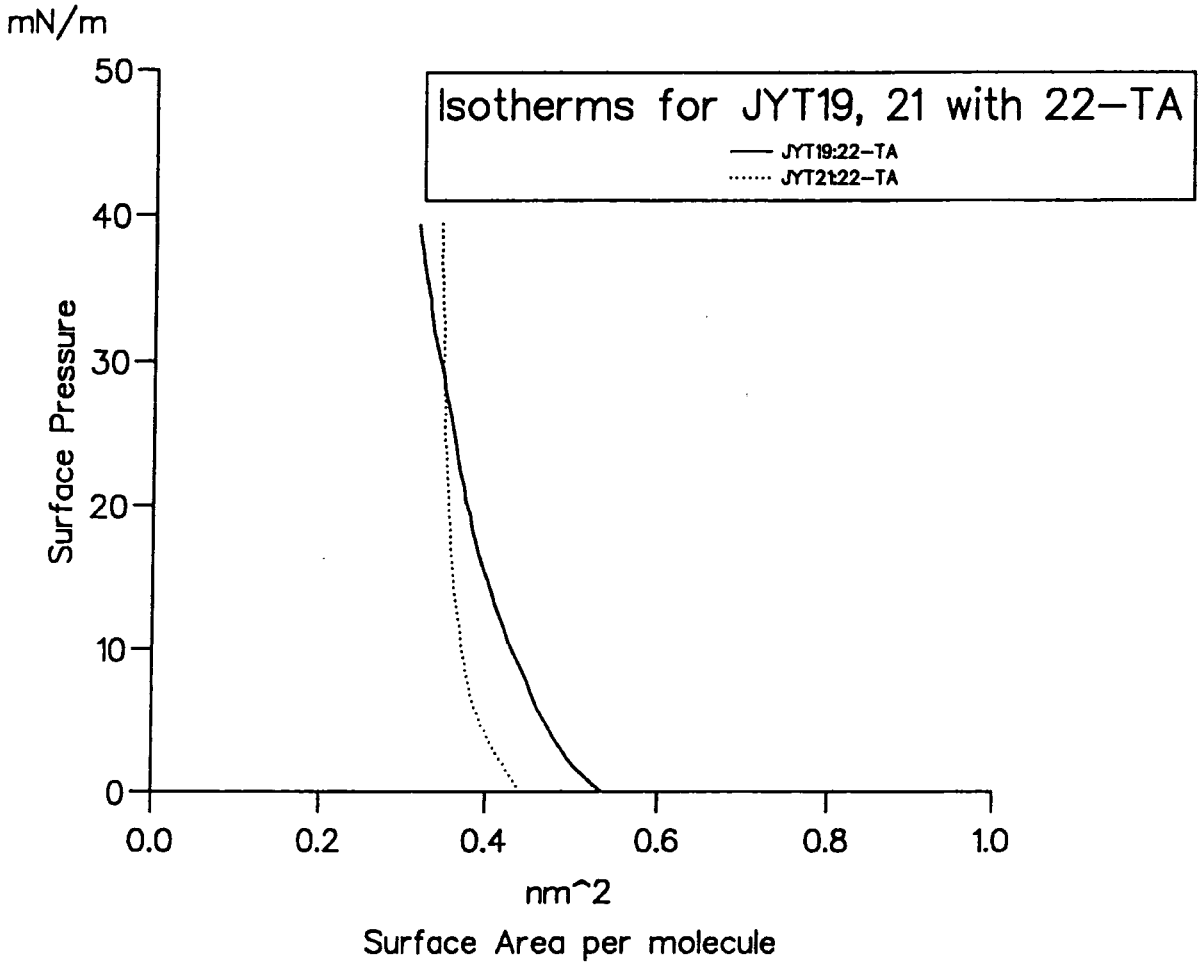

Figure 6.17 - Isotherms of JYT19 and JYT 21 mixed with 22-TA

Monolayers of the mixtures with 22-TA were transferred to silver coated glass for Pockels effect measurement and hydrophilic glass for second harmonic generation.

6.3.5 Aminonitrostilbene carboxylic acids and methyl esters

A solution was made of the first material in the series, 1-19A and an isotherm

produced (figure 6.18). Large amounts of the solution had to be spread before a pressure change could be observed on compression. The deduced area per molecule is only 0.02 nm^2. The anticipated arrangement with the carboxylic acid group in the subphase and the rest of the molecule near vertical would give a cross-section of 0.17 ± 0.01 nm^2 for all the molecules in this series[16]. It is likely that the molecules are in fact lying flat on the subphase in a multilayer.

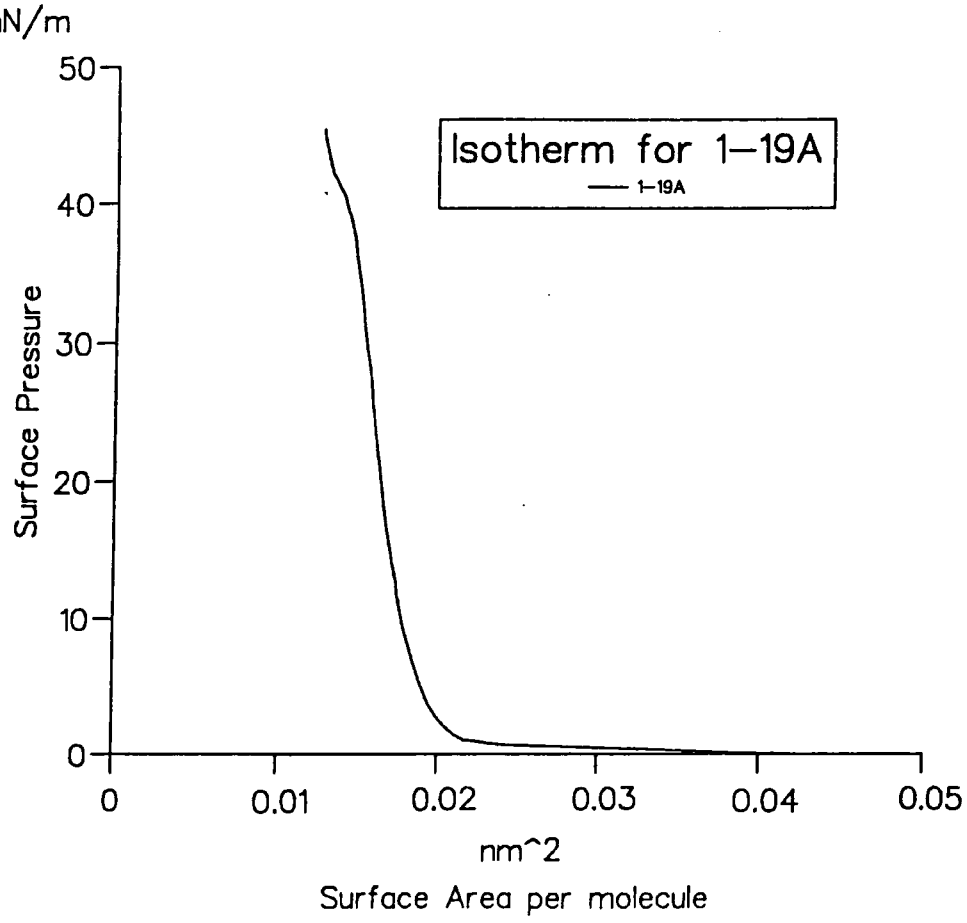

Figure 6.18 - Isotherm of 1-19A

The isotherm for MA (figure 6.19) shows a pair of inflections at approximately 0.13 nm^2 per molecule on first compression. Subsequent recompressions give a simple

isotherm with an area per molecule of 0.12 nm^2. It proved possible to control the floating monolayer at 30 mN m^{-1} but no deposition was achieved. On applying the suction test, the film was found to be extremely rigid.

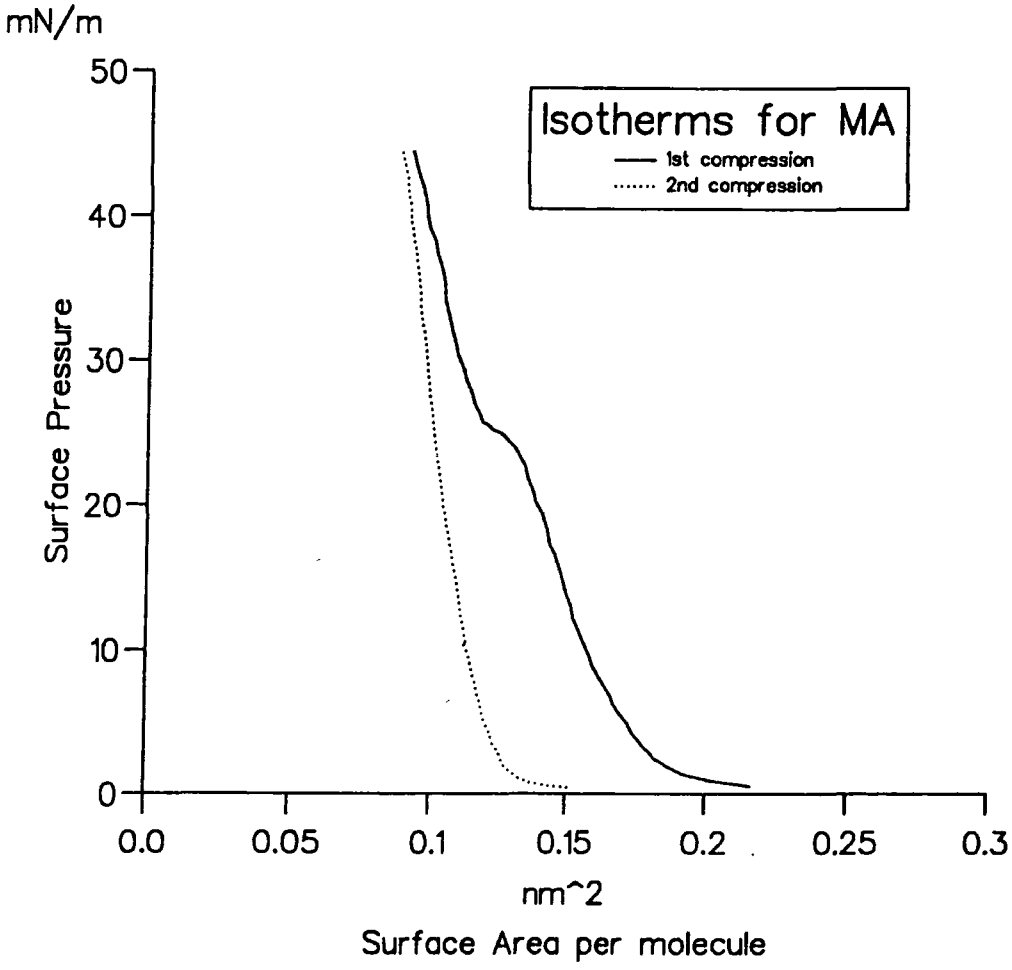

Figure 6.19 - Isotherm of MA

Figure 6.20 shows the isotherm of GSC; a single inflection occurred on the first compression only. The area per molecule taken from the second compression is 0.21 nm^2. Again, control at 30 mN m^{-1} was possible but no film transfer occurred. The suction test showed that the material was somewhat rigid, but less so than MA.

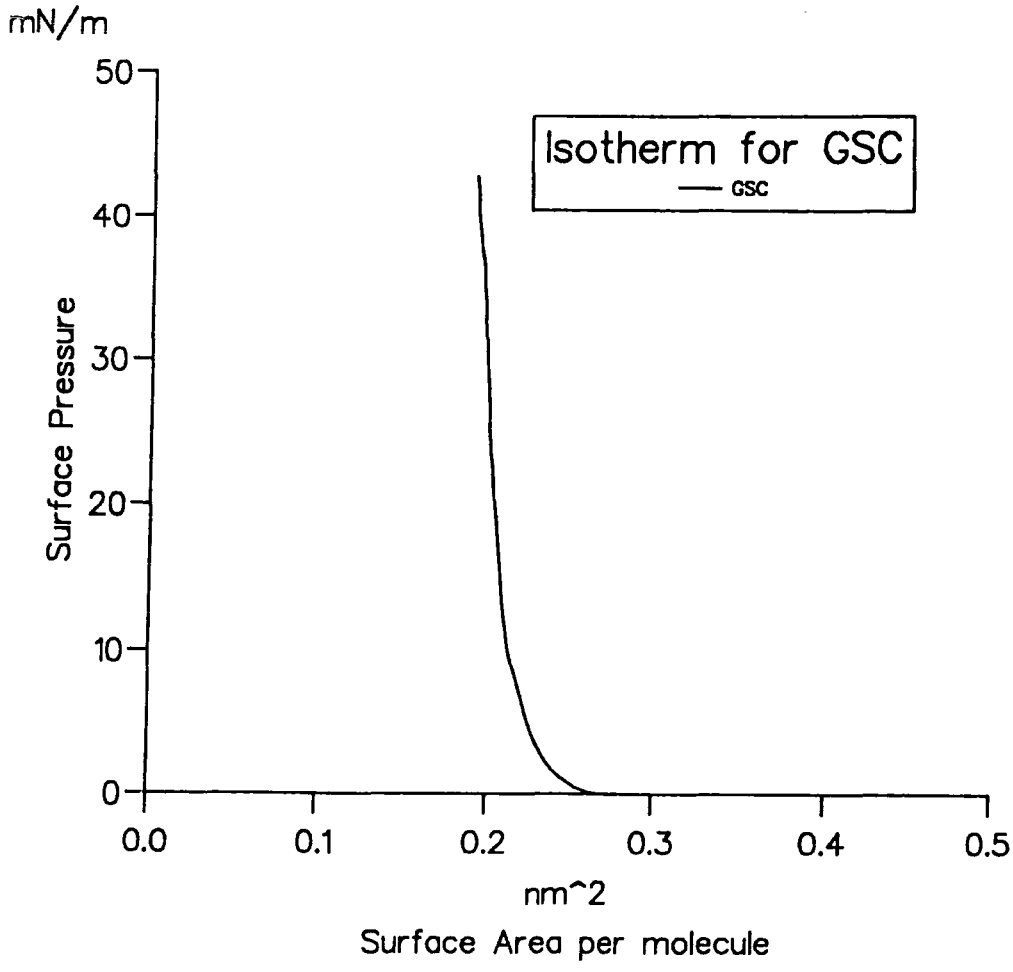

Figure 6.20 - Isotherm of GSC

The isotherm for 1-40A (figure 6.21) was very simple in form, consisting of a gradual progression between two straight line regions. Recompression gave only a slight change. The molecular area was extrapolated to be 0.46 nm^2. The monolayer was stable at 30 mN m^{-1} and the suction test showed it to be non rigid. Despite this, no deposition was possible.

The methyl ester 1-40II gave the isotherms in figure 6.22. Two molecular areas may be extrapolated, 0.30 nm^2 from the low pressure region of the first compression, and 0.17 nm^2 from the third compression. These areas will correspond to different packing of the molecules. A non-rigid film could be controlled at 30 mN m^{-1} but

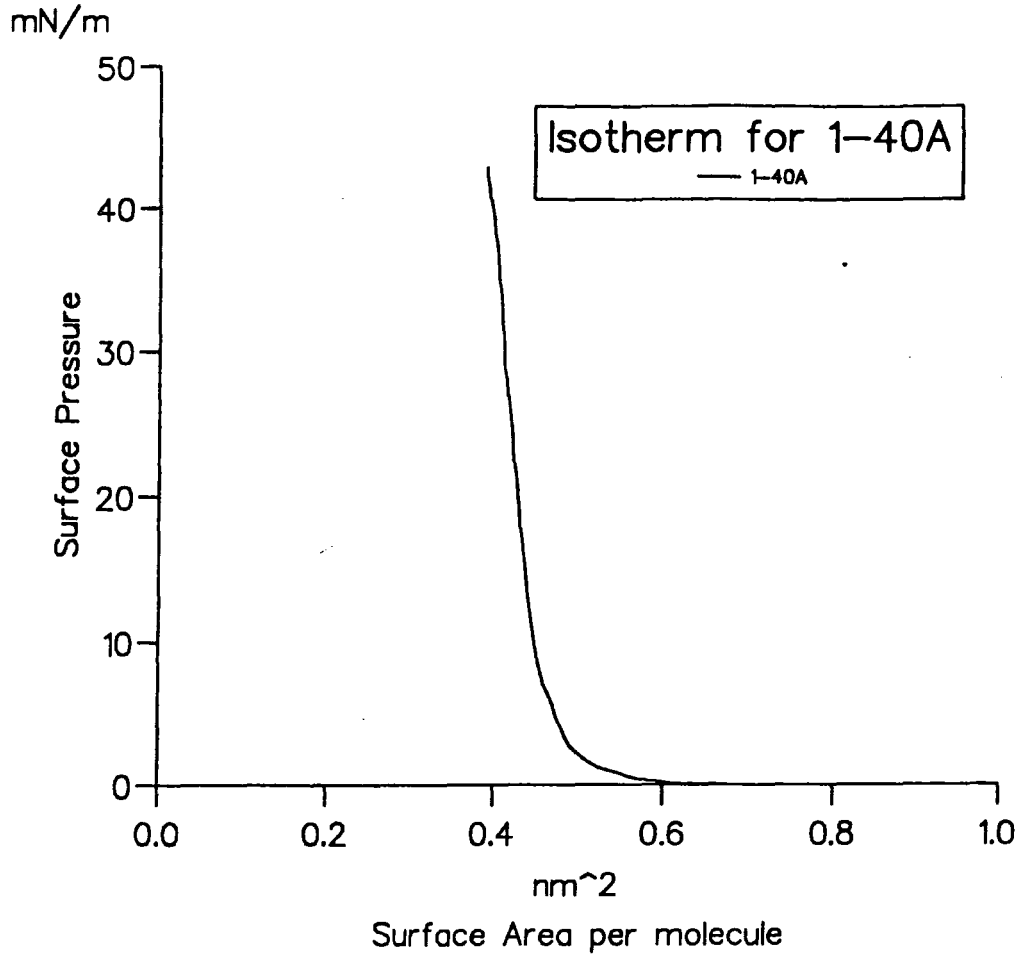

Figure 6.21 - Isotherm of 1-40A

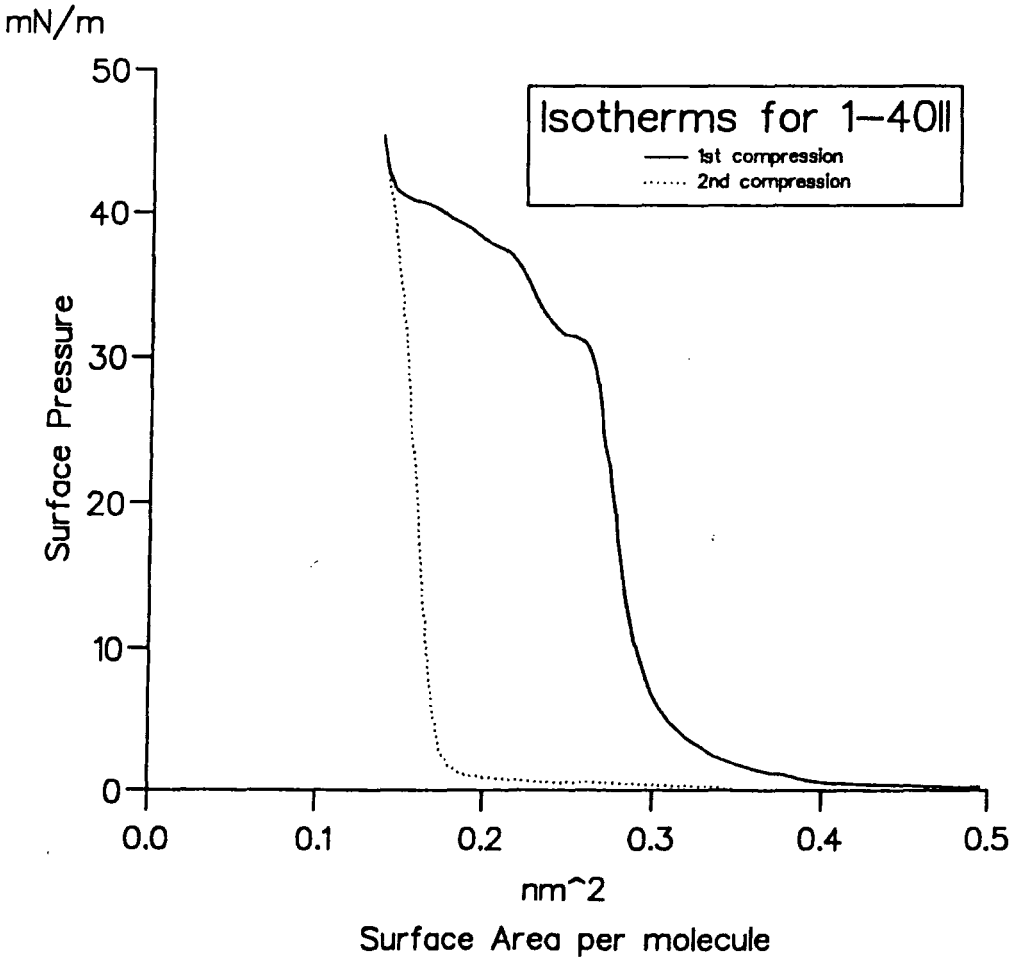

Figure 6.22 - Isotherm of 1-40II

no deposition occurred.

Taking this group of carboxylic acids as a whole it is clear that the two chain lengths (carboxylic acid and alkyl) have a marked effect on the area per molecule. As either chain increases in length the molecular area gets larger. This could not be the case if the chains were aligned normal to the subphase. The carboxylic acid group is the most hydrophilic part of the molecule. Taking this into account a possible molecular orientation is shown in figure 6.23.

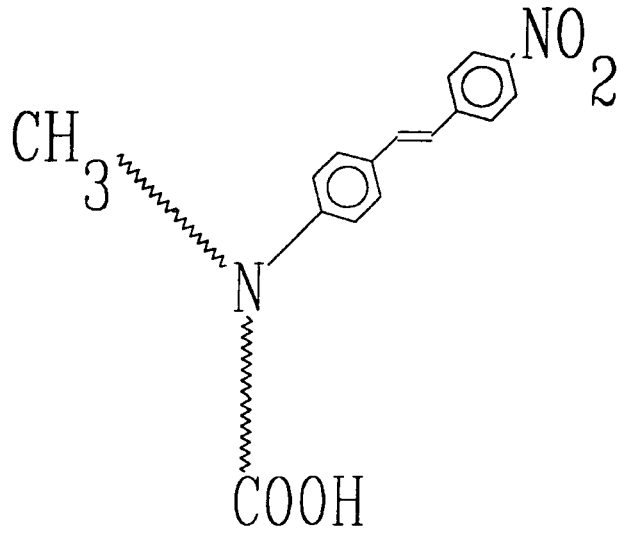

Figure 6.23 - Proposed orientation for aminonitrostilbene carboxylic acids

The increase in chain length also gave a reduction in rigidity. All the rigid materials identified in this thesis (4-HANS, JYT19, JYT21, MA, GSC) contained amine or amide donor groups and nitro acceptors. It appears possible that strong intermolecular binding forces are associated with one or both of these groups, perhaps involving the lone-pair of one of the nitrogen atoms. Rigidity can be reduced by mixing with a fatty acid. This probably separates the film into small rigid islands of the dye surrounded by more mobile fatty acid areas. In the case of the aminoni-

trostilbene carboxylic acids a longer chain length will separate the interacting parts of the molecules and so reduce the binding force.

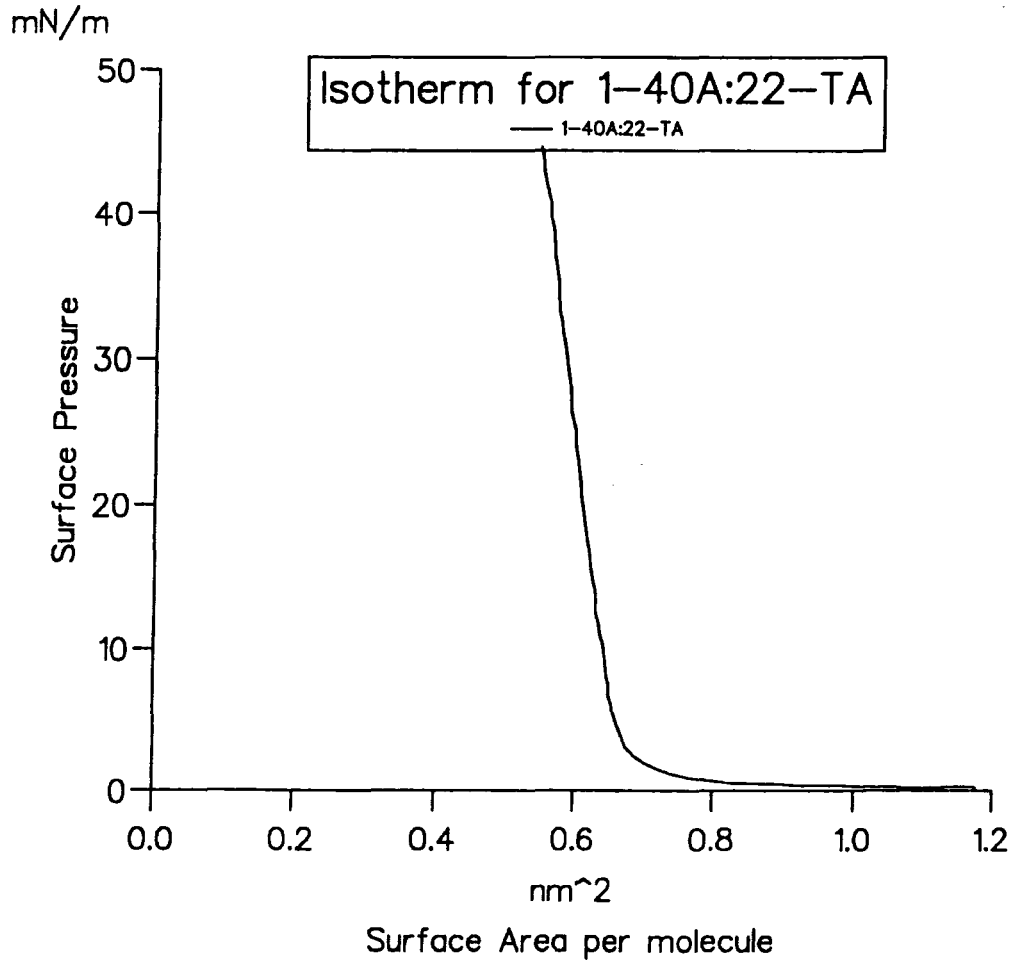

Figure 6.24 - Isotherm of 1-40A mixed with 22-TA

On the basis of the studies on the pure materials, 1-40A appeared to be the best candidate for further investigation. Not only was the film non-rigid but also the isotherm showed no signs of multiple phases. 1-40A was mixed with 63.0 molar% of 22-TA, giving the isotherm in figure 6.24 (as before the area per molecule is for 1-40A only, the area assumed to be occupied by the 22-TA has been subtracted). This mixed film controlled at 30 mN m^{-1} and gave variable gave Y/Z-type deposition

onto hydophilic and hydrophobic substrates. Up to 10 layers were deposited onto silicon for ellipsometry and a monolayer onto silver coated glass for measurement of the Pockels effect.

6.3.6 Oligomeric Materials

Appropriate deposition conditions for these materials had already been established by ICI[20] so no isotherms were produced. S119191 had been found to transfer at surface pressures of 30 mN m^{-1} to 35 mN m^{-1} and S122699 at 35 mN m^{-1}. The area per molecule of the former was 1.3 nm^2 and of the latter 1.2 nm^2. Monolayers of the two materials were prepared at rates of 15 to 20 mm min^{-1} onto hydrophilic glass (for second harmonic generation) and silver coated glass (for the Pockels effect). Y-type layers were deposited onto silicon for ellipsometry. Up to 49 layers were produced using S119191 but only 29 layers of S122699 could be obtained before the transfer ratio started to decrease.

6.3.7 Miscellaneous Materials

Isotherms for the two functionalised 4-pyrrolidino-pyridenes, JT9 and JT15, are shown in figure 6.25. Neither isotherm is of the condensed type, indicating that no solid like phase exists. In view of this, no further studies were undertaken.

The functionalised 4-N-dimethylaminopyridenes, JT10 and JT12, gave the isotherms shown in figure 6.26. Although JT12 shows no solid phase, the isotherm for JT10 has a region of reasonably steep gradient at around 30 mN m^{-1} and also a pressure maximum at a molecular area of 0.35 nm^2. It was impossible to control the monolayer at any pressure between 20 mN m^{-1} and 30 mN m^{-1} due a rapid loss of area (all the area was lost over a period of 30 minutes).

The isotherm of the asymmetrically disubstituted stilbene JT201 is given in figure 6.27. The material was spread from a solution of unknown concentration so no area calibration is provided. The isotherm contains numerous inflections. Control at 25 mN m^{-1} gave pressure oscillations of approximately 15 minute period. A layer was transferred onto hydrophilic glass at a single upstroke but the film consisted

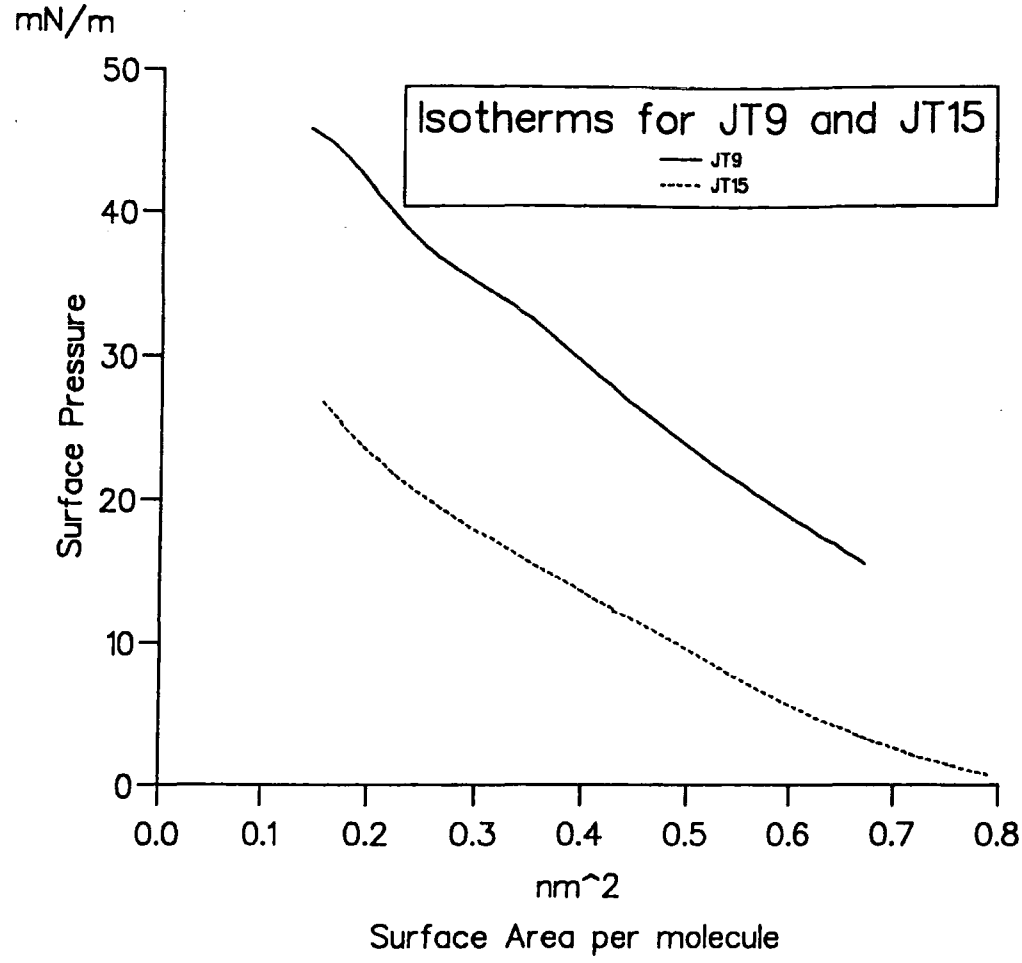

Figure 6.25 - Isotherms of JT9 and JT15

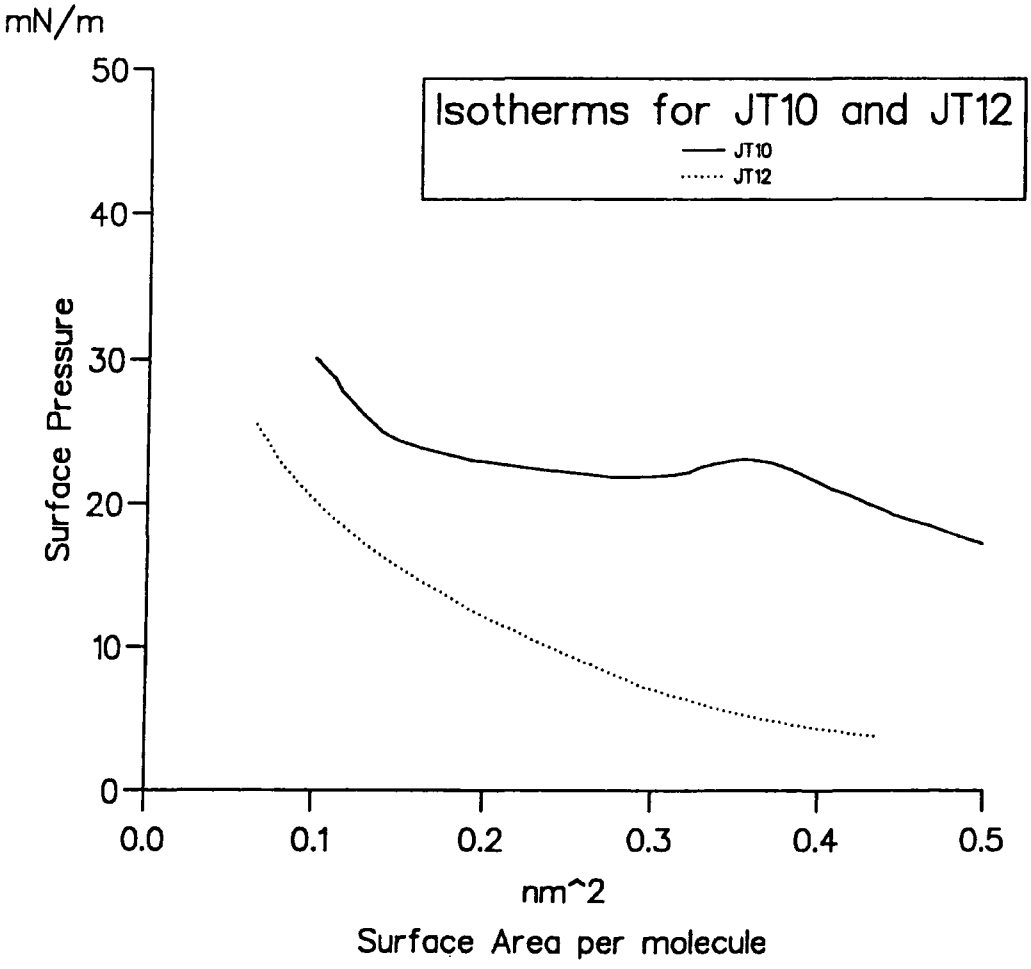

Figure 6.26 - Isotherms of JT10 and JT12

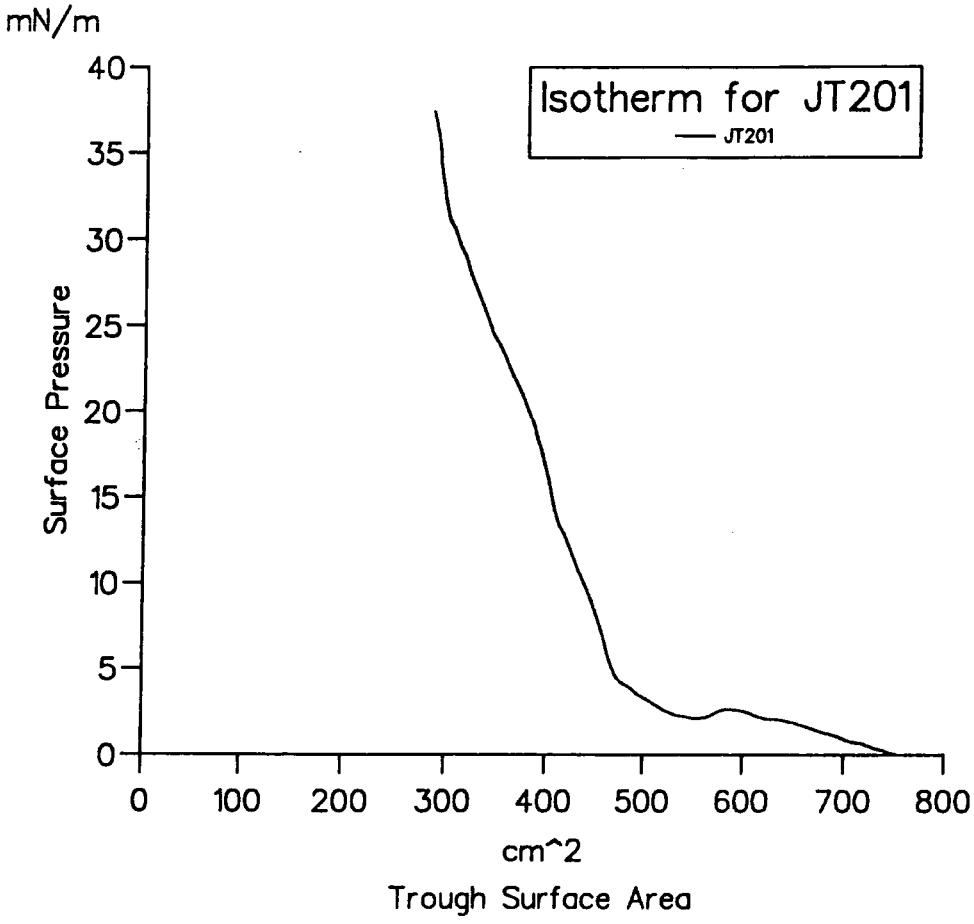

Figure 6.27 - Isotherm of JT201

of white flakes and was clearly not a monolayer.

6.4 Alternate-Layer Langmuir-Blodgett films

For any practical application of LB films for nonlinear optics it will be necessary to use multilayers. As the structure must be non-centrosymmetric, X-type, Z-type or Y-type alternate-layers are required.

None of the new materials studied showed a natural tendency to transfer X or Z-type. Although it would be possible to force this behaviour using an alternate-layer

trough with one side left unspread, better quality films are likely to result from the Y-type alternate-layer method. From the materials studied only a few suggested themselves as candidates for alternate-layer studies. It is obviously essential that the material should show good, reliable transfer properties if many layers are to be prepared. This effectively narrowed the choice to JT11 and the two ICI oligomers.

JT11 has a positive $\chi^{(2)}$ so it must be alternated with a negative material for the nonlinear effects to sum. 4-HANS was chosen as its partner as it is a well established material with excellent deposition properties. The two ICI materials were also used as a pair for alternate-layers (these materials were specifically designed for this purpose).

6.4.1 4-HANS/JT11 Films

These films[21] were prepared using a rotary type alternate-layer trough. The 4-HANS was mixed on a 1:1 molecular ratio with stearic acid to allow consistent film transfer, the JT11 was used undiluted. In each case a surface pressure of 30 mN m^{-1} was utilised. The correct choice of material to deposit on the upstroke was determined experimentally. It was found that a system of JT11 transferred on the upstroke and 4-HANS on the downstroke gave a faster drying time. However the dipping rate had to be continually reduced as the number of layers increased to allow time for drying. The initial rate of transfer was 35 mm min^{-1}, after approximately 30 bilayers this had to be reduced to 12 mm min^{-1} in order to maintain the transfer ratio. It was impossible to measure absolute transfer ratios on our rotary type Langmuir trough as an unknown quantity of material is transferred to the roller mechanism on each cycle. However, layer to layer comparision showed no reduction from the transfer ratios of the first layer, this suggests undiminished layer quality.

A large number of samples were prepared onto a range of substrates. Silver coated glass proved to be sufficiently hydrophobic to allow the first layer to be 4-HANS transferred on the downstroke. These substrates were coated with 1,3 and 10 bilayers for Pockels effect measurement. Hydrophobic and hydrophilic glass slides

were coated with 1, 7 ,25 and 50 bilayers for second harmonic generation. Despite some of the substrates being hydrophilic, all samples were prepared starting with transfer on a downstroke. This was to allow study of the effects of substrate treatment.

A 301 layer (150 bilayer) sample was produced on a hydrophilic substrate for waveguiding experiments. Transfer was carried out starting on an upstroke in order to maximise film quality. Second harmonic generation from this film was also investigated. The 25 bilayer films were also studied by X-ray diffraction. Layers were deposited onto silver coated glass and an ATR crystal for Fourier Transform Infra-Red measurements.

In order to study the effect of replacing one of the active materials with a passive spacer layer, 7 bilayer films of cadmium arachidate/JT11 and 4-HANS/cadmium arachidate were produced (the first mentioned material was deposited on the downstroke in both cases). These were then measured for second harmonic intensity and the results compared to those of 7 bilayer films of 4-HANS/JT11.

6.4.2 Oligomeric Alternate-Layers

As recommended by ICI, these films were prepared by transferring the active material (S119191) on the upstroke and the passive spacer (S122699) on the downstroke using conditions given in section 6.3.6. The rotary Langmuir trough was again used.

Films were deposited onto hydrophilic glass for second harmonic generation and onto silver coated glass for the Pockels effect. All substrates were first deposited on the upstroke giving an odd number of layers. Both 3 layer (active-passive-active - 'apa') and 5 layer ('apapa') samples were produced on both the substrate types. Thicker layers were not considered due to the disappointing nonlinear optical results (see section 8.2.2 and 8.3.2). For the small number of layers deposited, no reduction in transfer ratio was observed.

6.5 Summary

A large number of novel materials were investigated for their Langmuir-Blodgett deposition properties. For around a half of these it was possible to transfer films of sufficient quality to make nonlinear optical measurments worthwhile. Both of the diarylalkynes (JT3, JT11), all of the diphenyl butadiynes (JT301, JT666, JT777, JT999), the ICI oligomers, the nitroanaline derivatives (JYT19, JYT21) and one of the aminonitrostilbene carboxylic acids (1-40A) were chosen for further investigation. Mixed monolayers of hemicyanine with diacetylene and of the newly-available pure 4-HANS with fatty acids were also deposited. Two alternate-layer systems were investigated, 4-HANS/JT11, and one based on the two ICI oligomers.

References

1. I. Langmuir, *Trans. Faraday Society* **15** p62 (1920).

2. K.B. Blodgett, *J. Am. Chem. Soc.* **57** p1007 (1935).

3. A. Barraud, C. Rosilio, A. Ruaudel-Teixier, *J. Colloid Interface Sci.* **62** pp509-23 (1977).

4. G.L. Gaines, *Insoluble Monolayers at Liquid-Gas Interfaces* (Wiley-Interscience 1966).

5. B. Tieke, H.J. Graf, G. Wegner, B. Naegele, H. Ringsdorf, A. Banerjie, D.Day, J.B. Lande, *Colloid. Polym. Sci* **255** p251 (1977).

6. I.R. Girling, N.A. Cade, P.V. Kolinsky, R.J. Jones, I.R. Peterson, M.M. Ahmad, D.B. Neal, M.C. Petty, G.G. Roberts, W.J. Feast, *J. Opt. Soc. Am. B* **4** pp950-5 (1987).

7. G.H. Cross, I.R. Girling, I.R. Peterson, N.A. Cade, *Electronics Letters* **22** pp1111-3 (1986).

8. D.B. Neal, *PhD. Thesis*, University of Durham (1987).

9. D.B. Neal, M.C. Petty, G.G. Roberts, M.M. Ahmad, W.J. Feast, I.R. Girling,

N.A. Cade, P.V. Kolinsky, I.R. Peterson, Electronics Letters **22** p460 (1986).

10. J. Tsibouklis, J.P. Cresswell, N. Kalita, C.Pearson, P.J. Maddaford, H. Ancelin, J. Yarwood, M.J. Goodwin, N. Carr, W.J. Feast, M.C. Petty, *J. Phys. D Appl. Phys.* **22** pp1608-12 (1989).

11. N. Kalita, *PhD. Thesis*, University of Durham (1991).

12. J. Tsibouklis, J. Cresswell, C. Pearson, M.C. Petty, W.J. Feast, *Int. Phys. Conf. Ser.* **103** pp187-92 (1989).

13. S.T. Kowel, L. Ye, Y. Zhang, L.M. Hayden, *Optical Engineering* **26** pp107-112 (1987).

14. D. Lupo, W. Prass, U. Scheunemann, A. Laschewsky, H. Ringsdorf, I. Ledoux, *J. Opt. Soc. Am. B* **5** pp300-8 (1988).

15. N. Ratcliffe, *unpublished data.*

16. R.H. Tredgold, M.C.J. Young, R. Jones, P. Hodge, P. Kolinsky, R.J. Jones, *Electronic Letters* **24** p308 (1988).

17. W. Prass, *Hoechst High Chem Magazine* **7** p15 (1989).

18. S. Allen, T.G. Ryan, D.P. Devonald, M.G. Hutchings, A.N. Burgess, E.S. Froggatt, A. Hamilton, R.M. Swart, G.J. Ashwell, M. Malhotra, *Organic Materials for Nonlinear Optics 90* (Royal Society of Chemistry, London) in press.

19. J. Tsibouklis, S. Mukherjee, J. Cresswell, M.C. Petty, W.J. Feast, *J. Molecular Electronics* **6** pp221-223 (1990).

20. J.P. Cresswell, J. Tsibouklis, M.C. Petty, W.J. Feast, N. Carr, M. Goodwin, Y.M. Lvov, *SPIE Proceedings* **1337** pp358-63 (1990).

Chapter 7
Characterisation of Langmuir-Blodgett Monolayers

This chapter describes the nonlinear optical characterisation of monolayers of the materials discussed in Chapter 6. Their properties were measured by second harmonic generation and the Pockels effect. Ellipsometry results are also included because, although they are not carried out on monolayers, they were needed to find layer thicknesses or permittivities in order to fit the Pockels effect data.

The characterisation of LB multilayers is described in Chapter 8.

7.1 Ellipsometry

The calculation of $\chi^{(2)}(-\omega;\omega,0)$ from the Pockels effect experiment requires that the permittivity and thickness of the LB film be known. One of these values can be found from surface plasmon resonance but, as is discussed in section 5.2.2, the other must be found by an alternative method.

Ellipsometry provides a convenient method for measuring the permittivity and thickness of thin layers but unfortunately has two drawbacks for LB films. The first of these is that in ellipsometric calculations the layer is usually considered to be isotropic. This is not true for LB films but a suggested technique for dealing with uniaxial films is given in section 5.1.3. However the validity of this method must first be established. The second difficulty is that, by LB standards, relatively thick films are needed; a stepped structure of roughly 10, 20, 30 monolayers is required for uniaxial fitting and would also be the ideal for isotropic fitting. This limits the use of ellipsometry to those materials which deposit to this thickness. For the novel materials of this thesis, the method can only be used for JT11, 1-40A and the ICI oligomers.

7.1.1 Materials from the Literature

To allow comparision between the different methods of fitting ellipsometric data

the fatty acid 22-TA was chosen. This material deposits well up to a several hundred layers and figures for refractive index and layer thickness are available in the literature.

A stepped structure of 10, 20, 30, 40 and 50 layers was deposited on hydrophobic silicon at 30 mN m^{-1}. The ellipsometric angles Δ and ψ were then measured for each step using a wavelength of 633nm and 70 degree angle of incidence (table 7.1). Each region was individually fitted to a lossless isotropic model (see table 7.1). The six sets of ellipsometric angles were also fitted by the uniaxial model of section 5.1.3 (ie. assuming that the total film thickness is proportional to the number of layers). This gave an ordinary index of 1.5106 ± 0.0006, an extraordinary index of 1.5518 ± 0.006 and a layer thickness of 2.89 nm ± 0.01 nm. Finally, the data for all six regions were used together to give an isotropic best fit. This produced a refractive index of 1.5125 and a layer thickness of 2.89 nm.

No. of layers	Δ	ψ	n	d/nm
10	112.94	16.83	1.483	2.84
20	85.84	26.47	1.514	2.87
30	74.44	37.31	1.527	2.84
40	72.93	58.06	1.518	2.81
50	287.17	73.46	1.505	2.83
60	281.55	42.32	1.481	2.91

Table 7.1 - Ellipsometric angles and isotropic fit for 22-TA

The form of the results is found to be very similar to that reported by Den Engelsen in his experiments on arachidic acid[1]. Whichever model is used, the layer thickness varies only slightly and the isotropic refractive index is found to be close to the ordinary index of the uniaxial model. As in the case of arachidic acid the

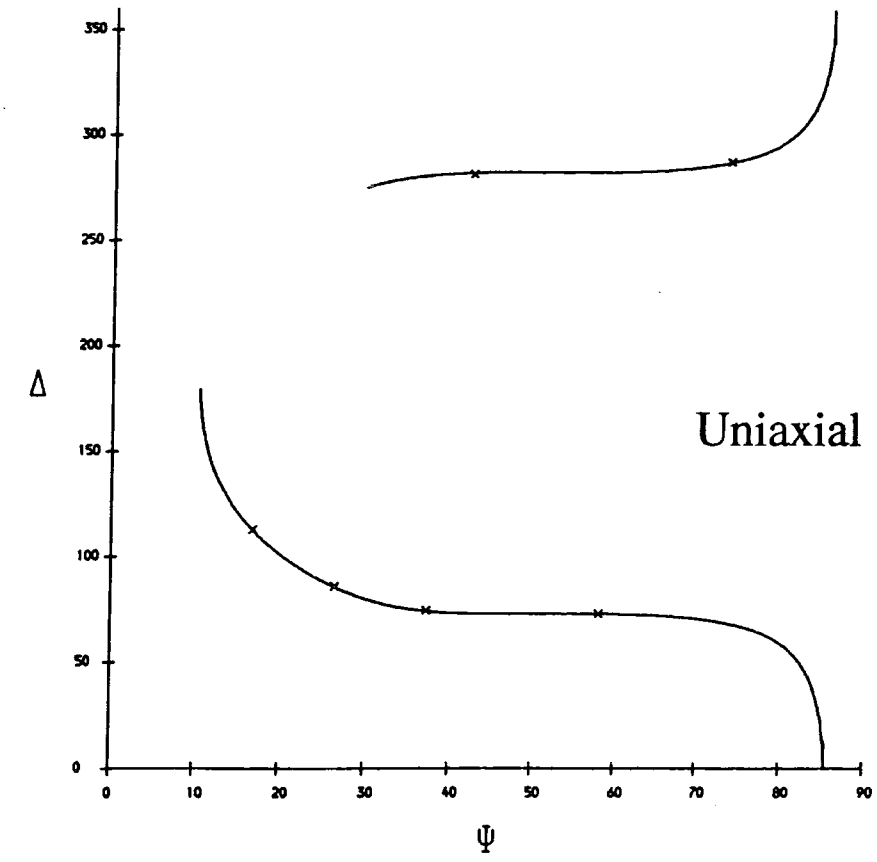

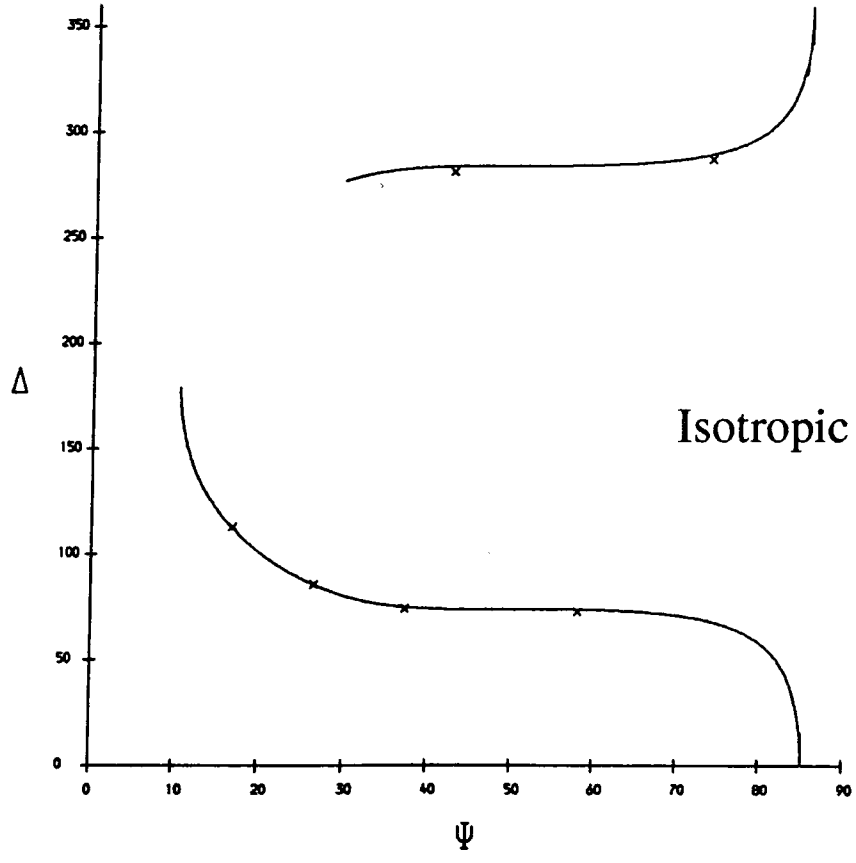

Figure 7.1 - Uniaxial and isotropic fits to 22-TA ellipsometric angles

extraordinary index is found to be to be larger than the ordinary, for 22-TA the birefringence is approximately 0.04. Confirmation of the greater accuracy of the uniaxial fit can be found by plotting the theoretical and experimental Δ and ψ on the same axes. Figure 7.1a shows the uniaxial data and Figure 7.1b shows that for an isotropic best fit (based on all six regions of the film). It is evident that better agreement between theory and experiment is obtained in the uniaxial case.

7.1.2 Functionalised diarylalkynes

Ellipsometry was performed on JT11 films deposited onto hydrophobic silicon; regions of 10, 20 and 30 layers were available. An isotropic fit gave $n = 1.492$ and a monolayer thickness of 4.02 nm for the 10-layer sample.

Analysis of the ellipsometric angles by a uniaxial model gave an in-plane index of $n_o = 1.496 \pm 0.005$ and a normal index of $n_e = 1.642 \pm 0.014$. The monolayer thickness was calculated to be 3.65 ± 0.01 nm. This is very much as anticipated from the molecular structure. The length of the molecule is 4.1 nm (CPK space filling model) which produces a tilt angle of 27 degrees. As the molecule is most highly polarisable in an axial direction, the greater value of n_e compared to n_o is in line with expectation.

7.1.3 Aminonitrostilbene carboxylic acids

Layers of the 1-40A mixture with 22-TA were deposited onto hydrophobic and hydrophilic silicon; unfortunately these proved to be of very poor quality. An isotropic fit to an 11 layer film gave a range of monolayer thicknesses from 0.7 nm to 1.3 nm and refractive indices of 1.21 to 1.46. Clearly these results reflect neither the molecular length nor its likely optical properties. Therefore another technique will be needed for estimating the layer thickness in order to analyse the Pockels data.

7.1.4 Oligomeric materials

The oligomer S119191 was deposited onto hydrophilic silicon in a stepped structure of 19, 29, 39 and 49 layers. The results of the isotropic fit are given in table 7.2. The variation is due to the reducing accuracy of this fitting method for thicker layers.

No. of layers	n	Layer thickness/nm
19	1.609	2.8
29	1.649	2.6
39	1.628	2.6
49	1.601	2.6

Table 7.2 - Isotropically fitted results for S119191

The uniaxial fit produced $n_o = 1.625 \pm 0.001$ and $n_e = 1.86 \pm 0.02$ with a monolayer thickness of 2.73 $\pm$ 0.01 nm. Again the anistropy is in the direction expected from the molecular design and the layer thickness is consistent with the molecular length (2.9 nm from a CPK space filling model).

The second ICI material, S122699, did not transfer with sufficient quality to allow formation of more than 15 and 25 layers. The isotropic fit is given in table 7.3, the number of regions is insufficient for uniaxial measurements. The smaller refractive index values (compared to S119191) are in line with the smaller polarisability of the molecule. The lower monolayer layer thickness is also to be expected as, although the alkyl chain is identical, the conjugated system is approximately 0.8 nm shorter.

7.2 Surface Plasmon Resonance and Pockels Effect

Each of the materials for which monolayer deposition was possible were studied for

No. of layers	n	Layer thickness/nm
15	1.504	2.04
25	1.513	2.11

Table 7.3 - Isotropically fitted results for S122699

their Pockels effect. Whilst the actual change in reflectivity in the surface plasmon arrangement is directly measurable, some estimate of the layer thickness or permittivity is needed to calculate $\chi^{(2)}(-\omega;\omega,0)$. For the functionalised diarylalkyne JT11 and the two oligomers, the thickness was available from ellipsometry but for the other materials different approaches had to be used. These are explained in the appropriate sections.

7.2.1 Materials from the Literature

Hemicyanine has already been studied for its Pockels effect[2]; hence it may be used to provide a comparision with results from other workers.

The results obtained depend critically on the assumptions made about the thickness and permittivity of the monolayer. One of these quantities can be obtained from surface plasmon resonance but the other must be determined or estimated independently. Values for the layer thickness are available from a number of methods, that chosen was a figure of 2.90 nm from capacitance measurements. In contrast, reference 2 instead assumes an arbitrary permittivity of 3.5, giving $\chi^{(2)}(-\omega;\omega,0) = (6.1 + 1.4j) \times 10^{-11}$ m V^{-1}. Fitted results based on both assumptions are given in table 7.4.

Comparing the results for $\epsilon_r = 3.5$ with those from reference 2 shows a difference of about 20%. Bearing in mind the major source of error in the method (estimating the electric field at the point of measurement), this is good agreement. It may

Fitting condition	ϵ_r	d/nm	$\chi^{(2)}(-\omega;\omega,0)$/m V^{-1}
$\epsilon_r = 3.5$	3.5+0.0j	2.60	$(4.9 + 2.2j) \times 10^{-11}$
d = 2.9nm	3.05-0.01j	2.90	$(3.3 + 1.2j) \times 10^{-11}$

Table 7.4 - Pockels effect in Hemicyanine monolayers

be reasonably assumed that the overall error on Pockels effect measurement is no more than 20% *provided that the either the layer thickness or permittivity is known.* In this case the result based on a layer thickness of 2.90 nm gives the best estimate of nonlinear susceptibility for hemicyanine at $\chi^{(2)}(-\omega;\omega,0) = (3.3 + 1.2j) \times 10^{-11}$ m V^{-1}.

Hemicyanine mixed with 53 mol % of 22-TA was also investigated for its Pockels effect. Assuming a layer thickness equal to that for a 22-TA layer (2.95 nm) gave a permittivity of $\epsilon_r = 3.43 + 0.00j$ and $\chi^{(2)}(-\omega;\omega,0) = (3.8 + 0.1j) \times 10^{-11}$ mV^{-1}.

The enhancement of the nonlinear effect and permittivity on dilution with a fatty acid is as expected from second harmonic generation measurements[3], but smaller in size. For a 50:50 molar mixture, a doubling of $\chi^{(2)}(-2\omega;\omega,\omega)$ occurred (ie. a factor of four increase in second harmonic). However there was only a 15% increase in $\chi^{(2)}(-\omega;\omega,0)$ for a similar mixed monolayer. To explain this difference, some discussion of the likely enhancement mechanism is required.

From the SHG results, mixing with a fatty acid was believed to alter the film properties in three ways: a bathochromic shift in absorption, an improvement in molecular alignment and a reduction in relative permittivity. All three of these changes would improve the second harmonic intensity. In fact it is clear from the SPR results that the permittivity is increased, thus the enhancement must be caused by the other two effects. The bathochromic shift gives an absorption increase in the red-yellow part of the spectrum, when this coincides with one of the wavelengths of measurement an enhancement in $\chi^{(2)}$ will result. This is clearly the case for Pockels effect at 633 nm and second harmonic generation with a 1064 nm

input (ie. 532 nm harmonic). The improvement in molecular alignment will also increase $\chi^{(2)}$ by ensuring that a greater proportion of the chromophores combine additively. The alignment change will also increase the birefringence of the film, in line with the increase in the component of permittivity monitored by surface plasmon resonance. The most likely explanation for the smaller increase in Pockels effect is that the absorption increase is greater at 532 nm than at 633 nm.

The Pockels effect of a monolayer of 4-HANS mixed with 46.0 mol % 22-TA was measured by again assuming a layer thickness equal to that of 22-TA (2.95 nm). The derived values were $\epsilon_r = 2.99 + 0.05j$, $\chi^{(2)}(-\omega;\omega,0) = -(8.0 + 0.3j) \times 10^{-12}$ m V^{-1}. As expected the sign of the effect is opposite to that for hemicyanine, this is due to the opposite positions of the donor and acceptor groups relative to the hydrophilic and hydrophobic ends of the molecule. The form of the differential reflectivity graph is shown in Figure 7.2; in contrast to materials with positive $\chi^2(-\omega;\omega,0)$ a decrease in reflectivity occurs at angles below resonance and in increase at angles above.

The fitting processes for both ϵ_r and $\chi^{(2)}(-\omega;\omega,0)$ produce complex values of the two quantities. The imaginary part of relative permittivity is interpreted as being due to the optical absorption in the film. If the real part of relative permittivity of ϵ_r' is much larger than the imaginary part ϵ_r'', then the absorption coefficient k is given by the following equation:

$$k = 8.868 \times 10^{-2} \times \frac{\epsilon_r''}{2\epsilon_r'}$$

(the constant factor converts the units of k to dB cm^{-1})

The effect of the imaginary part of permittivity on surface plasmon resonance is to broaden the reflectivity minimum and, like any optical absorption measurement, the effect is due to a mixture of true absorption (due to electronic transitions) and scattering. The results show a clear trend with film quality, the best LB materials

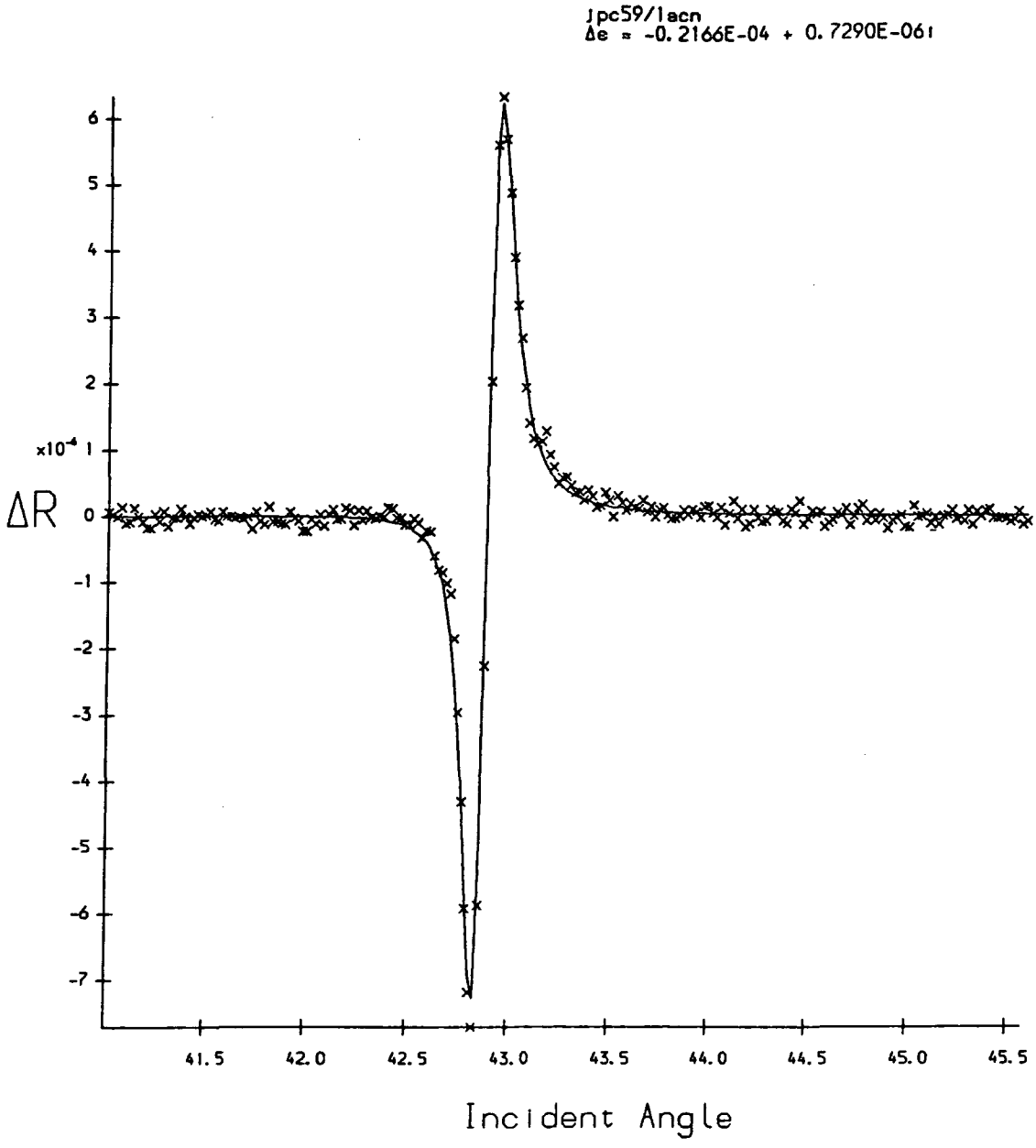

Figure 7.2 - Fitted Pockels effect curve for 4-HANS monolayer

such as 4-HANS and hemicyanine having values between 0.00 and 0.05. Materials with poor deposition properties exhibit larger ϵ_r'' (eg. JT3 has a value of 1.23). The imaginary part of $\chi^{(2)}(-\omega;\omega,0)$ is much harder to interpret. In theory it represents electrically induced loss or scattering in the film. In order to be detected at the same frequency as the applied field, only linear processes can be involved. This

rules out the Stark electroabsorption effect, which is a quadratic process. It is observed that, in general, the materials with the larger values of the imaginary part of $\chi^{(2)}(-\omega;\omega,0)$ also have large values of imaginary permittivity, suggesting that this may be some artefact of the fitting process.

7.2.2 Functionalised diarylalkynes

Ellipsometric measurements on JT11 films established the monolayer thickness as 3.65 nm. Given the similarity of molecular length, this figure will also be used for JT3[4] which did not deposit with sufficient quality to allow ellipsometric measurements.

Fitting the surface plasmon resonance and Pockels effect results for this thickness gave; for JT3 $\epsilon_r = 2.63 + 1.23j$, $\chi^{(2)}(-\omega;\omega,0) = (5.5 + 6.5j) \times 10^{-12}$ mV^{-1}; for JT11 $\epsilon_r = 2.74 + 1.05j$, $\chi^{(2)}(-\omega;\omega,0) = (7.4 + 1.5j) \times 10^{-12}$ mV^{-1}.

Compared to hemicyanine the nonlinear susceptibility values are somewhat low but they are of similar scale to those for 4-HANS. This suggests that the materials will be of value provided that their deposition properties remain good for a large number of layers. This is clearly not the case for JT3. However, JT11 is capable of producing many Y-type layers; furthermore the sign of the nonlinear effect is appropriate for alternation with 4-HANS (the characterisation of JT11/4-HANS alternate layers is discussed in chapter 8).

For both JT3 and JT11 the imaginary parts of ϵ_r and $\chi^{(2)}(-\omega;\omega,0)$ are much larger than for 4-HANS and hemicyanine. This implies that the film quality is poorer although, in the case of JT11, the consistency of the transfer ratio does not support this.

7.2.3 Diphenyl butadiynes

As these materials did not deposit to sufficient thickness for ellipsometry, the monolayer thicknesses were estimated to be equal to the molecular lengths (from a CPK space filling model).

The molecular length for JT666[5] was 3.6 nm, giving $\epsilon_r = 1.96 + 0.18j$ by fitting the surface plasmon data.. This figure is too small for a material designed to be highly polarisable, suggesting that the layer thickness has been overestimated.

As the donor group in the molecule is adjacent to the hydrophobic chain, it had been expected that $\chi^{(2)}(-\omega;\omega,0)$ would be negative (the same as 4-HANS); however the direction of the detected signal clearly showed it to be positive. This implies that the direction of the chromophore is reversed, ie the NO_2 group points away from the substrate. A likely orientation in the floating monolayer, consistent with this observation, is shown in figure 7.3. The molecule is folded with the central oxygen in the subphase and the chromophore and alkyl chain pointing upwards. This arrangement would give a monolayer thickness of 1.8 nm when transferred to the substrate. Fitting of the surface plasmon and Pockels effect results leads to $\epsilon_r = 5.21 + 1.00j$ and $\chi^{(2)}(-\omega;\omega,0) = (2.7 - 0.4j) \times 10^{-10}$ mV^{-1}.

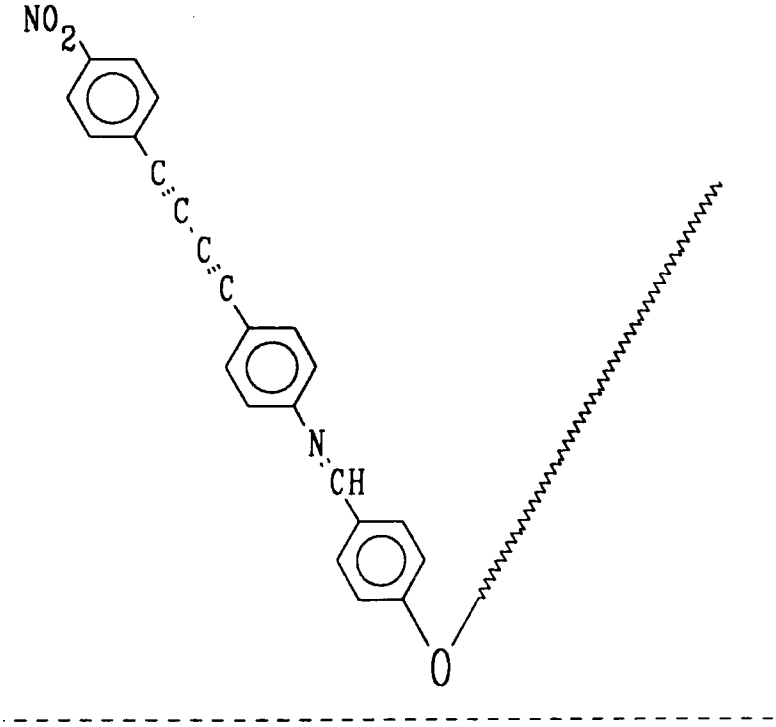

Figure 7.3 - Possible orientation of JT666 molecules

The sign of the Pockels effect for JT777 is also positive, again this suggests a folded molecule. Assuming a layer thickness of 2.1 nm gives $\epsilon_r = 2.40 + 0.12j$ and $\chi^{(2)}(-\omega;\omega,0) = (1.7 + 0.0j) \times 10^{-10}$ mV^{-1}.

A surface plasmon resonance curve for a monolayer of JT301 was fitted by assuming a layer thickness equal to the molecular length (2.6 nm from a CPK space filling model). This gave a relative permittivity of 35.2 + 2.0j. This impossibly high figure shows that the layer thickness was severely underestimated and that the 'monolayer' most likely consists of a thick multilayer film. A Pockels signal was detected but any attempt to fit a value to this would be meaningless without information on the layer thickness.

The poor deposition properties of these materials are largely explained by the deformation of the molecules within the monolayer, making stacking of subsequent layers extremely difficult.

7.2.4 pNA and mNA derivatives

The monolayers of JYT21 mixed with 22-TA gave an extremely small Pockels effect. Assuming a layer thickness of 2.95 nm (the thickness for pure 22-TA), led to $\epsilon_r = 1.39 + 0.09j$ and $\chi^{(2)}(-\omega;\omega,0) = (8.5 + 2.5j) \times 10^{-13}$ m V^{-1}. The permittivity value is unrealistically low for any solid and indicates that the layer is thinner than assumed. This may imply that no 22-TA was deposited at the point probed by the laser. The second-order susceptibility is on the threshold of detectability for this experiment. The molecular design would be expected to give greater nonlinear effects but the result may be due to poor alignment within the layer.

No Pockels effect was detectable for JYT19 mixed with 22-TA.

Given the small scale of the nonlinear properties and the probability of poor molecular alignment there is no value in further work on these materials.

7.2.5 Aminonitrostilbene carboxylic acids

Only one of these materials was investigated for the Pockels effect, namely 1-40A in a mixed monolayer with 22-TA. As multilayer quality was too poor for successful ellipsometry, the layer thickness was assumed to be equal to that for pure 22-TA (2.95 nm). Fitting of the surface plasmon resonance and Pockels effect results gave $\epsilon_r = 5.73 + 0.24j$ and $\chi^{(2)}(-\omega;\omega,0) = (1.43 - 0.02) \times 10^{-10}$ m V^{-1}. This second-order susceptibility is the largest so far recorded for the Pockels effect in an LB film (apart from that estimated for the folded JT666 molecule). However the relative permittivity appears to be overestimated, being approximately double that of other nitrostilbenes. This implies that the layer thickness must actually be greater than 2.9 nm and the true nonlinear susceptibility smaller than that quoted. Despite this qualification this type of material would be worthy of further study if derivatives can be synthesised with better deposition properties. This may, for example, be achieved by increasing the alkyl chain lengths in an effort to promote transfer of the pure material.

7.2.6 Oligomeric Materials

Ellipsometry on S119191 had given a layer thickness of 2.73 nm, which was used for interpreting the SPR and Pockels effect results. Permittivity was fitted to be $\epsilon_r = 5.1+0.81j$ and second-order susceptibility as $\chi^{(2)}(-\omega;\omega,0) = (1.42+0.17j)\times 10^{-10}$ m V^{-1}. This latter value is one of the largest for LB films. However, neutron diffraction results carried out by ICI[6] suggest that a 2 nm water layer is trapped between the film and substrate. When allowance is made for this the results become $\epsilon = 2.60 + 0.46j$ and $\chi^{(2)}(-\omega;\omega,0) = (3.4 + 1.0j) \times 10^{-11}$ m V^{-1}. Nevertheless, this value for nonlinear susceptibility is still among the highest for LB films. The new value for ϵ_r seems too small for such a polarisable material, implying that the water layer is really less than 2 nm in thickness. Refitting with a thinner water layer would lead to a slightly larger nonlinear susceptibility.

A further aspect of S119191's behaviour was also studied. By spacing the monolayer away from the substrate with 22-TA layers it was possible to investigate

whether the nonlinear effects are enhanced by substrate interactions. Samples were prepared with a monolayer of S119191 deposited onto 2, 4 and 6 layers of 22-TA on a silver coated glass slide. The results are given in table 7.5. For two layers of 22-TA, both the permittivity and second-order susceptibility are greater than found for more spacer layers. This suggests that some substrate interaction may be taking place. The second-order susceptibility is, in fact, larger than for deposition with no spacer layers. This could be due to better chromphore alignment when deposited onto 22-TA. However, the interpretation of the results is complicated by the fact that the permittivity with two 22-TA layers is greater than that for a monolayer deposited next to the substrate (when a water layer is assumed). This appears to place in doubt the presence of the water layer. The large value of permittivity for the monolayer with no spacer could then be explained by a substrate interaction. However, when spaced by 4 or 6 layers from the substrate the nonlinear properties fall to a constant value indicating that the limit of substrate interactions has been passed. This constant value, about $(9.0+0.0j)\times 10^{-11}$ mV^{-1}, is still large and confirms that this oligomer has potential for electroopic application.

Number of 22-TA layers	ϵ_r	$\chi^{(2)}(-\omega;\omega,0)$/m V^{-1}
2	5.56+0.07j	$(2.4+0.1j)\times 10^{-10}$
4	3.25+0.22j	$(7.0+0.0j)\times 10^{-11}$
6	3.85+0.15j	$(9.0+0.0j)\times 10^{-11}$

Table 7.5 - Effect of 22-TA spacer layers on Pockels effect in S119191

Although the material S122699 is designed as a passive spacer, it was also studied for its Pockels effect. Assuming the ellipsometric layer thickness of 2.04 nm produced $\epsilon_r = 2.36 + 0.21j$ and $\chi^{(2)}(-\omega;\omega,0) = (6.0 + 2.4j)\times 10^{-12}$ m V^{-1}. As expected, both the permittivity and nonlinearity are reduced due to the decreased

length and polarisation of the π-electron system. The figure is still, however, greater than that of some LB materials designed for nonlinear optics.

7.3 Second Harmonic Generation

The purpose of the second harmonic generation experiments was to provide a rapid indication of whether the materials possessed significant activity. Unless this was the case, there was clearly no value in attempting to determine individual tensor elements and structural information. Therefore the initial measurements were carried out for unpolarised inputs and outputs. The detected intensity is then due to the combined effect of many tensor components (see section 4.3.1).

In all cases, hemicyanine monolayers were used as reference samples. These monolayers were always freshly produced as their response has been found to decay with storage time. For monolayers kept in air at room temperature, 40% of the SHG was lost after 18 months and 95% after 5 years[7]. As both 4-HANS[8] and hemicyanine:fatty acid[3] mixtures have been previously studied for second harmonic generation only the novel materials and the hemicyanine:diacetylene mixtures were investigated.

7.3.1 Hemicyanine:Diacetylene Mixed Layers

The aim of mixing these two compounds was to form a system with hemicyanine dye within a polydiacetylene matrix. It was hoped that such a film would combine the second-order nonlinear properties of hemicyanine with the thermal and structural stability of polydiacetylene.

The 12-8 diacetylene polymerises on exposure to ultra-violet light[9]; this can then be detected by the formation of absorption peaks between 450 and 650 nm. The presence of hemicyanine dye within the film would be likely to inhibit polymerisation by separating the molecules of the diacetylene.

Films of different proportions (10 to 20 layers) were produced and exposed to ultra violet light in an EPROM eraser. Spectra were taken before and after exposure and the colours of the films were also noted. The results are shown in table 7.6.

mol% hemicyanine	colour before exposure	exposure time /minutes	colour after exposure
5.9	yellow	30 to 60 minutes	deep blue to mauve
12.4	orange	30 to 60 minutes	pink
19.5	orange	30 to 90 minutes	pink
27.4	orange	30 to 90 minutes	pale orange

Table 7.6 - The effect of uv exposure on mixed hemicyanine : diacetylene layers

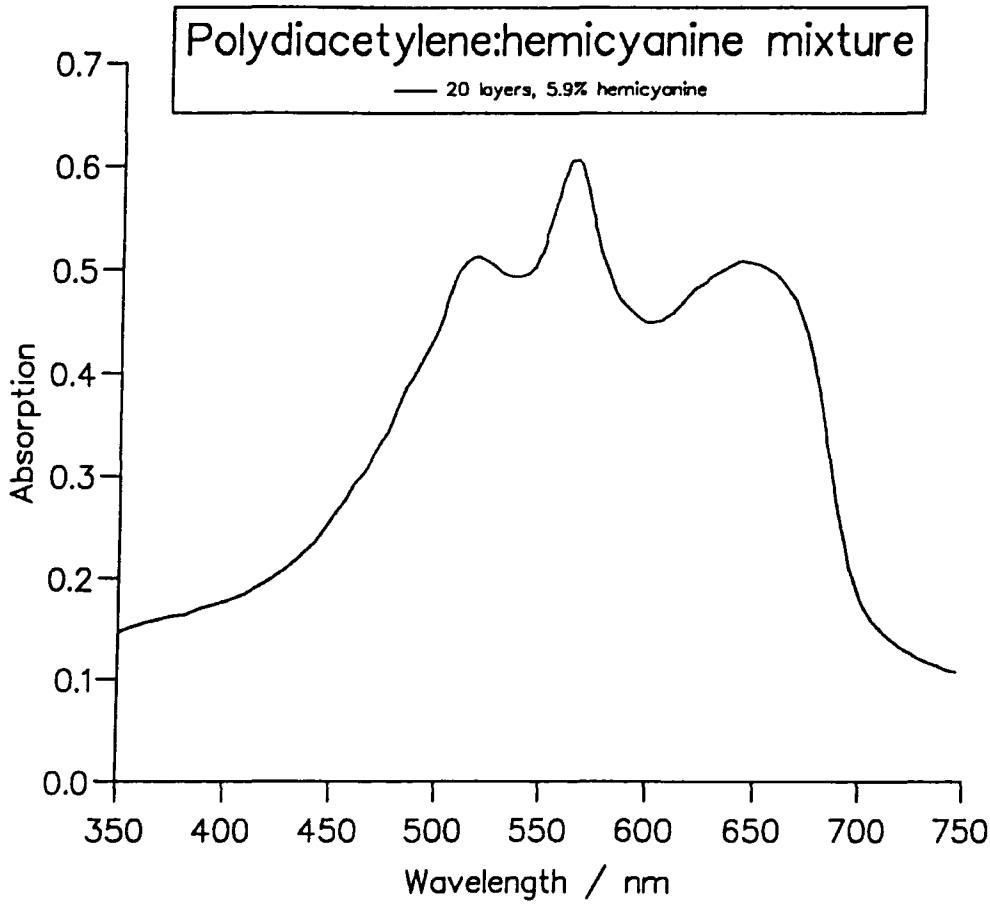

Figure 7.4 - Absorption spectra of uv exposed diacetylene:hemicyanine films

The blue-mauve-red colouration is indicative of the formation of polydiacetylene which exists in both red and blue forms. A typical spectrum is shown in figure 7.4. The blue form (type A) has an absorption band at 640 nm and the red form (type B) at 540 nm. This spectrum shows clearly that the polymerised films are a mixture of the two types.

For films with 5.9 mol% and 12.4 mol% hemicyanine polymerisation occurred after only 30 minutes; for 19.5 mol% this time increased and no sign of polymer formation was evident for 27.4 mol%. The colouration of the unexposed films is due to the hemicyanine dye - red in pure films but yellow/orange on dilution. The colour change of the 27.4 mol% film suggests that the hemicyanine is itself being changed in some way by the ultra-violet exposure.

Monolayers of four different concentrations (including pure hemicyanine) were studied for second harmonic generation both before and after exposure to ultra-violet (see table 7.7). The exposure time was 120 minutes for the film with 19.5 mol% hemicyanine and 30 minutes for the others. For all films it was observed that the second harmonic intensity fell after exposure.

SHG Intensity		
mol% hemicyanine	before exposure	after exposure
5.9	0.00	0.00
12.4	0.08	0.00
19.5	0.08	0.00
100.0	1.00	0.33

Table 7.7 - SHG from mixed hemicyanine:diacetylene monolayers

The above observations may be explained as follows. The ultra-violet exposure of the hemicyanine is causing the breaking of one of the double bonds at the centre of the chromophore and the formation of dimers (see figure 7.5). This cuts

the conjugated π-electron system and so reduces the nonlinear polarisability. For the unpolymerised films the activity is comparable to similar hemicyanine:fatty acids films. For example, the monolayers containing 12.4 mol% and 19.5 mol% of hemicyanine both gave a relative second harmonic intensity of 0.08. A hemicyanine: arachidic acid mixture with 14.9 area % of the dye produced an intensity of 0.12 (transmitted wave, p-polarised input and output)[3].

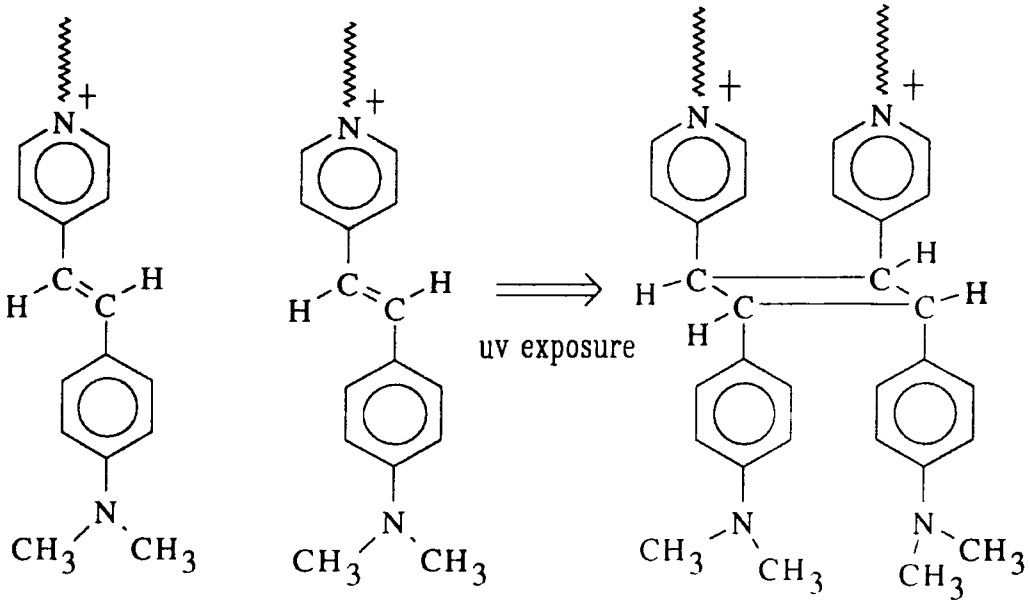

Figure 7.5 - Formation of hemicyanine dimers

Clearly, hemicyanine dye is unsuitable for use in an ultra-violet polymerised system but it may be possible to find other dyes which are not dimerised during the polymerisation process.

7.3.2 Functionalised diarylalkynes

The two materials gave very similar monolayer second harmonic intensities. Relative to a hemicyanine monolayer the values were 0.02 for JT3, and 0.03 for JT11. An approximately equimolar mixture of JT11 with 22-TA gave an intensity of 0.04.

These values are all quite small, but this is as would be expected from the Pockels effect results. The values of $\chi^{(2)}(-\omega;\omega,0)$ were less than one quarter of that for hemicyanine; neglecting dispersion and permittivity differences this translates to a relative SHG intensity of 0.05. The fact that the measured values are slightly below this can be explained by the differing frequencies of the two measurements.

7.3.3 Diphenyl butadiynes

A monolayer of JT666 mixed with about 20 mol % of 22-TA gave a second harmonic intensity of 0.08 (reference to a hemicyanine monolayer). This is quite a small value and the material was not amenable to multilayer formation. Also, the Pockels effect measurements suggest a folded molecule so it is unlikely that any method will be found to improve the transfer properties. Clearly, further work on this material is not worthwhile.

As the other materials in the series exhibit similar deposition and Pockels effect properties, they were not studied for second harmonic generation.

7.3.4 Oligomeric materials

Only the active material S119191 was studied for second harmonic generation as a monolayer. Two separate samples were investigated; although each showed negligible area to area variation individually, there was some inconsistency between the two samples. The output intensity can be stated as 0.99 ± 0.28 (relative to a hemicyanine monolayer).

This is a very promising result, especially as the material has good deposition properties. The results for alternation with its passive partner S122699 are given in chapter 8.

7.4 Summary

The nonlinear susceptibilities and second harmonic intensities for all the compounds are summarised in table 7.8. Of the materials investigated, only the ICI

oligomer S119191 combines good deposition properties with large nonlinear effects. This compund exhibits second harmonic generation and Pockels effect signals similar to those of hemicyanine and gives excellent Langmuir-Blodgett deposition for up to 50 layers.

JT11 has only small nonlinear properties but it forms good alternate-layers with 4-HANS. The fact that large thicknesses are possible may outweigh its relatively low monolayer response.

The diphenyl butadiynes and the aminonitrostilbene carboxylic acid 1-40A both give substantial nonlinear responses but are unable to form multilayers. This suggests that it will be worth combining the active chromophores with other groups in an effort to give a workable Langmuir-Blodgett material.

The nitroanilines showed negligible nonlinear effects and were unable to form high-quality multilayer films.

The hemicyanine:polydiacetylene mixtures also showed poor nonlinear properties due to the dimerisation of the dye on irradiation.

Material	$\chi^{(2)}(-\omega;\omega,0)$	Relative
	$\times 10^{12}$ m^{-1} V	SHG
Hemicyanine	33	1.00
Hemicyanine:22-TA	38	
4-HANS:22-TA	-8.0	
JT3	5.5	0.02
JT11	7.4	0.03
JT666	270	0.08
JT777	170	-
JYT21:22-TA	0.85	-
1-40A:22-TA	143	-
S119191	34	0.99
S122699	6.0	-

Table 7.8 - Summary of Pockels effect and SHG intensities

References

1. D. den Engelsen, *J. Opt. Soc. Am.* **61** pp1460-6 (1971).

2. G.H. Cross, I.R. Girling, I.R. Peterson, N.A. Cade, *Electronics Letters* **22** pp1111-3 (1986).

3. I.R. Girling, N.A. Cade, P.V. Kolinsky, R.J. Jones, I.R. Peterson, M.M. Ahmad, D.B. Neal, M.C. Petty, G.G. Roberts, W.J. Feast, *J. Opt. Soc. Am. B* **4** (6) pp950-5 (1987).

4. J. Tsibouklis, J.P. Cresswell, N. Kalita, C.Pearson, P.J. Maddaford, H. Ancelin, J. Yarwood, M.J. Goodwin, N. Carr, W.J. Feast, M.C. Petty, *J. Phys. D Appl. Phys.* **22** pp1608-12 (1989).

5. J. Tsibouklis, J. Cresswell, C. Pearson, M.C. Petty, W.J. Feast, *Int. Phys. Conf. Ser.* **103** pp187-92 (1989).

6. S. Allen, T.G. Ryan, D.P. Devonald, M.G. Hutchings, A.N. Burgess, E.S. Froggatt, A. Hamilton, R.M. Swart, G.J. Ashwell, M. Malhotra, *Organic Materials for Nonlinear Optics 90* (Royal Society of Chemistry, London) in press.

7. N. Carr, G. Ashwell, J. Cresswell, *unpublished data.*

8. D.B. Neal, M.C. Petty, G.G. Roberts, M.M. Ahmad, W.J. Feast, I.R. Girling, N.A. Cade, P.V. Kolinsky, I.R. Peterson, *Electronics Letters* **22** (9) pp460-2 (1986).

9. K. Saito, M. Saito, K. Ikegami, S. Kuroda, M. Sugi, *Jap. J. Appl. Phys.* **27** (6) pp1038-41 (1988).

Chapter 8
Characterisation of Langmuir-Blodgett Multilayers

Two different alternate-layer systems were studied; 4-HANS with JT11, and the partnership of the two ICI oligomers. These were characterised for their nonlinear properties (Pockels effect and second harmonic generation) and also by ellipsometry, Fourier transform infra-red spectroscopy, X-ray diffraction and waveguiding. These latter measurements were undertaken to provide structural information in order to explain the nonlinear properties. Much of this work is also described in references 1 and 2.

For a nonlinear film of consistent activity, independent of thickness, two relations are expected to be satisfied: firstly, that the second harmonic intensity will be proportional to the square of thickness; and secondly, that the susceptibility from the Pockels effect measurement $\chi^{(2)}(-\omega;\omega,0)$ will be independent of thickness. A failure to satisfy these criteria is an indication of variable quality across the thickness of the film.

8.1 Ellipsometry

8.1.1 4-HANS/JT11 alternate-layers

Alternate-layers of 4-HANS/JT11 were studied ellipsometrically to find their thicknesses and permittivities. A 5-bilayer region was fitted isotropically to give $n = 1.503 \pm 0.012$ and a bilayer thickness of 7.20 ± 0.30 nm. The error on the thickness is very large here due to point to point variation across the film. The value for thickness may be contrasted with that of 6.3 nm from X-ray diffraction (see section 8.4 for discussion).

8.1.2 Oligomeric alternate-layers

The ICI oligomers were not studied ellipsometrically as an alternate-layer system; however the layer thicknesses for the individual molecules had been previously

established (2.73 nm for S119191 and 2.04 nm for S122699).

8.2 Surface Plasmon Resonance and Pockels Effect

8.2.1 4-HANS/JT11 alternate-layers

Films of 4-HANS/JT11 were studied by surface plasmon resonance in thicknesses of 1, 3 and 10 bilayers. Thicker layers could not be considered as the surface plasmon resonance was shifted out of the angular range of the detector.

Two different bilayer thicknesses were available for fitting purposes; 6.3 nm from X-ray diffraction and 7.20 nm from ellipsometry. It was decided to use the former figure for two reasons. Firstly, X-ray diffraction derives the layer thickness independently of any other parameters whereas ellipsometry must attempt to match the results to a possible refractive index. Secondly, the value of 6.3 nm gave a realistic value of permittivity on fitting of the surface plasmon resonance results ($\epsilon_r = 2.35$).

Fitting the Pockels effect results with a thickness of 6.3 nm per bilayer gave the figures shown in table 8.1. The values for monolayers of JT11 and 4-HANS are also included for comparision. Within the estimated 20% accuracy of the experiments, the results are independent of the number of bilayers, suggesting undiminished film quality. The values are slightly smaller than for the monolayer materials, this may indicate that the chromophores of the two materials are not lining up exactly colinearly. The result of this would be incomplete summing of their hyperpolarisablities in the direction of the film normal. These results are encouraging for the construction of thick alternate-layer films.

8.2.2 Oligomeric alternate-layers

Alternate-layers of the active (S119191) and passive (S122699) ICI oligomers were produced. The active material was always transferred first on an upstroke, leading to films with an odd number of layers. A 3 layer (active-passive-active, 'apa') and

Number of bilayers	$\chi^{(2)}(-\omega;\omega,0)$/ m V^{-1}
1	2.6×10^{-12}
3	3.7×10^{-12}
10	3.2×10^{-12}
4-HANS monolayer	-4.5×10^{-12}
JT11 monolayer	4.3×10^{-12}

Table 8.1 - Pockels effect in 4-HANS/JT11 alternate-layers

a 5 layer ('apapa') film were deposited.

The Pockels results were fitted by using the layer thicknesses found by ellipsometry on Y-type layers of the individual materials. It was expected that, as in the case of S119191 monolayers, the films would include a 2 nm water layer between the first monolayer and the substrate. Results are shown in table 8.2 both allowing for and neglecting this layer. The value of $\chi^{(2)}(-\omega;\omega,0)$ for an S119191 monolayer is also given, the contribution of S122699 to the overall Pockels effect in the film may be neglected as its monolayer response was only 5% of the active material's.

Sample	$\chi^{(2)}(-\omega;\omega,0)$ m V^{-1}		ϵ_r	
	with water	without water	with water	without water
S119191 ×1	3.4×10^{-11}	1.4×10^{-10}	2.6	5.1
apa	4.2×10^{-12}	7.0×10^{-12}	2.12	2.63
apapa	1.2×10^{-12}	1.5×10^{-12}	2.54	2.90

Table 8.2 - Pockels effect and SPR results for oligomeric alternate-layers

It is difficult to establish whether all the films do indeed contain a trapped water layer from the results for ϵ_r. Although a more realistic value of permittivity is obtained for the monolayer of S119191 by assuming this layers presence, the situation is reversed for the 3-layer film. For the 5-layer film both values of permittivity are within the bounds of possibility. It appears that the trapping of the water layer may depend critically on the exact deposition conditions.

From the Pockels effect results, it is clear that the chromophores of the active material show no correlation from layer to layer. Whether the results are fitted with allowance for a water layer or not, it is seen that the nonlinear susceptibility falls to roughly 15% of its original value by 3 layers and to 5% by 5 layers. This is actually greater than the reduction that would occur if the second and third deposited layers of S119191 were non-electrooptic. In that case simple dilution of the effect would occur (ie to one-third after 3 layers and one-fifth after 5 layers). Obviously the direction of the dipoles in the later layers must be actually opposing that of the first layer. This alternate-layer system is clearly of no use for nonlinear optics, however S119191 has been shown to give excellent second harmonic generation when alternated with a quinolinium salt[4]. A different design of oligomeric partner may produce similar results.

8.3 Second Harmonic Generation

8.3.1 4-HANS/JT11 alternate-layers

The 4-HANS/JT11 structures of 1, 7, 25 and 49 bilayers were studied for their second harmonic generation deposited on both hydrophilic and hydrophobic substrates. The results are shown as a graph in figure 8.1, and also in table 8.3. All values are relative to a hemicyanine monolayer.

The dashed lines in figure 8.1 are to indicate the expected quadratic relationship of intensity to number of layers. It is clear that this relationship is not satisfied and that the increase in intensity gradually tails off. The response for a single bilayer is ten times greater for the hydrophobic substrate indicating that the active groups

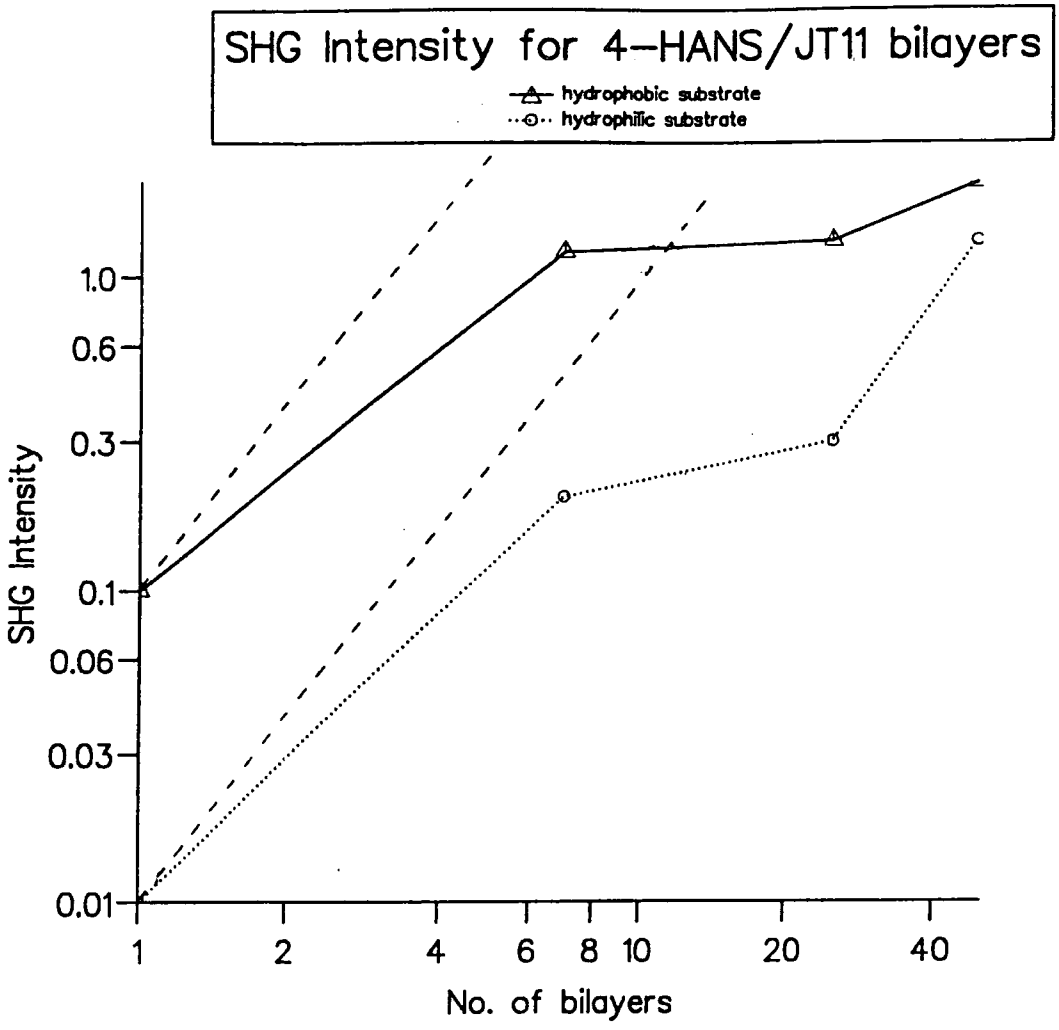

Figure 8.1 - SHG v number of bilayers for 4-HANS/JT11

Number of	SHG Intensity	
bilayers	hydrophobic	hydrophilic
1	0.10	0.01
7	1.20	0.20
25	1.30	0.30
49	2.00	1.30
150	-	0.8

Table 8.3 - SHG intensities for 4-HANS/JT11 alternate-layers

in the film must be better aligned. However, this greater order is not carried over into larger numbers of layers; the activity of the films on hydrophobic substrates gets closer and closer to those deposited onto hydrophilic glass.

Table 8.4 gives estimates of $\chi^{(2)}(-2\omega;\omega,\omega)$ for different thicknesses of films. These values are calculated by deriving the second-order susceptibility for hemicyanine from reference 3 ($\chi^{(2)}(-2\omega;\omega,\omega) = 1.3\times10^{-10}$ mV^{-1}), assuming the same permittivities as hemicyanine and then recalculating to take the various film thicknesses into account. Therefore, these figures can only be considered as estimates but, as they are internally consistent, the trend with number of layers is correct. It is observed that $\chi^{(2)}(-2\omega;\omega,\omega)$ falls markedly with increasing thickness; in the case of a hydrophobic substrate to only 10% of its original value by 49 bilayers. This is equivalent to a factor of 100 reduction in second harmonic intensity. Again it is clear that the activities of films on the different substrates converge for a large number of layers.

Number of	$\chi^{(2)}(-2\omega;\omega,\omega)$m V $^{-1}$	
bilayers	hydrophobic	hydrophilic
1	19×10^{-12}	6.1×10^{-12}
7	9.6×10^{-12}	3.9×10^{-12}
25	2.8×10^{-12}	1.4×10^{-12}
49	1.7×10^{-12}	1.4×10^{-12}

Table 8.4 - $\chi^{(2)}(-2\omega;\omega,\omega)$ estimates for 4-HANS/JT11 alternate-layers

The most likely explanation of these results is that the order within the films is poor and the alignment of chromophores decreases for an increase in thickness. This is in contradiction to the Pockels effect measurements which reveal no reduction in nonlinear properties for up to 10 bilayers. This may indicate better structure in the

films prepared on silver. The orders of magnitude for $\chi^{(2)}$ obtained from the two methods are in good agreement despite the difference in measurement frequencies.

In absolute terms, all the intensity values are much smaller than would be expected. A 4-HANS monolayer gave an SHG intensity of 0.13 relative to a hemicyanine monolayer[3]. Thus, neglecting any contribution from the JT11, a 50 bilayer sample should give a relative intensity of over 300, assuming perfect orientation of all layers. To further study the reasons for this discrepancy, structures were prepared with one of the active materials replaced with cadmium arachidate (CdAr) as a spacing layer (see table 8.5 for SHG results). For JT11/CdAr alternate-layers very little second harmonic was observed indicating a poor $\chi^{(2)}(-2\omega;\omega,\omega)$ for JT11. The 4-HANS/CdAr bilayers give slightly higher intensity than for equal numbers of bilayers of 4-HANS/JT11. Clearly the removal of one of the active components has been more than compensated for by an improvement in alignment. The results are, however, disappointingly low. This suggests that the degree of ordering is once again poor.

Materials (7 bilayers)	SHG intensity
4-HANS/CdAr	1.3
CdAr/JT11	0.05

Table 8.5 - SHG intensities for 4-HANS and JT11 alternated with cadmium arachidate

The 150 bilayer sample gave a relative second harmonic intensity of 0.8, a lower figure than for 49 bilayers. A possible explanation for this is that the measurement is not phase-matched. For the thinner films the interaction length would be too small for significant mismatch to build up. An absence of phase matching would lead to a reduction of measured intensity by a factor of

$$\mathrm{sinc}^2(\Delta k l)$$

where l is the interaction length and Δk is a wavevector mismatch term given by

$$\Delta k = 2k_\omega - k_{2\omega} = \frac{2\pi}{\lambda_{2\omega}}(n_\omega - n_{2\omega})$$

Although no measurements of the refractive indices of the alternate-layers are available at the Nd:YAG fundamental and harmonic, it is quite likely that the phase mismatch will become significant for the 150 bilayer film (1 micron thickness). A dispersion as small as 0.1 would halve the second harmonic intensity for this structure.

8.3.2 Oligomeric alternate-layers

As for the samples used for the Pockels effect, these films were prepared with the active material (S119191) transferred first, on an upstroke. Films of 3 layers ('apa') and 5 layers ('apapa') were produced, their second harmonic intensities relative to hemicyanine are given in table 8.6, along with a value for a monolayer of S119191. The results were expected to be in the ratio of the square of the number of active layers in the film, ie 1:4:9.

Sample	SHG intensity
S119191 ×1	0.99
apa	0.10
apapa	0.16

Table 8.6 - SHG intensities for oligomeric alternate-layers

In practice the data (table 8.6) reveal that the multilayers give much less second

harmonic than the monolayer. This is as expected from the Pockels effect results; the chromophores in the second and third S119191 layers must be aligned partly opposing those in the first layer. This reduces the overall $\chi^{(2)}(-2\omega;\omega,\omega)$ by a greater amount than if the subsequent layers were simply non-electrooptic. It is interesting to compare these results with those for S119191 alternated with a quinolinium salt[4]. In the latter case, a quadratic increase in intensity with number of layers was observed, showing that the active groups in the layers were correctly aligned.

8.4 X-ray diffraction in 4-HANS/JT11 alternate-layers

X-ray diffraction was performed on a 25-bilayer structure of 4-HANS/JT11 on hydrophobic glass; the results are presented in figure 8.2. Two diffraction peaks were observed at 2θ values of 1.4 and 4.2 degrees. These represent the first and third order Bragg reflections (the second diffraction order is systematically zero). A d-spacing (ie. the bilayer spacing in this case) of 6.3 nm $\pm$ 0.05 nm was calculated. As a CPK space filling model gave the sum of the molecular lengths to be 8.0 nm, this suggests a tilt angle of 38 degrees to the substrate normal. Further discussion of the film structure is given in section 8.5 in light of the Fourier transform infra-red results.

A second quantity which may be found from the diffraction results is the so called radius of correlation, which is an indication of the extent of long-range order within the film. This is calculated from the widths of the Bragg peaks. For this system it was measured to be 40 ± 5 nm which suggests that the interlayer order is confined to approximately 5 bilayers. Five *perfectly ordered* bilayers should give a second harmonic intensity of about 25 times that for a 4-HANS monolayer, ie. an intensity of 3.5 relative to hemicyanine monolayer. In fact, the definition of radius of correlation is not that it indicates a region of total order but rather that, after a distance equal to one radius, a stacking error of one half-layer has built up. Therefore, the fact that the second harmonic intensities seem to tend towards a relative

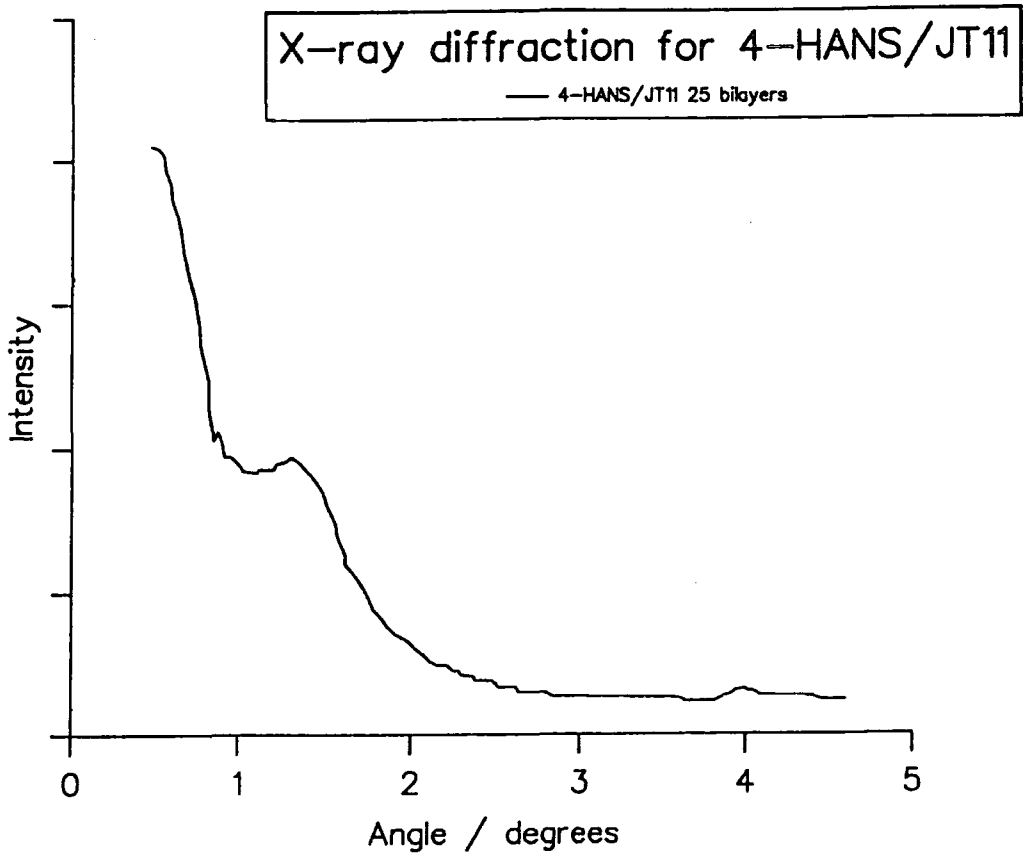

Figure 8.2 - X-ray diffraction from 4-HANS/JT11 bilayers

intensity of about 2 is in excellent agreement with the radius of correlation.

8.5 FTIR studies on 4-HANS/JT11 alternate-layers

Measurements of the infra-red linear dichroism were carried out on the 4-HANS/ JT11 system by Dr. Y. Song of the Department of Chemistry, University of Durham. These studies were designed to provide information on the bond orientations of the two materials and to allow an explanation of the nonlinear optical properties. Alternate-layers were deposited onto substrates of hydrophobic zinc selenide and silver coated glass. The layers on the ZnSe substrate were investigated by an attenuated total reflection (ATR) method and those on silvered glass by reflection absorption infra-red spectroscopy (RAIRS). Both types of measurements were performed in a Mattson Sirius 100 spectrometer.

Initially measurements were made on Y-type layers of JT11 alone to allow the assignment of the different absorption bands to the bonds. Similar studies have already been reported on 4-HANS[5]. For JT11 a RAIRS spectrum of 10 Y-type layers was compared to an ATR spectrum for a solution cast film. The RAIRS technique only couples transition dipoles normal to the substrate but ATR is direction independent (and the cast film will in any case be isotropic). Despite the differences in techniques and in type of film studied the two spectra are very similar (figure 8.3). This indicates that the order in the JT11 LB layers must be quite poor. Bond assignments were made to many of the absorption peaks (table 8.7).

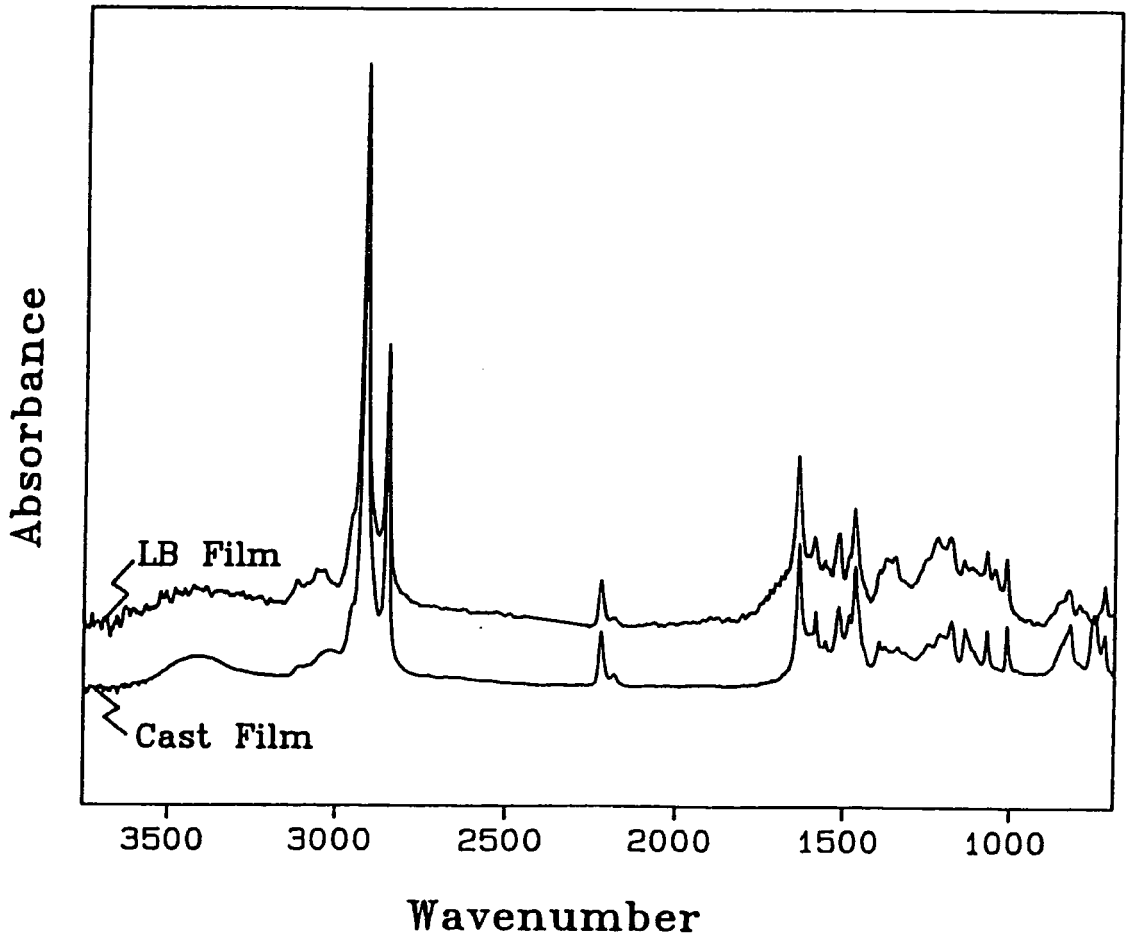

Figure 8.3 - RAIRS spectra for LB and cast films of JT11

$\bar{\nu}_{max}/cm^{-1}$	FWHM/cm^{-1}	bond
3412	185	H_2O, ν(OH)
3107	23	aromatic ν(C-H)
3017	52	aromatic ν(C-H)
2917	17	$\nu_{as}(CH_2)$
2851	12	$\nu_s(CH_2)$
2222	17	ν(C≡C)
2184	17	ν(C≡C)
1636	16	ν(C-N) of pyridinium ring
1584	10	aromatic ν(C-C) (disubstituted benzene)
1468	17	δ(C-H)
826	39	out-of-plane δ(C-H)
721	12	r(CH_2)

Table 8.7 - FTIR bond assignments for JT11 films

Spectra of alternate-layers were then compared for the RAIRS and ATR techniques (figure 8.4). Significant dichroism is apparent from the differing relative absorptions of various bands. For each band an angle of orientation can then be established for the assigned bond. As the absorption bands for the two materials can be individually identified, it is possible to find the orientation of the two dyes independently. The interpretation is that both molecules are well oriented and that their axial carbon chains lie at an angle of approximately 15 degrees to the substrate normal. Thus it can be concluded that JT11 is better ordered in this alternate-layer system than in the single component Y-type films.

The figure of 15 degrees for the tilt of the molecular axes is in contradiction to the figure of 38 degrees deduced by comparing the sum of the molecular lengths with

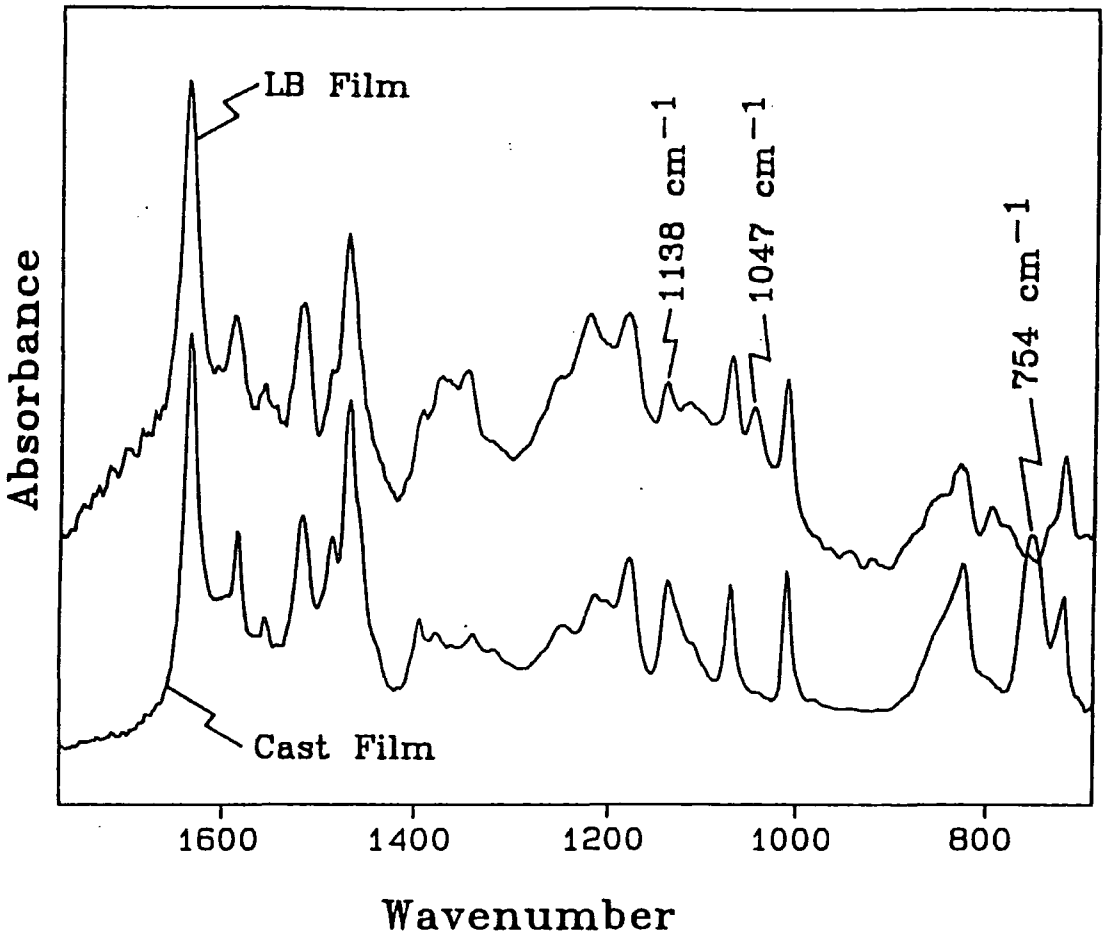

Figure 8.4 - ATR and RAIRS spectra for 4-HANS/JT11 alternate-layer films

the X-ray diffraction repeat distance. In fact, different parts of the molecules are tilted at different angles, the C≡C bond in JT11 is at 43 degrees to the normal and the orientation of the NO_2 group suggests that the stilbene system is tilted in the same direction. Summing the lengths of the alkyl chains at 15 degrees and the chromophores at 43 degrees gives a repeat distance of 7.0 nm which is still significantly larger than the figure of 6.3 nm from X-ray diffraction.

The structure proposed in figure 8.5 satisfies both the X-ray and FTIR measurements. The two chromophores are interdigitated, tilting at an engle of 43 degrees, and the alkyl chains are at 15 degrees to the normal. The layer thickness for such

an arrangement would be in the region of 6.0 nm, in excellent agreement with the X-ray repeat distance. Also shown in this diagram are the likely hydrogen bonds in the 4-HANS:stearic acid layer (these explain the good ordering for 4-HANS). The high order in the JT11 layers for the alternate-layer films is probably due to the interdigitation forcing the chromophores to take up the same angle as those of 4-HANS. This structure also helps to explain the relatively small values of $\chi^{(2)}(-\omega;\omega,0)$ for the alternate-layers as compared to those of the separate components. An interdigitated structure does not lead to such large values of nonlinear susceptibility as an 'end on' system would.

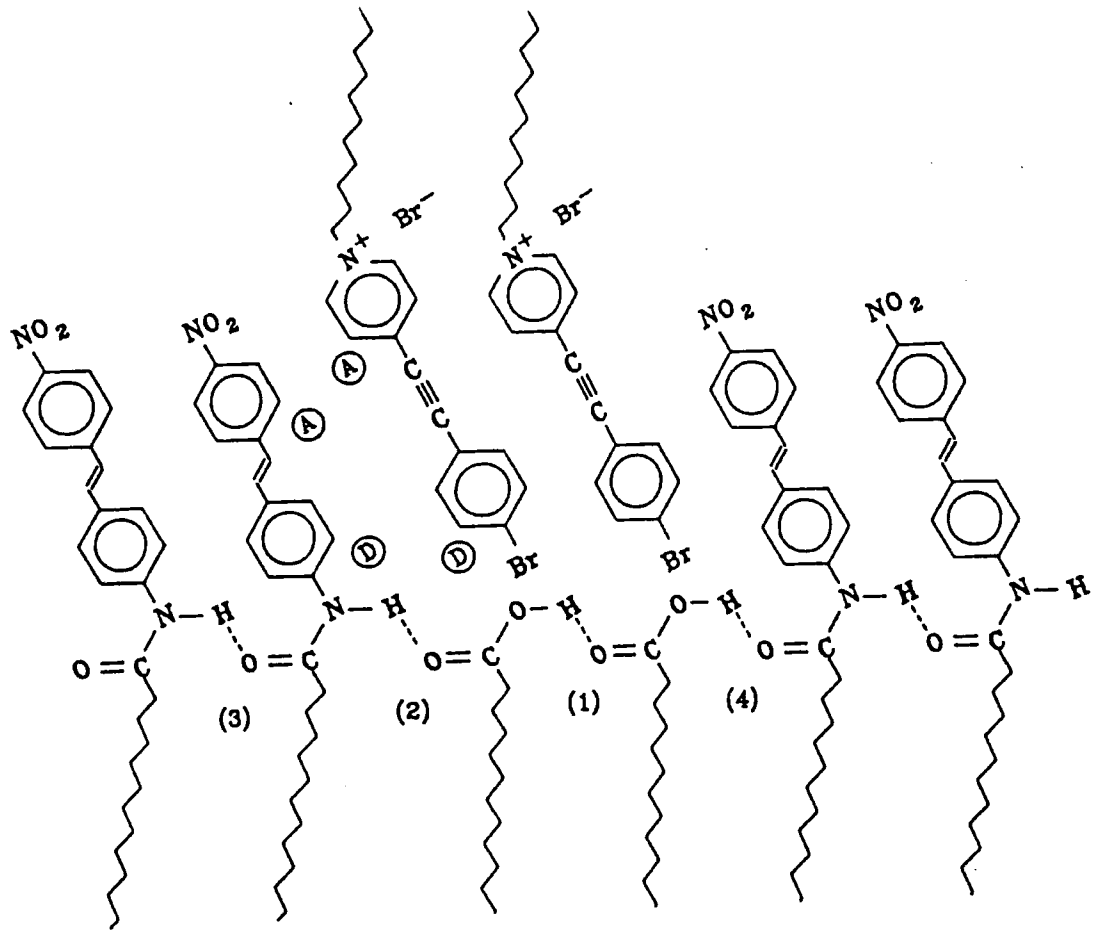

Figure 8.5 - Proposed interdigitated structure for 4-HANS/JT11 alternate-layers

8.6 Waveguiding in 4-HANS/JT11 alternate-layers

Waveguiding was performed using a 150 bilayer sample on a fused silica substrate. The film (see photo in figure 8.6) was strongly yellow coloured due to the 4-HANS and of poor optical transparency, indicating a high density of scattering centres (possibly due to dust or imperfections in the layer stacking). The film may be considered as uniaxial and, as the dipping direction was perpendicular to the propagation direction, some degree of polarisation mixing was to be expected.

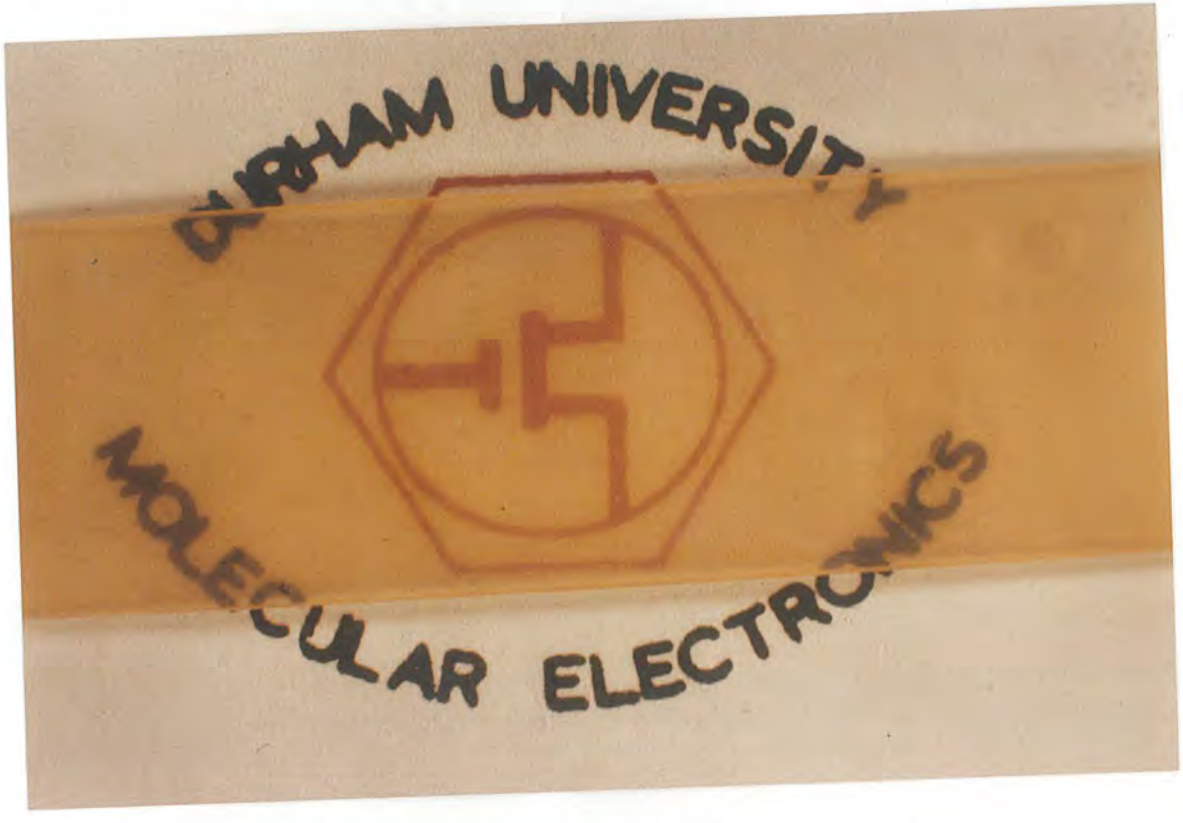

Figure 8.6 - 150 bilayer film of 4-HANS/JT11

Prism coupling at a wavelength of 633 nm revealed one TE and one TM mode. The former was excitable over an angular range of 2 degrees and the latter over 6 degrees. In each case propagation extended over a range of 1 to 2 cm. The effective indices were: $TE_0 = 1.51 \pm 0.1$ and $TM_0 = 1.52 \pm 0.3$. The broadness of

the excitation indicates a substantial degree of disorder and loss within the film. The likely causes of this are scattering, absorption and a distribution of molecular tilt angles giving a variation in refractive index. The refractive indices of the film were calculated by assuming a film thickness of 0.95 μm (150 times the repeat distance from X-ray diffraction). The values were 1.54 for TM and 1.53 for TE. As the molecules are designed to have a large polarisability in one direction only (along the conjugated π electron system) a greater birefringence would expected. The failure to observe this is yet more evidence of disorder within the films. Given the broadness of the mode excitation, it was impossible to observe polarisation mixing.

8.7 Summary

The 4-HANS/JT11 alternate-layer system has been extensively studied for layer thicknesses up to 150 bilayers. Although the results for the Pockels effect for 1 to 10 bilayers show that $\chi^{(2)}(-\omega;\omega,0)$ is maintained, this is not the case for second harmonic generation. The alignment of the molecules appears to be poor and this is supported by the X-ray diffraction and waveguide experiments. The Fourier transform infra-red results show that the chromophores of the materials are overlapped which reduces the overall nonlinearity of the films. The ICI oligomer alternate-layers also failed to show correct interlayer alignment of the active groups. Indeed, the alignment appeared to almost exactly opposite to that required and the properties were greatly degraded for films as thin as 3 layers.

References

1. J. Cresswell, J. Tsibouklis, M.C. Petty, W.J. Feast, N. Carr, M. Goodwin, Y.M. Lvov, *SPIE Proceedings* **1337** pp358-63 (1990).

2. Y.P. Song, J. Yarwood, J. Tsibouklis, W.J. Feast, J. Cresswell, M.C. Petty, *Langmuir* in press.

3. D.B. Neal, M.C. Petty, G.G. Roberts, M.M. Ahmad, I.R. Girling, N.A. Cade,

P.V. Kolinsky, I.R. Peterson, *Electronics Letters* **22** (9) pp460-3 (1986).

4. S. Allen, T.G. Ryan, D.P. Devonald, M.G. Hutchings, A.N. Burgess, E.S. Froggatt, A. Hamilton, R.M. Swart, G.J. Ashwell, M. Malhotra, *Organic Materials for Nonlinear Optics 90* (Royal Society of Chemistry, London) in press.

5. Y. Song, J.Yarwood, M.C. Petty, *Langmuir* in press.

Chapter 9
Langmuir-Blodgett Film/Polymer Waveguides

The work described in chapter 8 on thick alternate-layers of JT11 and 4-HANS demonstrated the major difficulties in forming waveguides from LB films. The minimum thickness requirement for guiding can only be satisfied by several hundred layers, this means that the fabrication time will be in the region of 50 hours. The layers produced were then found to have smaller nonlinear effects than expected by extrapolation from thin films. The guides also exhibited high propagation losses.

Conversely, low loss polymer waveguides may be rapidly produced by either solution dipping or spinning. However the materials are amorphous and cannot possess second order nonlinearities without further processing. This takes the form of poling in an electric field which aligns nonlinear groups either within the polymer or dopant dyes. Unfortunately the scale of effect so produced is much smaller than the best LB films and decays with time as the groups re-align thermally[1].

The work described in this chapter combines polymer layers for low loss propagation and rapid fabrication with LB layers to provide the nonlinear properties.

9.1 Initial Design of Waveguide

Langmuir-Blodgett films have already been combined with other materials as a waveguiding structure, for example with an ion-exchanged glass waveguide[2]. A similar approach could easily be used with a polymer waveguide, however the LB layer only guides the evanescent tail of the field profile. This means that only a small proportion of the light's power is in the nonlinear medium. Figure 9.1 shows the field in such a waveguide, the profile is for the H_y field of the TM_0 mode, the other fields and polarisation are of an approximately similar shape. Only 8% of the power power of the TM_0 mode is in the LB film. If the alignment of the molecules in the LB film is near-normal, then it is the TM modes which will interact with the nonlinear groups. All the guides were designed to be monomode so the TM_0 mode profile is ,in principle, the only mode with nonlinear properties. However, the TE_0

modes were also modelled as they were to be used as interferometer reference arms to convert a phase modulation of the TM_0 mode to an intensity change.

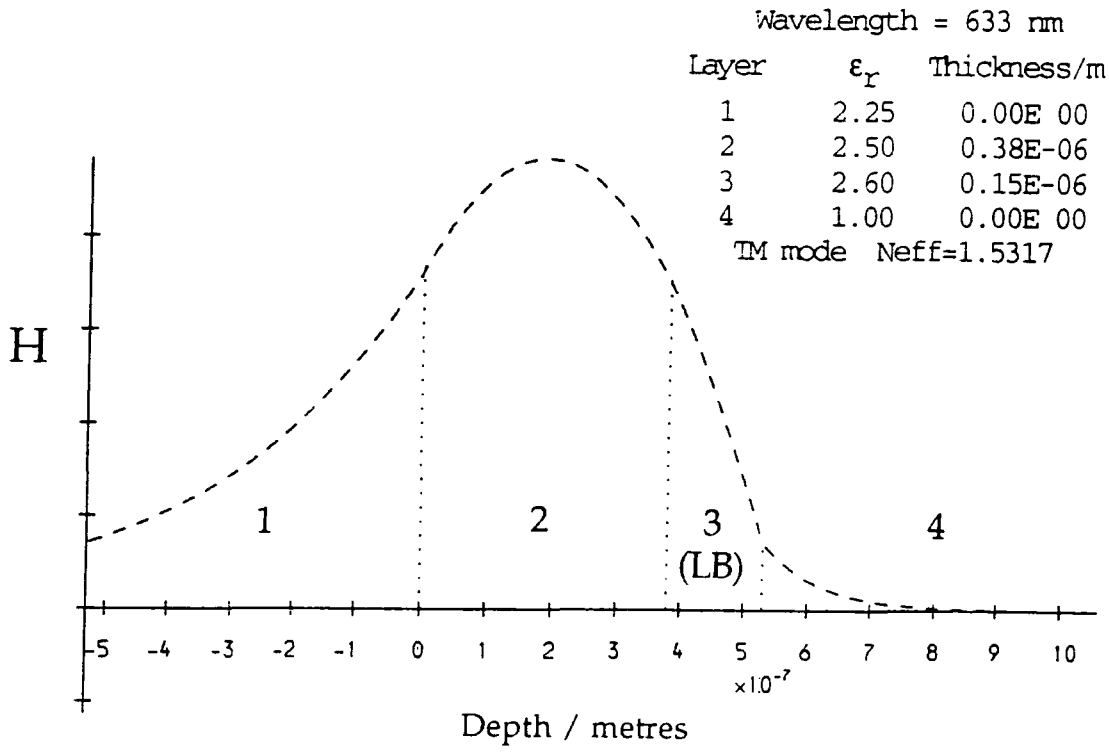

Figure 9.1 - Field in waveguide with LB film overlay

For the LB layer to guide a greater proportion of the power it must be placed at the field maximum, an example is shown in figure 9.2. In this case the high index 'core' of a symmetric guide has been split in two with the LB film placed between. 34% of the power of the TM_0 mode is in the LB layer. The refractive indices used are purely illustrative as no decision had yet been made on the polymers and LB materials to be used.

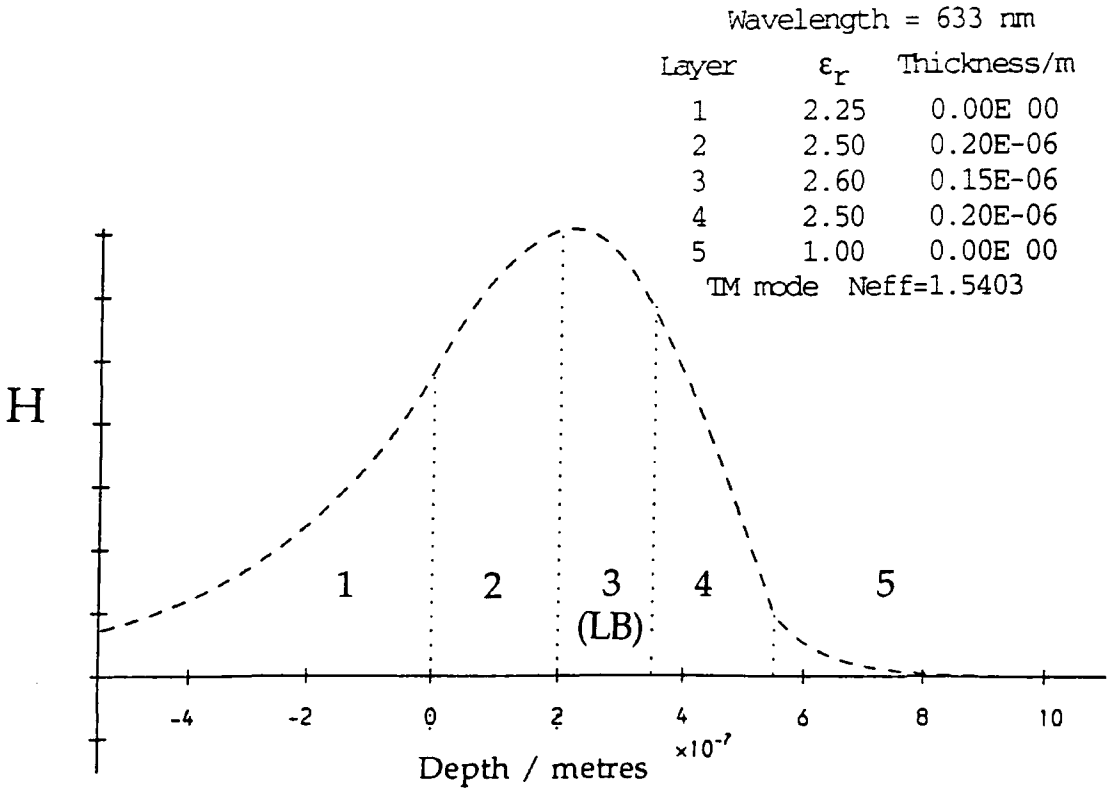

Figure 9.2 - Field in polymer/LB film sandwich guide

Further modelling showed that a similar effect could be achieved in asymmetric guides without splitting the core region. Figure 9.3 is a four layer structure - substrate/LB film/core/air - with the field maximum within the LB film. In this case 32 % of the power is in the LB region. It was found that for best results the LB layer must be placed on the high index side of the core (in this case the substrate side).

In order to investigate the electrooptic properties of the waveguide it is necessary to apply low frequency electric fields. The simplest electrode structure is to place one electrode beneath the waveguide (by either coating the substrate with

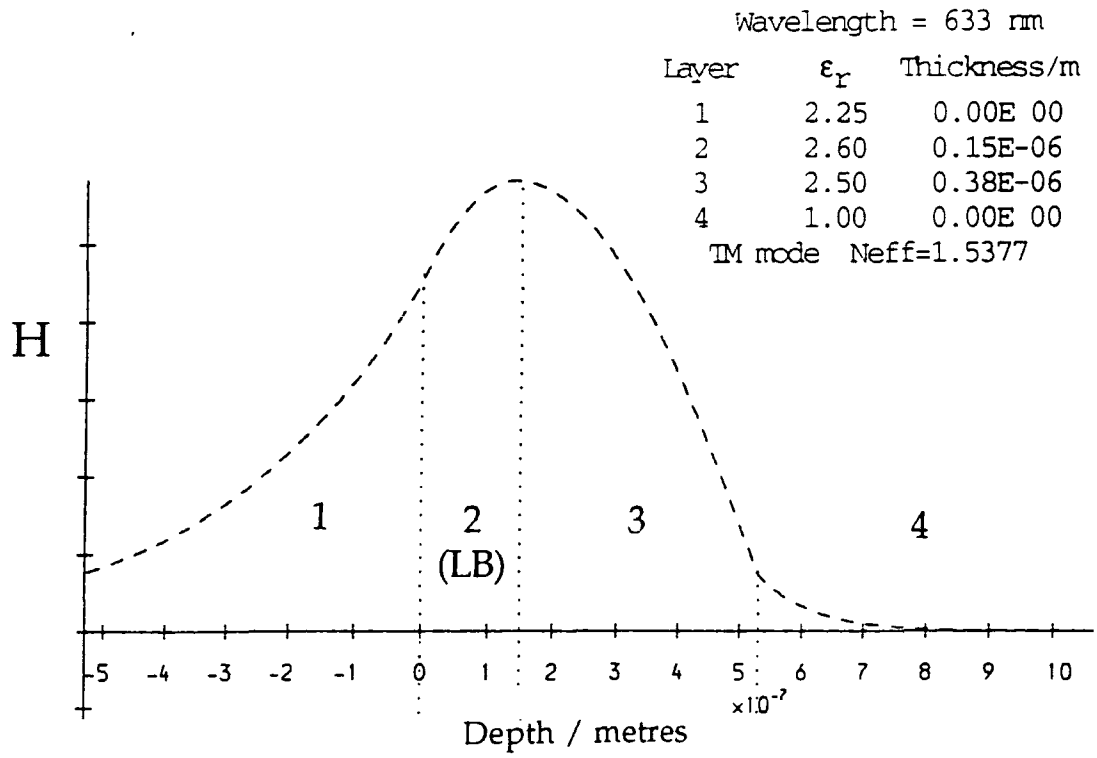

Figure 9.3 - Field in polymer/LB film waveguide

metal or using a conductive substrate) and the other on top of the structure. An alternative of patterning both electrodes on the top surface was rejected due to unnecessary complexity. Metal electrodes cannot be deposited directly onto the guiding region without causing optical attenuation. It is necessary to first deposit an optically transparent buffer of sufficient thickness for the mode profile to decay before the metal layer. This creates a five layer structure - substrate/LB film/core/buffer/metal - see figure 9.4 (the metal layer is not shown). The inclusion of a buffer layer and electrode inevitably reduces the proportion of the guided power that is in the LB layer but this fraction is still calculated to be 23 %.

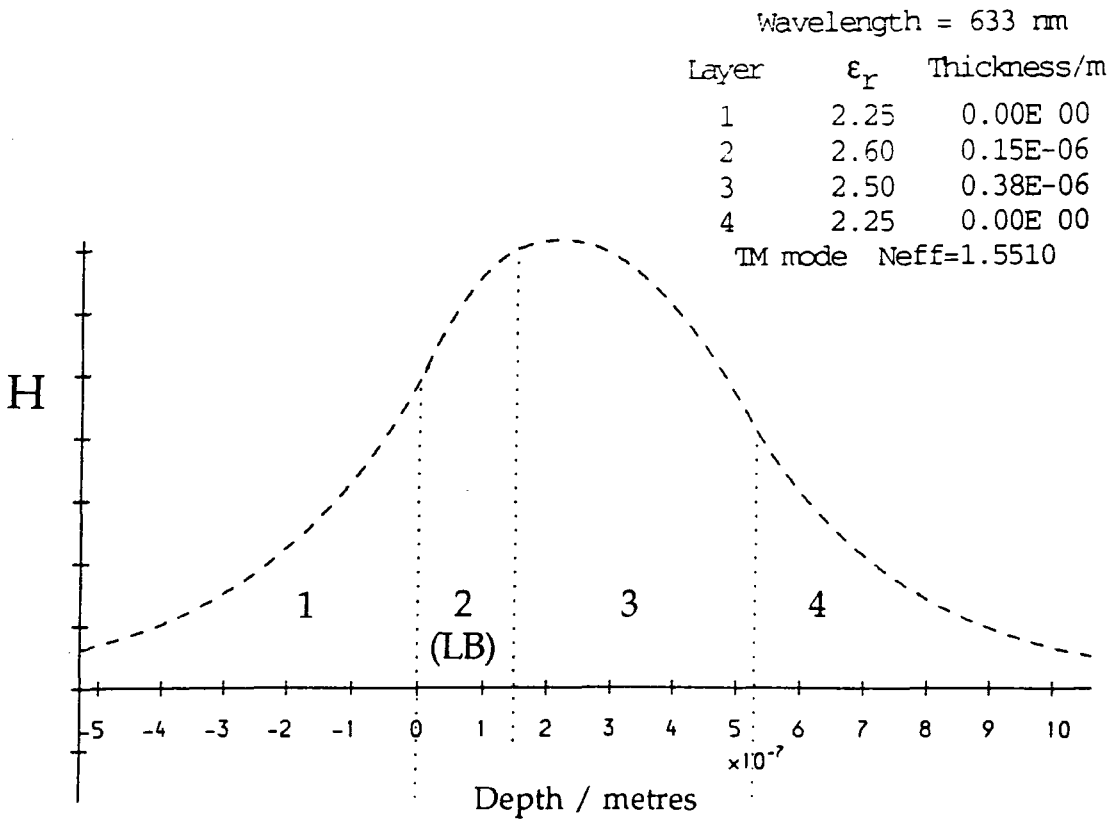

Figure 9.4 - Field in a 5-layer polymer/LB film waveguide

Theoretical modelling only gave an approximate design as many fabrication problems remained to be solved. For example, the actual refractive indices of the layers depended on the availability of appropriate polymers and it was essential that the deposition of a layer did not damage those prepared previously.

9.2 Fabrication Experiments

The polymers required can be divided into two types, low index polymers for buffer layers and high index polymers for the core. The dividing line for these two groups is somewhat arbitrary but may be set at n=1.52, the index of glass microscope slides. It was also necessary to know the solvent compatibility of each polymer to ensure both that suitable solvents were available and that solvents for the upper

layers did not attack the lower layers. Table 9.1 shows the relevant details for the polymers used[3].

Polymer	Abbreviation	Refractive Index	Solvents	Non-solvents
poly 4-vinyl pyridene	P4VP	1.577	propan-2-ol	cyclohexane ethyl acetate
poly methyl methacrylate	PMMA	1.490	dichloromethane ethyl acetate	propan-2-ol
telene^R	-	1.52	cyclohexane	

telene^R is a registered trademark of the BF Goodrich company

Table 9.1 - Polymer solvents and non-solvents

9.2.1 Deposition of Polymer layers

Solution dipping was used for depositing the polymer layers due to its simplicity. The substrate is lowered into a solution of the required polymer and then withdrawn at a controlled speed using a modified Langmuir trough dipping mechanism. Although the uniformity of the layer is less than for spin coating it is quite acceptable for waveguide fabrication, except that the bottom few millimetres of the slide must be discarded.

The thickness of the layer (t) increases with the viscosity of the solution and is related to the rate of withdrawal (v) by a simple formula:

$$t \approx v^{2/3} \tag{9.1}$$

This formula breaks down for high dipping speeds and for low viscosity solutions.

Table 9.2 shows some experimentally determined thicknesses for a number of polymers. The thicknesses were determined by measuring interference fringes on a spectrophotometer and using a Tencor AlphaStep 300.

Polymer	Solvent	Concentration	Dipping Speed/mm min^{-1}	Thickness/microns
P4VP	propan-2-ol	50 g/l	85	0.38
PMMA	dichloromethane	10% w/w	30	4.4
PMMA	ethyl acetate	200 g/l	85	5.1
telene	cyclohexane	200 g/l	10	11

Table 9.2 - Polymer dipping speeds and thicknesses

9.2.2 Deposition of Langmuir-Blodgett films onto Polymers

Langmuir-Blodgett films of hemicyanine:22-TA, 4-HANS:stearic acid and 22-TA deposited easily onto PMMA, polycarbonate and P4VP. The conditions were exactly as used for transfer onto glass ie. 30 mN m^{-1} surface pressure.

Preparation of multilayers of 4-HANS:22-TA proved impossible due to a gradual reduction in transfer ratio. After further study this was associated with ageing of the floating monolayer and occurred for all substrates including glass. The 4-HANS:stearic acid mixture showed no tendancy to age.

In order to compare the structures of films deposited on glass and PMMA a microscope slide was half coated with the polymer before deposition of 4-HANS:stearic acid alternated with 22-TA. X-ray diffraction measurements were then performed on the two regions. However, no diffraction could be obtained from the region transferred onto glass. On preparing a second sample it was observed that the problem was the behaviour of the meniscus at the transition point between the PMMA and glass. As PMMA is hydrophobic the meniscus is forced down, but as the boundary point is reached the meniscus is rapidly pulled up by the hydrophilic glass. The result was that most of the glass region remained uncoated. Clearly, for successful transfer, the glass should be treated to render it hydrophobic or two completely separate samples could be prepared.

9.2.3 Depositing Polymers onto Langmuir-Blodgett films

The choice of polymer to overlay the Langmuir-Blodgett film is determined by the properties of its solvent. It is obvious that the solvent must not dissolve any of the LB materials present; this effectively rules out the solvents used in preparing solutions for LB deposition, eg. chloroform, trichloroethane.

The first polymer tried was poly vinyl alcohol (PVA) as this is water soluble. Unfortunately LB films have a highly hydrophobic outer surface (because the hydrophobic end of the molecule faces away from the substrate on upstroke transfer) which causes the aqueous solution of PVA to form droplets on the surface instead of an even layer. Langmuir[4] describes a method for making the outer surface of the film hydrophilic by immersion in a solution containing aluminium (Al^{3+}) ions. It is unclear whether this effect is due to reversal of the final monolayer or its complete removal. A 0.1 M solution of $AlCl_3$ was prepared and used to treat LB films of 4-HANS:stearic acid/22-TA. No change in hydrophobicity was noted for up to ten minutes immersion, at this point the film fell off the substrate.

Due to the lack of published data on the solvent resistance of LB films it was decided to study experimentally the effect of a number of common solvents. Films were immersed for 30 seconds and then visually examined for signs of damage. It was found that acetone and cyclohexanone attacked the films but that propan-2-ol and cyclohexane had no effect. Ethyl acetate fell between these two extremes, slight damage being noted. Therefore propan-2-ol and cyclohexane were the first choices as solvents for applying overlayers to LB films, this limited the choice of polymer to P4VP (in propan-2-ol) for high index layers and telene (in cyclohexane) for low index layers.

9.2.4 Protection of lower layers

To test the protection (ie solvent isolation) properties of LB films a 49 layer structure of 4-HANS:stearic acid/22-TA was prepared on a P4VP layer. A second P4VP layer was then deposited on the LB film, this resulted in the LB layer peeling off as

the first P4VP layer dissolved. It is clear that LB films can provide no protection against solvent attack on underlayers.

A similar test was carried out by depositing a second telene layer onto a P4VP film deposited on telene. In this case it was found that the P4VP protected the lower telene layer.

9.3 Final Design of Waveguide

The information gained from the fabrication experiments was used to finalise the waveguide design. The actual refractive indices of the chosen polymers were measured by ellipsometry and modelling carried out to establish suitable layer thicknesses.

Silicon was chosen as the substrate material as it is conductive and easily cleaved. This second attribute is important in producing a good waveguide end-face for end-fire coupling. As silicon is non-transparent at the chosen wavelength of operation (633 nm) it must be coated by a transparent buffer layer of sufficient thickness to isolate the modal fields from the substrate. Two alternative methods were chosen for this, a 4.4 micron dip coated layer of PMMA (n=1.49), and a 2.5 micron layer of wet oxidation grown silicon dioxide (n=1.43 from ellipsometry).

The next two layers were the P4VP and LB film together forming the core. The order of these was as determined in section 9.1; the LB film is on the low index side. This completed the structure for the non-electroded guides, those with electrodes were coated with 11 microns of telene (n=1.52) and 50 nm of vacuum deposited silver.

The modal profiles of the waveguides are shown in figure 9.5, the refractive index of the LB film was estimated as 1.6 for TM and 1.51 for TE. The theoretical effective indices of the modes are also given in table 9.3. A number of guides were also produced omitting the LB layers for control purposes.

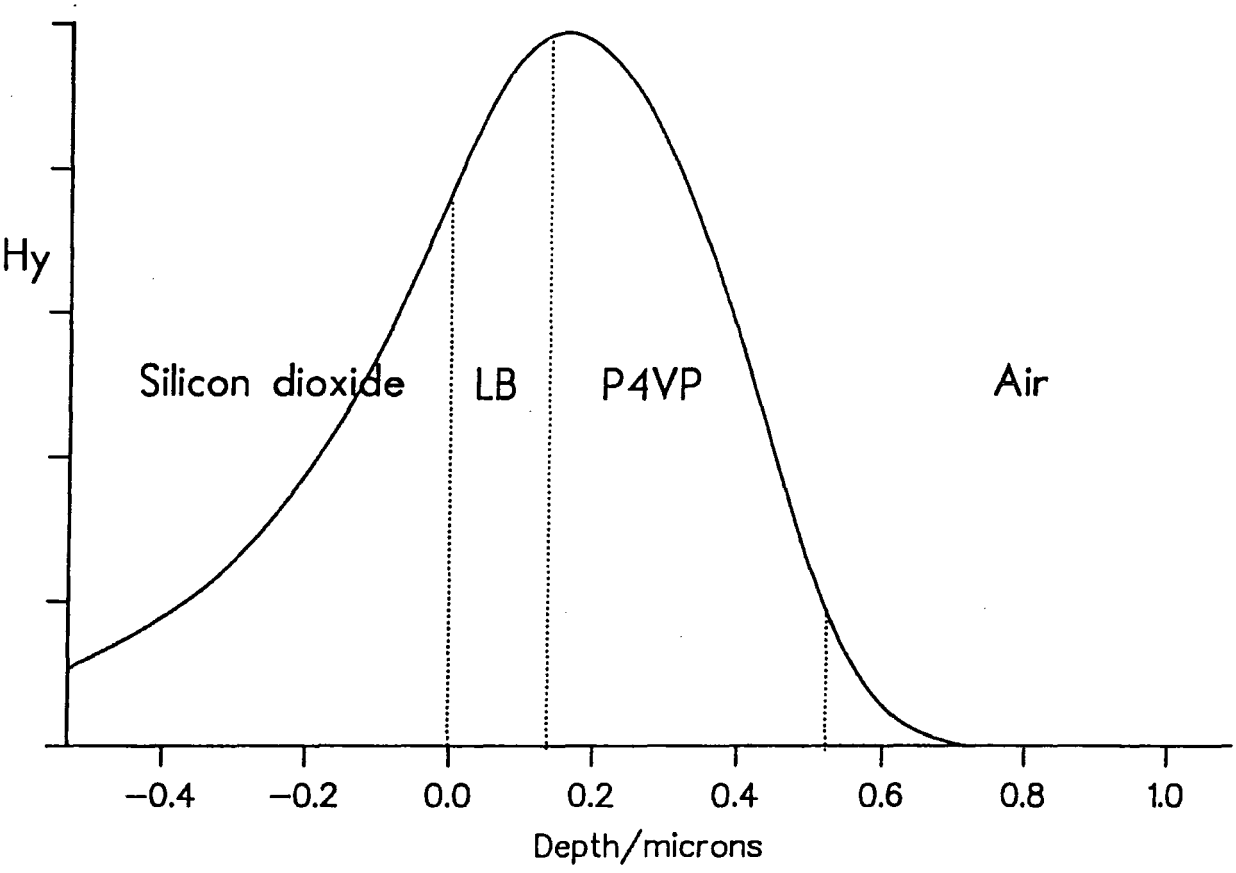

Figure 9.5a - Theoretical TM_0 profile for non-electroded guide

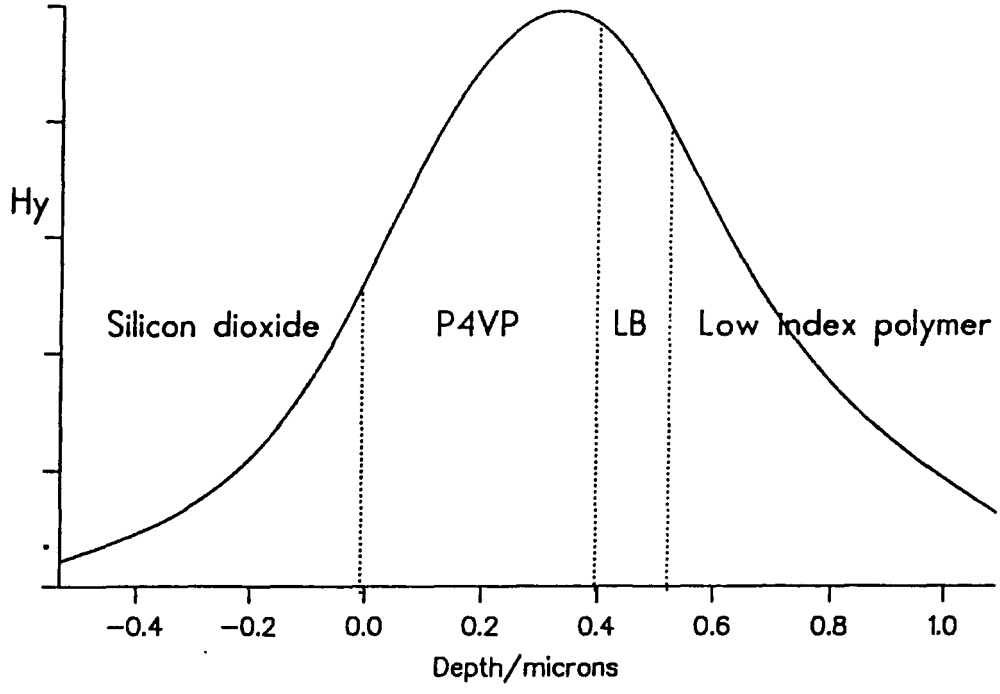

Figure 9.5b - Theoretical TM_0 profile for electroded guide

Layer No.	Material (Thickness/microns)					
1	SiO_2 (2.5)	PMMA (4.4)	PMMA (4.4)	SiO_2 (2.5)	SiO_2 (2.5)	SiO_2 (2.5)
2	LB† (0.15)	LB† (0.15)	P4VP (0.38)	P4VP (0.38)	P4VP (0.38)	P4VP (0.38)
3	P4VP (0.38)	P4VP (0.38)	-	LB† (0.15)	-	LB‡ (0.15)
4	air	air	air	telene (11)	telene (11)	PMMA (5)
TM_0 index	1.519	1.530	1.502	1.545	1.529	1.545
TE_0 index	1.530	1.537	1.511	1.548	1.531	1.548

LB† = 50 layers 4-HANS:stearic acid/22-TA

LB‡ = 50 layers Hemicyanine:22-TA/4-HANS:stearic acid

Table 9.3 - Waveguides produced and effective indices

9.4 Waveguiding

Following fabrication the waveguides were cleaved by scribing the edge of the silicon and applying pressure. In most cases this produced an excellent cleaved edge. However, there was a tendency for the telene layer to peel off, rendering the waveguide useless. The adhesion seemed to be worse on hemicyanine layers than on 4-HANS and it was impossible to produce a hemicyanine guide with a telene buffer layer. PMMA dipped from an ethyl acetate solution was used instead.

The guides were then mounted for end-fire coupling and wires applied to the silicon and silver using conductive paint. End-fire coupling was then carried out for both polarisations. An overhead view of waveguiding is shown in figure 9.6. The presence or absence of modes for each waveguide is shown in table 9.4.

All waveguides guided TE light but some showed no TM mode. This may be explained by theoretical effective indices for each mode. For all guides the TE_0 index is well above the cut-off effective index (equal to the larger of the refractive indices of the two confining layers). However, for the waveguides prepared using PMMA, the TM_0 index is very close to that of PMMA (1.490). This means that

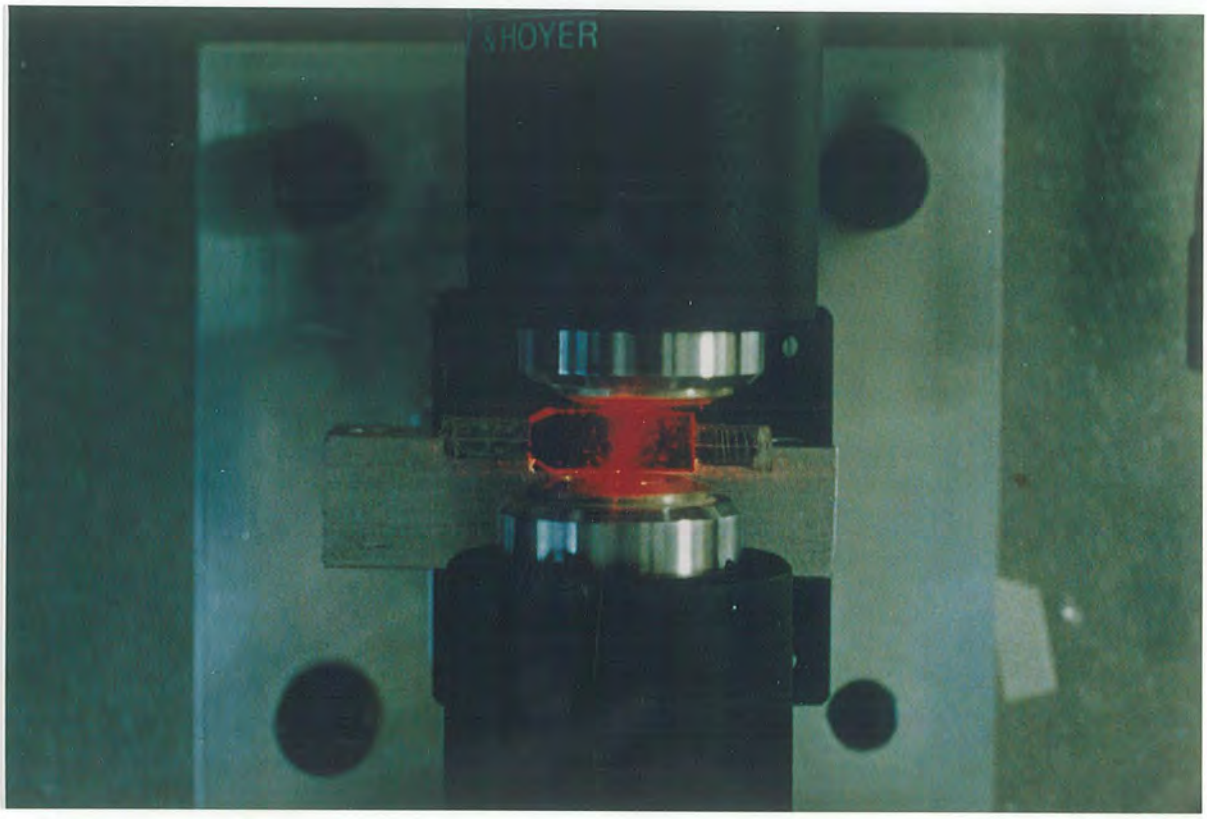

Figure 9.6 - Photograph of waveguide

the modes will be poorly confined and thus lossy. If the refractive index of the LB film is lower than estimated, the modes may well be cut-off. Therefore, the failure to guide TM light is not unexpected. In order to produce successful guides using PMMA, a thicker P4VP and/or LB layer should be used, or alternatively core materials of higher refractive indices.

9.5 Pockels Effect

An a.c. electric field was applied between the silicon and silver and the phase modulation properties of the waveguides were studied. The actual phase change measured is to the relative phase of the TM_0 and TE_0 modes. The values for the product of the voltage for a π phase change (V_π) and the device length (L) are

Layer No.	Material (Thickness/microns)					
1	SiO_2 (2.5)	PMMA (4.4)	PMMA (4.4)	SiO_2 (2.5)	SiO_2 (2.5)	SiO_2 (2.5)
2	LB† (0.15)	LB† (0.15)	P4VP (0.38)	P4VP (0.38)	P4VP (0.38)	P4VP (0.38)
3	P4VP (0.38)	P4VP (0.38)	-	LB† (0.15)	-	LB‡ (0.15)
4	air	air	air	telene (11)	telene (11)	PMMA (5)
TM mode	Yes	No	No	Yes	Yes	Yes
TE mode	Yes	Yes	Yes	Yes	Yes	Yes

LB† = 50 layers 4-HANS:stearic acid/22-TA

LB‡ = 50 layers Hemicyanine:22-TA/4-HANS:stearic acid

Table 9.4 - Modes observed in waveguides

given in table 9.5. This product is regarded is a figure of merit for waveguide phase modulators.

Layer No.	Material (Thickness/microns)		
1	SiO_2 (2.5)	SiO_2 (2.5)	SiO_2 (2.5)
2	P4VP (0.38)	P4VP (0.38)	P4VP (0.38)
3	4-HANS:SA/22-TA (0.15)	-	Hemi/4-HANS:SA (0.15)
4	telene (11)	telene (11)	PMMA (5)
$V_\pi.L$/Vm	130	30000	170
G	0.24	-	0.24
r/pm V^{-1}	0.07	-	0.03
$\chi^{(2)}(-\omega;\omega,0)$/pm V^{-1}	0.2	-	0.1

Electrooptic modulation in waveguides

The formula relating the phase modulation results to the r coefficient of the active layer is:

$$r = \frac{\lambda d}{n_{eff}^3 V_\pi L G} \tag{9.2}$$

where n_{eff} is the effective index of the mode, d is the electrode gap, λ the operating wavelength and G the fraction of the power within the active layer (this formula is readily derived from the equations given in reference 5).

It should be noted that this equation assumes that the phase modulation acts on a single mode only. For the type of waveguide considered here, this will be true if the chromophores of the LB film are aligned normally, in which case only the TM_0 mode will be modulated. In practice, any tilt of the chromophores would cause the phase of the TE_0 mode to be modulated in the same direction; this reduces the relative phase change. Therefore, the effect of tilt will be to understate the r coefficient for the LB layer.

Theoretically calculated G values and derived r coefficients for each waveguide are shown in table 9.5, the r values may be converted to $\chi^{(2)}(-\omega;\omega,0)$ and compared with the results of surface plasmon resonance measurements on monolayers. These are the first ever electrooptic measurements on a waveguide containing LB films.

All of the waveguides gave measurable modulation, but the device without LB layers has a much greater V_π. This proves that almost all of the observed effect is due to LB film. All of the V_π.length products are large compared to practical modulators (eg. 0.1 Vm for lithium niobate devices). The calculated $\chi^{(2)}(-\omega;\omega,0)$ figures show that part of the reason for this is the apparently poor activity of the LB materials in waveguide form. Comparing to monolayer measurements, a reduction of two orders of magnitude is seen. Possible reasons for this are damage to the LB film when applying the top layer, absorption of the TM mode and non-normal chromophore alignment giving TE modulation. The first two of these explanations probably explain the small response of the hemicyanine containing waveguide. Application of the overlayer from ethyl acetate may lead to partial dissolving of the LB film and hemicyanine dyes is absorbing at 633nm. However, the poor response of the 4-HANS:SA/22-TA waveguide is harder to explain. The overlayer

was applied from cyclohexane which appeared to leave the films unchanged and 4-HANS is only weakly absorbing at this wavelength. Clearly further work is needed to investigate and improve the small modulation observed.

9.6 Summary

A method of waveguide fabrication combining LB films and solution dipped polymer layers is described. This allows the rapid production of guides with active LB layers placed close to the field maximum of the modes. The design can be extended to allow electroded guides to be made.

Monomode guides were designed and fabricated, supporting TE_0 and TM_0 modes. For the first time, electrooptic measurements were carried out on an LB film waveguide. Comparision with a control device showed that the observed modulation was due to the presence of the LB layers.

References

1. H.L. Hampsch, J. Yang, G.K. Wong, J.M. Torkelson, *Macromolecules* **21** pp526-8 (1988).
2. F. Grunfeld, C.W. Pitt, *Thin Solid Films* **99** pp249-55 (1983).
3. J. Brandrup, E.H. Immergut, *Polymer Handbook* (Wiley 1989).
4. I. Langmuir, V.J. Schaefer, *J. Am. Chem. Soc.* **59** pp1762-3 (1937).
5. R.C. Alferness in *Guided-Wave Optoelectronics* ed T. Tamir p155 (Springer-Verlag 1990).

Chapter 10
Conclusions and Suggestions for further work

10.1 Conclusions

The application of Langmuir-Blodgett films to practical second-order nonlinear devices will require several advances from the current state of the art. Progress is needed in producing materials of greater stability and in devising practical waveguiding structures. It would also be advantageous to discover materials with larger values of nonlinear susceptibility. The work in this thesis has included the examination of a large number of novel monomeric materials and a pair of oligomeric compounds for their Langmuir-Blodgett deposition and nonlinear properties. The motivation behind the design of the monomers was to discover larger values of $\chi^{(2)}$ than for present materials whilst the oligomers were designed to combine high thermal stability with significant nonlinear effects. Mixtures of a hemicyanine dye and a uv-polymerisable diacetylene were also investigated in an effort to produce stable nonlinear films. Work was also carried out on fabricating waveguide systems, both by the conventional alternate-layer technique and by combining this with solution dipped polymer layers.

The results from the eighteen monomers studied were, on the whole, disappointing. Only half of the molecules were able to form Langmuir-Blodgett monolayers of sufficient quality for nonlinear optical measurements and just one (JT11) formed reliable multilayers (an essential requirement for practical application). Unfortunately, despite the apparent excellence of JT11 deposition, the nonlinear effects were found to be much smaller than those for the best existing materials. Among the materials which did not deposit well were the diphenyl butadiynes and an aminonitrostilbene carboxylic acid. However, their nonlinear properties were found to similar to those of hemicyanine, showing that the chromophores of these molecules are in fact very active. If these chromophores could be combined with other groups to give good deposition, a useful material could result, especially if the dye moieties could be linked to a polymer backbone.

The idea of combining hemicyanine with a diacetylene monomer and then polymerising the latter by ultra violet exposure did not give a successful second-order nonlinear film because a second optically induced reaction took place. This was the dimerisation of the hemicyanine, causing the breaking of the conjugated π-electron system. This bleaches the molecule and removes its nonlinear properties.

Two alternate-layer systems were studied but neither gave large nonlinear optical properties. 4-HANS/JT11 layers were studied in detail for thicknesses up to 150 bilayers. Characterisation by X-ray diffraction and waveguiding all showed that the degree of order in the layers was very poor and this was borne out by the low values of second harmonic intensity recorded. Fourier transform infra-red studies subsequently allowed an interdigitated molecular structure to be proposed for these layers which explained why the nonlinear effects were poor, even for small numbers of bilayers. The oligomeric alternate layer system was not studied in great detail because the results for films as thin as three layers showed that the chromophores were not aligning colinearly. In fact, the small values of second harmonic generation and Pockels effect implied that the alignment must be nearly anti-parallel. Despite this, it has been shown elsewhere[1] that the active oligomer forms films with large second harmonic generation when alternated with a quinolinium salt and it may therefore be possible to synthesise a successful, thermally stable oligomeric partner.

The novel combination of solution dipped polymer layers with Langmuir-Blodgett films in waveguide structures showed promising results. The fabrication time for these waveguides was much less than required for an all LB structure and the electroded system allowed electrooptic modulation to be observed. Although the scale of the response was small the use of other Langmuir-Blodgett materials should give a much larger effect.

10.2 Suggestions for further work

The work on novel monomeric Langmuir-Blodgett molecules has identified a potentially useful new chromophore, the diphenyl butadiyne, and confirmed the strong response of the aminonitrostilbene group. To produce useful, stable materials

these groups must be combined with polymers or oligomers. Examples of possible structures are shown in figure 10.1. These take existing examples of polymer backbone structures from the literature[2,3] and show how the chromophores could be attached. The first backbone (a) is based on a vinyl maleic acid anhydride copolymer; waveguiding has been reported in these materials[2] with the group R_1 as a hydrogen atom. However, it is stated in the paper that an active group could be attached at this point. Example (b) is a polysiloxane, second harmonic generation has been reported for a monolayer of this material[3] with an azo dye as R_1. The basic design could be adapted to other chromophores.

The ICI oligomer S119191 will require a more thermally stable alternation partner than a fatty acid in order to produce a useful overall system. The work in this thesis has already shown that the passive spacer S122699 led to poor alignment but there are a large number of alternative molecular designs which could be used. The second material could be either passive or active with the dipoles reversed relative to S119191. Figure 10.2 shows some possible active replacements for S122699. To reverse the sign of $\chi^{(2)}$, the relative positions of donor and acceptor groups must be changed. In S119191 the nitro group is the acceptor and the amine groups of the basic oligomer act as donors. A complementary material will require a donor group at the furthest point from the oligomer chain and an acceptor group closer to the chain with a conjugated system running between the two groups. The acceptor group must be isolated from the amine groups of unsubstituted oligomer. Example (a) of figure 10.2 shows the original azo dye chromophore reversed in orientation and (b) uses the JT666 diphenyl butadiyne group. However, the limitations of synthesis may require slight changes to these designs and many other variations could be proposed.

Although the 4-HANS/JT11 alternate-layers failed to show large nonlinear effects, a number of groups have recently reported combinations of materials which give significant values of $\chi^{(2)}$ for up to several hundred layers. Notable examples include the use of a hemicyanine dye with a so-called moleculer zip material[4] (figure 10.3)

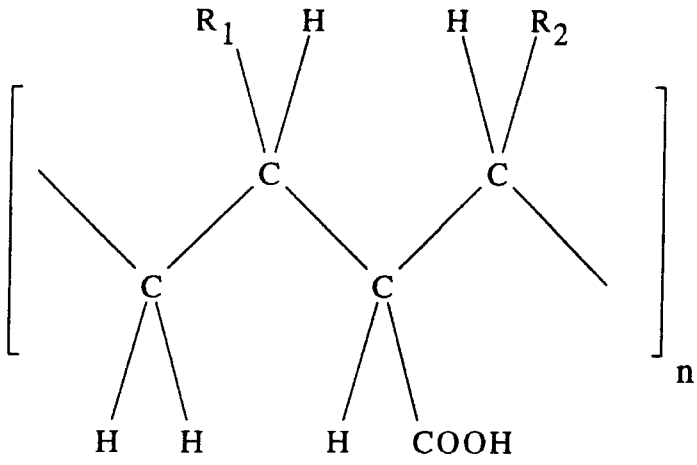

(a) vinyl - maleic acid anhydride copolymer derivatives

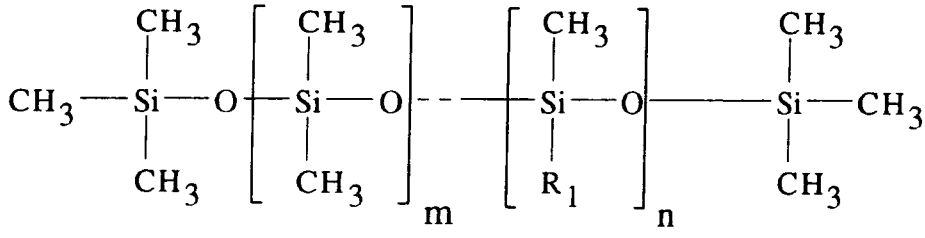

(b) polysiloxane derivatives

in both cases R1 can be an active chromophore

Figure 10.1 - Possible polymer backbones for NLO materials

and the alternation of polymer materials by Du Pont[5] These or similar structures could be combined with the polymer dipping method as described in this thesis to produce electrooptic modulators. The LB layers could either be dipped to a few hundred layers to form the guiding region alone (figure 10.4a) or just to around 50 layers and combined with a high index polymer (figure 10.4b).

Taking the example of the hemicyanine-molecular zip[4] system it is possible to

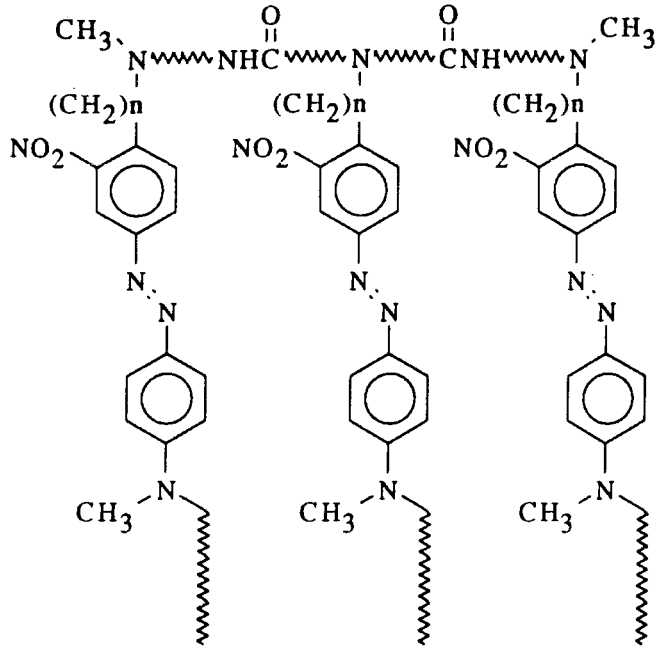

(a) Azo dye based complementary oligomer

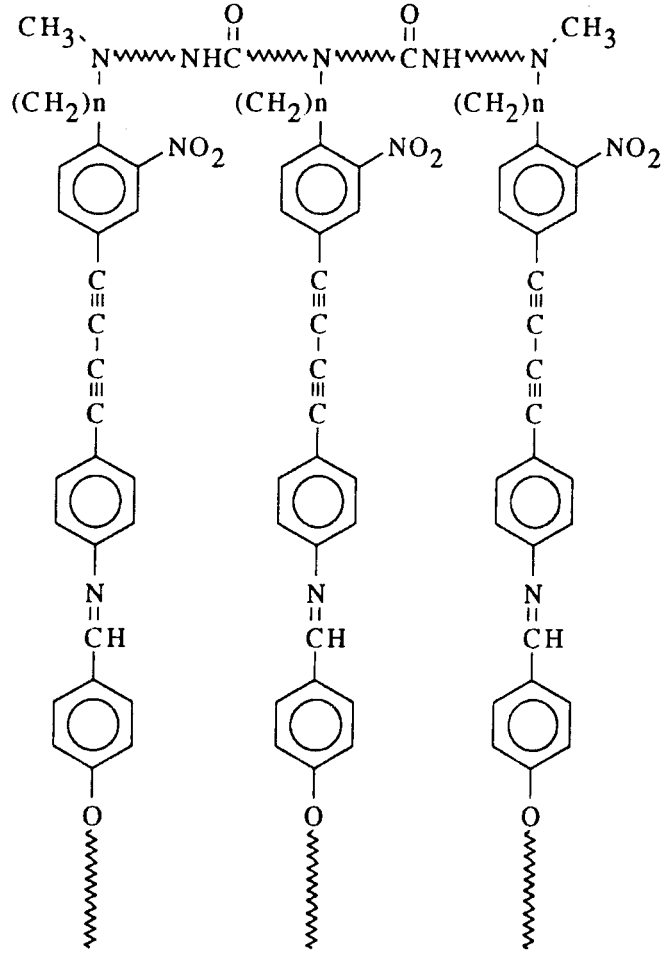

(b) JT666 based complementary oligomer

Figure 10.2 - Possible structures for complementary oligomer

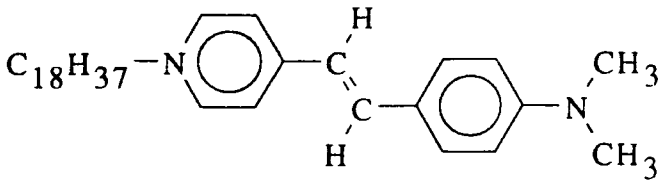

Hemicyanine

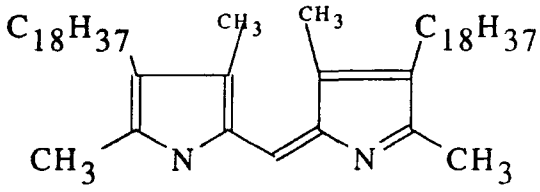

Molecular Zip

Figure 10.3 - Hemicyanine dye and the molecular zip material

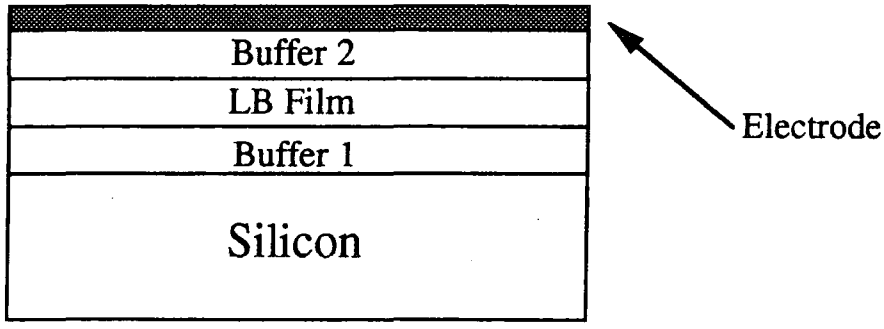

a) LB film modulator

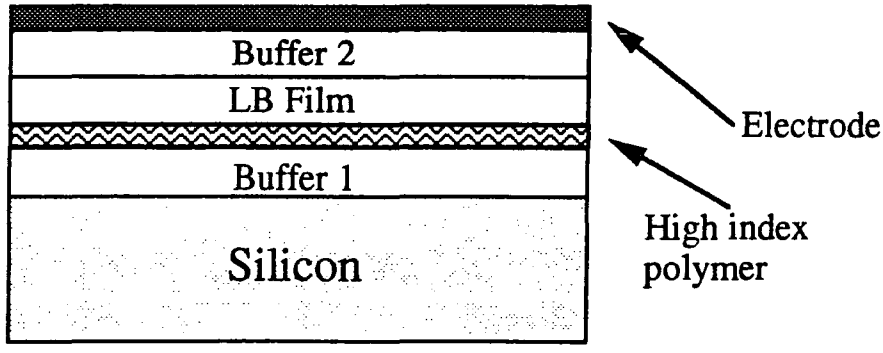

b) LB film modulator with polymer augmented guiding region

Figure 10.4 - Proposed LB film modulators

estimate a figure of merit for the modulator. Assuming that $\chi^{(2)}(-\omega;\omega,0) \sim 3 \times 10^{-11}$ m V^{-1} and $\epsilon_r = 3$, gives $r \sim 6 \times 10^{-12}$ m V^{-1}.

Using equation 9.2 with 75% of the guided energy in the LB layer, an electrode gap of 2 microns, a 1 micron wavelength and an effective index of 1.6 gives a figure of merit of:

$$V_\pi.L \sim 1 \text{ Vm}$$

.

This is comparable with polymer devices[6] (1 Vm) but an order of magnitude inferior to lithium niobate modulators (0.1 Vm). Clearly further work is required to produce molecules with larger nonlinear effects.

In conclusion, there is plenty of scope for further work in the field of Langmuir-Blodgett films for nonlinear optics, both in the search for active and stable molecules and in the design and fabrication of suitable device structures for practical applic-tion.

References

1. S. Allen, T.G. Ryan, D.P. Devonald, M.G. Hutchings, A.N. Burgess, E.S. Froggatt, A. Hamilton, R.M. Swart, G.J. Ashwell, M. Malhotra, *Organic Materials for Nonlinear Optics 90* (Royal Society of Chemistry, London) in press.

2. N. Carr, M.J. Goodwin, A.M. McRoberts, G.W. Gray, R. Marsden, R.M. Scrowston, *Makromo. Chem. Rapid Commun.* **8** pp487-93 (1987).

3. R.H. Tredgold, M.C.J. Young, P. Hodge, E. Khoshdel, *Thin Solid Films* **151** pp441-9 (1987).

4. a) G.J. Ashwell, *Thin Solid Films (Proc. Langmuir-Blodgett Films 5, Paris, August 1991)* in press.

   b) G.J. Ashwell, E.J.C. Dawnay, A.P. Kuczynski, P.J. Martin, *SPIE Proceed-*

ings **1361** (1990)

5. H. Hsiung, J. Rodriguez-Parada, R. Beckerbauer, M. Kaka, W. Tam, *Thin Solid Films (Proc. Langmuir-Blodgett Films 5, Paris, August 1991)* in press.

6. G.H. Cross, A. Donaldson, R.W. Gymer, S. Mann, N.J. Parsons, D.R. Haas, H.T. Man, H.N. Noon, *SPIE Proceedings* **1177** pp79-91 (1989).

Appendix 1

Converting between SI and e.s.u in Nonlinear Optics

Basic Units

Quantity	SI Unit	Multiply by for e.s.u	e.s.u unit
Potential	Volt	$\frac{1}{300}$	statvolt
Charge	Coulomb	3×10^9	statcoulomb
Length	Metre	100	centimetre

Nonlinear Optical Units

Second Order Susceptibility - $\chi^{(2)}$

Directly from Pockels effect measurement is in $mV^{-1} \Longrightarrow$ multiply by 3×10^4 for e.s.u.

If it has been multiplied by ϵ_o units are $CV^{-2} \Longrightarrow$ multiply by 2.7×10^{14} for e.s.u.

Second Order Surface Susceptibility - $\hat{\chi}^{(2)}$

This is Second Order Susceptibility multiplied by layer thickness.

Units are $CmV^{-2} \Longrightarrow$ multiply by 2.7×10^{16} for e.s.u.

Occasionally quoted before multiplication by ϵ_o in which case the units are m^2V^{-1}. Convert to CmV^{-2} before converting to e.s.u.

Molecular Hyperpolarisability - ß

This is Second Order Susceptibility divided by the volume density of molecules (or Second Order Surface Susceptibility divided by surface density).

Units are $Cm^3V^{-2} \equiv C^3m^3J^{-2} \Longrightarrow$ multiply by 2.7×10^{20} for e.s.u.

Note: the Second Order Susceptibility and Surface Susceptibility are sometimes quoted divided by $\epsilon_2\epsilon_1^2$ or some other combination of these.

Appendix 2

The effect of Electrostriction and Piezoelectricity on Pockels measurements

Electrostriction is a change in layer thickness proportional to the square of the applied electric field. Therefore, for an ac. electric field any thickness modulation will be at double the frequency and will not be detected by the phase sensitive detector. Hence electrostrictive effects may be neglected.

Piezoelectricity produces a thickness variation proportional to the electric field so the modulation will be at the applied frequency. For a film of thickness x the change in reflectivity R of the surface plasmon arrangement due to a thickness change Δx is given by:

$$\Delta R = \frac{\partial R}{\partial x} \Delta x$$

and the change in thickness due to the piezoelectric effect is:

$$\frac{\Delta x}{x} = P.E$$

where P is the piezoelectric coefficient and E is the applied electric field.

The field is of the $\sim 10^6$ V m^{-1} and the partial derivative $\frac{\partial R}{\partial x}$ is calculated numerically to be $\sim 3 \times 10^7$ for a 3 nm film. The most active materials known have piezoelectric coefficients of around 2 pC N^{-1}. Substituting these figure into the equations gives:

$$\Delta R \sim 2 \times 10^{-7}$$

This is much smaller than the change due to the Pockels effect and may be neglected.

Appendix 3
Computer Programs

All programs use GHOST 80 graphics and program 3 calls one NAG routine for numerical differentiation.

1. Reflection and Transmission of Multilayer Stack

```
C SOLVES MAXWELLS EQUATIONS THROUGH NLAYER STRUCTURE (UP TO 20 LAYERS)
C AND GIVES REFLECTIVITIES, TRANSMISSION, FIELD PROFILE
C FORTRAN 77 AND GHOST 80

      PROGRAM MULTIL
      COMPLEX E(20)
      REAL D(20),K0,ASTART,AEND,ASTEP,LAMDA
      INTEGER POLA,LAYERS,LFLAG

      COMMON /CONSTS/ PI,K0

      PI = 3.1415927
      LAYERS = 0
      LFLAG = 1

      CALL PAPER(1)
      WRITE(*,*) 'Multilayer reflectance program'
    5 WRITE(*,*) 'MAIN MENU'
      WRITE(*,*) '0=Exit program'
      WRITE(*,*) '1=Load data file'
      WRITE(*,*) '2=Change data'
      WRITE(*,*) '3=Go to function menu'
      READ (*,*) ANS
      IF(ANS.EQ.0) GOTO 15
      IF(ANS.EQ.1) THEN
         CALL LYDATA(E,D,LAYERS,POLA,LAMDA)
         CALL REDUCE(E,D,LAYERS)
         CALL SHOW(E,D,LAYERS,POLA,LAMDA,5)
         CALL SHOW(E,D,LAYERS,POLA,LAMDA,7)
         K0 = 2*PI/LAMDA
      ENDIF
      IF(ANS.EQ.2.AND.LAYERS.NE.0) THEN
         CALL CHANGE(E,D,LAYERS,POLA,LAMDA)
         CALL REDUCE(E,D,LAYERS)
         CALL SHOW(E,D,LAYERS,POLA,LAMDA,5)
         CALL SHOW(E,D,LAYERS,POLA,LAMDA,7)
         K0 = 2*PI/LAMDA
      ENDIF
      IF(ANS.EQ.3.AND.LAYERS.NE.0) GOTO 10
      IF(LAYERS.EQ.0) WRITE(*,*) 'No data loaded!'
      GOTO 5
```

```
   10  WRITE(*,*) 'FUNCTION MENU'
       WRITE(*,*) '0=Go to Main Menu'
       WRITE(*,*) '1=Reflectance Curve'
       WRITE(*,*) '2=Transmittance Curve'
       WRITE(*,*) '3=Field Profiles'
       WRITE(*,*) '4=Find minimum reflectivity'
       IF(LFLAG.EQ.1) WRITE(*,*) '5=Turn off graph labelling'
       IF(LFLAG.EQ.0) WRITE(*,*) '5=Turn on graph labelling'
       READ(*,*) ANS
       IF(ANS.EQ.1) CALL ROBLIQ(E,D,LAYERS,POLA,LFLAG)
       IF(ANS.EQ.2) CALL TOBLIQ(E,D,LAYERS,POLA,LFLAG)
       IF(ANS.EQ.3) THEN
          IF(POLA.EQ.0) CALL TEPROF(E,D,LAYERS,LFLAG)
          IF(POLA.EQ.1) CALL TMPROF(E,D,LAYERS,LFLAG)
       ENDIF
       IF(ANS.EQ.4) CALL GETMIN(E,D,LAYERS,POLA)
       IF(ANS.EQ.5) LFLAG = 1 - LFLAG
       IF(ANS.EQ.0) GOTO 5
       GOTO 10
   15  CALL GREND

       STOP
       END
C*************************END OF MAIN*****************************************

C*************************LYDATA**********************************************
C GATHERS DATA FOR LAYERS
       SUBROUTINE LYDATA(E,D,LAYERS,POLA,LAMDA)

       COMPLEX      E(20)
       REAL         D(20),LAMDA
       INTEGER      LAYERS,POLA
       CHARACTER*14 FILENM
       CHARACTER*80 TRASH

       WRITE(*,*) 'Filename for input'
       READ(*,999) FILENM
       OPEN(UNIT=10,FILE=FILENM,STATUS='OLD')
       REWIND(10)
       READ(10,'(A80)') TRASH
       READ(10,*) POLA
       READ(10,'(A80)') TRASH
       READ(10,*) LAMDA
       READ(10,'(A80)') TRASH
       READ(10,*) LAYERS
       READ(10,'(A80)') TRASH
       READ(10,*) (E(I),D(I), I=1,LAYERS)
       CLOSE(UNIT=10)
  999  FORMAT(A14)
       RETURN
       END
```

```
C************************END OF LYDATA*************************************

C*****************************SHOW*****************************************
C WRITES CURRENT DATA TO UNIT=WHERE
      SUBROUTINE SHOW(E,D,LAYERS,POLA,LAMDA,WHERE)
      COMPLEX E(20)
      REAL D(20),LAMDA
      INTEGER LAYERS,POLA,WHERE

      IF(POLA.EQ.0) WRITE(WHERE,*) 'TE Polarisation'
      IF(POLA.EQ.1) WRITE(WHERE,*) 'TM Polarisation'
      WRITE(WHERE,*) 'Wavelength =',LAMDA
      WRITE(WHERE,998) 'Layer','Permittivity','Depth'
      WRITE(WHERE,999) 1,E(1),0.0
      WRITE(WHERE,999) (I,E(I),D(I), I=2,LAYERS-1)
      WRITE(WHERE,999) LAYERS,E(LAYERS),0.0
  998 FORMAT(A5,A20,A10)
  999 FORMAT(I5,F14.4,',',F8.4,E15.6)
      RETURN
      END
C*************************END OF SHOW*************************************

C*****************************CHANGE***************************************
C CHANGES DATA
      SUBROUTINE CHANGE(E,D,LAYERS,POLA,LAMDA)
      COMPLEX E(20)
      REAL D(20),LAMDA
      INTEGER L,ANS,LAYERS,POLA

   10 WRITE(*,*) 'CHANGE PARAMETERS MENU'
      WRITE(*,*) '0=Return to main menu'
      WRITE(*,*) '1=Toggle Polarisation'
      WRITE(*,*) '2=Change Wavelength'
      WRITE(*,*) '3=Change Permittivity'
      WRITE(*,*) '4=Change Thickness'
      WRITE(*,*) '5=Show current parameters'
      WRITE(*,*) '6=Store new data in a file'
      READ(*,*) ANS
      IF(ANS.EQ.1) POLA=1-POLA
      IF(ANS.EQ.2) THEN
         WRITE(*,*) 'New Wavelength/m'
         READ(*,*) LAMDA
      ENDIF
      IF(ANS.EQ.3) THEN
         WRITE(*,*) 'Layer to change'
         READ(*,*) L
         WRITE(*,*) 'New Permittivity (real,imag)'
         READ(*,*) E(L)
      ENDIF
      IF(ANS.EQ.4) THEN
         WRITE(*,*) 'Layer to change'
```

```
          READ(*,*) L
          WRITE(*,*) 'New Thickness/m'
          READ(*,*) D(L)
        ENDIF
        IF(ANS.EQ.5) CALL SHOW(E,D,LAYERS,POLA,LAMDA,5)
        IF(ANS.EQ.6) CALL STORE(E,D,LAYERS,POLA,LAMDA)
        IF(ANS.EQ.0) GOTO 15
        GOTO 10
   15   RETURN
        END
C*************************END OF CHANGE************************************

C*****************************STORE****************************************
C WRITES LAYER DATA TO A FILE
        SUBROUTINE STORE(E,D,LAYERS,POLA,LAMDA)
        COMPLEX E(20)
        REAL D(20),LAMDA
        INTEGER LAYERS,POLA
        CHARACTER*14 FILENM

        WRITE(*,*) 'Filename for output'
        READ(*,999) FILENM
        OPEN(UNIT=10,FILE=FILENM,STATUS='UNKNOWN')
        REWIND(10)
        WRITE(10,*) 'Polarisation 1=TM 0=TE'
        WRITE(10,'(I1)') POLA
        WRITE(10,*) 'Wavelength/m'
        WRITE(10,'(E15.6)') LAMDA
        WRITE(10,*) 'Number of layers'
        WRITE(10,'(I2)') LAYERS
        WRITE(10,*) 'Real(e),Im(e),depth (0=semi infinite)'
        WRITE(10,998) (E(I),D(I), I=1,LAYERS)
        CLOSE(UNIT=10)
  998   FORMAT(F10.6,',',F10.6,',',E15.6)
  999   FORMAT(A14)
        RETURN
        END
C*************************END OF STORE*************************************

C****************************REDUCE****************************************
C LAYER REDUCTION ROUTINE - LOOKS FOR ADJACENT LAYERS OF SAME INDEX
        SUBROUTINE REDUCE (E,D,LAYERS)

        COMPLEX E(20)
        REAL D(20)
        INTEGER LAYERS,OLDLAY

        OLDLAY=LAYERS-1
    5   IF(OLDLAY.NE.LAYERS) THEN
          OLDLAY=LAYERS
          DO 9 I=1,LAYERS-1
```

```
            IF(E(I).EQ.E(I+1)) THEN
               D(I)=D(I)+D(I+1)
               DO 8 J=I+1,LAYERS-1
                  E(J)=E(J+1)
                  D(J)=D(J+1)
    8          CONTINUE
               LAYERS=LAYERS-1
            ENDIF
    9     CONTINUE
          GOTO 5
       ENDIF
       RETURN
       END
C**********************END OF REDUCE*****************************************

C*************************ROBLIQ*************************************************
C REFLECTION VERSUS ANGLE RESULTS
       SUBROUTINE ROBLIQ(E,D,LAYERS,POLA,LFLAG)

       COMPLEX E(20),RC,REFLEC
       REAL    D(20),K0,ASTART,AEND,ASTEP,ANGLE(10000),NEF,
     $         REFMAG(10000),REFARG(10000),PI,TEMP
       INTEGER LAYERS,POLA,I,LFLAG
       COMMON  /CONSTS/ PI,K0

       WRITE(*,*) 'Input start angle, finish angle, step size'
       READ(*,*) ASTART,AEND,ASTEP
       IF(ASTART.GT.AEND) THEN
          TEMP=AEND
          AEND=ASTART
          ASTART=TEMP
       ENDIF
       STEPS = INT((AEND-ASTART)/ASTEP)

       WRITE(7,998) 'Incident Angle','Reflection magnitude, phase','NEF'
       DO 10 I=1,STEPS
          ANGLE(I) = ASTART+I*ASTEP
          NEF = REAL(SQRT(E(1))) * SIN(ANGLE(I) * PI/180)
          RC = REFLEC(E,D,LAYERS,POLA,NEF)
          REFMAG(I) = ABS(RC)
          REFARG(I) = 180/PI * ATAN2(AIMAG(RC),REAL(RC))
          WRITE(7,999) ANGLE(I),REFMAG(I),REFARG(I),NEF
   10  CONTINUE

       CALL PSPACE(0.1,0.9,0.1,0.8)
       CALL MAP(ASTART,AEND,0.0,1.05)
       CALL WINDOW(ASTART,AEND,0.0,1.05)
       CALL AXORIG(ASTART,0)
       CALL AXES
       CALL POSITN(ANGLE(1),REFMAG(1))
       DO 20 I=2,STEPS
```

```
         CALL JOIN(ANGLE(I),REFMAG(I))
   20  CONTINUE
       CALL MAP(0.0,100.0,0.0,100.0)
       CALL CTRMAG(20)
       CALL PLOTCS(40.0,-10.0,'Incident Angle')
       CALL CTRORI(90.0)
       CALL PLOTCS(-10.0,40.0,'Reflectivity')
       CALL CTRORI(0.0)
       IF(LFLAG.EQ.1) CALL ANNOTA(E,D,LAYERS,POLA,0.0)
       CALL FRAME

       WRITE (*,*) 'Phase - angle graph required? 1=YES'
       READ (*,*) ANS

       IF(ANS.EQ.1) THEN
          CALL PSPACE(0.1,0.9,0.1,0.8)
          CALL MAP(ASTART,AEND,-180.0,180.0)
          CALL WINDOW(ASTART,AEND,-180.0,180.0)
          CALL AXORIG(ASTART,0)
          CALL AXES
          CALL POSITN(ANGLE(1),REFARG(1))
          DO 30 I=1,STEPS
             CALL JOIN(ANGLE(I),REFARG(I))
   30     CONTINUE
          CALL MAP(0.0,100.0,0.0,100.0)
          CALL CTRMAG(20)
          CALL PLOTCS(40.0,-10.0,'Incident Angle')
          CALL CTRORI(90.0)
          CALL PLOTCS(-10.0,40.0,'Phase Change')
          CALL CTRORI(0.0)
          IF(LFLAG.EQ.1) CALL ANNOTA(E,D,LAYERS,POLA,0.0)
          CALL FRAME
       ENDIF
  998  FORMAT(A16,A30,A5)
  999  FORMAT(F16.3,F15.3,',',F6.1,F14.3)
       RETURN
       END
C*************************END OF ROBLIQ*****************************************

C*************************TOBLIQ************************************************
C TRANSMISSION VERSUS ANGLE RESULTS
       SUBROUTINE TOBLIQ(E,D,LAYERS,POLA,LFLAG)

       COMPLEX E(20),TC,TRANSM
       REAL    D(20),K0,ASTART,AEND,ASTEP,ANGLE(10000),NEF,
     $         TRAMAG(10000),TRAARG(10000),PI,TEMP
       INTEGER LAYERS,POLA,I,LFLAG
       COMMON  /CONSTS/ PI,K0

       WRITE(*,*) 'Input start angle, finish angle, step size'
       READ(*,*) ASTART,AEND,ASTEP
```

```
      IF(ASTART.GT.AEND) THEN
         TEMP=AEND
         AEND=ASTART
         ASTART=TEMP
      ENDIF
      STEPS = INT((AEND-ASTART)/ASTEP)

      WRITE(7,998) 'Incident Angle','Transmiss. magnitude, phase','NEF'
      DO 10 I=1,STEPS
         ANGLE(I) = ASTART+I*ASTEP
         NEF = REAL(SQRT(E(1))) * SIN(ANGLE(I) * PI/180)
         TC = TRANSM(E,D,LAYERS,POLA,NEF)
         TRAMAG(I) = ABS(TC)
         IF(TC.NE.0) THEN
            TRAARG(I) = 180/PI * ATAN2(AIMAG(TC),REAL(TC))
         ELSE
            TRAARG(I) = 0
         ENDIF
         WRITE(7,999) ANGLE(I),TRAMAG(I),TRAARG(I),NEF
10    CONTINUE

      CALL PSPACE(0.1,0.9,0.1,0.8)
      CALL MAP(ASTART,AEND,0.0,1.05)
      CALL WINDOW(ASTART,AEND,0.0,1.05)
      CALL AXORIG(ASTART,0)
      CALL AXES
      CALL POSITN(ANGLE(1),TRAMAG(1))
      DO 20 I=2,STEPS
         CALL JOIN(ANGLE(I),TRAMAG(I))
20    CONTINUE
      CALL MAP(0.0,100.0,0.0,100.0)
      CALL CTRMAG(20)
      CALL PLOTCS(40.0,-10.0,'Incident Angle')
      CALL CTRORI(90.0)
      CALL PLOTCS(-10.0,40.0,'Transmission')
      CALL CTRORI(0.0)
      IF(LFLAG.EQ.1) CALL ANNOTA(E,D,LAYERS,POLA,0.0)
      CALL FRAME

      WRITE (*,*) 'Phase - angle graph required? 1=YES'
      READ (*,*) ANS

      IF(ANS.EQ.1) THEN
         CALL PSPACE(0.1,0.9,0.1,0.8)
         CALL MAP(ASTART,AEND,-180.0,180.0)
         CALL WINDOW(ASTART,AEND,-180.0,180.0)
         CALL AXORIG(ASTART,0)
         CALL AXES
         CALL POSITN(ANGLE(1),TRAARG(1))
         DO 30 I=1,STEPS
            CALL JOIN(ANGLE(I),TRAARG(I))
```

```
   30     CONTINUE
          CALL MAP(0.0,100.0,0.0,100.0)
          CALL CTRMAG(20)
          CALL PLOTCS(40.0,-10.0,'Incident Angle')
          CALL CTRORI(90.0)
          CALL PLOTCS(-10.0,40.0,'Phase Change')
          CALL CTRORI(0.0)
          IF(LFLAG.EQ.1) CALL ANNOTA(E,D,LAYERS,POLA,0.0)
          CALL FRAME
       ENDIF
  998  FORMAT(A16,A30,A5)
  999  FORMAT(F16.3,F15.3,',',F6.1,F14.3)
       RETURN
       END
C*************************END OF TOBLIQ*************************************

C*************************ANNOTA********************************************
C* ANNOTATES GRAPH
       SUBROUTINE ANNOTA(E,D,LAYERS,POLA,ANGLE)
       COMPLEX E(20)
       REAL D(20),ANGLE,PI,K0,LAMDA
       INTEGER LAYERS,POLA
       COMMON /CONSTS/ PI,K0
       LAMDA = 2 * PI/K0
       CALL CSPACE(0.0,1.0,0.0,1.0)
       CALL CTRMAG(12)
       CALL PLACE(58,1)
       CALL TYPECS('Wavelength = ')
       CALL PLACE(70,1)
       CALL TYPENE(LAMDA,4)
       CALL PLACE(58,2)
       IF(POLA.EQ.1) CALL TYPECS('TM Polarisation')
       IF(POLA.EQ.0) CALL TYPECS('TE Polarisation')

       CALL PLACE(50,3)
       CALL TYPECS('Layer     Permittivity   Thickness/m')
       DO 10 I=1,LAYERS
          CALL PLACE(51,3+I)
          CALL TYPENI(I)
          CALL PLACE(57,3+I)
          CALL TYPENF(REAL(E(I)),4)
          CALL PLACE(65,3+I)
          CALL TYPECS('+')
          CALL PLACE(65,3+I)
          CALL TYPENF(AIMAG(E(I)),4)
          CALL PLACE(72,3+I)
          CALL TYPECS('i')
          CALL PLACE(75,3+I)
          CALL TYPENE(D(I),4)
   10  CONTINUE
       IF(ANGLE.NE.0.0) THEN
```

```
            CALL PLACE(65,4+LAYERS)
            CALL TYPECS('Angle= ')
            CALL PLACE(71,4+LAYERS)
            CALL TYPENF(ANGLE,4)
         ENDIF
         CALL CSPACE(0.0,0.0,0.0,0.0)
         RETURN
         END
C*************************END OF ANNOTA*************************************

C*************************FINDMIN*******************************************
C LOCATES MINIMUM OF SPR CURVE - VERY UNRELIABLE!!
         SUBROUTINE GETMIN(E,D,LAYERS,POLA)

         REAL KO,D(20),NEF,PI,ANGLE,STEP,FNEXT,FNOW,DELTA,GRAD
         COMPLEX E(20),REFLEC
         INTEGER LAYERS,POLA
         COMMON /CONSTS/ PI,KO

         STEP = 1.0
         WRITE(*,*) 'Input angle close to minimum'
         READ (*,*) ANGLE
         NEF = REAL(SQRT(E(1))) * SIN(ANGLE * PI/180)
         FNEXT = ABS(REFLEC(E,D,LAYERS,POLA,NEF))
         DELTA = 0.001
   10    FNOW = FNEXT
         ANGLE = ANGLE + DELTA
         NEF = REAL(SQRT(E(1))) * SIN(ANGLE * PI/180)
         GRAD = (ABS(REFLEC(E,D,LAYERS,POLA,NEF)) - FNOW)/DELTA
         ANGLE = ANGLE - DELTA
         IF(GRAD.GT.0.0) THEN
            ANGLE = ANGLE - STEP
         ELSE
            ANGLE = ANGLE + STEP
         ENDIF
         NEF = REAL(SQRT(E(1))) * SIN(ANGLE*PI/180)
         FNEXT = ABS(REFLEC(E,D,LAYERS,POLA,NEF))
         IF(FNEXT.GT.FNOW) STEP = STEP/2
         IF(STEP.GT.0.0001.AND.ANGLE.GT.0.0.AND.ANGLE.LT.90.0) GOTO 10

         WRITE (*,999) 'Minimum at angle = ',ANGLE
         WRITE (*,999) 'Reflectance = ',FNEXT
  999    FORMAT(A20,F8.4)
         RETURN
         END
C*************************END OF FINDMD*************************************

C*************************REFLEC********************************************
C****** CALCULATES THE INTENSITY REFLECTION COEFFICIENT OF STRUCTURE
         COMPLEX FUNCTION REFLEC(E,D,LAYERS,POLA,NEF)
```

```
      COMPLEX E(20),MATRIX(40,40),VECTOR(40),RESULT(40)
      REAL D(20),K0,NEF,PI
      INTEGER LAYERS,POLA
      COMMON /CONSTS/ PI,K0

      CALL MAKEQN(NEF,E,D,LAYERS,MATRIX,VECTOR,POLA)
      CALL GAUSSE(MATRIX,2*LAYERS-2,VECTOR,RESULT)
C SQUARE TO CONVERT FROM FIELD TO AMPLITUDE
      REFLEC = RESULT(1) * RESULT(1)

      RETURN
      END
C************************END OF REFLEC*************************************

C*************************TRANSM*****************************************
C****** CALCULATES THE INTENSITY TRANSMISSION COEFFICIENT OF STRUCTURE
      COMPLEX FUNCTION TRANSM(E,D,LAYERS,POLA,NEF)

      COMPLEX E(20),MATRIX(40,40),VECTOR(40),RESULT(40),KINC,KTRA
      REAL D(20),K0,NEF,PI
      INTEGER LAYERS,POLA
      COMMON /CONSTS/ PI,K0

      CALL MAKEQN(NEF,E,D,LAYERS,MATRIX,VECTOR,POLA)
      CALL GAUSSE(MATRIX,2*LAYERS-2,VECTOR,RESULT)
C SQUARE TO CONVERT FROM FIELD TO AMPLITUDE
      KINC=K0*CSQRT(E(1)-CMPLX(NEF*NEF))
      KTRA=K0*CSQRT(E(LAYERS)-CMPLX(NEF*NEF))
      IF(POLA.EQ.0) TRANSM = RESULT(2*LAYERS-2) * RESULT(2*LAYERS-2) *
     $                       KTRA / KINC
      IF(POLA.EQ.1) TRANSM = RESULT(2*LAYERS-2) * RESULT(2*LAYERS-2) *
     $                       KINC * E(LAYERS)/(KTRA * E(1))
      IF(NEF*NEF.GT.REAL(E(LAYERS))) TRANSM = 0
      RETURN
      END
C************************END OF REFLEC*************************************

C*************************TMPROF*****************************************
C CALCULATES AND PLOTS FIELD PROFILES FOR TM CASE
      SUBROUTINE TMPROF(E,D,LAYERS,LFLAG)

      COMPLEX E(20),MATRIX(40,40),VECTOR(40),RESULT(40),K(20),
     $     FIELD1(2000),FIELD2(2000),A,EZ(2000),HY(2000)
      REAL D(20),ANGLE,NEF,PI,K0,DTOTAL,X(2000),SX(2000),SZ(2000)
      INTEGER LAYERS,I,J,T,LFLAG
      COMMON /CONSTS/ PI,K0

      WRITE(*,*) 'Input angle of incidence'
      READ(*,*) ANGLE
      NEF = REAL(SQRT(E(1))) * SIN(ANGLE * PI/180)
      CALL MAKEQN(NEF,E,D,LAYERS,MATRIX,VECTOR,1)
```

```
      CALL GAUSSE(MATRIX,2*LAYERS-2,VECTOR,RESULT)
      DTOTAL = 0
      DO 10 I=1,LAYERS
         K(I)=K0*CSQRT(E(I)-CMPLX(NEF*NEF))
         DTOTAL = DTOTAL + D(I)
   10 CONTINUE
      IF(DTOTAL.EQ.0.0) DTOTAL = 1E-6
C GET FIELD PROFILES FOR FIRST LAYER
      DO 20 J=1,100
         X(J) = -DTOTAL + J*DTOTAL/100
         A = EXP(K(1)*(0,1)*X(J))
         FIELD1(J) = A + RESULT(1)/A
         FIELD2(J) = E(1)/K(1) * (A-RESULT(1)/A)
   20 CONTINUE
C GET FIELD PROFILES FOR INSIDE LAYERS
      DO 40 I=2,LAYERS-1
         DO 30 J=1,100
            T = I*100 - 100 + J
            X(T) = X(T-J) + J*D(I)/100
            A = EXP(K(I)*(0,1)*J*D(I)/100)
            FIELD1(T) = A*RESULT(I*2-2) + RESULT(I*2-1)/A
            FIELD2(T) = E(I)/K(I)*(A*RESULT(I*2-2)-RESULT(I*2-1)/A)
   30    CONTINUE
   40 CONTINUE
C GET FIELD PROFILES FOR LAST LAYER
      DO 50 J=1,100
         T = LAYERS*100 - 100 + J
         X(T) = X(T-J) + J*DTOTAL/100
         A = EXP(K(LAYERS)*(0,1)*J*DTOTAL/100)
         FIELD1(T) = RESULT(LAYERS*2-2)*A
         FIELD2(T) = E(LAYERS)/K(LAYERS)*RESULT(2*LAYERS-2)*A
   50 CONTINUE
      DO 60 I = 1,LAYERS*100
         EZ(I) = FIELD1(I)
         HY(I) = FIELD2(I)
C        EX = (0,1)*K0*NEF*FIELD2
         SZ(I) = REAL(K0*NEF*FIELD2(I)*CONJG(FIELD2(I)))
         SX(I) = REAL(FIELD1(I)*CONJG(FIELD1(I)))
   60 CONTINUE

      CALL PROFIL(X,EZ,DTOTAL,LAYERS,'Ez',E,D,1,LFLAG,ANGLE)
      CALL PROFIL(X,HY,DTOTAL,LAYERS,'Hy',E,D,1,LFLAG,ANGLE)

      CALL POYNT(X,SZ,SX,DTOTAL,LAYERS,E,D,1,LFLAG,ANGLE)
      RETURN
      END
C************************END OF TMPROF*************************************

C***************************TEPROF*****************************************
C CALCULATES AND PLOTS FIELD PROFILES FOR TE CASE
      SUBROUTINE TEPROF(E,D,LAYERS,LFLAG)
```

```
      COMPLEX E(20),MATRIX(40,40),VECTOR(40),RESULT(40),K(20),
     $     FIELD1(2000),FIELD2(2000),A,EY(2000),HZ(2000)
      REAL D(20),ANGLE,NEF,PI,K0,DTOTAL,X(2000),SX(2000),SZ(2000)
      INTEGER LAYERS,I,J,T,LFLAG
      COMMON /CONSTS/ PI,K0

      WRITE(*,*) 'Input angle of incidence'
      READ(*,*) ANGLE
      NEF = REAL(SQRT(E(1))) * SIN(ANGLE * PI/180)
      CALL MAKEQN(NEF,E,D,LAYERS,MATRIX,VECTOR,0)
      CALL GAUSSE(MATRIX,2*LAYERS-2,VECTOR,RESULT)
      DTOTAL = 0
      DO 10 I=1,LAYERS
         K(I)=K0*CSQRT(E(I)-CMPLX(NEF*NEF))
         DTOTAL = DTOTAL + D(I)
   10 CONTINUE
      IF(DTOTAL.EQ.0.0) DTOTAL = 1E-6
C GET FIELD PROFILE FOR FIRST LAYER
      DO 20 J=1,100
         X(J) = -DTOTAL + J*DTOTAL/100
         A = EXP(K(1)*(0,1)*X(J))
         FIELD1(J) = A + RESULT(1)/A
         FIELD2(J) = K(1) * (A - RESULT(1)/A)
   20 CONTINUE
C GET FIELD PROFILES FOR INSIDE LAYERS
      DO 40 I=2,LAYERS-1
         DO 30 J=1,100
            T = I*100 - 100 + J
            X(T) = X(T-J) + J*D(I)/100
            A = EXP(K(I)*(0,1)*J*D(I)/100)
            FIELD1(T) = A*RESULT(I*2-2) + RESULT(I*2-1)/A
            FIELD2(T) = K(I) * (A*RESULT(I*2-2) - RESULT(I*2-1)/A)
   30    CONTINUE
   40 CONTINUE
C GET FIELD PROFILES FOR LAST LAYER
      DO 50 J=1,100
         T = LAYERS*100 - 100 + J
         X(T) = X(T-J) + J*DTOTAL/100
         A = EXP(K(LAYERS)*(0,1)*J*DTOTAL/100)
         FIELD1(T) = RESULT(LAYERS*2-2)*A
         FIELD2(T) = K(LAYERS)*RESULT(2*LAYERS-2)*A
   50 CONTINUE

      DO 60 I=1,LAYERS*100
         EY(I) = FIELD1(I)
         HZ(I) = (0,1)*FIELD2(I)
C        HX = K0*NEF*FIELD1
         SZ(I) = REAL(K0*NEF*FIELD1(I)*CONJG(FIELD1(I)))
         SX(I) = REAL(FIELD1(I)*CONJG((0,1)*FIELD2(I)))
   60 CONTINUE
```

```
      CALL PROFIL(X,EY,DTOTAL,LAYERS,'Ey',E,D,0,LFLAG,ANGLE)
      CALL PROFIL(X,HZ,DTOTAL,LAYERS,'Hz',E,D,0,LFLAG,ANGLE)

      CALL POYNT(X,SZ,SX,DTOTAL,LAYERS,E,D,0,LFLAG,ANGLE)
      RETURN
      END
C************************END OF TEPROF*************************************

C*************************PROFIL*******************************************
C* PLOTS FIELD PROFILES
      SUBROUTINE PROFIL(X,FIELD,DTOTAL,LAYERS,LABEL,E,D,POLA,LFLAG,
     $                                                        ANGLE)
      COMPLEX FIELD(2000),E(20)
      REAL X(2000),AFIELD(2000),RFIELD(2000),DTOTAL,SCALE,D(20),ANGLE
      INTEGER I,LAYERS,POLA,LFLAG
      CHARACTER*2 LABEL

      DO 10 I=1,100*LAYERS
         AFIELD(I) = ABS(FIELD(I))
         RFIELD(I) = REAL(FIELD(I))
 10   CONTINUE
      SCALE = AFIELD(1)
      DO 20 I=2,LAYERS*100
         IF (AFIELD(I).GT.SCALE) SCALE=AFIELD(I)
 20   CONTINUE

      CALL PSPACE(0.1,0.9,0.1,0.8)
      CALL MAP(-DTOTAL,2*DTOTAL,-SCALE,SCALE)
      CALL WINDOW(-DTOTAL,2*DTOTAL,-SCALE,SCALE)
      CALL AXORIG(-DTOTAL,0.0)
      CALL AXES
      CALL BROKEN(1,10,1,10)
      DO 30 I=1,LAYERS-1
          CALL POSITN(X(I*100),-SCALE)
          CALL JOIN(X(I*100),SCALE)
 30   CONTINUE
      CALL FULL
      CALL POSITN(X(1),AFIELD(1))
      DO 40 I=1,100*LAYERS
          CALL JOIN(X(I),AFIELD(I))
 40   CONTINUE
      CALL POSITN(X(1),-AFIELD(1))
      DO 50 I=1,100*LAYERS
          CALL JOIN(X(I),-AFIELD(I))
 50   CONTINUE
      CALL BROKEN(10,10,10,10)
      CALL POSITN(X(1),RFIELD(1))
      DO 60 I=1,LAYERS*100
          CALL JOIN(X(I),RFIELD(I))
 60   CONTINUE
```

```
      CALL MAP(0.0,100.0,0.0,100.0)
      CALL WINDOW(0.0,100.0,0.0,100.0)
      CALL CTRMAG(15)
      CALL FULL
      CALL PLOTCS(90.0,15.0,LABEL)
      CALL POSITN(80.0,15.0)
      CALL JOIN(85.0,15.0)
      CALL BROKEN(10,10,10,10)
      CALL PLOTCS(90.0,10.0,LABEL//':t=0')
      CALL POSITN(80.0,10.0)
      CALL JOIN(85.0,10.0)
      CALL FULL
      CALL PLOTCS(40.0,-10.0,'Depth / metres')
      CALL CTRORI(90.0)
      IF(LABEL(1:1).EQ.'E') THEN
         CALL PLOTCS(-10.0,25.0,'E Field / arbitrary units')
      ELSE
         CALL PLOTCS(-10.0,25.0,'H Field / arbitrary units')
      ENDIF
      CALL CTRORI(0.0)
      IF(LFLAG.EQ.1) CALL ANNOTA(E,D,LAYERS,POLA,ANGLE)
      CALL FRAME
      RETURN
      END
C************************END OF PROFIL************************************

C*************************POYNT*****************************************
C PLOTS OUT POYNTING VECTOR PROFILE
      SUBROUTINE POYNT(X,SZ,SX,DTOTAL,LAYERS,E,D,POLA,LFLAG,ANGLE)

      COMPLEX E(20)
      REAL X(2000),SZ(2000),SX(2000),SCALE,DTOTAL,D(20),ANGLE
      INTEGER I,LAYERS,POLA,LFLAG
      SCALE=SZ(1)
      DO 38 I=2,LAYERS*100
         IF (SZ(I).GT.SCALE) SCALE=SZ(I)
   38 CONTINUE

      CALL PSPACE(0.1,0.9,0.1,0.8)
      CALL MAP(-DTOTAL,2*DTOTAL,0.0,SCALE)
      CALL WINDOW(-DTOTAL,2*DTOTAL,0.0,SCALE)
      CALL AXORIG(-DTOTAL,0.0)
      CALL AXES
      CALL BROKEN(1,10,1,10)
      DO 39 I=1,LAYERS-1
          CALL POSITN(X(I*100),0.0)
          CALL JOIN(X(I*100),SCALE)
   39 CONTINUE
      CALL FULL
      CALL POSITN(X(1),SZ(1))
      DO 40 I=1,100*LAYERS
```

```
            CALL JOIN(X(I),SZ(I))
   40   CONTINUE
        CALL MAP(0.0,100.0,0.0,100.0)
        CALL CTRMAG(20)
        CALL PLOTCS(40.0,-10.0,'Depth / metres')
        CALL CTRORI(90.0)
        CALL PLOTCS(-10.0,25.0,'Poynting Vector / arbitrary units')
        CALL CTRORI(0.0)
        IF(LFLAG.EQ.1) CALL ANNOTA(E,D,LAYERS,POLA,ANGLE)
        CALL FRAME

        RETURN
        END
C*************************END OF POYNT*********************************

C*************************MAKEQN***************************************
C GENERATES THE SIMULTANEOUS EQUATIONS IN MATRIX FORM
C
        SUBROUTINE MAKEQN(NEF,E,D,LAYERS,MATRIX,VECTOR,POLA)


        REAL NEF,D(20),K0,PI
        COMPLEX K(20),MATRIX(40,40),A,B,E(20),VECTOR(40)
        INTEGER LAYERS,I,J,POLA
        COMMON /CONSTS/ PI,K0
        DO 2 I=1,40
           VECTOR(I)=0.0
           DO 1 J=1,40
              MATRIX(I,J) = 0.0
    1      CONTINUE
    2   CONTINUE

        DO 5 I=1,LAYERS
           K(I)=K0*CSQRT(E(I)-CMPLX(NEF*NEF))
    5   CONTINUE

        IF(LAYERS.GT.2) THEN
C FIELD CONTINUITY AT E1:E2 - THIS IS AT DEPTH=0
           VECTOR(1) = -1
           MATRIX(1,1) = 1
           MATRIX(1,2) = -1
           MATRIX(1,3) = -1
C FIELD CONTINUITY AT OTHER BOUNDARIES EXCLUDING LAST ONE
           DO 10 I=2,LAYERS-2
              A=EXP(K(I)*(0,1)*D(I))
              J=2*I
              MATRIX(J-1,J-2) = A
              MATRIX(J-1,J-1) = 1/A
              MATRIX(J-1,J) = -1
              MATRIX(J-1,J+1) = -1
   10      CONTINUE
```

```
C FIELD CONTINUITY AT LAST BOUNDARY
          A=EXP(K(LAYERS-1)*(0,1)*D(LAYERS-1))
          J=2*(LAYERS-1)
          MATRIX(J-1,J-2)=A
          MATRIX(J-1,J-1)=1/A
          MATRIX(J-1,J)=-1
          IF(POLA.EQ.0) THEN
C TE CONDITIONS - GRADIENT CONTINUITY
             VECTOR(2)=-K(1)
             MATRIX(2,1)=-K(1)
             MATRIX(2,2)=-K(2)
             MATRIX(2,3)=K(2)
             DO 20 I=2,LAYERS-2
                A = EXP(K(I)*(0,1)*D(I))
                J = 2*I
                MATRIX(J,J-2) = A*K(I)
                MATRIX(J,J-1) = -K(I)/A
                MATRIX(J,J) = -K(I+1)
                MATRIX(J,J+1) = K(I+1)
  20         CONTINUE
             A = EXP(K(LAYERS-1)*(0,1)*D(LAYERS-1))
             J = 2*(LAYERS-1)
             MATRIX(J,J-2)=K(LAYERS-1)*A
             MATRIX(J,J-1)=-K(LAYERS-1)/A
             MATRIX(J,J)=-K(LAYERS)
          ELSE
C TM CONDITIONS - INTEGRAL FIELD * PERMITTIVITY CONTINUITY
             VECTOR(2)=-E(1)/K(1)
             MATRIX(2,1)=-E(1)/K(1)
             MATRIX(2,2)=-E(2)/K(2)
             MATRIX(2,3)=E(2)/K(2)
             DO 30 I=2,LAYERS-2
                A = EXP(K(I)*(0,1)*D(I))
                J = 2*I
                MATRIX(J,J-2) = A*E(I)/K(I)
                MATRIX(J,J-1) = -E(I)/(K(I)*A)
                MATRIX(J,J) = -E(I+1)/K(I+1)
                MATRIX(J,J+1) = E(I+1)/K(I+1)
  30         CONTINUE
             A = EXP(K(LAYERS-1)*(0,1)*D(LAYERS-1))
             J = 2*(LAYERS-1)
             MATRIX(J,J-2)=E(LAYERS-1)*A/K(LAYERS-1)
             MATRIX(J,J-1)=-E(LAYERS-1)/(K(LAYERS-1)*A)
             MATRIX(J,J)=-E(LAYERS)/K(LAYERS)
          ENDIF

       ELSE
C SINGLE INTERFACE CASE
          VECTOR(1) = -1
          MATRIX(1,1) = 1
          MATRIX(1,2) = -1
```

```
            IF(POLA.EQ.0) THEN
               VECTOR(2) = -K(1)
               MATRIX(2,1) = -K(1)
               MATRIX(2,2) = -K(2)
            ELSE
               VECTOR(2) = -E(1)/K(1)
               MATRIX(2,1) = -E(1)/K(1)
               MATRIX(2,2) = -E(2)/K(2)
            ENDIF
         ENDIF
         RETURN
         END
C******************END OF MAKEQN*********************************************

C ************************GAUSSELIM*******************************************
C SOLVES SIMULTANEOUS EQUATIONS A.Y=X WHERE A IS AN NxN MATRIX
C RESULT CONTAINS ANSWERS
         SUBROUTINE GAUSSE(A,M,V,RESULT)

         INTEGER M,SWAP,I,J,R,Y
         COMPLEX A(40,40),V(40),RESULT(40),FACTOR,TEMP

         IF(M.EQ.2) THEN
            FACTOR = A(2,1)/A(1,1)
            A(2,1) = 0
            A(2,2) = A(2,2) - FACTOR * A(1,2)
            V(2) = V(2) - FACTOR * V(1)
            RESULT(2) = V(2)/A(2,2)
            RESULT(1) = (V(1) - A(1,2) * RESULT(2))/A(1,1)
         ELSE
            DO 60 R=1,M-1
C CHECKS FOR ZERO PIVOT
               SWAP=R
   10          IF(A(SWAP,SWAP).NE.0) THEN
                  GOTO 30
               ELSE
                  SWAP=SWAP+1
                  IF(SWAP.EQ.M) THEN
                     PRINT *,'No solutions.'
                     STOP
                  ENDIF
                  GOTO 10
               ENDIF

C ROW SWAP - ONLY SWAPS NON ZERO PARTS OF COURSE
               IF(R.NE.SWAP) THEN
                  DO 20 Y=R,M
                     TEMP=A(SWAP,Y)
                     A(SWAP,Y)=A(R,Y)
                     A(R,Y)=TEMP
   20             CONTINUE
```

```
                TEMP=V(SWAP)
                V(SWAP)=V(R)
                V(R)=TEMP
             ENDIF


   30        DO 50 I=R+1,M
                FACTOR=A(I,R)/A(R,R)
                A(I,R)=0
                DO 40 J=R+1,M
                   A(I,J)=A(I,J)-FACTOR*A(R,J)
   40           CONTINUE
                V(I)=V(I)-FACTOR*V(R)
   50        CONTINUE
   60     CONTINUE
C NOW MATRIX IS TRIANGULAR - CAN SUBSTITUTE BACK FOR RESULTS
          RESULT(M)=V(M)/A(M,M)
          DO 80 I=M-1,1,-1
             RESULT(I)=V(I)
             DO 70 J=M,I+1,-1
                RESULT(I)=RESULT(I)-RESULT(J)*A(I,J)
   70        CONTINUE
             RESULT(I)=RESULT(I)/A(I,I)
   80     CONTINUE
       ENDIF
       RETURN
       END
```

2. SPR curve fitting program

```
C SOLVES MAXWELLS EQUATIONS THROUGH NLAYER STRUCTURE (UP TO 20 LAYERS)
C AND FITS UNKNOWN PERMITTIVITY AND THICKNESS TO SPRCURVE

       PROGRAM SPRFIT
       COMPLEX E(20)
       INTEGER POLA,LAYERS,M,UNKNOW,I,ANS,PMASK(3)
       REAL D(20),LAMDA,ANGLE(10000),MEASUR(10000),PI,K0,X(3),SUMSQ,NS
       CHARACTER*14 FILENM
       COMMON /DATA/ E,D,LAYERS,POLA,UNKNOW,ANGLE,MEASUR,M
       COMMON /CONSTS/ PI,K0

       PI = 3.1415927
       LAYERS = 0

       WRITE(*,*) 'SPR Curve fitting program'
```

```
      WRITE(*,*) 'Filename for reflectivity data'
      READ(*,999) FILENM
      CALL DATADC(ANGLE,MEASUR,M,FILENM)
C REDUCE NUMBER OF DATA POINTS
      WRITE(*,*) 'Will use every n th point. Enter n'
      READ(*,*) N
      M = M/N
      DO 20 I=1,M
         ANGLE(I) = ANGLE(I*N)
         MEASUR(I) = MEASUR(I*N)
   20 CONTINUE

      CALL LYDATA(E,D,LAYERS,POLA,LAMDA)
      CALL REDUCE(E,D,LAYERS)
      CALL SHOW(E,D,LAYERS,POLA,LAMDA,5)
      K0 = 2*PI/LAMDA
      WRITE(*,*) 'Which is the unknown layer?'
      READ (*,*) UNKNOW
      X(1) = REAL(E(UNKNOW))
      X(2) = AIMAG(E(UNKNOW))
      X(3) = D(UNKNOW)*1E8
C MASK OUT PARAMETERS NOT BENG FITTED
      PMASK(1) = 1
      PMASK(2) = 1
      PMASK(3) = 1
   30 WRITE(*,*) 'Parameters to fit for'
      WRITE(*,*) '1=All'
      WRITE(*,*) '2=Thickness only'
      WRITE(*,*) '3=Permittivity only'
      WRITE(*,*) '4=Lossless film'
      WRITE(*,*) '5=Loss and thickness only'
      WRITE(*,*) '6=Loss only'
      READ(*,*) ANS
      IF(ANS.GT.6.OR.ANS.LT.1) GOTO 30
      IF(ANS.EQ.2) THEN
         PMASK(1) = 0
         PMASK(2) = 0
      ENDIF
      IF(ANS.EQ.3) PMASK(3) = 0
      IF(ANS.EQ.4) THEN
         PMASK(2) = 0
         X(2) = 0
      ENDIF
      IF(ANS.EQ.5) PMASK(1) = 0
      IF(ANS.EQ.6) THEN
         PMASK(1) = 0
         PMASK(3) = 0
      ENDIF
      CALL FIT(X,PMASK,M)
      E(UNKNOW) = X(1) + (0,1)*X(2)
      D(UNKNOW) = X(3)/1E8
```

```
      CALL SHOW(E,D,LAYERS,POLA,LAMDA,5)
      CALL CURVES(FILENM)
      CALL STORE(E,D,LAYERS,POLA,LAMDA)
  999 FORMAT(A14)
      STOP
      END
C************************END OF MAIN*************************************

C*************************LYDATA*****************************************
C GATHERS DATA FOR LAYERS
      SUBROUTINE LYDATA(E,D,LAYERS,POLA,LAMDA)

      COMPLEX      E(20)
      REAL         D(20),LAMDA
      INTEGER      LAYERS,POLA
      CHARACTER*14 FILNAM
      CHARACTER*80 TRASH

      WRITE(*,*) 'Filename for layer data'
      READ(*,999) FILNAM
      OPEN(UNIT=10,FILE=FILNAM,STATUS='OLD')
      REWIND(10)
      READ(10,'(A80)') TRASH
      READ(10,*) POLA
      READ(10,'(A80)') TRASH
      READ(10,*) LAMDA
      READ(10,'(A80)') TRASH
      READ(10,*) LAYERS
      READ(10,'(A80)') TRASH
      READ(10,*) (E(I),D(I), I=1,LAYERS)
      CLOSE(UNIT=10)
  999 FORMAT(A14)
      RETURN
      END
C************************END OF LYDATA**********************************

C*****************************SHOW****************************************
      SUBROUTINE SHOW(E,D,LAYERS,POLA,LAMDA,WHERE)
      COMPLEX E(20)
      REAL D(20),LAMDA
      INTEGER LAYERS,POLA,WHERE

      IF(POLA.EQ.0) WRITE(WHERE,*) 'TE Polarisation'
      IF(POLA.EQ.1) WRITE(WHERE,*) 'TM Polarisation'
      WRITE(WHERE,*) 'Wavelength =',LAMDA
      WRITE(WHERE,998) 'Layer','Permittivity','Depth'
      WRITE(WHERE,999) 1,E(1),0.0
      WRITE(WHERE,999) (I,E(I),D(I), I=2,LAYERS-1)
      WRITE(WHERE,999) LAYERS,E(LAYERS),0.0
  998 FORMAT(A5,A20,A10)
  999 FORMAT(I5,F14.4,',',F8.4,E15.6)
```

```
      RETURN
      END
C*************************END OF SHOW*************************************

C*****************************STORE***************************************
      SUBROUTINE STORE(E,D,LAYERS,POLA,LAMDA)
      COMPLEX E(20)
      REAL D(20),LAMDA
      INTEGER LAYERS,POLA
      CHARACTER*14 FILNAM

      WRITE(*,*) 'Filename for output'
      READ(*,999) FILNAM
      OPEN(UNIT=10,FILE=FILNAM,STATUS='UNKNOWN')
      REWIND(10)
      WRITE(10,*) 'Polarisation 1=TM 0=TE'
      WRITE(10,'(I1)') POLA
      WRITE(10,*) 'Wavelength/m'
      WRITE(10,'(E15.6)') LAMDA
      WRITE(10,*) 'Number of layers'
      WRITE(10,'(I2)') LAYERS
      WRITE(10,*) 'Real(e),Im(e),depth (0=semi infinite)'
      WRITE(10,998) (E(I),D(I), I=1,LAYERS)
      CLOSE(UNIT=10)
  998 FORMAT(F10.6,',',F10.6,',',E15.6)
  999 FORMAT(A14)
      RETURN
      END
C************************END OF STORE*************************************

C****************************REDUCE***************************************
      SUBROUTINE REDUCE (E,D,LAYERS)
C LAYER REDUCTION ROUTINE - LOOKS FOR ADJACENT LAYERS OF SAME INDEX

      COMPLEX E(20)
      REAL D(20)
      INTEGER LAYERS,OLDLAY

      OLDLAY=LAYERS-1
    5 IF(OLDLAY.NE.LAYERS) THEN
        OLDLAY=LAYERS
        DO 9 I=1,LAYERS-1
          IF(E(I).EQ.E(I+1)) THEN
            D(I)=D(I)+D(I+1)
            DO 8 J=I+1,LAYERS-1
              E(J)=E(J+1)
              D(J)=D(J+1)
    8       CONTINUE
            LAYERS=LAYERS-1
          ENDIF
    9   CONTINUE
```

```
         GOTO 5
       ENDIF
       RETURN
       END
C**********************END OF REDUCE*****************************************

C***************************FIT*************************************************
C* PEFORMS ACTUAL FITTING
       SUBROUTINE FIT(X,PMASK,M)
       REAL X(3),FSUMSQ,GRAD(3),FNOW,LENGTH,FNEXT,ERROR
       INTEGER M,COUNT,ITER,PMASK(3),BETTER

       GRAD(1) = 0
       GRAD(2) = 0
       GRAD(3) = 0

       WRITE(*,*) 'Enter average error required (0.01 suggested)'
       READ(*,*) ERROR
       WRITE(*,*) 'Enter iterations limit'
       READ(*,*) ITER
       CALL AUTNOR
       FNEXT = FSUMSQ(X,0.0,0.0,0.0)
       COUNT = 0
       WRITE(*,998) 'Permittivity','Depth','Average Error'
  10   FNOW = FNEXT
       BETTER = 0
       WRITE(*,999) X(1),X(2),X(3)/1E8,SQRT(FNOW/M)
       IF(PMASK(1).EQ.1) THEN
          GRAD(1) = (FSUMSQ(X,0.001,0.0,0.0) - FNOW)/0.001
       ENDIF
       IF(PMASK(2).EQ.1) THEN
          GRAD(2) = (FSUMSQ(X,0.0,0.001,0.0) - FNOW)/0.001
       ENDIF
       IF(PMASK(3).EQ.1) THEN
          GRAD(3) = (FSUMSQ(X,0.0,0.0,0.001) - FNOW)/0.001
       ENDIF
       LENGTH=SQRT(GRAD(1)*GRAD(1)+GRAD(2)*GRAD(2)+GRAD(3)*GRAD(3))
       GRAD(1) = - 0.0001 * GRAD(1)/LENGTH
       GRAD(2) = - 0.0001 * GRAD(2)/LENGTH
       GRAD(3) = - 0.0001 * GRAD(3)/LENGTH

  20   GRAD(1) = GRAD(1) * 2
       GRAD(2) = GRAD(2) * 2
       GRAD(3) = GRAD(3) * 2
       FNEXT = FSUMSQ(X,GRAD(1),GRAD(2),GRAD(3))
       IF(FNEXT.LT.FNOW) THEN
          BETTER = 1
          FNOW = FNEXT
          GOTO 20
       ELSE
          X(1) = X(1) + GRAD(1)/2
```

```
            X(2) = X(2) + GRAD(2)/2
            X(3) = X(3) + GRAD(3)/2
         ENDIF

         CALL AUTNOR
         FNEXT = FSUMSQ(X,0.0,0.0,0.0)
         COUNT = COUNT + 1
         IF(FNOW.GT.M*ERROR*ERROR.AND.COUNT.LT.ITER.AND.BETTER.EQ.1)
        $                                                    GOTO 10
   30    WRITE(*,999) X(1),X(2),X(3)/1E8,SQRT(FSUMSQ(X,0.0,0.0,0.0)/M)
  998    FORMAT(A16,A15,A19)
  999    FORMAT(F10.4,',',F8.4,E15.3,F13.4)
         RETURN
         END
C************************END OF FIT*****************************************

C*************************FSUMSQ*******************************************
C* CALCULATES SUM OF SQUARES OF ERRORS
         REAL FUNCTION FSUMSQ(X,DX1,DX2,DX3)
         INTEGER M,POLA,LAYERS,I,UNKNOW
         REAL D(20),PI,K0,ERROR,ANGLE(10000),MEASUR(10000),X(3),NEF,DX1
        $      DX2,DX3
         COMPLEX E(20),REFLEC
         COMMON /DATA/ E,D,LAYERS,POLA,UNKNOW,ANGLE,MEASUR,M
         COMMON /CONSTS/ PI,K0

         E(UNKNOW) = X(1) + DX1 + (0,1) * (X(2)+DX2)
         D(UNKNOW) = (X(3)+DX3)/1E8
         F = 0
         DO 10 I = 1,M
            NEF = REAL(SQRT(E(1))) * SIN(ANGLE(I) * PI/180)
            ERROR = ABS(REFLEC(E,D,LAYERS,POLA,NEF)) - MEASUR(I)
            F = F + ERROR * ERROR
   10    CONTINUE
         FSUMSQ = F
         RETURN
         END
C************************END OF FSUMSQ*************************************

C*************************CURVES*******************************************
C REFLECTION VERSUS ANGLE RESULTS
         SUBROUTINE CURVES(FILENM)

         COMPLEX E(20),RC,REFLEC
         REAL    D(20),K0,ANGLE(10000),NEF,REFMAG(10000),PI,MAX,MIN,
        $        MEASUR(10000),ERROR(10000)
         INTEGER LAYERS,POLA,I,M,UNKNOW
         CHARACTER*14 FILENM
         COMMON /DATA/ E,D,LAYERS,POLA,UNKNOW,ANGLE,MEASUR,M
         COMMON /CONSTS/ PI,K0
```

```
      DO 10 I=1,M
         NEF = REAL(SQRT(E(1))) * SIN(ANGLE(I) * PI/180)
         RC = REFLEC(E,D,LAYERS,POLA,NEF)
         REFMAG(I) = ABS(RC)
10    CONTINUE

      CALL PAPER(1)
      CALL PSPACE(0.1,0.9,0.1,0.9)
      CALL MAP(ANGLE(1),ANGLE(M),0.0,1.05)
      CALL WINDOW(ANGLE(1),ANGLE(M),0.0,1.05)
      CALL AXORIG(ANGLE(1),0)
      CALL AXES
      CALL POSITN(ANGLE(1),REFMAG(1))
      DO 20 I=2,M
         CALL JOIN(ANGLE(I),REFMAG(I))
20    CONTINUE
      DO 30 I=1,M
         CALL PLOTNC(ANGLE(I),MEASUR(I),248)
30    CONTINUE
      CALL MAP(0.0,100.0,0.0,100.0)
      CALL CTRMAG(20)
      CALL PLOTCS(40.0,-10.0,'Incident Angle')
      CALL CTRORI(90.0)
      CALL PLOTCS(-10.0,40.0,'Reflectivity')
      CALL CTRORI(0.0)
      CALL ANNOTA(E,D,LAYERS,POLA,FILENM)
      CALL FRAME
      DO 40 I=1,M
         ERROR(I) = REFMAG(I) - MEASUR(I)
         IF(ERROR(I).LT.MIN) MIN = ERROR(I)
         IF(ERROR(I).GT.MAX) MAX = ERROR(I)
40    CONTINUE
      CALL PSPACE(0.1,0.9,0.1,0.9)
      CALL MAP(ANGLE(1),ANGLE(M),MIN,MAX)
      CALL WINDOW(ANGLE(1),ANGLE(M),MIN,MAX)
      CALL AXORIG(ANGLE(1),0)
      CALL AXES
      CALL POSITN(ANGLE(1),ERROR(1))
      DO 50 I=2,M
         CALL JOIN(ANGLE(I),ERROR(I))
50    CONTINUE
      CALL MAP(0.0,100.0,0.0,100.0)
      CALL CTRMAG(20)
      CALL PLOTCS(40.0,-10.0,'Incident Angle')
      CALL CTRORI(90.0)
      CALL PLOTCS(-10.0,20.0,'Deviation: Theory - Experiment')
      CALL CTRORI(0.0)
      CALL ANNOTA(E,D,LAYERS,POLA,FILENM)
      CALL GREND
      RETURN
      END
```

```
C*************************END OF CURVES*****************************************

C*************************ANNOTA************************************************
C* ANNOTATES GRAPHS
      SUBROUTINE ANNOTA(E,D,LAYERS,POLA,FILENM)
      COMPLEX E(20)
      REAL D(20)
      INTEGER LAYERS,POLA
      CHARACTER*14 FILENM
      CALL CSPACE(0.0,1.0,0.0,1.0)
      CALL CTRMAG(12)
      CALL PLACE(52,1)
      IF(POLA.EQ.1) CALL TYPECS('TM Pol. ')
      IF(POLA.EQ.0) CALL TYPECS('TE Pol. ')
      CALL PLACE(61,1)
      CALL TYPECS(FILENM)

      CALL PLACE(50,2)
      CALL TYPECS('Layer     Permittivity   Thickness/m')
      DO 10 I=1,LAYERS
         CALL PLACE(51,2+I)
         CALL TYPENI(I)
         CALL PLACE(57,2+I)
         CALL TYPENF(REAL(E(I)),4)
         CALL PLACE(65,2+I)
         CALL TYPECS('+')
         CALL PLACE(65,2+I)
         CALL TYPENF(AIMAG(E(I)),4)
         CALL PLACE(72,2+I)
         CALL TYPECS('i')
         CALL PLACE(75,2+I)
         CALL TYPENE(D(I),4)
   10 CONTINUE
      CALL CSPACE(0.0,0.0,0.0,0.0)
      RETURN
      END
C*************************END OF ANNOTA*****************************************

C*************************REFLEC************************************************
C****** CALCULATES THE INTENSITY REFLECTION COEFFICIENT OF STRUCTURE
      COMPLEX FUNCTION REFLEC(E,D,LAYERS,POLA,NEF)

      COMPLEX E(20),MATRIX(40,40),VECTOR(40),RESULT(40)
      REAL D(20),K0,NEF,PI
      INTEGER LAYERS,POLA
      COMMON /CONSTS/ PI,K0

      CALL MAKEQN(NEF,E,D,LAYERS,MATRIX,VECTOR,POLA)
      CALL GAUSSE(MATRIX,2*LAYERS-2,VECTOR,RESULT)
C SQUARE TO CONVERT FROM FIELD TO AMPLITUDE
      REFLEC = RESULT(1) * RESULT(1)
```

```
      RETURN
      END
C************************END OF REFLEC*************************************

C*************************MAKEQN*****************************************
C GENERATES THE SIMULTANEOUS EQUATIONS IN MATRIX FORM
C
      SUBROUTINE MAKEQN(NEF,E,D,LAYERS,MATRIX,VECTOR,POLA)

      REAL NEF,D(20),K0,PI
      COMPLEX K(20),MATRIX(40,40),A,B,E(20),VECTOR(40)
      INTEGER LAYERS,I,J,POLA
      COMMON /CONSTS/ PI,K0
      DO 2 I=1,40
         VECTOR(I)=0.0
         DO 1 J=1,40
            MATRIX(I,J) = 0.0
    1    CONTINUE
    2 CONTINUE

      DO 5 I=1,LAYERS
         IF(NEF.NE.SQRT(E(I))) THEN
            K(I)=K0*CSQRT(E(I)-CMPLX(NEF*NEF))
                        ELSE
            K(I)=0
         END IF
    5 CONTINUE

      IF(LAYERS.GT.2) THEN
C FIELD CONTINUITY AT E1:E2 - THIS IS AT DEPTH=0
         VECTOR(1) = -1
         MATRIX(1,1) = 1
         MATRIX(1,2) = -1
         MATRIX(1,3) = -1
C FIELD CONTINUITY AT OTHER BOUNDARIES EXCLUDING LAST ONE
         DO 10 I=2,LAYERS-2
            A=EXP(K(I)*(0,1)*D(I))
            J=2*I
            MATRIX(J-1,J-2) = A
            MATRIX(J-1,J-1) = 1/A
            MATRIX(J-1,J) = -1
            MATRIX(J-1,J+1) = -1
   10    CONTINUE
C FIELD CONTINUITY AT LAST BOUNDARY
         A=EXP(K(LAYERS-1)*(0,1)*D(LAYERS-1))
         J=2*(LAYERS-1)
         MATRIX(J-1,J-2)=A
         MATRIX(J-1,J-1)=1/A
         MATRIX(J-1,J)=-1
         IF(POLA.EQ.0) THEN
```

```
C TE CONDITIONS - GRADIENT CONTINUITY
              VECTOR(2)=-K(1)
              MATRIX(2,1)=-K(1)
              MATRIX(2,2)=-K(2)
              MATRIX(2,3)=K(2)
              DO 20 I=2,LAYERS-2
                 A = EXP(K(I)*(0,1)*D(I))
                 J = 2*I
                 MATRIX(J,J-2) = A*K(I)
                 MATRIX(J,J-1) = -K(I)/A
                 MATRIX(J,J) = -K(I+1)
                 MATRIX(J,J+1) = K(I+1)
   20         CONTINUE
              A = EXP(K(LAYERS-1)*(0,1)*D(LAYERS-1))
              J = 2*(LAYERS-1)
              MATRIX(J,J-2)=K(LAYERS-1)*A
              MATRIX(J,J-1)=-K(LAYERS-1)/A
              MATRIX(J,J)=-K(LAYERS)
           ELSE
C TM CONDITIONS - INTEGRAL FIELD * PERMITTIVITY CONTINUITY
              VECTOR(2)=-E(1)/K(1)
              MATRIX(2,1)=-E(1)/K(1)
              MATRIX(2,2)=-E(2)/K(2)
              MATRIX(2,3)=E(2)/K(2)
              DO 30 I=2,LAYERS-2
                 A = EXP(K(I)*(0,1)*D(I))
                 J = 2*I
                 MATRIX(J,J-2) = A*E(I)/K(I)
                 MATRIX(J,J-1) = -E(I)/(K(I)*A)
                 MATRIX(J,J) = -E(I+1)/K(I+1)
                 MATRIX(J,J+1) = E(I+1)/K(I+1)
   30         CONTINUE
              A = EXP(K(LAYERS-1)*(0,1)*D(LAYERS-1))
              J = 2*(LAYERS-1)
              MATRIX(J,J-2)=E(LAYERS-1)*A/K(LAYERS-1)
              MATRIX(J,J-1)=-E(LAYERS-1)/(K(LAYERS-1)*A)
              MATRIX(J,J)=-E(LAYERS)/K(LAYERS)
           ENDIF

        ELSE
C SINGLE INTERFACE CASE
           VECTOR(1) = -1
           MATRIX(1,1) = 1
           MATRIX(1,2) = -1
           IF(POLA.EQ.0) THEN
              VECTOR(2) = -K(1)
              MATRIX(2,1) = -K(1)
              MATRIX(2,2) = -K(2)
           ELSE
              VECTOR(2) = -E(1)/K(1)
              MATRIX(2,1) = -E(1)/K(1)
```

```
            MATRIX(2,2) = -E(2)/K(2)
          ENDIF
        ENDIF
      RETURN
        END
C******************END OF MAKEQN*********************************************

C ***************************GAUSSELIM*************************************
C SOLVES SIMULTANEOUS EQUATIONS A.Y=X WHERE A IS AN NxN MATRIX
C RESULT CONTAINS ANSWERS
        SUBROUTINE GAUSSE(A,M,V,RESULT)

        INTEGER M,SWAP,I,J,R,Y
        COMPLEX A(40,40),V(40),RESULT(40),FACTOR,TEMP

        DO 60 R=1,M-1
C CHECKS FOR ZERO PIVOT
           SWAP=R
   10      IF(A(SWAP,SWAP).NE.0) THEN
              GOTO 30
                                ELSE
              SWAP=SWAP+1
              IF(SWAP.EQ.M) THEN
                 PRINT *,'No solutions.'
                 STOP
              ENDIF
              GOTO 10
           ENDIF

C ROW SWAP - ONLY SWAPS NON ZERO PARTS OF COURSE
           IF(R.NE.SWAP) THEN
              DO 20 Y=R,M
                 TEMP=A(SWAP,Y)
                 A(SWAP,Y)=A(R,Y)
                 A(R,Y)=TEMP
   20         CONTINUE
              TEMP=V(SWAP)
              V(SWAP)=V(R)
              V(R)=TEMP
           ENDIF


   30      DO 50 I=R+1,M
              FACTOR=A(I,R)/A(R,R)
              A(I,R)=0
              DO 40 J=R+1,M
                 A(I,J)=A(I,J)-FACTOR*A(R,J)
   40         CONTINUE
              V(I)=V(I)-FACTOR*V(R)
   50      CONTINUE
   60   CONTINUE
```

```
C NOW MATRIX IS TRIANGULAR - CAN SUBSTITUTE BACKFOR RESULTS
      RESULT(M)=V(M)/A(M,M)
      DO 80 I=M-1,1,-1
         RESULT(I)=V(I)
         DO 70 J=M,I+1,-1
            RESULT(I)=RESULT(I)-RESULT(J)*A(I,J)
   70    CONTINUE
         RESULT(I)=RESULT(I)/A(I,I)
   80 CONTINUE

      RETURN
      END
C ********************* END OF GAUSSE ***************************************

C*****************************REFP*****************************************
C* P POLARISATION REFLECTION COEFFICIENT
C* USED TO ALLOW FOR PRISM REFLECTANCE LOSSES
      REAL FUNCTION REFP(THETA,N)
C N IS RATIO N2/N1, THETA IS IN RADIANS (MEASURED IN N1)
      REAL THETA,N,TERM1,TERM2

      TERM1 = N * N * COS(THETA)
      TERM2 = SQRT(N * N - SIN(THETA) * SIN(THETA))
      REFP = ABS((TERM1 - TERM2)/(TERM1 + TERM2))
      RETURN
      END
C************************END OF REFP*****************************************

C****************************TRANSM*****************************************
C TRANSMISSION AT INTERNAL ANGLE PHI THROUGH TWO PRISM FACES
      REAL FUNCTION TRANSM(PHI)
      REAL PHI,PI,REFP
      PI = 3.1415927
      TRANSM = (1-REFP(ASIN(1.52*SIN(PI/4-PI*PHI/180)),1.52) *
     $          REFP(ASIN(1.52*SIN(PI/4-PI*PHI/180)),1.52)) *
     $          (1-REFP(PI/4-PI*PHI/180,1/1.52) *
     $          REFP(PI/4-PI*PHI/180,1/1.52))
      RETURN
      END
C************************END OF TRANSM ***************************************

C****************************DATADC*****************************************
      SUBROUTINE DATADC(ANGLE,MEASUR,M,FILENM)
      CHARACTER*14 FILENM
      REAL ANGLE(10000),MEASUR(10000),MAXIMR,TRANSM
      INTEGER M,I

      OPEN(UNIT=10,FILE=FILENM,STATUS='OLD')
      I=1
    5 READ(10,*,END=6) ANGLE(I),MEASUR(I)
      I=I+1
```

```
      GOTO 5
    6 M = I-1
      WRITE(*,*) M,' points read in'
      CLOSE(UNIT=10)

      DO 30 I = 1,M
         MEASUR(I) = MEASUR(I)/TRANSM(ANGLE(I))
   30 CONTINUE

  999 FORMAT(A14)
      RETURN
      END
C********************** END OF DATADC ***********************************
C* NORMALISATION OF DATA BY MATCHING THEORETICAL AND PRACTICAL MAXIMA
      SUBROUTINE AUTNOR

      REAL ANGLE(10000),MEASUR(10000),D(20),PI,K0,RATIO,MAXIMR,NEF
      COMPLEX E(20),REFLEC
      INTEGER LAYERS,POLA,UNKNOW,I,M,TOP

      COMMON /DATA/ E,D,LAYERS,POLA,UNKNOW,ANGLE,MEASUR,M
      COMMON /CONSTS/ PI,K0

      MAXIMR = MEASUR(1)
      TOP = 1
      DO 10 I =2,M
         IF(MEASUR(I).GT.MAXIMR) THEN
            MAXIMR = MEASUR(I)
            TOP = I
         ENDIF
   10 CONTINUE

      I = TOP
      NEF = REAL(SQRT(E(1))) * SIN(ANGLE(I) * PI/180)
      RATIO = MEASUR(I)/ABS(REFLEC(E,D,LAYERS,POLA,NEF))

      DO 20 I = 1,M
         MEASUR(I) = MEASUR(I)/RATIO
   20 CONTINUE
      RETURN
      END
```

3. Pockels effect fitting program

```
C POCKELS EFFECT FITTING PROGRAM
```

```
C NEEDS INPUT POCKELS CURVE AND LAYER THICKNESSES AND PERMITTIVITIES

      PROGRAM POKFIT
      COMPLEX E(20)
      INTEGER POLA,LAYERS,M,UNKNOW,I,ELAYER
      REAL D(20),LAMDA,ANGLE(10000),MEASUR(10000),PI,K0,X(3),NEF,
     $     DERIVR(10000),DERIVI(10000),DELER,DELEI,OFFSET
      CHARACTER*14 FILENM
      COMMON /FITDAT/ M,ANGLE,MEASUR,DERIVR,DERIVI
      COMMON /NAGDAT/ E,D,LAYERS,POLA,NEF,ELAYER
      COMMON /CONSTS/ PI,K0

      PI = 3.1415927
      LAYERS = 0

      WRITE(*,*) 'Pockels Effect fitting program'
      CALL LYDATA(E,D,LAYERS,POLA,LAMDA)
      CALL SHOW(E,D,LAYERS,POLA,LAMDA,5)
      K0 = 2*PI/LAMDA
      WRITE(*,*) 'Filename for reflectivity data'
      READ(*,999) FILENM
      OPEN(UNIT=10,FILE=FILENM,STATUS='OLD')
      I=1
    5 READ(10,*,END=6) ANGLE(I),MEASUR(I)
      I=I+1
      GOTO 5
    6 M = I-1
      CLOSE(UNIT=10)
      WRITE(*,*) M,' points read in'

C Calculate theoretical derivatives wrt. real and imag parts of permittivity
      CALL DIFFER(FILENM)

      X(1) = 0.0
      X(2) = 0.0
      CALL FIT(X)
      DELER = X(1)/1E8
      DELEI = X(2)/1E8
      OFFSET = X(3)
      CALL CURVES(DELER,DELEI,OFFSET,FILENM)
  999 FORMAT(A14)
      STOP
      END
C*************************END OF MAIN*****************************************

C*************************LYDATA**********************************************
C GATHERS DATA FOR LAYERS
      SUBROUTINE LYDATA(E,D,LAYERS,POLA,LAMDA)

      COMPLEX      E(20)
      REAL         D(20),LAMDA
```

```
      INTEGER      LAYERS,POLA
      CHARACTER*14 FILNAM
      CHARACTER*80 TRASH

      WRITE(*,*) 'Filename for layer data'
      WRITE(*,*) 'This file MUST contain data fitted using dc. results'
      READ(*,999) FILNAM
      OPEN(UNIT=10,FILE=FILNAM,STATUS='OLD')
      REWIND(10)
      READ(10,'(A80)') TRASH
      READ(10,*) POLA
      READ(10,'(A80)') TRASH
      READ(10,*) LAMDA
      READ(10,'(A80)') TRASH
      READ(10,*) LAYERS
      READ(10,'(A80)') TRASH
      READ(10,*) (E(I),D(I), I=1,LAYERS)
      CLOSE(UNIT=10)
  999 FORMAT(A14)
      RETURN
      END
C***********************END OF LYDATA*************************************

C*****************************SHOW*****************************************
      SUBROUTINE SHOW(E,D,LAYERS,POLA,LAMDA,WHERE)
      COMPLEX E(20)
      REAL D(20),LAMDA
      INTEGER LAYERS,POLA,WHERE

      IF(POLA.EQ.0) WRITE(WHERE,*) 'TE Polarisation'
      IF(POLA.EQ.1) WRITE(WHERE,*) 'TM Polarisation'
      WRITE(WHERE,*) 'Wavelength =',LAMDA
      WRITE(WHERE,998) 'Layer','Permittivity','Depth'
      WRITE(WHERE,999) 1,E(1),0.0
      WRITE(WHERE,999) (I,E(I),D(I), I=2,LAYERS-1)
      WRITE(WHERE,999) LAYERS,E(LAYERS),0.0
  998 FORMAT(A5,A20,A10)
  999 FORMAT(I5,F14.4,',',F8.4,E15.6)
      RETURN
      END
C***************************END OF SHOW*************************************

C*****************************STORE****************************************
      SUBROUTINE STORE(E,D,LAYERS,POLA,LAMDA)
      COMPLEX E(20)
      REAL D(20),LAMDA
      INTEGER LAYERS,POLA
      CHARACTER*14 FILNAM

      WRITE(*,*) 'Filename for output'
      READ(*,999) FILNAM
```

```
      OPEN(UNIT=10,FILE=FILNAM,STATUS='UNKNOWN')
      REWIND(10)
      WRITE(10,*) 'Polarisation 1=TM 0=TE'
      WRITE(10,'(I1)') POLA
      WRITE(10,*) 'Wavelength/m'
      WRITE(10,'(E15.6)') LAMDA
      WRITE(10,*) 'Number of layers'
      WRITE(10,'(I2)') LAYERS
      WRITE(10,*) 'Real(e),Im(e),depth (0=semi infinite)'
      WRITE(10,998) (E(I),D(I), I=1,LAYERS)
      CLOSE(UNIT=10)
  998 FORMAT(F10.6,',',F10.6,',',E15.6)
  999 FORMAT(A14)
      RETURN
      END
C************************END OF STORE*****************************************

C************************DIFFER***********************************************
C* NUMERICAL DIFFERENTIATION USING D04AAF
      SUBROUTINE DIFFER(FILENM)
      COMPLEX E(20),REFLEC
      REAL D(20),ANGLE(10000),DERIVR(10000),DERIVI(10000),NEF,PI,K0,
     $     MAX,MEASUR(10000),MIN,REFMAG(10000)
      DOUBLE PRECISION HBASE,DER(14),EREST(14),FUNR,FUNI,RVAL,IVAL,DVAL
      INTEGER LAYERS,POLA,M,I,IFAIL,ELAYER
      CHARACTER*14 FILENM
      COMMON /FITDAT/ M,ANGLE,MEASUR,DERIVR,DERIVI
      COMMON /NAGDAT/ E,D,LAYERS,POLA,NEF,ELAYER
      COMMON /CONSTS/ PI,K0
      EXTERNAL FUNR,FUNI

      WRITE(*,*) 'Which is the electrooptic layer?'
      READ(*,*) ELAYER
      IFAIL = 0
      RVAL = DBLE(REAL(E(ELAYER)))
      IVAL = DBLE(AIMAG(E(ELAYER)))
      DVAL = DBLE(D(ELAYER))

      WRITE(*,*) 'Calculating derivatives...'
      DO 10 I = 1,M
         WRITE(*,999) I
         HBASE = 1D-4
         NEF = REAL(SQRT(E(1))) * SIN(ANGLE(I) * PI/180)
         CALL D04AAF(RVAL,1,HBASE,DER,EREST,FUNR,IFAIL)
         DERIVR(I) = REAL(DER(1))
         CALL D04AAF(IVAL,1,HBASE,DER,EREST,FUNI,IFAIL)
         DERIVI(I) = REAL(DER(1))
  10  CONTINUE
      DO 20 I = 1,M
         NEF = REAL(SQRT(E(1))) * SIN(ANGLE(I) * PI/180)
         REFMAG(I) = ABS(REFLEC(E,D,LAYERS,POLA,NEF))
```

```
20  CONTINUE

    CALL PAPER(1)
    CALL PSPACE(0.1,0.9,0.1,0.9)
    CALL MAP(ANGLE(1),ANGLE(M),0.0,1.05)
    CALL WINDOW(ANGLE(1),ANGLE(M),0.0,1.05)
    CALL AXORIG(ANGLE(1),0)
    CALL AXES
    CALL POSITN(ANGLE(1),REFMAG(1))
    DO 30 I=2,M
       CALL JOIN(ANGLE(I),REFMAG(I))
30  CONTINUE
    CALL MAP(0.0,100.0,0.0,100.0)
    CALL CTRMAG(20)
    CALL PLOTCS(40.0,-10.0,'Incident Angle')
    CALL ANNOTA(E,D,LAYERS,POLA,FILENM)
    CALL FRAME

    MAX = DERIVR(1)
    MIN = DERIVR(1)
    IF(DERIVI(1).GT.MAX) MAX = DERIVI(1)
    IF(DERIVI(1).LT.MIN) MIN = DERIVI(1)
    DO 50 I = 1,M
       IF(DERIVR(I).LT.MIN) MIN = DERIVR(I)
       IF(DERIVR(I).GT.MAX) MAX = DERIVR(I)
       IF(DERIVI(I).LT.MIN) MIN = DERIVI(I)
       IF(DERIVI(I).GT.MAX) MAX = DERIVI(I)
50  CONTINUE

    CALL MAP(ANGLE(1),ANGLE(M),MIN,MAX)
    CALL WINDOW(ANGLE(1),ANGLE(M),MIN,MAX)
    CALL AXORIG(ANGLE(1),0)
    CALL AXES
    CALL POSITN(ANGLE(1),DERIVR(1))
    DO 80 I=2,M
       CALL JOIN(ANGLE(I),DERIVR(I))
80  CONTINUE
    CALL BROKEN(10,10,10,10)
    CALL POSITN(ANGLE(1),DERIVI(1))
    DO 90 I=2,M
       CALL JOIN(ANGLE(I),DERIVI(I))
90  CONTINUE
    CALL BROKEN(10,5,10,5)

    CALL FULL
    CALL MAP(0.0,100.0,0.0,100.0)
    CALL CTRMAG(20)
    CALL PLOTCS(40.0,-10.0,'Incident Angle')
    CALL CTRORI(90.0)
    CALL PLOTCS(-10.0,25.0,'Theoretical derivatives')
    CALL CTRORI(0.0)
```

```
      CALL ANNOTA(E,D,LAYERS,POLA,FILENM)
      CALL FRAME
  999 FORMAT('+[',I3,']')
      RETURN
      END
C**********************END OF DIFFER*****************************************

C***************************FUNR*************************************************
C* REAL FUNCTION TO DIFFERENTIATE FOR D04AAF
      DOUBLE PRECISION FUNCTION FUNR(X)
      DOUBLE PRECISION X
      COMPLEX E(20),REFLEC,TEMP
      REAL D(20),NEF
      INTEGER LAYERS,POLA,ELAYER
      COMMON /NAGDAT/ E,D,LAYERS,POLA,NEF,ELAYER
      TEMP = E(ELAYER)
      E(ELAYER) = REAL(X) + (0,1)*AIMAG(E(ELAYER))
      FUNR = DBLE(ABS(REFLEC(E,D,LAYERS,POLA,NEF)))
      E(ELAYER) = TEMP
      RETURN
      END
C***************************END OF FUNR*************************************

C*******************************FUNI*************************************************
C* IMAGINARY FUNCTION TO DIFFERENTIATE FOR D04AAF
      DOUBLE PRECISION FUNCTION FUNI(X)
      DOUBLE PRECISION X
      COMPLEX E(20),REFLEC,TEMP
      REAL D(20),NEF
      INTEGER LAYERS,POLA,ELAYER
      COMMON /NAGDAT/ E,D,LAYERS,POLA,NEF,ELAYER

      TEMP = E(ELAYER)
      E(ELAYER) = REAL(E(ELAYER)) + (0,1) * REAL(X)
      FUNI = DBLE(ABS(REFLEC(E,D,LAYERS,POLA,NEF)))
      E(ELAYER) = TEMP
      RETURN
      END
C***************************END OF FUNI*************************************

C***************************FIT*************************************************
      SUBROUTINE FIT(X)
      REAL X(3),FSUMSQ,FNOW,LENGTH,DX,MOVE,FNEXT,ERROR,
     $     ANGLE(10000),MEASUR(10000),DERIVR(10000),DERIVI(10000)
      INTEGER M,COUNT,ITER
      COMMON /FITDAT/ M,ANGLE,MEASUR,DERIVR,DERIVI

      ITER=10
      COUNT = 0
      WRITE(*,998) 'deltaE: Real,Imaginary','Average error'
  1   MOVE = 1E8
```

```
      X(1) = 0.0
      FNOW = FSUMSQ(X)
   10 X(1) = X(1) + MOVE
      FNEXT = FSUMSQ(X)
      IF(FNEXT.GT.FNOW) MOVE = - MOVE/10
      FNOW = FNEXT
      IF(ABS(MOVE).GT.1E-2) GOTO 10
      WRITE(*,999) X(1)/1E8,X(2)/1E8,SQRT(FNOW/M)
      MOVE = 1E8
      X(2) = 0.0
      FNOW = FSUMSQ(X)
   20 X(2) = X(2) + MOVE
      FNEXT = FSUMSQ(X)
      IF(FNEXT.GT.FNOW) MOVE = - MOVE/10
      FNOW = FNEXT
      IF(ABS(MOVE).GT.1E-2) GOTO 20
      WRITE(*,999) X(1)/1E8,X(2)/1E8,SQRT(FNOW/M)
      COUNT = COUNT + 1
      IF(COUNT.LT.ITER) GOTO 1
C FIT OFFSET ON PSD
      MOVE = 1E-3
      X(3) = 0.0
      FNOW = FSUMSQ(X)
   30 X(3) = X(3) +MOVE
      FNEXT = FSUMSQ(X)
      IF(FNEXT.GT.FNOW) MOVE = - MOVE/10
      FNOW = FNEXT
      IF(ABS(MOVE).GT.1E-10) GOTO 30
      WRITE(*,*) 'Fitting complete'
  998 FORMAT(A30,A19)
  999 FORMAT(E15.4,E15.4,E15.4)
      RETURN
      END
C************************END OF FIT*****************************************

C************************FSUMSQ*********************************************
C* CALCULATES SUM OF SQUARES OF ERRORS
      REAL FUNCTION FSUMSQ(X)
      INTEGER M
      REAL ERROR,ANGLE(10000),MEASUR(10000),X(3),F,DERIVR(10000),
     $     DERIVI(10000),DELER,DELEI,OFFSET
      COMMON /FITDAT/ M,ANGLE,MEASUR,DERIVR,DERIVI

      F = 0
      DELER = X(1)/1E8
      DELEI = X(2)/1E8
      OFFSET = X(3)
      DO 10 I = 1,M
         ERROR = DELER*DERIVR(I) + DELEI*DERIVI(I) - MEASUR(I) + OFFSET
         F = F + ERROR * ERROR
   10 CONTINUE
```

```
      FSUMSQ = F
      RETURN
      END
C**********************END OF FSUMSQ*****************************************

C*************************CURVES*********************************************
C REFLECTION VERSUS ANGLE RESULTS
      SUBROUTINE CURVES(DELER,DELEI,OFFSET,FILENM)

      COMPLEX E(20)
      REAL    ANGLE(10000),MEASUR(10000),ERROR(10000),DERIVR(10000),
     $        DERIVI(10000),THEORY(10000),DELER,DELEI,MAX,MIN,NEF,
     $        D(20),OFFSET
      INTEGER M,LAYERS,POLA,ELAYER
      CHARACTER*14 FILENM
      COMMON /FITDAT/ M,ANGLE,MEASUR,DERIVR,DERIVI
      COMMON /NAGDAT/ E,D,LAYERS,POLA,NEF,ELAYER

      DO 10 I = 1,M
         THEORY(I) = DELER*DERIVR(I) + DELEI*DERIVI(I)
         MEASUR(I) = MEASUR(I)- OFFSET
 10   CONTINUE

      MIN = 0
      MAX = 0
      DO 15 I = 1,M
         IF(THEORY(I).LT.MIN) MIN = THEORY(I)
         IF(MEASUR(I).LT.MIN) MIN = MEASUR(I)
         IF(MEASUR(I).GT.MAX) MAX = MEASUR(I)
         IF(THEORY(I).GT.MAX) MAX = THEORY(I)
 15   CONTINUE

      CALL PSPACE(0.1,0.9,0.1,0.9)
      CALL MAP(ANGLE(1),ANGLE(M),MIN,MAX)
      CALL WINDOW(ANGLE(1),ANGLE(M),MIN,MAX)
      CALL AXORIG(ANGLE(1),MIN)
      CALL AXES
      CALL POSITN(ANGLE(1),THEORY(1))
      DO 20 I=2,M
         CALL JOIN(ANGLE(I),THEORY(I))
 20   CONTINUE
      DO 30 I=1,M
         CALL PLOTNC(ANGLE(I),MEASUR(I),248)
 30   CONTINUE
      CALL MAP(0.0,100.0,0.0,100.0)
      CALL CTRMAG(20)
      CALL PLOTCS(40.0,-10.0,'Incident Angle')
      CALL CTRMAG(30)
      CALL CTRFNT(2)
      CALL PLOTNC(-10.0,55.0,68)
      CALL CTRFNT(1)
```

```
      CALL PLOTNC(-7.0,55.0,82)
      CALL CTRMAG(20)
      CALL ANNOTB(DELER,DELEI,FILENM)
      CALL FRAME
      DO 40 I=1,M
         ERROR(I) = THEORY(I) - MEASUR(I)
   40 CONTINUE
      MIN = 0
      MAX = 0
      DO 45 I = 1,M
         IF(ERROR(I).LT.MIN) MIN = ERROR(I)
         IF(ERROR(I).GT.MAX) MAX = ERROR(I)
   45 CONTINUE
      CALL PSPACE(0.1,0.9,0.1,0.9)
      CALL MAP(ANGLE(1),ANGLE(M),MIN,MAX)
      CALL WINDOW(ANGLE(1),ANGLE(M),MIN,MAX)
      CALL AXORIG(ANGLE(1),MIN)
      CALL AXES
      CALL POSITN(ANGLE(1),ERROR(1))
      DO 50 I=2,M
         CALL JOIN(ANGLE(I),ERROR(I))
   50 CONTINUE
      CALL MAP(0.0,100.0,0.0,100.0)
      CALL CTRMAG(20)
      CALL PLOTCS(40.0,-10.0,'Incident Angle')
      CALL CTRORI(90.0)
      CALL PLOTCS(-10.0,10.0,'Deviation: Theory - Experiment')
      CALL CTRORI(0.0)
      CALL ANNOTB(DELER,DELEI,FILENM)
      CALL GREND
      RETURN
      END
C*************************END OF CURVES*****************************************

C*************************ANNOTA************************************************
C* ANNOTATES GRAPHS
      SUBROUTINE ANNOTA(E,D,LAYERS,POLA,FILENM)
      COMPLEX E(20)
      REAL D(20)
      INTEGER LAYERS,POLA
      CHARACTER*14 FILENM
      CALL CSPACE(0.0,1.0,0.0,1.0)
      CALL CTRMAG(12)
      CALL PLACE(52,1)
      IF(POLA.EQ.1) CALL TYPECS('TM Pol. ')
      IF(POLA.EQ.0) CALL TYPECS('TE Pol. ')
      CALL PLACE(61,1)
      CALL TYPECS(FILENM)

      CALL PLACE(50,2)
      CALL TYPECS('Layer     Permittivity   Thickness/m')
```

```
      DO 10 I=1,LAYERS
         CALL PLACE(51,2+I)
         CALL TYPENI(I)
         CALL PLACE(57,2+I)
         CALL TYPENF(REAL(E(I)),4)
         CALL PLACE(65,2+I)
         CALL TYPECS('+')
         CALL PLACE(65,2+I)
         CALL TYPENF(AIMAG(E(I)),4)
         CALL PLACE(72,2+I)
         CALL TYPECS('i')
         CALL PLACE(75,2+I)
         CALL TYPENE(D(I),4)
   10  CONTINUE
       CALL CSPACE(0.0,0.0,0.0,0.0)
       RETURN
       END
C*************************END OF ANNOTA*************************************

C*************************ANNOTB*******************************************
C* ANNOTATES OTHER GRAPHS
       SUBROUTINE ANNOTB(DELER,DELEI,FILENM)
       REAL DELER,DELEI
       CHARACTER*14 FILENM
       CALL CSPACE(0.0,1.0,0.0,1.0)
       CALL CTRMAG(12)

       CALL PLACE(50,2)
       CALL TYPECS(FILENM)
       CALL PLACE(50,3)
       CALL CTRFNT(2)
       CALL TYPECS('De =')
       CALL PLACE(55,3)
       CALL CTRFNT(1)
       CALL TYPENE(DELER,4)
       CALL PLACE(67,3)
       IF(DELEI.GE.0.0) CALL TYPECS('+')
       CALL PLACE(68,3)
       CALL TYPENE(DELEI,4)
       CALL PLACE(79,3)
       CALL TYPECS('i')
   10  CONTINUE
       CALL CSPACE(0.0,0.0,0.0,0.0)
       RETURN
       END
C*************************END OF ANNOTB*************************************

C*************************REFLEC*******************************************
C****** CALCULATES THE INTENSITY REFLECTION COEFFICIENT OF STRUCTURE
       COMPLEX FUNCTION REFLEC(E,D,LAYERS,POLA,NEF)
```

```
      COMPLEX E(20),MATRIX(40,40),VECTOR(40),RESULT(40)
      REAL D(20),K0,NEF,PI
      INTEGER LAYERS,POLA
      COMMON /CONSTS/ PI,K0

      CALL MAKEQN(NEF,E,D,LAYERS,MATRIX,VECTOR,POLA)
      CALL GAUSSE(MATRIX,2*LAYERS-2,VECTOR,RESULT)
C SQUARE TO CONVERT FROM FIELD TO AMPLITUDE
      REFLEC = RESULT(1) * RESULT(1)

      RETURN
      END
C************************END OF REFLEC*************************************

C*************************MAKEQN*****************************************
C GENERATES THE SIMULTANEOUS EQUATIONS IN MATRIX FORM
C
      SUBROUTINE MAKEQN(NEF,E,D,LAYERS,MATRIX,VECTOR,POLA)


      REAL NEF,D(20),K0,PI
      COMPLEX K(20),MATRIX(40,40),A,B,E(20),VECTOR(40)
      INTEGER LAYERS,I,J,POLA
      COMMON /CONSTS/ PI,K0
      DO 2 I=1,40
         VECTOR(I)=0.0
         DO 1 J=1,40
            MATRIX(I,J) = 0.0
    1    CONTINUE
    2 CONTINUE

      DO 5 I=1,LAYERS
         IF(NEF.NE.SQRT(E(I))) THEN
            K(I)=K0*CSQRT(E(I)-CMPLX(NEF*NEF))
                        ELSE
            K(I)=0
         END IF
    5 CONTINUE

      IF(LAYERS.GT.2) THEN
C FIELD CONTINUITY AT E1:E2 - THIS IS AT DEPTH=0
         VECTOR(1) = -1
         MATRIX(1,1) = 1
         MATRIX(1,2) = -1
         MATRIX(1,3) = -1
C FIELD CONTINUITY AT OTHER BOUNDARIES EXCLUDING LAST ONE
         DO 10 I=2,LAYERS-2
            A=EXP(K(I)*(0,1)*D(I))
            J=2*I
            MATRIX(J-1,J-2) = A
            MATRIX(J-1,J-1) = 1/A
```

```
            MATRIX(J-1,J) = -1
            MATRIX(J-1,J+1) = -1
   10     CONTINUE
C FIELD CONTINUITY AT LAST BOUNDARY
          A=EXP(K(LAYERS-1)*(0,1)*D(LAYERS-1))
          J=2*(LAYERS-1)
          MATRIX(J-1,J-2)=A
          MATRIX(J-1,J-1)=1/A
          MATRIX(J-1,J)=1
          IF(POLA.EQ.0) THEN
C TE CONDITIONS - GRADIENT CONTINUITY
            VECTOR(2)=-K(1)
            MATRIX(2,1)=-K(1)
            MATRIX(2,2)=-K(2)
            MATRIX(2,3)=K(2)
            DO 20 I=2,LAYERS-2
               A = EXP(K(I)*(0,1)*D(I))
               J = 2*I
               MATRIX(J,J-2) = A*K(I)
               MATRIX(J,J-1) = -K(I)/A
               MATRIX(J,J) = -K(I+1)
               MATRIX(J,J+1) = K(I+1)
   20       CONTINUE
            A = EXP(K(LAYERS-1)*(0,1)*D(LAYERS-1))
            J = 2*(LAYERS-1)
            MATRIX(J,J-2)=K(LAYERS-1)*A
            MATRIX(J,J-1)=-K(LAYERS-1)/A
            MATRIX(J,J)=K(LAYERS)
          ELSE
C TM CONDITIONS - INTEGRAL FIELD * PERMITTIVITY CONTINUITY
            VECTOR(2)=-E(1)/K(1)
            MATRIX(2,1)=-E(1)/K(1)
            MATRIX(2,2)=-E(2)/K(2)
            MATRIX(2,3)=E(2)/K(2)
            DO 30 I=2,LAYERS-2
               A = EXP(K(I)*(0,1)*D(I))
               J = 2*I
               MATRIX(J,J-2) = A*E(I)/K(I)
               MATRIX(J,J-1) = -E(I)/(K(I)*A)
               MATRIX(J,J) = -E(I+1)/K(I+1)
               MATRIX(J,J+1) = E(I+1)/K(I+1)
   30       CONTINUE
            A = EXP(K(LAYERS-1)*(0,1)*D(LAYERS-1))
            J = 2*(LAYERS-1)
            MATRIX(J,J-2)=E(LAYERS-1)*A/K(LAYERS-1)
            MATRIX(J,J-1)=-E(LAYERS-1)/(K(LAYERS-1)*A)
            MATRIX(J,J)=E(LAYERS)/K(LAYERS)
          ENDIF

       ELSE
C SINGLE INTERFACE CASE
```

```
            VECTOR(1) = -1
            MATRIX(1,1) = 1
            MATRIX(1,2) = -1
            IF(POLA.EQ.0) THEN
               VECTOR(2) = -K(1)
               MATRIX(2,1) = -K(1)
               MATRIX(2,2) = -K(2)
            ELSE
               VECTOR(2) = -E(1)/K(1)
               MATRIX(2,1) = -E(1)/K(1)
               MATRIX(2,2) = -E(2)/K(2)
            ENDIF
         ENDIF
         RETURN
         END
C******************END OF MAKEQN*********************************************

C ***************************GAUSSELIM*************************************
C SOLVES SIMULTANEOUS EQUATIONS A.Y=X WHERE A IS AN NxN MATRIX
C RESULT CONTAINS ANSWERS
         SUBROUTINE GAUSSE(A,M,V,RESULT)

         INTEGER M,SWAP,I,J,R,Y
         COMPLEX A(40,40),V(40),RESULT(40),FACTOR,TEMP

         DO 60 R=1,M-1
C CHECKS FOR ZERO PIVOT
            SWAP=R
   10       IF(A(SWAP,SWAP).NE.0) THEN
               GOTO 30
                                 ELSE
               SWAP=SWAP+1
               IF(SWAP.EQ.M) THEN
                  PRINT *,'No solutions.'
                  STOP
               ENDIF
               GOTO 10
            ENDIF

C ROW SWAP - ONLY SWAPS NON ZERO PARTS OF COURSE
            IF(R.NE.SWAP) THEN
               DO 20 Y=R,M
                  TEMP=A(SWAP,Y)
                  A(SWAP,Y)=A(R,Y)
                  A(R,Y)=TEMP
   20          CONTINUE
               TEMP=V(SWAP)
               V(SWAP)=V(R)
               V(R)=TEMP
            ENDIF
```

```
   30      DO 50 I=R+1,M
              FACTOR=A(I,R)/A(R,R)
              A(I,R)=0
              DO 40 J=R+1,M
                 A(I,J)=A(I,J)-FACTOR*A(R,J)
   40         CONTINUE
              V(I)=V(I)-FACTOR*V(R)
   50      CONTINUE
   60   CONTINUE
C NOW MATRIX IS TRIANGULAR - CAN SUBSTITUTE BACKFOR RESULTS
        RESULT(M)=V(M)/A(M,M)
        DO 80 I=M-1,1,-1
           RESULT(I)=V(I)
           DO 70 J=M,I+1,-1
              RESULT(I)=RESULT(I)-RESULT(J)*A(I,J)
   70      CONTINUE
           RESULT(I)=RESULT(I)/A(I,I)
   80   CONTINUE

        RETURN
        END
```

4. Waveguide mode detection program

```
C SEARCHES FOR MODES IN AN N LAYER STRUCTURE
C FOR VALID NEF (EFFECTIVE INDEX) THE DETERMINANT IS ZERO
C ALSO THE SIGN OF THE IMAGINARY PART OF DETERMINANT CHANGES AT EACH MODE
C THE VALID NEF FOUND BY LOOKING FOR THIS SIGN CHANGE
C

        PROGRAM NLAYER
        COMPLEX MATRIX(40,40),E(20),VECTOR(40)
        REAL KO,D(20),PI,LAMDA
        INTEGER LAYERS,POLA,ANS

        COMMON /CONSTS/ PI,KO

        PI = 3.1415927
        LAYERS = 0
        CALL PAPER(1)
   10   WRITE(*,*) 'Main menu'
        WRITE(*,*) '0=Exit program'
        WRITE(*,*) '1=Load data file'
        WRITE(*,*) '2=Change data'
```

```
      WRITE(*,*) '3=Find effective indices'
      READ(*,*) ANS

      IF(ANS.EQ.1) THEN
         CALL LYDATA(E,D,LAYERS,POLA,LAMDA)
         CALL SHOW(E,D,LAYERS,POLA,LAMDA,5)
         CALL SHOW(E,D,LAYERS,POLA,LAMDA,7)
         K0 = 2*PI/LAMDA
      ENDIF
      IF(LAYERS.NE.0) THEN
         IF(ANS.EQ.2) THEN
            CALL CHANGE(E,D,LAYERS,POLA,LAMDA)
            CALL SHOW(E,D,LAYERS,POLA,LAMDA,5)
            CALL SHOW(E,D,LAYERS,POLA,LAMDA,7)
            K0 = 2*PI/LAMDA
         ENDIF
         IF(ANS.EQ.3) CALL MODES(E,D,LAYERS,POLA,LAMDA)
      ELSE
         WRITE(*,*) 'No data loaded'
      ENDIF
      IF(ANS.NE.0) GOTO 10
      CALL GREND
      STOP
      END
C ******************************END OF MAIN*************************************

C ********************************MODES*****************************************
C SEARCHES FOR DETERMINANT IMAGINARY PART SIGN CHANGE
      SUBROUTINE MODES(E,D,LAYERS,POLA,LAMDA)

      COMPLEX E(20),MATRIX(40,40),VECTOR(40)
      REAL D(20),LAMDA,NMAX,NMIN,NEF,NESTEP
      INTEGER POLA,LAYERS,I,SIGN,LSTSIG,DETSIG,VALID

      IF(POLA.EQ.0) THEN
         WRITE(7,*) 'TE Modes'
         WRITE(*,*) 'TE Modes'
      ELSE
         WRITE(*,*) 'TM Modes'
         WRITE(7,*) 'TM Modes'
      ENDIF
      NMIN = SQRT(REAL(E(1)))
      IF(SQRT(REAL(E(LAYERS))).LT.NMIN) NMIN = SQRT(REAL(E(LAYERS)))
      NMAX = SQRT(REAL(E(2)))
      DO 10 I = 2,LAYERS-1
         IF(SQRT(REAL(E(I))).GT.NMAX) NMAX = SQRT(REAL(E(I)))
 10   CONTINUE
      NESTEP=(NMAX-NMIN)/100
      NEF=NMIN+0.000001

      WRITE(*,*) 'Searching for modes between ',NMIN,' and ',NMAX
```

```
   20    IF(NEF.LE.NMAX) THEN
            CALL MAKEQN(NEF,E,D,LAYERS,MATRIX,VECTOR,POLA)
            SIGN=DETSIG(MATRIX,2*LAYERS-2)
            LSTSIG=SIGN

   30       IF(ABS(NESTEP).GT.1E-6) THEN
   40          IF(SIGN.EQ.LSTSIG.AND.NEF.LE.NMAX) THEN
                  NEF=NEF+NESTEP
                  CALL MAKEQN(NEF,E,D,LAYERS,MATRIX,VECTOR,POLA)
                  SIGN=DETSIG(MATRIX,2*LAYERS-2)
                  GOTO 40
               ENDIF
               LSTSIG=SIGN
               NESTEP=-NESTEP/10
               GOTO 30
            ENDIF

C CHECK VALIDITY OF EFFECTIVE INDEX
            IF(VALID(E,NEF,LAYERS).EQ.1.AND.NEF.LT.NMAX) THEN
               IF(MINCHK(E,D,NEF,LAYERS).EQ.1) THEN
                  WRITE(7,*) ' Mode at Neff=', NEF
                  WRITE(*,*) ' Mode at Neff=', NEF
               ELSE
                  WRITE(7,*) ' Phase zero at Neff=', NEF
                  WRITE(*,*) ' Phase zero at Neff=', NEF
               ENDIF
               IF(POLA.EQ.0) CALL TEPROF(E,D,LAYERS,1,NEF)
               IF(POLA.EQ.1) CALL TMPROF(E,D,LAYERS,1,NEF)
            ENDIF
            NESTEP=(NMAX-NMIN)/100
            NEF=NEF+NESTEP
            GOTO 20
         ENDIF
         RETURN
         END
C ************************END OF MODES*****************************************

C *********************************DETSIGN*************************************
C EVALUATES SIGN OF IMAGINARY PART OF DETERMINANT
C - RETURNS 1 IF +VE, -1 IF -VE

         INTEGER FUNCTION DETSIG(A,N)

         INTEGER N
         COMPLEX A(40,40),DET
         REAL IDET

         IDET=IMAG(DET(A,N))

         IF(IDET.EQ.ABS(IDET)) THEN
            DETSIG=1
```

```
                              ELSE
         DETSIG=-1
       ENDIF
       RETURN
       END
C ****************************END OF DETSIGN ***********************************

C ****************************DET***********************************************
C EVALUATES DETERMINANT
       COMPLEX FUNCTION DET(A,M)

       INTEGER M,SWAP,SSIGN,I,J,R,Y
       COMPLEX A(40,40),PROD,FACTOR,TEMP

       SSIGN=1
       PROD=1

       DO 35 R=1,M-1
          SWAP=R
   10     IF(A(SWAP,R).NE.0) THEN
             GOTO 30
                              ELSE
             SWAP=SWAP+1
             IF(SWAP.EQ.M+1) THEN
                DET=0
                GOTO 60
             ENDIF
             GOTO 10
          ENDIF

C ROW SWAP - ONLY SWAPS NON ZERO PARTS OF COURSE
          IF(R.NE.SWAP) THEN
             DO 20 Y=R,M
                TEMP=A(SWAP,Y)
                A(SWAP,Y)=A(R,Y)
                A(R,Y)=TEMP
   20        CONTINUE
C ROW SWAP LEADS TO SIGN SWAP
             SSIGN=-SSIGN
          ENDIF


   30     DO 34 I=R+1,M
             FACTOR=A(I,R)/A(R,R)
             A(I,R)=0
             DO 33 J=R+1,M
                A(I,J)=A(I,J)-FACTOR*A(R,J)
   33        CONTINUE
   34     CONTINUE
   35  CONTINUE
```

```
   40  DO 50 I=1,M
          PROD=PROD*A(I,I)
   50  CONTINUE
       DET=PROD*SSIGN

   60  RETURN
       END
C ***************************END OF DET*****************************************

C***************************LYDATA*****************************************
C GATHERS DATA FOR LAYERS
       SUBROUTINE LYDATA(E,D,LAYERS,POLA,LAMDA)

       COMPLEX      E(20)
       REAL         D(20),LAMDA
       INTEGER      LAYERS,POLA
       CHARACTER*14 FILENM
       CHARACTER*80 TRASH

       WRITE(*,*) 'Filename for input'
       READ(*,999) FILENM
       OPEN(UNIT=10,FILE=FILENM,STATUS='OLD')
       REWIND(10)
       READ(10,'(A80)') TRASH
       READ(10,*) POLA
       READ(10,'(A80)') TRASH
       READ(10,*) LAMDA
       READ(10,'(A80)') TRASH
       READ(10,*) LAYERS
       READ(10,'(A80)') TRASH
       READ(10,*) (E(I),D(I), I=1,LAYERS)
       CLOSE(UNIT=10)
  999  FORMAT(A14)
       RETURN
       END
C************************END OF LYDATA*************************************

C*****************************SHOW*****************************************
C WRITES CURRENT DATA TO UNIT=WHERE
       SUBROUTINE SHOW(E,D,LAYERS,POLA,LAMDA,WHERE)
       COMPLEX E(20)
       REAL D(20),LAMDA
       INTEGER LAYERS,POLA,WHERE

       IF(POLA.EQ.0) WRITE(WHERE,*) 'TE Polarisation'
       IF(POLA.EQ.1) WRITE(WHERE,*) 'TM Polarisation'
       WRITE(WHERE,*) 'Wavelength =',LAMDA
       WRITE(WHERE,998) 'Layer','Permittivity','Depth'
       WRITE(WHERE,999) 1,E(1),0.0
       WRITE(WHERE,999) (I,E(I),D(I), I=2,LAYERS-1)
       WRITE(WHERE,999) LAYERS,E(LAYERS),0.0
```

```
  998  FORMAT(A5,A20,A10)
  999  FORMAT(I5,F14.4,',',F8.4,E15.6)
       RETURN
       END
C*************************END OF SHOW*************************************

C*************************CHANGE******************************************
C CHANGES DATA
       SUBROUTINE CHANGE(E,D,LAYERS,POLA,LAMDA)
       COMPLEX E(20)
       REAL D(20),LAMDA
       INTEGER L,ANS,LAYERS,POLA

   10  WRITE(*,*) 'CHANGE PARAMETERS MENU'
       WRITE(*,*) '0=Return to main menu'
       WRITE(*,*) '1=Toggle Polarisation'
       WRITE(*,*) '2=Change Wavelength'
       WRITE(*,*) '3=Change Permittivity'
       WRITE(*,*) '4=Change Thickness'
       WRITE(*,*) '5=Show current parameters'
       WRITE(*,*) '6=Store new data in a file'
       READ(*,*) ANS
       IF(ANS.EQ.1) POLA=1-POLA
       IF(ANS.EQ.2) THEN
          WRITE(*,*) 'New Wavelength/m'
          READ(*,*) LAMDA
       ENDIF
       IF(ANS.EQ.3) THEN
          WRITE(*,*) 'Layer to change'
          READ(*,*) L
          WRITE(*,*) 'New Permittivity (real,imag)'
          READ(*,*) E(L)
       ENDIF
       IF(ANS.EQ.4) THEN
          WRITE(*,*) 'Layer to change'
          READ(*,*) L
          WRITE(*,*) 'New Thickness/m'
          READ(*,*) D(L)
       ENDIF
       IF(ANS.EQ.5) CALL SHOW(E,D,LAYERS,POLA,LAMDA,5)
       IF(ANS.EQ.6) CALL STORE(E,D,LAYERS,POLA,LAMDA)
       IF(ANS.EQ.0) GOTO 15
       GOTO 10
   15  RETURN
       END
C************************END OF CHANGE************************************

C*************************STORE*******************************************
C WRITES LAYER DATA TO A FILE
       SUBROUTINE STORE(E,D,LAYERS,POLA,LAMDA)
       COMPLEX E(20)
```

```
      REAL D(20),LAMDA
      INTEGER LAYERS,POLA
      CHARACTER*14 FILENM

      WRITE(*,*) 'Filename for output'
      READ(*,999) FILENM
      OPEN(UNIT=10,FILE=FILENM,STATUS='UNKNOWN')
      REWIND(10)
      WRITE(10,*) 'Polarisation 1=TM 0=TE'
      WRITE(10,'(I1)') POLA
      WRITE(10,*) 'Wavelength/m'
      WRITE(10,'(E15.6)') LAMDA
      WRITE(10,*) 'Number of layers'
      WRITE(10,'(I2)') LAYERS
      WRITE(10,*) 'Real(e),Im(e),depth (0=semi infinite)'
      WRITE(10,998) (E(I),D(I), I=1,LAYERS)
      CLOSE(UNIT=10)
  998 FORMAT(F10.6,',',F10.6,',',E15.6)
  999 FORMAT(A14)
      RETURN
      END
C************************END OF STORE*************************************


C************************VALID*******************************************
C CHECKS TO SEE WHETHER NEF DEFINES CONFINED MODE
      INTEGER FUNCTION VALID(E,NEF,LAYERS)

      COMPLEX E(20)
      REAL    NEF
      INTEGER CONF1,CONF2

      VALID=0
C FINDS FIRST LAYER WITH EXPONENTIAL FIELD PROFILE COUNTING UP FROM FIRST
      CONF1=1
   10 IF(NEF*NEF.GT.REAL(E(CONF1))) GOTO 20
      IF(CONF1.LT.LAYERS) THEN
         CONF1=CONF1+1
         GOTO 10
      ENDIF
   20 CONF2=LAYERS
C FINDS FIRST LAYER WITH EXPONENTIAL FIELD PROFILE COUNTING DOWN FROM LAST
   30 IF(NEF*NEF.GT.REAL(E(CONF2))) GOTO 40
      IF(CONF2.GT.1) THEN
         CONF2=CONF2-1
         GOTO 30
      ENDIF
   40 IF(CONF2.GT.CONF1) VALID=1
      RETURN
      END
C************************ END OF VALID ***********************************
```

```
C*************************MINCHK*****************************************
C* CHECKS FOR DETERMINANT MINIMUM - RETURNS 1 IF TRUE
       INTEGER FUNCTION MINCHK(E,D,NEF,LAYERS)

       COMPLEX E(20),MATRIX(40,40),VECTOR(40),DET
       REAL D(20),NEF,DETM,DET1,DET2
       INTEGER LAYERS

       CALL MAKEQN(NEF,E,D,LAYERS,MATRIX,VECTOR,1)
       DETM = ABS(DET(MATRIX,2*LAYERS-2))
       NEF = NEF + 0.000001
       CALL MAKEQN(NEF,E,D,LAYERS,MATRIX,VECTOR,1)
       DET1 = ABS(DET(MATRIX,2*LAYERS-2))
       NEF = NEF - 0.000002
       CALL MAKEQN(NEF,E,D,LAYERS,MATRIX,VECTOR,1)
       DET2 = ABS(DET(MATRIX,2*LAYERS-2))

       MINCHK = 0
       IF(DETM.LT.DET1.AND.DETM.LT.DET2) MINCHK = 1
       RETURN
       END
C*********************END OF MINCHK*************************************

C*************************TMPROF*****************************************
C CALCULATES FIELD PROFILES FOR TM CASE
       SUBROUTINE TMPROF(E,D,LAYERS,LFLAG,NEF)

       COMPLEX E(20),MATRIX(40,40),VECTOR(40),RESULT(40),K(20),
     $      FIELD1(2000),FIELD2(2000),A,EZ(2000),HY(2000)
       REAL D(20),ANGLE,NEF,PI,K0,DTOTAL,X(2000),SX(2000),SZ(2000)
       INTEGER LAYERS,I,J,T,LFLAG
       COMMON /CONSTS/ PI,K0

       CALL MAKEQN(NEF,E,D,LAYERS,MATRIX,VECTOR,1)
       CALL GAUSSE(MATRIX,2*LAYERS-2,VECTOR,RESULT)
       DTOTAL = 0
       DO 10 I=1,LAYERS
          K(I)=K0*CSQRT(E(I)-CMPLX(NEF*NEF))
          DTOTAL = DTOTAL + D(I)
   10  CONTINUE
       IF(DTOTAL.EQ.0.0) DTOTAL = 1E-6
C GET FIELD PROFILES FOR FIRST LAYER
       DO 20 J=1,100
          X(J) = -DTOTAL + J*DTOTAL/100
          A = EXP(K(1)*(0,1)*X(J))
          FIELD1(J) = RESULT(1)/A
          FIELD2(J) = - E(1)/K(1) * RESULT(1)/A
   20  CONTINUE
C GET FIELD PROFILES FOR INSIDE LAYERS
       DO 40 I=2,LAYERS-1
```

```
            DO 30 J=1,100
               T = I*100 - 100 + J
               X(T) = X(T-J) + J*D(I)/100
               A = EXP(K(I)*(0,1)*J*D(I)/100)
               FIELD1(T) = A*RESULT(I*2-2) + RESULT(I*2-1)/A
               FIELD2(T) = E(I)/K(I)*(A*RESULT(I*2-2)-RESULT(I*2-1)/A)
   30       CONTINUE
   40    CONTINUE
C GET FIELD PROFILES FOR LAST LAYER
         DO 50 J=1,100
            T = LAYERS*100 - 100 + J
            X(T) = X(T-J) + J*DTOTAL/100
            A = EXP(K(LAYERS)*(0,1)*J*DTOTAL/100)
            FIELD1(T) = RESULT(LAYERS*2-2)*A
            FIELD2(T) = E(LAYERS)/K(LAYERS)*RESULT(2*LAYERS-2)*A
   50    CONTINUE
         DO 60 I = 1,LAYERS*100
            EZ(I) = FIELD1(I)
            HY(I) = FIELD2(I)
C           EX = (0,1)*K0*NEF*FIELD2
            SZ(I) = REAL(K0*NEF*FIELD2(I)*CONJG(FIELD2(I)))
            SX(I) = REAL(FIELD1(I)*CONJG(FIELD1(I)))
   60    CONTINUE

C        CALL PROFIL(X,EZ,DTOTAL,LAYERS,'Ez',E,D,1,LFLAG,NEF)
         CALL PROFIL(X,HY,DTOTAL,LAYERS,'Hy',E,D,1,LFLAG,NEF)

C        CALL POYNT(X,SZ,SX,DTOTAL,LAYERS,E,D,1,LFLAG,NEF)
         RETURN
         END
C************************END OF TMPROF*************************************

C*************************TEPROF*******************************************
C CALCULATES FIELD PROFILES FOR TE CASE
         SUBROUTINE TEPROF(E,D,LAYERS,LFLAG,NEF)

         COMPLEX E(20),MATRIX(40,40),VECTOR(40),RESULT(40),K(20),
     $        FIELD1(2000),FIELD2(2000),A,EY(2000),HZ(2000)
         REAL D(20),NEF,PI,K0,DTOTAL,X(2000),SX(2000),SZ(2000)
         INTEGER LAYERS,I,J,T,LFLAG
         COMMON /CONSTS/ PI,K0

         CALL MAKEQN(NEF,E,D,LAYERS,MATRIX,VECTOR,0)
         CALL GAUSSE(MATRIX,2*LAYERS-2,VECTOR,RESULT)
         DTOTAL = 0
         DO 10 I=1,LAYERS
            K(I)=K0*CSQRT(E(I)-CMPLX(NEF*NEF))
            DTOTAL = DTOTAL + D(I)
   10    CONTINUE
         IF(DTOTAL.EQ.0.0) DTOTAL = 1E-6
C GET FIELD PROFILE FOR FIRST LAYER
```

```
      DO 20 J=1,100
         X(J) = -DTOTAL + J*DTOTAL/100
         A = EXP(K(1)*(0,1)*X(J))
         FIELD1(J) = RESULT(1)/A
         FIELD2(J) = - K(1) * RESULT(1)/A
   20 CONTINUE
C GET FIELD PROFILES FOR INSIDE LAYERS
      DO 40 I=2,LAYERS-1
         DO 30 J=1,100
            T = I*100 - 100 + J
            X(T) = X(T-J) + J*D(I)/100
            A = EXP(K(I)*(0,1)*J*D(I)/100)
            FIELD1(T) = A*RESULT(I*2-2) + RESULT(I*2-1)/A
            FIELD2(T) = K(I) * (A*RESULT(I*2-2) - RESULT(I*2-1)/A)
   30    CONTINUE
   40 CONTINUE
C GET FIELD PROFILES FOR LAST LAYER
      DO 50 J=1,100
         T = LAYERS*100 - 100 + J
         X(T) = X(T-J) + J*DTOTAL/100
         A = EXP(K(LAYERS)*(0,1)*J*DTOTAL/100)
         FIELD1(T) = RESULT(LAYERS*2-2)*A
         FIELD2(T) = K(LAYERS)*RESULT(2*LAYERS-2)*A
   50 CONTINUE

      DO 60 I=1,LAYERS*100
         EY(I) = FIELD1(I)
         HZ(I) = (0,1)*FIELD2(I)
C        HX = K0*NEF*FIELD1
         SZ(I) = REAL(K0*NEF*FIELD1(I)*CONJG(FIELD1(I)))
         SX(I) = REAL(FIELD1(I)*CONJG((0,1)*FIELD2(I)))
   60 CONTINUE

      CALL PROFIL(X,EY,DTOTAL,LAYERS,'Ey',E,D,0,LFLAG,NEF)
C     CALL PROFIL(X,HZ,DTOTAL,LAYERS,'Hz',E,D,0,LFLAG,NEF)

C     CALL POYNT(X,SZ,SX,DTOTAL,LAYERS,E,D,0,LFLAG,NEF)
      RETURN
      END
C************************END OF TEPROF*************************************

C*************************PROFIL*****************************************
C* PLOTS FIELD PROFILES
      SUBROUTINE PROFIL(X,FIELD,DTOTAL,LAYERS,LABEL,E,D,POLA,LFLAG,NEF)
      COMPLEX FIELD(2000),E(20)
      REAL X(2000),AFIELD(2000),RFIELD(2000),DTOTAL,SCALE,D(20),NEF
      INTEGER I,LAYERS,POLA,LFLAG
      CHARACTER*2 LABEL

      DO 10 I=1,100*LAYERS
C        AFIELD(I) = ABS(FIELD(I))
```

```
         RFIELD(I) = REAL(FIELD(I))
   10  CONTINUE
       SCALE = ABS(RFIELD(1))
       DO 20 I=2,LAYERS*100
          IF (ABS(RFIELD(I)).GT.SCALE) SCALE=ABS(RFIELD(I))
   20  CONTINUE
       IF (RFIELD(1).LT.0.0) THEN
          DO 25 I=1,LAYERS*100
             RFIELD(I) = - RFIELD(I)
   25     CONTINUE
       ENDIF

       CALL PSPACE(0.1,0.9,0.1,0.8)
       CALL MAP(-DTOTAL,2*DTOTAL,-SCALE,SCALE)
       CALL WINDOW(-DTOTAL,2*DTOTAL,-SCALE,SCALE)
       CALL AXORIG(-DTOTAL,0.0)
       CALL CTRMAG(12)
       CALL AXNOTA(0)
       CALL YAXISI(0.0)
       CALL AXNOTA(1)
       CALL XAXISI(0.0)
       CALL BROKEN(1,10,1,10)
       DO 30 I=1,LAYERS-1
           CALL POSITN(X(I*100),-SCALE)
           CALL JOIN(X(I*100),SCALE)
   30  CONTINUE
C      CALL FULL
C      CALL POSITN(X(1),AFIELD(1))
C      DO 40 I=1,100*LAYERS
C          CALL JOIN(X(I),AFIELD(I))
C  40  CONTINUE
C      CALL POSITN(X(1),-AFIELD(1))
C      DO 50 I=1,100*LAYERS
C          CALL JOIN(X(I),-AFIELD(I))
C  50  CONTINUE
       CALL BROKEN(10,10,10,10)
       CALL POSITN(X(1),RFIELD(1))
       DO 60 I=1,LAYERS*100
           CALL JOIN(X(I),RFIELD(I))
   60  CONTINUE
       CALL MAP(0.0,100.0,0.0,100.0)
       CALL WINDOW(0.0,100.0,0.0,100.0)
       CALL CTRMAG(15)
C      CALL FULL
C      CALL PLOTCS(90.0,15.0,LABEL)
C      CALL POSITN(80.0,15.0)
C      CALL JOIN(85.0,15.0)
       CALL BROKEN(10,10,10,10)
       CALL PLOTCS(90.0,10.0,LABEL//':t=0')
       CALL POSITN(80.0,10.0)
       CALL JOIN(85.0,10.0)
```

```
      CALL FULL
      CALL PLOTCS(40.0,-10.0,'Depth / metres')
      CALL CTRMAG(30)
      IF(LABEL(1:1).EQ.'E') THEN
         CALL PLOTCS(-10.0,60.0,'E')
      ELSE
         CALL PLOTCS(-10.0,60.0,'H')
      ENDIF
      IF(LFLAG.EQ.1) CALL ANNOTA(E,D,LAYERS,POLA,NEF)
      CALL FRAME
      RETURN
      END
C************************END OF PROFIL*************************************

C*************************POYNT*******************************************
C PLOTS OUT POYNTING VECTOR PROFILE
      SUBROUTINE POYNT(X,SZ,SX,DTOTAL,LAYERS,E,D,POLA,LFLAG,NEF)

      COMPLEX E(20)
      REAL X(2000),SZ(2000),SX(2000),SCALE,DTOTAL,D(20),NEF
      INTEGER I,LAYERS,POLA,LFLAG
      SCALE=SZ(1)
      DO 38 I=2,LAYERS*100
         IF (SZ(I).GT.SCALE) SCALE=SZ(I)
  38  CONTINUE

      CALL PSPACE(0.1,0.9,0.1,0.8)
      CALL MAP(-DTOTAL,2*DTOTAL,0.0,SCALE)
      CALL WINDOW(-DTOTAL,2*DTOTAL,0.0,SCALE)
      CALL AXORIG(-DTOTAL,0.0)
      CALL AXES
      CALL BROKEN(1,10,1,10)
      DO 39 I=1,LAYERS-1
          CALL POSITN(X(I*100),0.0)
          CALL JOIN(X(I*100),SCALE)
  39  CONTINUE
      CALL FULL
      CALL POSITN(X(1),SZ(1))
      DO 40 I=1,100*LAYERS
          CALL JOIN(X(I),SZ(I))
  40  CONTINUE
      CALL MAP(0.0,100.0,0.0,100.0)
      CALL CTRMAG(20)
      CALL PLOTCS(40.0,-10.0,'Depth / metres')
      CALL CTRORI(90.0)
      CALL PLOTCS(-10.0,25.0,'Poynting Vector / arbitrary units')
      CALL CTRORI(0.0)
      IF(LFLAG.EQ.1) CALL ANNOTA(E,D,LAYERS,POLA,NEF)
      CALL FRAME

      RETURN
```

```
      END
C*************************END OF POYNT*********************************

C*************************MAKEQN***************************************
C GENERATES THE SIMULTANEOUS EQUATIONS IN MATRIX FORM
C
      SUBROUTINE MAKEQN(NEF,E,D,LAYERS,MATRIX,VECTOR,POLA)


      REAL NEF,D(20),K0,PI
      COMPLEX K(20),MATRIX(40,40),A,B,E(20),VECTOR(40)
      INTEGER LAYERS,I,J,POLA
      COMMON /CONSTS/ PI,K0
      DO 2 I=1,40
         VECTOR(I)=0.0
         DO 1 J=1,40
            MATRIX(I,J) = 0.0
    1    CONTINUE
    2 CONTINUE

      DO 5 I=1,LAYERS
         K(I)=K0*CSQRT(E(I)-CMPLX(NEF*NEF))
    5 CONTINUE

      IF(LAYERS.GT.2) THEN
C FIELD CONTINUITY AT E1:E2 - THIS IS AT DEPTH=0
         VECTOR(1) = -1
         MATRIX(1,1) = 1
         MATRIX(1,2) = -1
         MATRIX(1,3) = -1
C FIELD CONTINUITY AT OTHER BOUNDARIES EXCLUDING LAST ONE
         DO 10 I=2,LAYERS-2
            A=EXP(K(I)*(0,1)*D(I))
            J=2*I
            MATRIX(J-1,J-2) = A
            MATRIX(J-1,J-1) = 1/A
            MATRIX(J-1,J) = -1
            MATRIX(J-1,J+1) = -1
   10    CONTINUE
C FIELD CONTINUITY AT LAST BOUNDARY
         A=EXP(K(LAYERS-1)*(0,1)*D(LAYERS-1))
         J=2*(LAYERS-1)
         MATRIX(J-1,J-2)=A
         MATRIX(J-1,J-1)=1/A
         MATRIX(J-1,J)=-1
         IF(POLA.EQ.0) THEN
C TE CONDITIONS - GRADIENT CONTINUITY
            VECTOR(2)=-K(1)
            MATRIX(2,1)=-K(1)
            MATRIX(2,2)=-K(2)
            MATRIX(2,3)=K(2)
```

```
            DO 20 I=2,LAYERS-2
               A = EXP(K(I)*(0,1)*D(I))
               J = 2*I
               MATRIX(J,J-2) = A*K(I)
               MATRIX(J,J-1) = -K(I)/A
               MATRIX(J,J) = -K(I+1)
               MATRIX(J,J+1) = K(I+1)
 20         CONTINUE
            A = EXP(K(LAYERS-1)*(0,1)*D(LAYERS-1))
            J = 2*(LAYERS-1)
            MATRIX(J,J-2)=K(LAYERS-1)*A
            MATRIX(J,J-1)=-K(LAYERS-1)/A
            MATRIX(J,J)=-K(LAYERS)
         ELSE
C TM CONDITIONS - INTEGRAL FIELD * PERMITTIVITY CONTINUITY
            VECTOR(2)=-E(1)/K(1)
            MATRIX(2,1)=-E(1)/K(1)
            MATRIX(2,2)=-E(2)/K(2)
            MATRIX(2,3)=E(2)/K(2)
            DO 30 I=2,LAYERS-2
               A = EXP(K(I)*(0,1)*D(I))
               J = 2*I
               MATRIX(J,J-2) = A*E(I)/K(I)
               MATRIX(J,J-1) = -E(I)/(K(I)*A)
               MATRIX(J,J) = -E(I+1)/K(I+1)
               MATRIX(J,J+1) = E(I+1)/K(I+1)
 30         CONTINUE
            A = EXP(K(LAYERS-1)*(0,1)*D(LAYERS-1))
            J = 2*(LAYERS-1)
            MATRIX(J,J-2)=E(LAYERS-1)*A/K(LAYERS-1)
            MATRIX(J,J-1)=-E(LAYERS-1)/(K(LAYERS-1)*A)
            MATRIX(J,J)=-E(LAYERS)/K(LAYERS)
         ENDIF

      ELSE
C SINGLE INTERFACE CASE
         VECTOR(1) = -1
         MATRIX(1,1) = 1
         MATRIX(1,2) = -1
         IF(POLA.EQ.0) THEN
            VECTOR(2) = -K(1)
            MATRIX(2,1) = -K(1)
            MATRIX(2,2) = -K(2)
         ELSE
            VECTOR(2) = -E(1)/K(1)
            MATRIX(2,1) = -E(1)/K(1)
            MATRIX(2,2) = -E(2)/K(2)
         ENDIF
      ENDIF
      RETURN
      END
```

```
C*******************END OF MAKEQN*********************************************

C ***************************GAUSSELIM*****************************************
C SOLVES SIMULTANEOUS EQUATIONS A.Y=X WHERE A IS AN NxN MATRIX
C RESULT CONTAINS ANSWERS
      SUBROUTINE GAUSSE(A,M,V,RESULT)

      INTEGER M,SWAP,I,J,R,Y
      COMPLEX A(40,40),V(40),RESULT(40),FACTOR,TEMP

      IF(M.EQ.2) THEN
         FACTOR = A(2,1)/A(1,1)
         A(2,1) = 0
         A(2,2) = A(2,2) - FACTOR * A(1,2)
         V(2) = V(2) - FACTOR * V(1)
         RESULT(2) = V(2)/A(2,2)
         RESULT(1) = (V(1) - A(1,2) * RESULT(2))/A(1,1)
      ELSE
         DO 60 R=1,M-1
C CHECKS FOR ZERO PIVOT
            SWAP=R
   10       IF(A(SWAP,SWAP).NE.0) THEN
               GOTO 30
            ELSE
               SWAP=SWAP+1
               IF(SWAP.EQ.M) THEN
                  PRINT *,'No solutions.'
                  STOP
               ENDIF
               GOTO 10
            ENDIF

C ROW SWAP - ONLY SWAPS NON ZERO PARTS OF COURSE
            IF(R.NE.SWAP) THEN
               DO 20 Y=R,M
                  TEMP=A(SWAP,Y)
                  A(SWAP,Y)=A(R,Y)
                  A(R,Y)=TEMP
   20          CONTINUE
               TEMP=V(SWAP)
               V(SWAP)=V(R)
               V(R)=TEMP
            ENDIF


   30       DO 50 I=R+1,M
               FACTOR=A(I,R)/A(R,R)
               A(I,R)=0
               DO 40 J=R+1,M
                  A(I,J)=A(I,J)-FACTOR*A(R,J)
   40          CONTINUE
```

```
                V(I)=V(I)-FACTOR*V(R)
   50         CONTINUE
   60      CONTINUE
C NOW MATRIX IS TRIANGULAR - CAN SUBSTITUTE BACK FOR RESULTS
           RESULT(M)=V(M)/A(M,M)
           DO 80 I=M-1,1,-1
              RESULT(I)=V(I)
              DO 70 J=M,I+1,-1
                 RESULT(I)=RESULT(I)-RESULT(J)*A(I,J)
   70         CONTINUE
              RESULT(I)=RESULT(I)/A(I,I)
   80      CONTINUE
        ENDIF
        RETURN
        END

C*************************ANNOTA*************************************************
C* GRAPH ANNOTATION
        SUBROUTINE ANNOTA(E,D,LAYERS,POLA,NEF)
        COMPLEX E(20)
        REAL D(20),PI,KO,LAMDA,NEF
        INTEGER LAYERS,POLA
        COMMON /CONSTS/ PI,KO
        LAMDA = 2 * PI/KO
        CALL CSPACE(0.0,1.0,0.0,1.0)
        CALL CTRMAG(12)
        CALL PLACE(58,1)
        CALL TYPECS('Wavelength = ')
        CALL PLACE(70,1)
        CALL TYPENE(LAMDA,4)
        CALL PLACE(58,2)
        IF(POLA.EQ.1) CALL TYPECS('TM Polarisation')
        IF(POLA.EQ.0) CALL TYPECS('TE Polarisation')

        CALL PLACE(50,3)
        CALL TYPECS('Layer  Rel. Permittivity  Thickness/m')
        DO 10 I=1,LAYERS
           CALL PLACE(51,3+I)
           CALL TYPENI(I)
           CALL PLACE(57,3+I)
           CALL TYPENF(REAL(E(I)),4)
           CALL PLACE(65,3+I)
           CALL TYPECS('+')
           CALL PLACE(65,3+I)
           CALL TYPENF(AIMAG(E(I)),4)
           CALL PLACE(72,3+I)
           CALL TYPECS('i')
           CALL PLACE(75,3+I)
           CALL TYPENE(D(I),4)
   10   CONTINUE
        CALL PLACE(65,4+LAYERS)
```

```
      CALL TYPECS('Neff= ')
      CALL PLACE(71,4+LAYERS)
      CALL TYPENF(NEF,4)
      CALL CSPACE(0.0,0.0,0.0,0.0)
      RETURN
      END
```

5. Uniaxial Ellipsometry program

```
C PRODUCES ELLIPSOMETRY RESULTS FOR UNIAXIAL FILMS
      PROGRAM UNIAX
      REAL K0,D1,PI,PHI0,DELTAM(20),PSIM(20),X(3)
      INTEGER NRESUL,PMASK(3),NLAYRS(20)
      COMPLEX N10,N1E,N2
      COMMON /PARAMS/ N10,N1E,N2,D1,PHI0,DELTAM,PSIM,NLAYRS,NRESUL
      COMMON /CONSTS/ PI,K0

      PI = 3.1415927

      WRITE(*,*) 'Uniaxial Ellipsometry program'
      CALL LYDATA

      PHI0 = PI*PHI0/180
      CALL SHOW(5)

      X(1) = REAL(N10)
      X(2) = REAL(N1E)
      X(3) = D1*1E9
      PMASK(1) = 1
      PMASK(2) = 1
      PMASK(3) = 1

      CALL FIT(X,PMASK,NRESUL)
      N10 = X(1) + (0,1) * 0.0
      N1E = X(2) + (0,1) * 0.0
      D1 = X(3)/1E9

      CALL CURVES

      CALL GREND
      STOP
      END

C*****************************DELPSI*****************************************
C* CALCULATES ELLIPSOMETRIC ANGLES
      COMPLEX FUNCTION DELPSI(N10,N1E,N2,D1,K0,PHI0)
```

```
      REAL D1,K0,PHI0,PHI2,PI
      COMPLEX BETAP,BETAS,N10,N1E,N2,R01SS,R01PP,R12SS,R12PP,RSS,RPP

      PI = 3.1415927
      PHI2 = ASIN(1/REAL(N2)*SIN(PHI0))

      BETAP = K0*D1*(N10/N1E)*SQRT(N1E*N1E-SIN(PHI0)*SIN(PHI0))
      BETAS = K0*D1*SQRT(N10*N10-SIN(PHI0)*SIN(PHI0))

      R01PP = (N10*N1E*COS(PHI0)-SQRT(N1E*N1E-SIN(PHI0)*SIN(PHI0)))/
     $        (N10*N1E*COS(PHI0)+SQRT(N1E*N1E-SIN(PHI0)*SIN(PHI0)))
      R12PP = (-N10*N1E*COS(PHI2)+N2*SQRT(N1E*N1E-N2*N2*SIN(PHI2)
     $         *SIN(PHI2)))/(N10*N1E*COS(PHI2)+N2*SQRT(N1E*N1E-N2*N2*
     $         SIN(PHI2)*SIN(PHI2)))
      R01SS = (COS(PHI0)-SQRT(N10*N10-SIN(PHI0)*SIN(PHI0)))/
     $        (COS(PHI0)+SQRT(N10*N10-SIN(PHI0)*SIN(PHI0)))
      R12SS = (-N2*COS(PHI2)+SQRT(N10*N10-N2*N2*SIN(PHI2)*SIN(PHI2)))/
     $        (N2*COS(PHI2)+SQRT(N10*N10-N2*N2*SIN(PHI2)*SIN(PHI2)))

      RPP = (R01PP+R12PP*EXP(-(0,1)*2*BETAP))/
     $      (1+R01PP*R12PP*EXP(-(0,1)*2*BETAP))
      RSS = (R01SS+R12SS*EXP(-(0,1)*2*BETAS))/
     $      (1+R01SS*R12SS*EXP(-(0,1)*2*BETAS))

      DELPSI = RPP/RSS
      RETURN
      END
C********************* END OF DELPSI ***************************************

C*************************LYDATA*********************************************
C GATHERS DATA FOR LAYERS
      SUBROUTINE LYDATA

      COMPLEX      N10,N1E,N2
      REAL         PI,K0,LAMDA,PHI0,DELTAM(20),PSIM(20),D1
      INTEGER      NRESUL,NLAYRS(20)
      CHARACTER*14 FILNAM
      CHARACTER*80 TRASH

      COMMON /PARAMS/ N10,N1E,N2,D1,PHI0,DELTAM,PSIM,NLAYRS,NRESUL
      COMMON /CONSTS/ PI,K0

      WRITE(*,*) 'Filename for layer data'
      READ(*,999) FILNAM
      OPEN(UNIT=10,FILE=FILNAM,STATUS='OLD')
      REWIND(10)
      READ(10,'(A80)') TRASH
      READ(10,*) LAMDA
      READ(10,'(A80)') TRASH
      READ(10,*) PHI0
```

```
      READ(10,'(A80)') TRASH
      READ(10,*) N2
      READ(10,'(A80)') TRASH
      READ(10,*) N1O
      READ(10,'(A80)') TRASH
      READ(10,*) N1E
      READ(10,'(A80)') TRASH
      READ(10,*) D1
      READ(10,'(A80)') TRASH
      READ(10,*) NRESUL
      READ(10,'(A80)') TRASH
      READ(10,*) (DELTAM(I),PSIM(I),NLAYRS(I), I=1,NRESUL)

      KO = 2*PI/LAMDA

      CLOSE(UNIT=10)

  999 FORMAT(A14)
      RETURN
      END
C************************END OF LYDATA*************************************

C*****************************SHOW*****************************************
      SUBROUTINE SHOW(WHERE)
      COMPLEX N1O,N1E,N2
      REAL PHIO,LAMDA,PI,KO,D1,DELTAM(20),PSIM(20)
      INTEGER WHERE,NRESUL,NLAYRS(20)

      COMMON /PARAMS/ N1O,N1E,N2,D1,PHIO,DELTAM,PSIM,NLAYRS,NRESUL
      COMMON /CONSTS/ PI,KO


      LAMDA = 2*PI/KO
      WRITE(WHERE,997) 'Wavelength =',LAMDA
      WRITE(WHERE,999) 'Incident angles =',PHIO*180/PI
      WRITE(WHERE,998) 'Substrate Index =',N2
      WRITE(WHERE,998) 'Film ordinary Index =',N1O
      WRITE(WHERE,998) 'Film extraordinary Index =',N1E

  997 FORMAT(A30,E10.5)
  998 FORMAT(A30,F8.3,',',F8.3)
  999 FORMAT(A30,F8.3)
      RETURN
      END

C*************************FIT*****************************************
C* FITS THEORY AND EXPERIMENT
      SUBROUTINE FIT(X,PMASK,M)
      REAL X(3),FSUMSQ,GRAD(3),FNOW,LENGTH,FNEXT,ERROR
      INTEGER M,COUNT,ITER,PMASK(3),BETTER
```

```
      GRAD(1) = 0
      GRAD(2) = 0
      GRAD(3) = 0

      WRITE(*,*) 'Enter iterations limit'
      READ(*,*) ITER
      FNEXT =  FSUMSQ(X,0.0,0.0,0.0)
      COUNT = 0
      WRITE(*,998) 'Ordinary Index','Extraord Index','Monolayer d',
     $                                                    'Error'
   10 FNOW = FNEXT
      BETTER = 0
      WRITE(*,999) X(1),X(2),X(3)/1E9,SQRT(FNOW/M)
      IF(PMASK(1).EQ.1) THEN
         GRAD(1) = (FSUMSQ(X,0.001,0.0,0.0) - FNOW)/0.001
      ENDIF
      IF(PMASK(2).EQ.1) THEN
         GRAD(2) = (FSUMSQ(X,0.0,0.001,0.0) - FNOW)/0.001
      ENDIF
      IF(PMASK(3).EQ.1) THEN
         GRAD(3) = (FSUMSQ(X,0.0,0.0,0.001) - FNOW)/0.001
      ENDIF
      LENGTH=SQRT(GRAD(1)*GRAD(1)+GRAD(2)*GRAD(2)+GRAD(3)*GRAD(3))
      GRAD(1) = - 0.00001 * GRAD(1)/LENGTH
      GRAD(2) = - 0.00001 * GRAD(2)/LENGTH
      GRAD(3) = - 0.00001 * GRAD(3)/LENGTH

   20 GRAD(1) = GRAD(1) * 2
      GRAD(2) = GRAD(2) * 2
      GRAD(3) = GRAD(3) * 2
      FNEXT = FSUMSQ(X,GRAD(1),GRAD(2),GRAD(3))
      IF(FNEXT.LT.FNOW) THEN
         BETTER = 1
         FNOW = FNEXT
         GOTO 20
      ELSE
         X(1) = X(1) + GRAD(1)/2
         X(2) = X(2) + GRAD(2)/2
         X(3) = X(3) + GRAD(3)/2
      ENDIF

      FNEXT = FSUMSQ(X,0.0,0.0,0.0)
      COUNT = COUNT + 1
      IF(COUNT.LT.ITER.AND.BETTER.EQ.1) GOTO 10
   30 WRITE(*,999) X(1),X(2),X(3)/1E9,SQRT(FSUMSQ(X,0.0,0.0,0.0)/M)
  998 FORMAT(A20,A15,A15,A19)
  999 FORMAT(F20.4,F15.4,E15.3,F13.4)
      RETURN
      END
C************************END OF FIT*****************************************
```

```
C*************************FSUMSQ*****************************************
C* CALCULATES SUM OF SQUARES OF ERRORS
      REAL FUNCTION FSUMSQ(X,DX1,DX2,DX3)
      INTEGER I,NRESUL,NLAYRS(20)
      REAL PI,K0,PHI0,DELTAM(20),PSIM(20),ERROR,X(3),DX1,
     $         DX2,DX3,PSIT,DELTAT,D1
      COMPLEX N10,N1E,N2,ELLIPS,DELPSI
      COMMON /PARAMS/ N10,N1E,N2,D1,PHI0,DELTAM,PSIM,NLAYRS,NRESUL
      COMMON /CONSTS/ PI,K0

      N10 = X(1) + DX1 + (0,1) * 0.0
      N1E = X(2) + DX2 + (0,1) * 0.0
      D1 = (X(3) + DX3)/1E9
      F = 0
      DO 10 I = 1,NRESUL
         ELLIPS = DELPSI(N10,N1E,N2,D1*NLAYRS(I),K0,PHI0)
         PSIT = ATAN(ABS(ELLIPS))*180/PI
         DELTAT = ATAN2(AIMAG(ELLIPS),REAL(ELLIPS))*180/PI
         IF(DELTAT.LT.0.0) DELTAT=DELTAT+360.0

         F = F + (PSIT - PSIM(I)) * (PSIT - PSIM(I))
         F = F + (DELTAT - DELTAM(I)) * (DELTAT - DELTAM(I))
   10 CONTINUE
      FSUMSQ = F
      RETURN
      END
C*********************END OF FSUMSQ*************************************

C*************************CURVES*****************************************
C REFLECTION VERSUS ANGLE RESULTS
      SUBROUTINE CURVES

      INTEGER I,NRESUL,NLAYRS(20)
      REAL PI,K0,PHI0,DELTAM(20),PSIM(20),ERROR,PSIT,DELTAT,DEPTH,D1
      COMPLEX N10,N1E,N2,ELLIPS,DELPSI
      COMMON /PARAMS/ N10,N1E,N2,D1,PHI0,DELTAM,PSIM,NLAYRS,NRESUL
      COMMON /CONSTS/ PI,K0

      CALL PAPER(1)
      CALL PSPACE(0.1,0.9,0.1,0.9)
      CALL MAP(0.0,90.0,0.0,360.0)
      CALL WINDOW(0.0,90.0,0.0,360.0)
      CALL AXORIG(0,0)
      CALL AXES

      DEPTH = 10E-10
      ELLIPS = DELPSI(N10,N1E,N2,DEPTH,K0,PHI0)
      PSIT = ATAN(ABS(ELLIPS))*180/PI
      DELTAT = ATAN2(AIMAG(ELLIPS),REAL(ELLIPS))*180/PI
      IF(DELTAT.LT.0.0) DELTAT=DELTAT+360.0
      CALL POSITN(PSIT,DELTAT)
```

```
   10  DEPTH = DEPTH + 1E-10
       ELLIPS = DELPSI(N10,N1E,N2,DEPTH,K0,PHI0)
       PSIT = ATAN(ABS(ELLIPS))*180/PI
       DELTAT = ATAN2(AIMAG(ELLIPS),REAL(ELLIPS))*180/PI
       IF(DELTAT.LT.0.0) DELTAT=DELTAT+360.0
       CALL JOIN(PSIT,DELTAT)
       IF(DEPTH.LT.2000E-10) GOTO 10

       DO 20 I = 1,NRESUL
          CALL PLOTNC(PSIM(I),DELTAM(I),248)
   20  CONTINUE
       CALL CTRFNT(2)
       CALL MAP(0.0,100.0,0.0,100.0)
       CALL CTRMAG(20)
       CALL PLOTCS(50.0,-10.0,'V')
       CALL PLOTCS(-10.0,50.0,'D')
       CALL CTRFNT(1)

       RETURN
       END
```

6. Input file formats

The SPR, Pockels effect and waveguide programs all take a data file of the following form:

```
 Polarisation 1=TM 0=TE
1
 Wavelength/m
   0.632800E-06
 Number of layers
 3
 Real(e),Im(e),depth (0=semi infinite)
  2.319529,  0.000000,   0.000000E+00
-17.500000,  0.730000,   0.500000E-07
  1.000000,  0.000000,   0.000000E+00
```

The fitting programs also use files containing reflectivity or differential reflectivity against angle; these simply consist of the set of datum points delimited as follows:

```
angle1 , data1
angle2 , data2
```

```
angle3 , data3
etc.
```

The uniaxial ellipsometry program takes a single input data file:

```
Wavelength in metres
0.633E-6
Angle of Incidence in degrees
70.0
Substrate index (real,imag)
3.861,0.178
Film ordinary index (real,imag)
1.4900,0.0
Film extraordinary index (real,imag)
1.5700,0.0
Monolayer thickness (metres)
30E-10
Number of data points
6
Delta, Psi, Number of monolayers
112.00 , 16.81 , 10
85.83 , 26.45 , 20
74.25, 37.04 , 30
72.87, 58.00 , 40
286.70, 72.77, 50
281.41, 41.47, 60
```